Nesprin-1/-2 Ortholog ANC-1 Regulates Organelle Positioning and Subcellular Crowding in *C. elegans*

By

HONGYAN HAO
DISSERTATION/THESIS

Submitted in partial satisfaction of the requirements for the degree of

DOCTOR OF PHILOSOPHY

in

Biochemistry, Molecular, Cellular and Developmental Biology

in the

OFFICE OF GRADUATE STUDIES

of the

UNIVERSITY OF CALIFORNIA

DAVIS

Approved:

Daniel A. Starr, Chair

JoAnne Engebrecht

Kassandra Ori-McKenney

Committee in Charge

2022

Acknowledgement

The journey to my Ph.D. has been joyful with support and help from many. I am very lucky to be surrounded by helpful mentors, wonderful labmates, cheerful friends, and thoughtful families.

First, I sincerely thank my supervisor Dr. Daniel Starr for his consistent guidance, patience, support, and feedback on the project in the past few years. I am grateful that he supported me to work on this fascinating protein ANC-1 with trust. He taught me how to think about science, how to read and write, how to connect to people, how to collaborate with others, and most importantly, how to stay positive. My success is attributable to his visionary leadership and dedicated support. Working with him is but a joy.

I would also like to thank my other thesis committee members Dr. JoAnne Engebrecht and Dr. Kassandra Ori-McKenney for their guidance, advice, and support both on my scientific project and career development. I would also like to thank Dr. Harri Reddi for his support and advice.

I would also like to thank my collaborators in and out of the Starr-Luxton Laboratory for their helpful discussions and reliable work. I have learned so much from them. I also would like to thank Dr. Michael Paddy and Dr. Thomas Wilkop from the UCDavis MCB imaging facility, Dr. Danielle Jorgens from the UC Berkeley Electron Microscope Lab and Bradley Shibata from the UCDavis Biological Electron Microscopy Facility for their help.

I am thankful to the past and present Starr-Luxton lab members and the BESt lab members, especially those who contributed to this project, for insightful discussion on my project, as well as being great labmates and friends.

I would like to thank the members of Friday Cell Biology group for their inspiring talks, constructive criticism, and helpful discussion on my project. I especially am thankful to Dr. Frank McNally, Dr. Rick McKenny, Dr. Ben Montpetit, Dr. Lesilee Rose and Dr. Bo Liu for their intelligent suggestions.

I would also like to thank the faculty and students of the Biochemistry, Molecular, Cellular and Developmental Biology (BMCDB) graduate group, especially the 2016 BMCDB cohort, for creating this supportive environment to help each other to succeed. Being aware of how supportive our graduate group is has enabled me to just focus on the science, which is the most fun part of this journey besides working with awesome people along the way.

My family has been supporting me in the past many years to follow my dream. I specially want to thank my mom and dad, who never had a chance to go to high school, trusted me with their love and blessing to pursue my dream of doing science.

I would like to thank my husband Yu Ji for all his love, support, understanding, inspiring ideas and everything else.

There are still many more important people who are missing on the list. I am grateful that our path has crossed. Thank you to everyone else who has helped and supported me with kindness!

RIGHTS & ACCESS

Elsevier Ltd

Article:	**Conserved SUN-KASH interfaces mediate LINC complex-dependent nuclear movement and positioning**
Corresponding author:	**Dr. Daniel A. Starr**
E-mail address:	**dastarr@ucdavis.edu**
Journal:	**Current Biology**
Our reference	**CURBIO14875**
PII:	**S0960-9822(18)31046-7**
DOI:	**10.1016/j.cub.2018.08.001**

YOUR STATUS

I am one author signing on behalf of all co-authors of the manuscript

ASSIGNMENT OF COPYRIGHT

I hereby assign to Elsevier Ltd the copyright in the manuscript identified above (where Crown Copyright is asserted, authors agree to grant an exclusive publishing and distribution license) and any tables, illustrations or other material submitted for publication as part of the manuscript (the "Article"). This assignment of rights means that I have granted to Elsevier Ltd, the exclusive right to publish and reproduce the Article, or any part of the Article, in print, electronic and all other media (whether now known or later developed), in any form, in all languages, throughout the world, for the full term of copyright, and the right to license others to do the same, effective when the Article is accepted for publication. This includes the right to enforce the rights granted hereunder against third parties.

SUPPLEMENTAL MATERIALS

"Supplemental Materials" shall mean materials published as a supplemental part of the Article, including but not limited to graphical, illustrative, video and audio material.

With respect to any Supplemental Materials that I submit, Elsevier Ltd shall have a perpetual worldwide, non-exclusive right and license to publish, extract, reformat, adapt, build upon, index, redistribute, link to and otherwise use all or any part of the Supplemental Materials in all forms and media (whether now known or later developed), and to permit others to do so.

RESEARCH DATA

"Research Data" shall mean the result of observations or experimentation that validate research findings and that are published separate to the Article, which can include but are not limited to raw data, processed data, software, algorithms, protocols, and methods.

With respect to any Research Data that I wish to make accessible on a site or through a service of Elsevier Ltd, Elsevier Ltd shall have a perpetual worldwide, non-exclusive right and license to publish, extract, reformat, adapt, build upon, index, redistribute, link to and otherwise use all or any part of the Research Data in all forms and media (whether now known or later developed) and to permit others to do so. Where I have selected a specific end user license under which the Research Data is to be made available on a site or through a service, the publisher shall apply that end user license to the Research Data on that site or service.

REVERSION OF RIGHTS

Articles may sometimes be accepted for publication but later rejected in the publication process, even in some cases after public posting in "Articles in Press" form, in which case all rights will revert to the author (see https://www.elsevier.com/about/our-business/policies/article-withdrawal).

REVISIONS AND ADDENDA

I understand that no revisions, additional terms or addenda to this Journal Publishing Agreement can be accepted without Elsevier Ltd's express written consent. I understand that this Journal Publishing Agreement supersedes any previous agreements I have entered into with Elsevier Ltd in relation to the Article from the date hereof.

AUTHOR RIGHTS FOR SCHOLARLY PURPOSES

I understand that I retain or am hereby granted (without the need to obtain further permission) the Author Rights (see description below), and that no rights in patents, trademarks or other intellectual property rights are transferred to Elsevier Ltd.

The Author Rights include the right to use the Preprint, Accepted Manuscript and the Published Journal Article for Personal Use and Internal Institutional Use. They also include the right to use these different versions of the Article for Scholarly Sharing purposes, which include sharing:

the Preprint on any website or repository at any time;
the Accepted Manuscript on certain websites and usually after an embargo period;

the Published Journal Article only privately on certain websites, unless otherwise agreed by Elsevier Ltd.

In the case of the Accepted Manuscript and the Published Journal Article the Author Rights exclude Commercial Use (unless expressly agreed in writing by Elsevier Ltd), other than use by the author in a subsequent compilation of the author's works or to extend the Article to book length form or re-use by the author of portions or excerpts in other works (with full acknowledgment of the original publication of the Article).

AUTHOR REPRESENTATIONS / ETHICS AND DISCLOSURE / SANCTIONS

I affirm the Author Representations noted below, and confirm that I have reviewed and complied with the relevant Instructions to Authors, Ethics in Publishing policy, Declarations of Interest disclosure and information for authors from countries affected by sanctions (Iran, Cuba, Sudan, Burma, Syria, or Crimea). Please note that some journals may require that all co-authors sign and submit Declarations of Interest disclosure forms. I am also aware of the publisher's policies with respect to retractions and withdrawal (https://www.elsevier.com/about/our-business/policies/article-withdrawal).
For further information see the publishing ethics page at https://www.elsevier.com/about/our-business/policies/publishing-ethics and the journal home page. For further information on sanctions, see https://www.elsevier.com/about/our-business/policies/trade-sanctions

Author representations

The Article I have submitted to the journal for review is original, has been written by the stated authors and has not been previous
The Article was not submitted for review to another journal while under review by this journal and will not be submitted to any oth
The Article and the Supplemental Materials do not infringe any copyright, violate any other intellectual property, privacy or other ri
entity, or contain any libellous or other unlawful matter.
I have obtained written permission from copyright owners for any excerpts from copyrighted works that are included and have cre
Article or the Supplemental Materials.
Except as expressly set out in this Journal Publishing Agreement, the Article is not subject to any prior rights or licenses and, if my
authors' institution has a policy that might restrict my ability to grant the rights required by this Journal Publishing Agreement (tak
Author Rights permitted hereunder, including Internal Institutional Use), a written waiver of that policy has been obtained.
If I and/or any of my co-authors reside in Iran, Cuba, Sudan, Burma, Syria, or Crimea, the Article has been prepared in a personal
capacity and not as an official representative or otherwise on behalf of the relevant government or institution.
If I am using any personal details or images of patients, research subjects or other individuals, I have obtained all consents require
and complied with the publisher's policies relating to the use of such images or personal information. See https://www.elsevier.com
/policies/patient-consent for further information.
Any software contained in the Supplemental Materials is free from viruses, contaminants or worms.
If the Article or any of the Supplemental Materials were prepared jointly with other authors, I have informed the co-author(s) of th
Publishing Agreement and that I am signing on their behalf as their agent, and I am authorized to do so.

GOVERNING LAW AND JURISDICTION

This Agreement will be governed by and construed in accordance with the laws of the country or state of Elsevier Ltd ("the Governing State"), without regard to conflict of law principles, and the parties irrevocably consent to the exclusive jurisdiction of the courts of the Governing State.

For information on the publisher's copyright and access policies, please see http://www.elsevier.com/copyright.
For more information about the definitions relating to this agreement click here.

☑ **I have read and agree to the terms of the Journal Publishing Agreement.**

1st August 2018 T-copyright-v22/2017

Abstract

Organelle positioning is important in many cellular and developmental processes, especially for the function of polarized and spatially extended cells. For example, in mammalian myofibers, most nuclei are evenly spaced out at the periphery of the fiber, except for a few that group into small clusters anchored under the neuromuscular junction. Disruption of nuclear positioning is found in many muscular diseases. Nuclear positioning is mediated by the conserved bridge termed the LINC (Linker of nucleoskeleton and cytoskeleton) complex, which is formed by the interaction between inner nuclear membrane SUN domain proteins and the outer nuclear membrane KASH domain proteins. The SUN proteins pair with different KASH proteins which contains various cytoskeleton interacting domains, to perform distinct functions. For example, in *Caenorhabditis elegans*, SUN protein UNC-84 either interacts with the KASH protein UNC-83 to move nuclei during development, or the KASH protein ANC-1 to anchor nuclei in the hyp7 syncytium. Interestingly, UNC-83 KASH is shorter and lacks the conserved cysteine predicted to be important to stabilize SUN/KASH interaction by structural and molecular dynamic simulations.

In collaboration with other lab mates, we showed that the conserved intermolecular disulfide bond plays important roles for UNC-84/ANC-1 mediated nuclear anchorage but is dispensable for UNC-84/UNC-83 mediated nuclear migration. In addition, the longer KASH containing the DDEY residues predicted to be associated with the membrane also is necessary for ANC-1 KASH to function.

ANC-1 has been proposed to physically tether nuclei to the actin cytoskeleton through its C-terminal KASH domain and the N-terminal calponin homology (CH) actin-binding domains. However, I found that deletion of the KASH domain causes less severe nuclear anchorage defects than null mutations. Moreover, the short isoform *anc-1b* lacking CH domains is sufficient for hyp7 nuclear anchorage. It was completely unknown how ANC-1 functions without CH and

KASH domains. Interestingly, other than nuclear anchorage defects, the ER, mitochondria, and lipid-droplets were also severely unanchored and sometimes moved throughout the cytoplasm in *anc-1* but not *unc-84* null mutants. Unlike most KASH proteins which are enriched on the nuclear envelope, I found that GFP-tagged ANC-1 was mostly colocalized with the ER. To understand the mechanism by which ANC-1 regulates organelle positioning, I used CRISPR/Cas9 gene editing to delete different domains of ANC-1 and found that the spectrin-like repeat structures and the transmembrane domain play important roles in organelle anchorage. Deletion of the spectrin-like repeat region disrupted the protein's ER-localization. These results led to a cytoplasmic integrity model where ANC-1 localizes to the ER and functions in positioning nuclei, the ER, mitochondria, and likely other organelles in place.

The cytoplasm is a crowded environment filled with macromolecules. To test if ANC-1 anchors organelles through regulating the intracellular crowding, I expressed and analyzed the diffusion of 40nm GEMs (genetically encoded multimeric nanoparticles) in *C. elegans* hypodermal and intestine tissues. The diffusion of the 40nm GEMs is significantly increased in the cytoplasm of *anc-1* null mutants in both tissues, indicating that ANC-1 may regulate the crowding of the cytoplasm. Ribosome concentration has been reported to play an important role in cytoplasmic crowding. RNAi of small ribosome protein *rps-15* or *rps-18* caused nuclear anchorage defects. In addition, in *anc-1* mutants, the ribosome distribution is altered. These results indicate that ANC-1 may regulate the biophysical properties of the cytoplasm through the ER and ribosomes.

Table of Contents

Chapter I

Introduction: SUN/KASH interactions facilitate force transmission across the nuclear envelope

Hongyan Hao and Daniel A. Starr

Nucleus March 2019

Hongyan Hao and Daniel A. Starr wrote and edited the Extra View article together. Hongyan Hao created the figure.

Nucleus

ISSN: 1949-1034 (Print) 1949-1042 (Online) Journal homepage: https://www.tandfonline.com/loi/kncl20

SUN/KASH interactions facilitate force transmission across the nuclear envelope

Hongyan Hao & Daniel A. Starr

To cite this article: Hongyan Hao & Daniel A. Starr (2019) SUN/KASH interactions facilitate force transmission across the nuclear envelope, Nucleus, 10:1, 73-80, DOI: 10.1080/19491034.2019.1595313

To link to this article: https://doi.org/10.1080/19491034.2019.1595313

Published online: 19 Mar 2019.

NUCLEUS
2019, VOL. 10, NO. 1, 73–80
https://doi.org/10.1080/19491034.2019.1595313

Taylor & Francis
Taylor & Francis Group

EXTRA VIEW

OPEN ACCESS Check for updates

SUN/KASH interactions facilitate force transmission across the nuclear envelope

Hongyan Hao and Daniel A. Starr

Department of Molecular and Cellular Biology, University of California, Davis, CA USA

ABSTRACT

LINC complexes (Linker of Nucleoskeleton and Cytoskeleton), consisting of inner nuclear membrane SUN (Sad1, UNC-84) proteins and outer nuclear membrane KASH (Klarsicht, ANC-1, and Syne Homology) proteins, are essential for nuclear positioning, cell migration and chromosome dynamics. To test the in vivo functions of conserved interfaces revealed by crystal structures, Cain et al used a combination of Caenorhabditis elegans genetics, imaging in cultured NIH 3T3 fibroblasts, and Molecular Dynamic simulations, to study SUN-KASH interactions. Conserved aromatic residues at the -7 position of the C-termini of KASH proteins and conserved disulfide bonds in LINC complexes play important roles in force transmission across the nuclear envelope. Other properties of LINC complexes, such as the helices preceding the SUN domain, the longer coiled-coils spanning the perinuclear space and higher-order organization may also function to transmit mechanical forces generated by the cytoskeleton across the nuclear envelope.

ARTICLE HISTORY
Received 19 December 2018
Revised 4 March 2019
Accepted 7 March 2019

KEYWORDS
LINC complex; mechanical force transduction; nuclear envelope; nuclear positioning

LINC complexes are essential for force transmission across the nuclear envelope

Eukaryotes are distinguishable from prokaryotes by the presence of a nuclear envelope separating the genetic material from the cytoplasm. The nuclear envelope is composed of two lipid bilayers and a perinuclear space continuous with the lumen of the endoplasmic reticulum (ER). Communication between the nucleoplasm and the cytoplasm is crucial for cellular functions [2]. There are three independent ways to transmit information across the nuclear envelope. Classically, small proteins and molecules can diffuse through nuclear pores while larger complexes, including ribosomal subunits, can be specifically transported through nuclear pores [3]. Alternatively, other complexes, including some virus coats, bleb from the inner nuclear membrane, diffuse across the perinuclear space in membrane-bound compartments, and fuse to the outer nuclear membrane [4]. Third, mechanical forces can be transferred directly across the nuclear envelope through conserved physical bridges termed LINC (**Li**nker of **N**ucleoskeleton and **C**ytoskeleton) complexes. Such mechanical force transmission across the nuclear envelope is essential for nuclear positioning and meiotic chromosome dynamics [5,6].

LINC complexes are made of SUN (**S**ad1, **UN**C-84) proteins in the inner nuclear membrane and KASH (**K**larsicht, **A**NC-1, and **S**yne **H**omology) proteins in the outer nuclear membrane [7]. The central interaction occurs in the lumen of the nuclear envelope near the outer nuclear membrane, between a trimer of conserved SUN domains about 175 residues each and C-terminal KASH peptides of 10 to 32 residues (Figure 1) [8–12]. SUN proteins then extend across the perinuclear space, cross the inner nuclear membrane and interact with lamins or other proteins in the nucleus, including chromatin and telomeric proteins [6,13,14]. The large, cytoplasmic portions of KASH proteins associate with various components of the cytoskeleton, including actin filaments, microtubule motors, or intermediate filaments [7,15].

LINC complexes are conserved across eukaryotes, and likely played a role in the formation of the nuclear envelope before the last eukaryotic common ancestor [16]. Furthermore, LINC complexes facilitate diverse functions, ranging from pronuclear migration, skeletal muscle nuclear positioning, nuclear migration in the hair cells of the inner ear, and chromosome pairing during meiosis [5,6,17,18]. A common feature of these processes is that mechanical forces generated by the cytoskeleton need to be transferred across the nuclear envelope to the nucleoskeleton. Mutations in

CONTACT Daniel A. Starr dastarr@ucdavis.edu Department of Molecular and Cellular Biology, University of California, Davis, CA USA

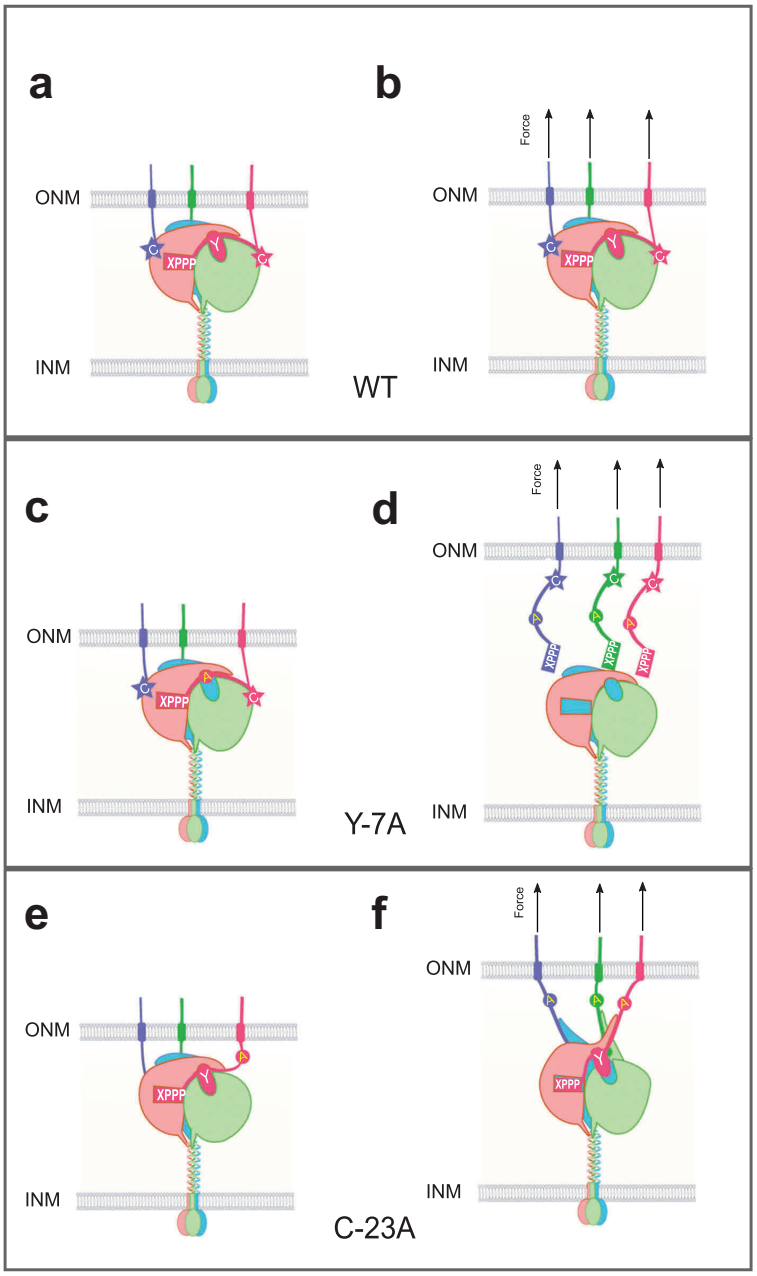

Figure 1. Conserved residues at SUN-KASH interfaces function in LINC complex assembly and force transmission at the nuclear envelope. Each panel shows a cartoon simulation focusing on the SUN-KASH interface. SUN proteins (salmon, light green and blue) trimerize and span the inner nuclear membrane (INM). Coiled-coils reach toward the outer nuclear membrane (ONM). A trimer of conserved SUN domains (at the top of the coils) interacts with three KASH peptides in the ONM (blue, green, and red) to form a hetero-hexamer. In wild type, the PPPX motif (rectangle) at the C terminus of KASH fits into a pocket in one SUN protomer (P1), the −7 tyrosine (oval) interacts with a hydrophobic binding site between the KASH lid of SUN P1 and the SUN core of second protomer (P2) and the −23 cysteine forms an intermolecular disulfide bond (star) with SUN. (A, C, and E) Representations of the LINC complexes without any forces. (B, D, and F) Representations of LINC complexes under mechanical strain from pulling forces generated in the cytoplasm. (A-B) wild type; when force is applied on the LINC complex, a stable LINC transfers forces across the nuclear envelope to the nucleoskeleton, resulting in nuclear movements. (C-D) KASH with a tyrosine mutation at position −7 from the C terminus; LINC complexes still form, but fail when force is applied. (E-F) KASH with a mutation in the −23 cysteine. LINC complexes form, and are able to transfer some forces across the nuclear envelope to move nuclei. However, without the intermolecular disulfide bond, LINC will break under maximal force in some systems (not shown).

LINC components are linked to a wide variety of diseases including muscular diseases, hearing loss, neurological disorders, and cancers [19]. Thus, it is critical to study the molecular mechanisms for the assembly of the LINC complexes as well as how forces are transmitted through the LINC complex.

Crystal structure of the SUN/KASH complex

A major breakthrough for understanding LINC complexes came in 2012 when the crystal structures of the interaction between human SUN and KASH domains were revealed [8,20]. Overall, three SUN domains ($SUN2_{540-717}$) and their adjacent, short, coiled trimerization domains ($SUN2_{525-540}$) interact with C-terminal 29 residues of Nesprin-1 or Nesprin-2 KASH domains to form a clover-like heterohexamer complex [8]. The SUN domain folds into a β-sandwich core with a protruding 20-residue β-hairpin ($SUN2_{567-587}$) termed the KASH-lid. Each KASH peptide interacts with three interfaces of a SUN trimer. First, the core of a SUN2 protomer formed by hydroxyl groups of S641, Y703 and Y707, together with H628 and stabilized by the C601-C705 intermolecular disulfide bond, forms a binding pocket for the three prolines of a PPPX motif at the C terminus of the KASH peptides (Figure 1a). Second, the KASH-lid of SUN2 protomer 1 (P1) and the β-sandwich core of protomer 2 (P2) form a groove that interacts with the −4 to −14 residues of the KASH peptide. The −4, −5 and −6 residues of KASH do not interact strongly with SUN2, while a Y at −7 and a L at −9 are buried into the cleft between P1 and P2 (Figure 1a). Third, the KASH peptide kinks between the P-11 and −12 residues. Next, residues −13 to −23 of the KASH peptide bind along the surface of SUN2 P2, except for a large, conserved hydrophobic residue at −17 buried into a hydrophobic pocket. Finally, the crystal structures showed that a cysteine at −23 of the KASH peptide forms a disulfide bond with a conserved cysteine in SUN2 (C563), to further stabilize the interaction (Figure 1a) [8]. Thus, the crystal structures predict that a number of conserved residues that are likely important for the interaction between SUN and KASH proteins and their ability to transfer mechanical forces across the nuclear envelope (Figure 1b).

To test the crystal structure predictions, Sosa et al. [8], performed *in vitro* pull-down assays with SUN and KASH domains. They showed that a disulfide bond is formed between SUN and KASH proteins in HeLa cells. However, a truncated KASH peptide of only 14 amino acids still interacts with SUN proteins *in vitro*, indicating that the cysteine at −23 and the disulfide bond between SUN and KASH are not required for their interaction. In contrast, extending the C terminus of the KASH peptide by a single alanine residue, or mutating conserved residues at −7 or −9 of KASH peptides abolishes SUN-KASH interactions *in vitro* [8]. The *in vivo* functional significance of the different SUN-KASH interaction interfaces and the implications for LINC complex mechanisms were yet to be uncovered. It was hypothesized that strong interactions between SUN and KASH domains are required to resist forces generated from the cytoskeleton and to ensure effective force transmission across the nuclear envelope. We set out to test this model in live cells.

Conserved residues are required for functional LINC complex in live cells

In our recent study [1], we tested the ability of conserved residues for SUN-KASH interactions and force transmission. To examine these processes in cells, we used *C. elegans* developing hypodermal tissues. During *C. elegans* embryogenesis, hypodermal precursor nuclei migrate to the opposite side of the cell in a SUN-KASH dependent manner [21]. The SUN protein UNC-84 recruits the KASH protein UNC-83 to the outer nuclear membrane [22]. UNC-83 then serves as the cargo adaptor to recruit microtubule motors kinesin-1 and dynein to the surface of nuclei [7,23,24]. The motors facilitate nuclear migration towards the plus end of microtubules [24]. Failure of this nuclear migration leads to ectopic localization of nuclei in the dorsal cord of the L1 larva [25]. After nuclear migration, hypodermal cells fuse to form a syncytium and nuclei are anchored in place. In adult *C. elegans* more than a hundred nuclei are evenly spaced in the hyp7 syncytium [26]. The KASH protein ANC-1 interacts with the SUN protein UNC-84 to anchor nuclei to the actin cytoskeleton. In *unc-84* and *anc-1* null mutants, hyp7 nuclei form clusters [27,28].

We used a mammalian tissue culture model to complement our *C. elegans* studies. NIH3T3 fibroblasts cultured in a monolayer polarize with

centrosomes in front of nuclei in response to a scratch wound [29]. To achieve this polarization, nuclei move rearward, away from the wound edge [30]. The forces to move nuclei arise by tethering nuclei to rearward-moving actin cables. During migration, the N-terminal calponin homology (CH) domains of Nesprin-2G bind actin while its KASH domain connects to SUN2 in the nuclear envelope to form a LINC complex [31]. The LINC complex is under tension in this process, indicated by a fluorescence resonance energy transfer (FRET)-based tension biosensor [32]. A mini-Nesprin-2G (EGFP-mini-N2G) construct containing CH domains and the KASH domain is sufficient for the nuclear movement in polarizing NIH3T3 fibroblasts [31]. Interestingly, the luminal domains of KASH proteins differ in length; Nesprin-2G and ANC-1 contain a long KASH domain that harbors the −23 conserved cysteine while the UNC-83 KASH domain only contains 18 residues and is missing the conserved cysteine.

To test the function of conserved residues of SUN-KASH interfaces in live cells, our collaborators, Natalie Cain and Gant Luxton, led teams that tested predictions from the crystal structure and *in vitro* assays in the context of nuclear positioning in developing *C. elegans* hypodermal cells and polarizing NIH 3T3 fibroblasts, respectively [1]. We first showed that extending the C terminus of the UNC-83 KASH domain by a single alanine completely disrupts nuclear migration during *C. elegans* embryonic hypodermal development. Moreover, the SUN-KASH interaction is likely abolished since UNC-83(KASH+A) was undetectable on the nuclear envelope by immunostaining. These results fit the crystal structure and the *in vitro* pull-down data [8]. However, not all of our findings matched the crystal structural predictions. Mutating the −7 tyrosine of the UNC-83 KASH domain did not completely block the SUN-KASH interaction (Figure 1c). UNC-83(Y967A) still localized to the nuclear envelope prior to nuclear migration, suggesting that it was able to at least weakly interact with UNC-84. However, nuclear migration failed, indicating that the UNC-83(Y967A) mutant could not interact with UNC-84 SUN domains strongly enough to transfer the mechanical forces needed to move nuclei across the nuclear envelope (Figure 1d). Since the UNC-83 KASH domain is normally only 18 amino acids in length and the 18-mer KASH peptide used in the pulldown assay to introduce the Y-7A mutation also lacks the conserved −23 cysteine, it remained unclear how the mutation at the −7 aromatic residue could be tolerated in long KASH domains with intermolecular disulfide bonds between SUN and KASH. We developed nuclear positioning assays in adult *C. elegans* hypodermal syncytia as a model to test the function of longer KASH domains [25]. Interestingly, mutating the phenylalanine residue at −7 of the ANC-1 KASH domain did not cause nuclear anchorage defects [1]. This indicates that nuclear anchorage in *C. elegans* hyp7 syncytia might not require as high of forces to be transmitted through LINC complexes as nuclear migration does. In contrast, mutating the Nesprin-2G KASH tyrosine at −7 to an alanine disrupted rearward nuclear movement in polarizing NIH 3T3 fibroblasts, indicating that Y-7 is important for force transmission across the SUN2/Nesprin-2 LINC complex (Figure 1d). Thus, the −7 conserved aromatic residue is important for LINC complexes under mechanical tension, but not required for initial interactions between SUN and KASH domains.

Conserved cysteines regulate LINC complex function during nuclear positioning

The longer KASH domains of *C. elegans* ANC-1 and mammalian Nesprin-2 harbor a conserved cysteine at position −23, which forms an intermolecular disulfide bond with SUN trimers in the crystal structures. However, the shorter KASH domain of *C. elegans* UNC-83 does not contain the interface with P2 or the −23 cysteine. We, therefore, tested the role of the −23 cysteine in nuclear anchorage in *C. elegans* and nuclear rearward movement in polarizing NIH 3T3 fibroblasts. In support of our model, mutating the −23 cysteine in ANC-1, Nesprin-2, or their partner cysteines in UNC-84 or SUN2, disrupted nuclear positioning [1]. Since the cysteine is not required for the SUN/KASH interaction in the in vitro pulldown assay [8], we proposed that the nuclear positioning defects might be caused by insufficient force transmission across the LINC complex (Figure 1e-f). To further test our hypothesis that a disulfide bridge is needed for maximal force transduction across LINC complexes, our collaborators Zeinab Jahed and

Mohammad Mofrad used Molecular Dynamic simulations to apply a constant velocity of 0.05m/s pulling on the N termini of KASH peptides associated with the wild type or C953A SUN2 trimer. When an intermolecular disulfide bond was present, the pulling forces were transmitted effectively through the LINC complex to the coiled-coil regions (Figure 1b). However, in the cysteine mutant, the SUN/KASH interactions were not strong enough to withstand the forces and the KASH peptide and KASH lid of the SUN protein underwent significant stretching (Figure 1f) [1]. Taken together, our cellular and modeling data support the hypothesis that an intermolecular disulfide bridge is needed to stabilize SUN-KASH interactions to transmit maximal forces through LINC complexes.

Many other KASH domains, including mammalian KASH5 and *C. elegans* UNC-83 and ZYG-12, contain short KASH domains without the conserved cysteine. All three of these proteins function during brief windows in development to move nuclei and/or chromosomes inside meiotic prophase nuclei. In our assay, UNC-83-mediated nuclear migration was not affected in *unc-84 (C953A)* mutants. Thus, short KASH domains can interact with SUN domains in the absence of disulfide bonds and can transmit enough force to move nuclei or chromosomes. Interestingly, the *anc-1(CC-23, −24-AA)* mutation caused nuclear anchorage defects while the *anc-1(F-7A)* mutant was nearly wild type [1]. Further molecular dynamic simulations or *in vivo* assays are required to investigate force transmission across LINC complexes formed by longer or shorter KASH domains, with or without the disulfide bond, and with or without the −7 aromatic amino acid. In addition, it could be valuable to use FRET tension biosensors to determine the amplitude and direction of force across the LINC complex during different processes [32].

Other factors that influence force transmission through LINC complex

Besides the strong interaction between SUN and KASH domains, four other properties of LINC complexes may be important for force transmission across the nuclear envelope. First, helical domains of SUN proteins are predicted to regulate when SUN domains interact with KASH proteins to turn LINC complexes on and off. Second, the predicted extended coiled-coils in SUN proteins transmit forces by spanning the perinuclear space. Third, SUN and KASH domains could directly interact with the inner nuclear membrane. Finally, coiled-coils and other domains in LINC complexes appear to contribute to higher order oligomerization of LINC complexes. Together, these properties of LINC complexes would maximize the transfer of mechanical forces from the cytoskeleton to the nucleoskeleton. Further studies of these mechanisms are required to fully understand how LINC complexes function.

The timing of SUN protein activation and LINC complex assembly must be regulated. Structural and biochemical studies revealed that the helical region closest to the SUN domain serves as the minimal trimerization domain [8,33]. Moreover, recent crystal structures identified a nearby short alpha-helical bundle that is able to engage with a single SUN domain through the KASH-lid, locking the protein in a monomeric, presumably inactive state [34,35]. Mutating residues at the interface between this alpha helix and the KASH-lid restored the KASH-binding capacity of the SUN domain [35]. Interestingly, the KASH-lid is released from the autoinhibited state in the presence of the trimerization coiled-coil in Molecular Dynamic simulations [36]. Both the crystal model and simulations indicate that a calcium ion can occupy a cation loop formed in the extended coiled-coil domain of the SUN protein, which might play a role in activating the LINC complex. When a conserved residue (E452) in the mouse SUN2 trimerization coil is not occupied by Ca^{2+}, it interacts with the SUN domain and potentially inactivates LINC complex formation. Both the E452 mutation in SUN2 and Ca^{2+} concentration changes monomer to trimer ratios in gel filtration assays [36]. Notably, the E452D mutation in human SUN2 was identified in muscular dystrophy patients [34–36]. Further *in vivo* studies are needed to demonstrate the significance and mechanisms for the SUN protein activation, which is essential to form LINC complex and transfer force across the nuclear envelope.

A second mechanism influencing force transmission involves predicted coiled-coils in SUN proteins. These coiled-coils are thought to span the perinuclear space and connect SUN domains near the outer nuclear membrane to the inner nuclear membrane.

Coiled-coil domains are elastic structures often found in cytoskeletal proteins such as kinesin, myosin and vimentin intermediate filaments [37,38]. How SUN proteins span the perinuclear space is not clear at a structural level. Mammalian germ cell-specific SUN proteins, SUN3-SUN5, contain shorter coiled-coil domains, which is predicted to bring the two nuclear envelope membranes closer together [39]. However, shortening the coiled-coil domains of UNC-84 did not shrink the perinuclear space and had little effect on UNC-83-mediated nuclear migration in *C. elegans* [40]. It will be interesting to further test the role of the coiled-coils in force transmission across LINC complexes in other processes and to determine more complete structures of LINC complexes.

The third potential aspect of force transmission across the nuclear envelope is how LINC components could directly interact with the lipid bilayer or chromatin to further stabilize the complex. How LINC complexes interact with lipid membranes is poorly understood. For example, *in vitro* reconstituted LINC complexes on artificial nuclear membranes indicate that SUN2 contains a single transmembrane domain while SUN1 has three [41]. In addition, hydrophobic patches in the nucleoplasmic region of SUN proteins may associate with the inner nuclear membrane and the lamin network to distribute forces inside the nucleus [41]. Additional studies are required to determine how SUN and KASH domains might be directly interacting with the outer nuclear membrane. Crystal structures showed that a conserved hydrophobic patch exists on the surface of the SUN domain at a position facing the outer nuclear membrane, suggesting that SUN domains are extending into the outer nuclear membrane lipid bilayer when binding KASH [8,20,34]. Finally, the interaction between KASH proteins and the cytoplasmic leaflet of the outer nuclear membrane is potentially stabilized to maximize force transmission. Recently, an outer nuclear membrane protein Kuduk was shown to interact with LINC complexes in the outer nuclear membrane in *Drosophila*. Kuduk (TMEM258 in mammals) has a cytoplasmic amphipathic helix as well as a trans-membrane helix that both interact with the outer nuclear membrane and stabilize LINC [42]. Future experiments should uncover how Kuduk/TMEM258 might function to stabilize the LINC complexes *in vivo*.

A fourth mechanism that may allow LINC complexes to maximize the force transfer across the nuclear envelope might involve assembly into higher-order structures. There are many examples of LINC complexes organizing in larger groups. In *C. elegans*, immunostaining of UNC-84 and UNC-83 shows punctate distribution of LINC complexes on the nuclear envelope during nuclear migration [21,22]. SUN1 punctate are also observed in Hela cells [43–45]. Another case for higher-order organization of LINC complex involves how nuclei move rearward in wounded NIH3T3 fibroblasts. During nuclear migration, linear arrays of SUN2-Nesprin-2G LINC complexes, termed transmembrane actin-associated nuclear (TAN) lines, assemble to tether the nuclei to moving actin cables [9,31]. As a more extreme example, LINC complex proteins involved in meiotic chromosome dynamics and telomere bouquet formation redistribute and concentrate in large patches associated with chromosome ends [6,46–48].

Recent studies suggest possible mechanisms for LINC complexes to assemble into larger structures., Mammalian SUN1 proteins form oligomers larger than trimers detected in living cells by fluorescence fluctuation spectroscopy [49]. SUN1 has also been observed to form clusters in a reconstituted, cell-free expression system on artificial lipid bilayers [41]. Computer modeling predicts that SUN1 trimers can associate with each other laterally through their SUN domains to form higher-order clusters [41,43]. It has also been proposed that a cysteine adjacent to the SUN domain of SUN1 protein is able to form intermolecular disulfide bonds with neighboring SUN trimers [44,50]. The specific requirement of mammalian SUN1, but not SUN2, during meiotic chromosome pairing, might be associated with the ability of SUN1 to more easily form higher-order structures than SUN2 [9,43,44,49]. Interestingly, a recent study has shown different mechanisms involved in homeostatic nuclear positioning under centrifugal force. Rearward nuclear recentration requires TAN lines formed by SUN2 and Nesprin-2G while the same KASH protein Nesprin-2G interacts with SUN1 and the microtubule motor dynein to facilitate forward recentration [51]. It is not clear if distinct higher-order structures are specialized for force transmission or if oligomerization states of SUN protein are involved in selection between

SUN1 and SUN2 by Nesprin-2G in different nuclear positioning processes. Further studies are required to determine the physiological significance and molecular mechanism of higher-order LINC organization and force transmission.

Acknowledgments

We thank all the co-authors of Cain et al. [1] for insightful discussions throughout the project and current members of the Starr lab for comments on the manuscript.

Disclosure statement

No potential conflict of interest was reported by the authors.

Funding

This work was supported by the National Institute of General Medical Sciences [R01 GM073874].

References

[1] Cain NE, Jahed Z, Schoenhofen A, *et al*. Conserved SUN-KASH interfaces mediate LINC complex-dependent nuclear movement and positioning. Curr Biol. 2018;28:3086–3097 e3084.
[2] D'Angelo MA, Hetzer MW. The role of the nuclear envelope in cellular organization. Cell Mol Life Sci. 2006;63:316–332.
[3] Wente SR, Rout MP. The nuclear pore complex and nuclear transport. Cold Spring Harb Perspect Biol. 2010;2:a000562.
[4] Ungricht R, Kutay U. Mechanisms and functions of nuclear envelope remodelling. Nat Rev Mol Cell Biol. 2017;18:229–245.
[5] Lee YL, Burke B. LINC complexes and nuclear positioning. Semin Cell Dev Biol. 2018;82:67–76.
[6] Burke B. LINC complexes as regulators of meiosis. Curr Opin Cell Biol. 2018;52:22–29.
[7] Starr DA, Fridolfsson HN. Interactions between nuclei and the cytoskeleton are mediated by SUN-KASH nuclear-envelope bridges. Annu Rev Cell Dev Bi. 2010;26:421–444.
[8] Sosa BA, Rothballer A, Kutay U, et al. LINC complexes form by binding of three KASH peptides to domain interfaces of trimeric SUN proteins. Cell. 2012;149:1035–1047.
[9] Hieda M. Implications for diverse functions of the LINC complexes based on the structure. Cells. 2017;6.
[10] Crisp M, Liu Q, Roux K, et al. Coupling of the nucleus and cytoplasm: role of the LINC complex. J Cell Biol. 2006;172:41–53.
[11] McGee MD, Rillo R, Anderson AS, et al. UNC-83 is a KASH protein required for nuclear migration and is recruited to the outer nuclear membrane by a physical interaction with the SUN protein UNC-84. Mol Biol Cell. 2006;17:1790–1801.
[12] Padmakumar VC, Libotte T, Lu W, et al. The inner nuclear membrane protein Sun1 mediates the anchorage of Nesprin-2 to the nuclear envelope. J Cell Sci. 2005;118:3419–3430.
[13] Haque F, Lloyd DJ, Smallwood DT, et al. SUN1 interacts with nuclear lamin A and cytoplasmic nesprins to provide a physical connection between the nuclear lamina and the cytoskeleton. Mol Cell Biol. 2006;26:3738–3751.
[14] Bone CR, Tapley EC, Gorjanacz M, et al. The Caenorhabditis elegans SUN protein UNC-84 interacts with lamin to transfer forces from the cytoplasm to the nucleoskeleton during nuclear migration. Mol Biol Cell. 2014;25:2853–2865.
[15] Luxton GW, Starr DA. KASHing up with the nucleus: novel functional roles of KASH proteins at the cytoplasmic surface of the nucleus. Curr Opin Cell Biol. 2014;28:69–75.
[16] Baum DA, Baum B. An inside-out origin for the eukaryotic cell. BMC Biol. 2014;12:76.
[17] Mejat A, Misteli T. LINC complexes in health and disease. Nucleus. 2010;1:40–52.
[18] Meinke P, Nguyen TD, Wehnert MS. The LINC complex and human disease. Biochem Soc Trans. 2011;39:1693–1697.
[19] Janin A, Bauer D, Ratti F, et al. Nuclear envelopathies: a complex LINC between nuclear envelope and pathology. Orphanet J Rare Dis. 2017;12:147.
[20] Zhou Z, Du X, Cai Z, *et al*. Structure of Sad1-UNC84 homology (SUN) domain defines features of molecular bridge in nuclear envelope. J Biol Chem. 2012;287:5317–5326.
[21] Malone CJ, Fixsen WD, Horvitz HR, et al. UNC-84 localizes to the nuclear envelope and is required for nuclear migration and anchoring during C. elegans development. . Development. 1999;126:3171–3181.
[22] Starr DA, Hermann GJ, Malone CJ, et al. unc-83 encodes a novel component of the nuclear envelope and is essential for proper nuclear migration. Development. 2001;128:5039–5050.
[23] Meyerzon M, Fridolfsson HN, Ly N, et al. UNC-83 is a nuclear-specific cargo adaptor for kinesin-1-mediated nuclear migration. Development. 2009;136:2725–2733.
[24] Fridolfsson HN, Ly N, Meyerzon M, et al. UNC-83 coordinates kinesin-1 and dynein activities at the nuclear envelope during nuclear migration. Dev Biol. 2010;338:237–250.
[25] Fridolfsson HN, Herrera LA, Brandt JN, et al. Genetic analysis of nuclear migration and anchorage to study LINC complexes during development of caenorhabditis elegans. Methods Mol Biol. 2018;1840:163–180.

[26] Hedgecock EM, Thomson JN. A gene required for nuclear and mitochondrial attachment in the nematode Caenorhabditis elegans. Cell. 1982;30:321–330.
[27] Starr DA, Han M. Role of ANC-1 in tethering nuclei to the actin cytoskeleton. Science. 2002;298:406–409.
[28] D'Alessandro M, Hnia K, Gache V, *et al*. Amphiphysin 2 orchestrates nucleus positioning and shape by linking the nuclear envelope to the actin and microtubule cytoskeleton. Dev Cell. 2015;35:186–198.
[29] Palazzo AF, Joseph HL, Chen YJ, et al. Cdc42, dynein, and dynactin regulate MTOC reorientation independent of Rho-regulated microtubule stabilization. Curr Biol. 2001;11:1536–1541.
[30] Gomes ER, Jani S, Gundersen GG. Nuclear movement regulated by Cdc42, MRCK, myosin, and actin flow establishes MTOC polarization in migrating cells. Cell. 2005;121:451–463.
[31] Luxton GW, Gomes ER, Folker ES, et al. Linear arrays of nuclear envelope proteins harness retrograde actin flow for nuclear movement. Science. 2010;329:956–959.
[32] Arsenovic PT, Ramachandran I, Bathula K, et al. Nesprin-2G, a component of the nuclear LINC complex, is subject to myosin-dependent tension. Biophys J. 2016;110:34–43.
[33] Wang WJ, Shi ZB, Jiao S, et al. Structural insights into SUN-KASH complexes across the nuclear envelope. Cell Res. 2012;22:1440–1452.
[34] Nie S, Ke H, Gao F, et al. Coiled-coil domains of SUN proteins as intrinsic dynamic regulators. Structure. 2016;24:80–91.
[35] Xu Y, Li W, Ke H, et al. Structural conservation of the autoinhibitory domain in SUN proteins. Biochem Biophys Res Commun. 2018;496:1337–1343.
[36] Jahed Z, Vu UT, Fadavi D, et al. A molecular model for LINC complex regulation: activation of SUN2 for KASH binding. Mol Biol Cell. 2018b;29:2012–2023.
[37] Schwaiger I, Sattler C, Hostetter DR, et al. The myosin coiled-coil is a truly elastic protein structure. Nat Mater. 2002;1:232–235.
[38] Rose A, Meier I. Scaffolds, levers, rods and springs: diverse cellular functions of long coiled-coil proteins. Cell Mol Life Sci. 2004;61:1996–2009.
[39] Sosa BA, Kutay U, Schwartz TU. Structural insights into LINC complexes. Curr Opin Struct Biol. 2013;23:285–291.
[40] Cain NE, Tapley EC, McDonald KL, et al. The SUN protein UNC-84 is required only in force-bearing cells to maintain nuclear envelope architecture. J Cell Biol. 2014;206:163–172.
[41] Majumder S, Willey PT, DeNies MS, et al. A synthetic biology platform for the reconstitution and mechanistic dissection of LINC complex assembly. J Cell Sci. 2018;132:1–16.
[42] Ding ZY, Wang YH, Huang YC, et al. Outer nuclear membrane protein Kuduk modulates the LINC complex and nuclear envelope architecture. J Cell Biol. 2017;216:2827–2841.
[43] Jahed Z, Fadavi D, Vu UT, et al. Molecular insights into the mechanisms of SUN1 oligomerization in the nuclear envelope. Biophys J. 2018a;114:1190–1203.
[44] Lu W, Gotzmann J, Sironi L, *et al*. Sun1 forms immobile macromolecular assemblies at the nuclear envelope. Biochim Biophys Acta. 2008;1783:2415–2426.
[45] Liu Q, Pante N, Misteli T, et al. Functional association of Sun1 with nuclear pore complexes. J Cell Biol. 2007;178:785–798.
[46] Penkner A, Tang L, Novatchkova M, et al. The nuclear envelope protein Matefin/SUN-1 is required for homologous pairing in C. elegans meiosis. Dev Cell. 2007;12:873–885.
[47] Ding X, Xu R, Yu J, et al. SUN1 is required for telomere attachment to nuclear envelope and gametogenesis in mice. Dev Cell. 2007;12:863–872.
[48] Chikashige Y, Tsutsumi C, Yamane M, et al. Meiotic proteins bqt1 and bqt2 tether telomeres to form the bouquet arrangement of chromosomes. Cell. 2006;125:59–69.
[49] Hennen J, Saunders CA, Mueller JD, et al. Fluorescence fluctuation spectroscopy reveals differential SUN protein oligomerization in living cells. Mol Biol Cell. 2018;29:1003–1011.
[50] Link J, Leubner M, Schmitt J, et al. Analysis of meiosis in SUN1 deficient mice reveals a distinct role of SUN2 in mammalian meiotic LINC complex formation and function. PLoS Genet. 2014;10:e1004099.
[51] Zhu R, Antoku S, Gundersen GG. Centrifugal displacement of nuclei reveals multiple LINC complex mechanisms for homeostatic nuclear positioning. Curr Biol. 2017;27:3097–3110 e3095.

Chapter II

Conserved SUN-KASH interfaces mediate LINC complex-dependent nuclear movement and positioning

Natalie E. Cain, Zeinab Jahed, Amy Schoenhofen, Venecia A. Valdez, Baila Elkin, **Hongyan Hao**, Nathan J. Harris, Leslie A. Herrera, Brian M. Woolums, Mohammad R.K. Mofrad, G.W. Gant Luxton, and Daniel A. Starr

Current Biology, October 2018

Hongyan Hao participated in generating the *anc-1(CC-23-24AA)* and *anc-1(F-7A)* CRISPR strain and conducted the nuclear anchorage assay in Figure 4. Natalie E. Cain and the rest of the Starr lab, Mofrad lab and Luxton lab members designed, and performed the rest of the experiments and wrote the manuscript.

Article

Current Biology

Conserved SUN-KASH Interfaces Mediate LINC Complex-Dependent Nuclear Movement and Positioning

Graphical Abstract

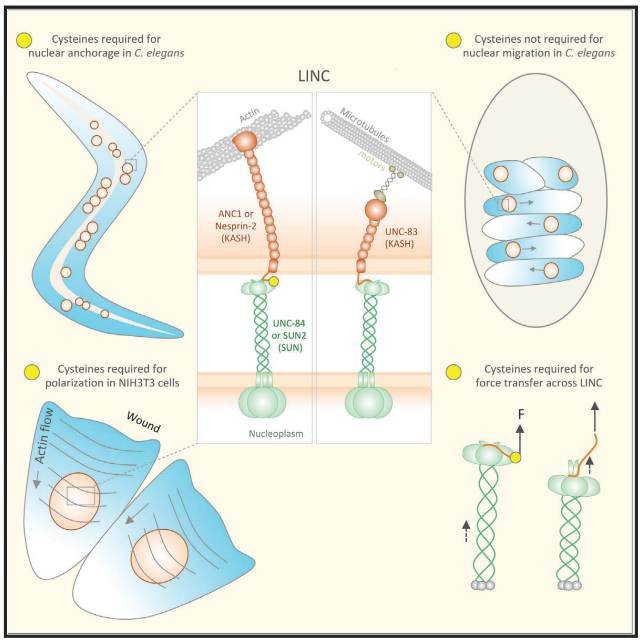

Authors

Natalie E. Cain, Zeinab Jahed, Amy Schoenhofen, ..., Mohammad R.K. Mofrad, G.W. Gant Luxton, Daniel A. Starr

Correspondence

dastarr@ucdavis.edu

In Brief

Cain et al. test the function of mutant SUN and KASH proteins in *C. elegans* nuclear positioning, NIH 3T3 fibroblast polarization, and simulations of LINC complexes under mechanical strain to gain mechanistic insights into how SUN-KASH interactions might be regulated to transfer forces from the cytoskeleton to the nucleus.

Highlights

- Mutating conserved residues at SUN-KASH interfaces disrupts LINC function
- Cysteines in LINC are required to anchor, but not to move, *C. elegans* nuclei
- Cysteines in LINC are needed for nuclear movement in wound-edge fibroblasts
- Simulations show disulfide bridges maximize forces transferred across LINC

Cain et al., 2018, Current Biology *28*, 3086–3097
October 8, 2018
https://doi.org/10.1016/j.cub.2018.08.001

CellPress

CellPress

Current Biology
Article

Conserved SUN-KASH Interfaces Mediate LINC Complex-Dependent Nuclear Movement and Positioning

Natalie E. Cain,[1] Zeinab Jahed,[2] Amy Schoenhofen,[3] Venecia A. Valdez,[1] Baila Elkin,[3] Hongyan Hao,[1] Nathan J. Harris,[3] Leslie A. Herrera,[1] Brian M. Woolums,[3] Mohammad R.K. Mofrad,[2] G.W. Gant Luxton,[3] and Daniel A. Starr,[1,4,*]

[1]Department of Molecular and Cellular Biology, University of California, Davis, 1 Shields Avenue, Davis, CA 95616, USA
[2]Molecular Cell Biomechanics Laboratory, Departments of Bioengineering and Mechanical Engineering, University of California, Berkeley, 208A Stanley Hall, Berkeley, CA 94720, USA
[3]Department of Genetics, Cell Biology, and Development, University of Minnesota, 420 Washington Avenue SE, Minneapolis, MN 55455, USA
[4]Lead Contact
*Correspondence: dastarr@ucdavis.edu
https://doi.org/10.1016/j.cub.2018.08.001

SUMMARY

Many nuclear positioning events involve linker of nucleoskeleton and cytoskeleton (LINC) complexes, which transmit forces generated by the cytoskeleton across the nuclear envelope. LINC complexes are formed by trans-luminal interactions between inner nuclear membrane SUN proteins and outer nuclear membrane KASH proteins, but how these interactions are regulated is poorly understood. We combine *in vivo C. elegans* genetics, *in vitro* wounded fibroblast polarization, and *in silico* molecular dynamics simulations to elucidate mechanisms of LINC complexes. The extension of the KASH domain by a single alanine residue or the mutation of the conserved tyrosine at −7 completely blocked the nuclear migration function of *C. elegans* UNC-83. Analogous mutations at −7 of mouse nesprin-2 disrupted rearward nuclear movements in NIH 3T3 cells, but did not disrupt ANC-1 in nuclear anchorage. Furthermore, conserved cysteines predicted to form a disulfide bond between SUN and KASH proteins are important for the function of certain LINC complexes, and might promote a developmental switch between nuclear migration and nuclear anchorage. Mutations of conserved cysteines in SUN or KASH disrupted ANC-1-dependent nuclear anchorage in *C. elegans* and Nesprin-2G-dependent nuclear movements in polarizing fibroblasts. However, the SUN cysteine mutation did not disrupt nuclear migration. Moreover, molecular dynamics simulations showed that a disulfide bond is necessary for the maximal transmission of cytoskeleton-generated forces by LINC complexes *in silico*. Thus, we have demonstrated functions for SUN-KASH binding interfaces, including a predicted intermolecular disulfide bond, as mechanistic determinants of nuclear positioning that may represent targets for regulation.

INTRODUCTION

The precise intracellular positioning of the nucleus is essential for many cellular and developmental processes including fertilization, cell migration, cell polarization, gametogenesis, neuronal development, and muscle development. Defects in nuclear positioning result in developmental disorders in tissues, including the central nervous system, reproductive organs, and skeletal muscle [1–4]. Most nuclei are positioned by the cytoskeleton, which is physically coupled to the nuclear envelope via a conserved nuclear envelope-spanning molecular bridge known as the linker of nucleoskeleton and cytoskeleton (LINC) complex [5].

The LINC complex is formed by a trans-luminal direct interaction between Sad1/UNC-84 (SUN) proteins in the inner nuclear membrane and Klarsicht/ANC-1/Syne homology (KASH) proteins spanning the outer nuclear membrane (Figure 1) [7–10]. SUN proteins contain a conserved KASH protein-binding luminal C-terminal SUN domain [11] and divergent N termini that interact with lamins and chromatin within the nucleoplasm [9, 12, 13]. KASH proteins contain a conserved C-terminal KASH domain, comprising a trans-membrane domain followed by the ~10- to 32-residue luminal KASH peptide [14]. The divergent N termini of KASH proteins extend into the cytoplasm and engage the cytoskeleton [5, 15, 16]. Thus, LINC complexes enable force transmission across the nuclear envelope [5, 15].

Crystal structures of mammalian SUN2 in complex with KASH peptides from Nesprin-1 or -2 provide insights into the molecular mechanisms of LINC complex-dependent mechanotransmission and nuclear positioning [6, 17]. The structures predict that SUN2 functions as a homo-trimer where each protomer consists of a non-conventional coiled-coil region followed by a β sandwich core with an ~20-residue β hairpin extension, known as the KASH lid. Three independent KASH peptides interact with a single SUN2 homo-trimer [6, 17]. Our recent studies show that the luminal domain of SUN2 does homo-trimerize in living cells [18, 19].

Each KASH peptide forms three binding interfaces with a SUN trimer (Figure 1C) [6, 20]. First, the last four residues of KASH proteins (0 to −3; gray in Figure 1C), consisting of the PPPX motif, fit into a binding pocket formed primarily by a single SUN protomer (P1; green in Figure 1C). Second, positions −4 to −14 of KASH

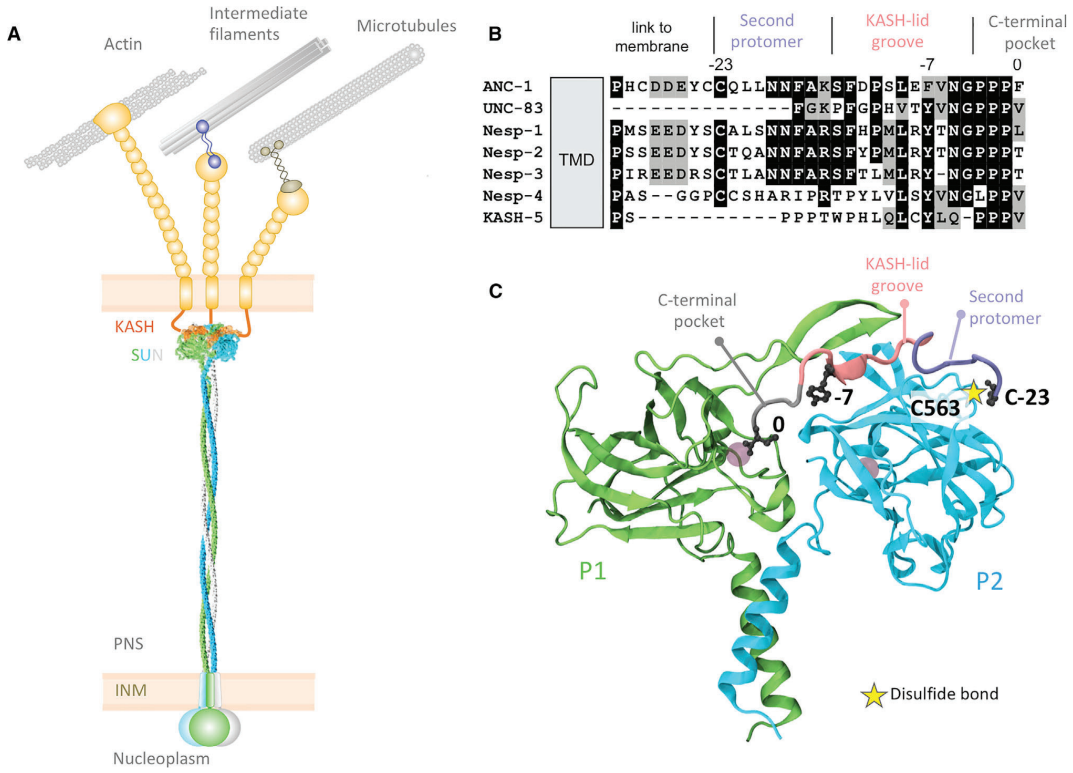

Figure 1. SUN and KASH Proteins Form a Bridge across the Nuclear Envelope

(A) SUN trimers (gray, blue, and green) cross the inner nuclear membrane (INM) and span most of the perinuclear space (PNS). SUN proteins interact with the luminal domains of KASH proteins (orange and tan), extending from the outer nuclear membrane (ONM). Cytoplasmic domains of KASH proteins interact with a variety of cytoskeletal components.

(B) Sequence alignment of *C. elegans* and human KASH domains.

(C) A close-up of the interaction between a KASH peptide (Nesprin-2; gray, pink, and purple) and two SUN2 protomers (green and blue). The gray circles in the SUN protomers represent cations. Based on PDB: 4DXS [6].

proteins (pink in Figure 1C) fit into a groove between two SUN protomers (P1 and P2), with the conserved hydrophobic residues at −7 and −9 facing into the cleft between P1 and P2. Third, residues −15 to −23 (purple in Figure 1C) bind along the surface of P2. At position −23 of the KASH peptide, a conserved cysteine is oriented to form a disulfide bond (yellow star in Figure 1C) with a conserved cysteine in SUN2 (C563 in human SUN2, C577 in mouse SUN2, and C953 in *C. elegans* UNC-84) [20]. Furthermore, an intermolecular disulfide bond was detected between transiently expressed SUN and KASH domains in HeLa cells [6, 20]. Although this covalent bridge was determined by *in vitro* pull-downs to be dispensable for the SUN2-KASH interaction, it was hypothesized to be important for LINC complexes to resist the considerable cytoskeleton-generated forces necessary for nuclear positioning [6, 20]. However, the physiological relevance of each of the three conserved SUN-KASH interaction domains and the conserved disulfide bond during intracellular nuclear movement and positioning remains to be tested experimentally. Here, we examine the effect of disrupting SUN-KASH interactions in two established experimental assays for intracellular nuclear positioning: nuclear migration and anchorage in developing *C. elegans* hypodermal cells [21, 22], and rearward nuclear positioning during centrosome orientation in migrating fibroblasts [23–25]. Furthermore, we used molecular dynamics simulations of SUN2-KASH complexes under tension to model how disrupting SUN-KASH interactions might influence the ability of LINC complexes to withstand the mechanical forces required for nuclear positioning.

Nuclear positioning in *C. elegans* consists of two related processes—nuclear migration to a specific location and then anchoring in place. Nuclear migration in hyp7 precursors requires the SUN protein UNC-84 and the KASH protein UNC-83, which recruit microtubule motors to the surface of nuclei [11, 26, 27]. After the hyp7 syncytium is formed, UNC-84 and the KASH protein ANC-1 anchor nuclei to the actin cytoskeleton [11, 14]. In mammals, KASH proteins Nesprin-4 and KASH5 play

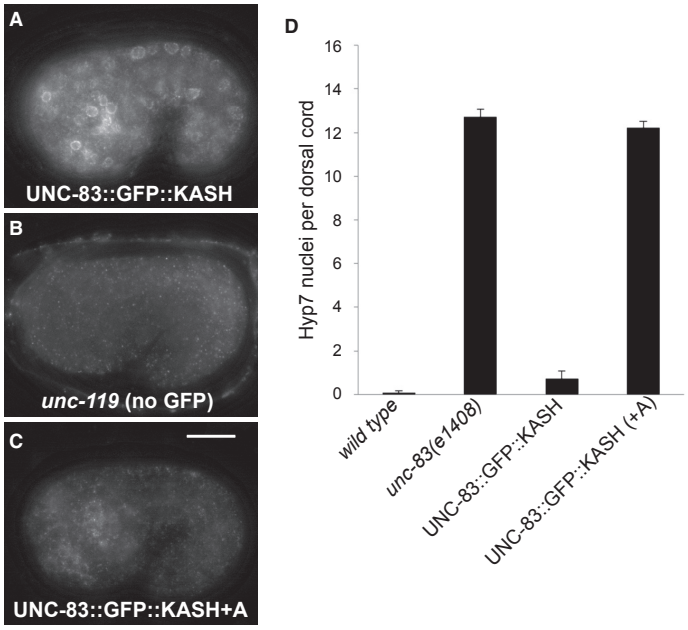

Figure 2. Extension of the KASH Domain of UNC-83 Blocks Nuclear Migration

(A–C) GFP expression in comma-stage embryos with the version of UNC-83 indicated. Anterior is left; dorsal is up. Scale bar, 10 μm.

(A) UNC-83::GFP::KASH.

(B) *unc-119*, which serves as the wild-type UNC-83 (no GFP) control.

(C) UNC-83::GFP::KASH+A.

(D) Quantification of nuclear migration defects by counting the average number of hyp7 nuclei in the dorsal cords of larval stage (L)1 animals. Error bars are 95% CI.

analogous roles recruiting microtubule motors to the surface of nuclei [28, 29]. In other mammalian cell types, giant isoforms of Nesprin-1 and -2 tether mammalian nuclei to actin networks [30–32]. However, it remains unknown how UNC-84-UNC-83 complexes that move nuclei eventually yield to UNC-84-ANC-1 complexes to mediate nuclear anchorage. Interestingly, the KASH domain in UNC-83 is much shorter than in ANC-1; the UNC-83 perinuclear luminal domain is only 17 residues and lacks the cysteine at −23 (Figure 1B) [7]. We hypothesized that an intermolecular disulfide bond formed between conserved cysteines at −23 of KASH peptides and at 563 of human SUN2 (residue 577 of mouse SUN2) or 953 of *C. elegans* UNC-84 plays a central role in LINC complex function. In order to elucidate potential molecular mechanisms for LINC complex regulation, we addressed the following. How important is the interaction between conserved residues in SUN and the PPPX motif of KASH? What happens when the interaction between the aromatic residue at the −7 position of KASH and the cleft between P1 and P2 is disrupted? And, what is the physiological relevance of the disulfide bond between SUN and KASH domains?

RESULTS

Extension of the C Terminus of the UNC-83 KASH Domain Disrupts Nuclear Migration *In Vivo*

The crystal structures of mammalian SUN-KASH complexes show the C terminus of KASH pointed into the SUN protomer P1, where it is coordinated by conserved hydroxyl groups [6, 17] (Figure 1C). Furthermore, the addition of a single alanine to the end of KASH peptides was shown to abolish *in vitro* pull-down interactions between SUN2 and KASH [6], whereas the extension of KASH peptides by 13 residues blocks their function in binding assays and acts as a dominant-negative construct in tissue-culture cells [33]. Therefore, we predicted that the extension of the KASH domain of UNC-83 by one residue would disrupt the interaction between UNC-84 and UNC-83 and disrupt nuclear migration *in vivo*. We used UNC-83::GFP::KASH, which has normal function for nuclear migration [34], as a starting point (Figures 2A and 2D) and added a single alanine onto the C terminus of UNC-83 to express UNC-83::GFP::KASH+A at endogenous levels. UNC-83::GFP::KASH+A failed to localize to the nuclear envelope, similar to when the entire KASH domain of UNC-83 was deleted [7]. As a control, we measured the relative fluorescence in the GFP channel in a standardized region of interest. UNC-83::GFP::KASH+A had 48.7 ± 7.6 (mean ± SD) arbitrary units of fluorescence per embryo compared to 27.1 ± 6.5 arbitrary units in wild-type embryos (t test; $p < 0.0001$), suggesting that the UNC-83::GFP::KASH+A construct was expressed but failed to localize to the nuclear envelope. The resulting animal had a severe nuclear migration defect (Figures 2C and 2D). Thus, the KASH+A mutation blocks SUN-KASH function *in vivo*.

Mutation of the Tyrosine at –7 of KASH Disrupts SUN-KASH Function *In Vivo*

Residues −5 to −14 of KASH proteins (pink in Figure 1) fit into a cleft between two SUN protomers. The conserved hydrophobic aromatic residue at −7 faces directly into the cleft in the crystal structure and a KASH(Y-7A) mutation blocked SUN2-KASH interactions *in vitro* [6]. Overexpressed mutant UNC-83(Y-7A) in a transgenic animal localized to the nuclear envelope, but did not rescue *unc-83(null)* nuclear migration defects [7]. To rule out the effects of overexpression and test the role of Y-7 more directly, we used CRISPR/Cas9 genome editing to introduce the Y-7A mutation into the *unc-83* locus. The resulting *unc-83(Y-7A)* mutant animal completely blocked nuclear migration in hyp7 cells (Figures 3A–3E). However, UNC-83(Y-7A) localized normally to the nuclear envelope of hyp7 cells (Figures 3C and 3D), suggesting that unlike UNC-83(KASH+A), the UNC-83(Y-7A) mutant protein can partially interact with the SUN domain of UNC-84 for localization but that the interaction fails to withstand forces across the nuclear envelope required to move nuclei in these cells.

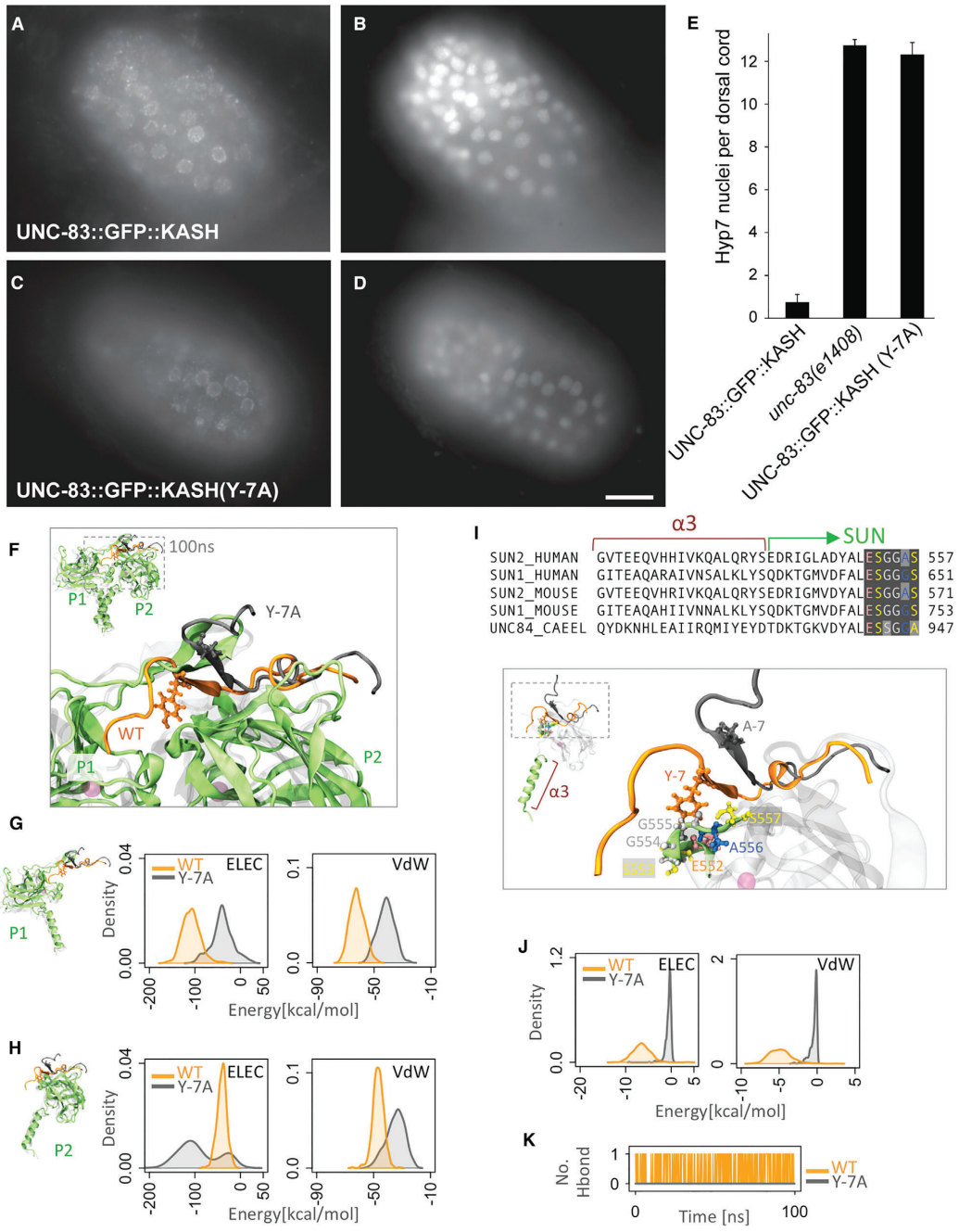

Figure 3. Mutation of Tyrosine –7 of KASH Disrupts SUN-KASH Interactions

(A–D) Anti-GFP immunolocalization (A and C) and DAPI staining (B and D) in pre-bean embryos around the time of hyp7 nuclear migration. Scale bar, 10 μm.

(E) Quantification of nuclear migration defects as in Figure 2. Error bars are 95% CI.

(legend continued on next page)

We used molecular dynamics simulations to examine the extent to which the KASH(Y-7A) mutation might compromise SUN-KASH interactions. We performed simulations of the human SUN2 trimer bound to wild-type Nesprin-2 or Nesprin-2(Y-7A) KASH peptides. Within 100 ns of simulation time, the KASH(Y-7A) peptides partially detached from the SUN2 trimer (Figure 3F). We calculated the non-bonded interaction energies between the KASH(Y-7A) peptide and P1 or P2 over the 100-ns simulation and compared it with wild-type (Figures 3G and 3H). Because the KASH domain of UNC-83 only contains residues 0 to −17, we included the analogous 18 residues of the Nesprin-2 KASH peptide in our energy calculations. The van der Waals (VdW) and electrostatic (ELEC) interactions between the 17 residues of KASH(Y-7A) and P1 were significantly reduced compared with wild-type (Figure 3G). Because the KASH(Y-7A) peptide was partially released from P1, it attempted to form new ELEC contacts with P2 during the simulation time before it partially detached from P2 as well (hence the two peaks in the density of ELEC energies of KASH(Y-7A) with P2 in Figure 3H). Note that the KASH(Y-7A) peptide did not fully detach from P1 or P2 during our simulation (Figures 3G and 3H), which supports our *in vivo* data. We further examined SUN-KASH crystal structures to identify the main interacting partners of SUN2 for the tyrosine at −7 of KASH. The side chain of tyrosine −7 reaches into the trimer and interacts with a highly conserved motif of SUN2 (E552–S557) in P2 (Figure 3I). An alanine at position −7 is not able to reach this motif. To verify this, we computed the non-bonded interaction energies between the residue at position −7 and the E552–S557 motif in P2. This interaction was completely lost with the KASH(Y-7A) mutation (Figure 3J). Additionally, a hydrogen bond between tyrosine −7 of KASH and the E552–S557 motif was lost in simulations with the Y-7A mutation (Figure 3K). Thus, these simulations support *in vivo* data that the tyrosine at −7 of KASH is necessary to transfer forces across the nuclear envelope.

The Cysteine at –23 of the ANC-1 KASH Domain Is Required for Nuclear Anchorage

Residues −15 to −23 of KASH peptides (purple in Figure 1) traverse along the surface of P2 before they disengage from SUN proteins and extend toward the outer nuclear membrane. This interaction domain has been proposed to stabilize LINC complexes and allow for maximal force to be transferred across the nuclear envelope [35]. We hypothesized that mutating the conserved cysteine at −23 of the KASH domain of ANC-1 would disrupt nuclear anchorage in *C. elegans*.

Previous assays for nuclear anchorage defects were qualitative and tended to overestimate anchorage defects [11, 36]. To quantify nuclear anchorage, we expressed nuclear GFP in adult syncytial hypodermal cells. In wild-type young adults, an average of 2.4% ± 1.3% (mean ± 95% confidence interval [CI]) GFP-positive nuclei per lateral side of an animal were clustered (Figures 4A and 4H). In contrast, an *anc-1(e1873)* null animal had an average of 57.3% ± 6.1% ($p < 0.0001$ in a t test) clustered nuclei per lateral side (Figures 4B and 4H). Also, ANC-1 nuclei appear smaller and misshapen. Surprisingly, this assay showed that *unc-84(n369)* null animals have a much less severe nuclear anchorage defect, with only 26.5% ± 5.3% clustered nuclei per lateral side ($p < 0.0001$ in a t test compared to wild-type or *anc-1(e1873)*) (Figures 4C and 4H). This suggests that ANC-1 functions to anchor nuclei through at least two pathways—one through UNC-84 and a second, KASH-independent pathway that will require future investigation.

To test the contribution of the cysteine at −23 of the ANC-1 KASH domain to nuclear anchorage, we edited the conserved cysteine at −23 of the ANC-1 KASH domain and an unconserved cysteine at −24 (Figure 1B) to alanines to make *anc-1(CC-23,-24AA)*. The double-cysteine mutant had a significant nuclear anchorage defect of 11.3% ± 6.0% clustered nuclei ($p < 0.0001$ in a t test compared to wild-type) (Figures 4D and 4H). Thus, the cysteines near −23 of ANC-1 are necessary for normal anchoring of nuclei.

The Cysteine at 953 of the SUN Domain of UNC-84 Is Required for Nuclear Anchorage but Dispensable for Nuclear Migration

Although ANC-1 has a full-length KASH domain with the conserved cysteine at −23, UNC-83 lacks the third interaction domain and connects from residue −18 directly to the transmembrane domain [7]. We therefore hypothesized that an intermolecular disulfide bridge between SUN and KASH would be dispensable for nuclear migration but needed for nuclear anchorage. Genome editing was used to make *unc-84::gfp(C953A)*. We previously reported that the CRISPR/Cas9-edited strain *unc-84::gfp* is functional (Figures 3E, 3H, 5B, and 5C) [37]. In two independent lines, UNC-84::GFP(C953A) localized in a pattern indistinguishable from otherwise wild-type UNC-84::GFP (Figures 5A and 5C), recruited UNC-83 to the nuclear envelope (Figures 5B and 5D), and displayed nearly normal levels of nuclear migration (Figure 5E). In contrast, *unc-84::gfp(C953A)* mutant animals had significant nuclear anchorage defects with 16.2% ± 4.0% and 17.2% ± 2.6% clustered nuclei per lateral side of an adult ($p < 0.0001$ compared to UNC-84::GFP for both t tests) (Figures 4F–4H). We conclude that the conserved cysteine at 953 of UNC-84 is dispensable for nuclear migration but required for normal nuclear anchorage.

(F–K) Modeling the effect of Y-7A on SUN-KASH interactions.
(F) Superimposed structures of wild-type (orange) and Y-7A (gray) after 100 ns of molecular dynamics simulation time. Only two of three SUN2 protomers are shown (P1 and P2).
(G and H) Electrostatic (ELEC) and van der Waals (VdW) energies between KASH (residues 0 to −17) and the P1 (G) or P2 (H) SUN2 protomer for wild-type (WT) (orange) and Y-7A (gray) (shown as densities over a 100-ns simulation time).
(I) Sequence and structure of α3 and the first few residues of the SUN domain showing that the major interacting partners of Y-7 on SUN P2 (E552–S557) are highly conserved.
(J) ELEC and VdW energies between residue −7 and residues E552–S557 on SUN2 P2 for wild-type (orange) and Y-7A (gray) (shown as densities over a 100-ns simulation time).
(K) Number of H bonds between residue −7 and residues E552–S557 on SUN2 P2 for wild-type (orange) and Y-7A (gray).

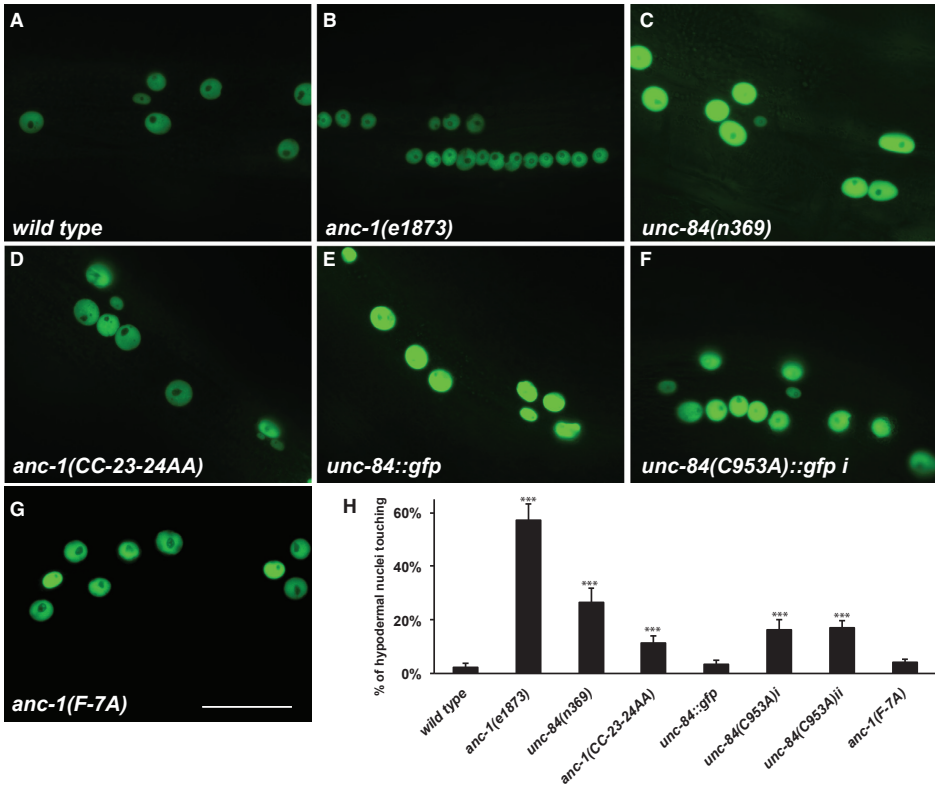

Figure 4. Mutating Conserved Cysteines in UNC-84 or ANC-1 Disrupts Nuclear Anchorage

(A–G) Lateral views of L4 or young adult animals expressing GFP in hypodermal nuclei in the following genotypes: (A) wild-type; (B) *anc-1(e1873)*; (C) *unc-84(n369)*; (D) *anc-1(CC-23-24AA)*; (E) *unc-84::gfp*; (F) *unc-84(C953A)::gfp* line I; and (G) *anc-1(F-7A)*. Scale bar, 25 μm.

(H) Quantification of nuclear anchorage defects assayed by counting the average number of hypodermal nuclei in clusters of two or more nuclei on one lateral side of an animal. Error bars are 95% CI; ***$p < 0.0001$ in a t test when compared to wild-type; all sample sizes are ≥20 animals.

Cysteines 577 of Mouse SUN2 and –23 of Nesprin-2 Are Required for Rearward Nuclear Positioning in Migrating NIH 3T3 Fibroblasts

Our results in *C. elegans* are consistent with a role for a covalent link between UNC-84 and ANC-1 in nuclear anchoring. We next tested whether a similar role could be observed during mammalian nuclear positioning. Actin-dependent rearward nuclear positioning in wounded monolayers of fibroblasts polarizing for migration is an established assay for LINC complex-dependent nuclear positioning [23, 38, 39]. Following serum starvation, monolayers of NIH 3T3 fibroblasts are wounded and stimulated with lysophosphatidic acid (LPA), which induces the movement of nuclei away from the wound edge [24]. This process is mediated by the retrograde flow of perinuclear actin cables, which are coupled to the nuclear envelope via linear arrays of LINC complexes [23, 40]. As previously shown, knockdown of either SUN2 or Nesprin-2 blocked rearward nuclear movements and centrosome orientation (Figure 6) [23]. The SUN2 and Nesprin-2 small interfering RNA (siRNA) defects were efficiently rescued by transient expression of EGFP-SUN2^{WT} or EGFP-mini-Nesprin-2G^{WT}, respectively (Figure 6) [23].

The siRNA rescue assays were used to test the importance of the predicted disulfide bond between SUN2 and Nesprin-2G. Mutating either conserved cysteine, in EGFP-SUN2^{C577S} or EGFP-mini-Nesprin-2G$^{C\text{-}23S}$, blocked the rescue of centrosome orientation (Figure 6B) and the rearward nuclear positioning defects (Figure 6C) caused by the depletion of SUN2 or Nesprin-2G, respectively. These results suggest that the ability of SUN2 to form an intermolecular disulfide bond with Nesprin-2G is critical for actin-mediated rearward nuclear positioning in migrating fibroblasts.

The Role of the Conserved Aromatic Residues at –7 of KASH Domains in the Presence of the Disulfide Bond

We next tested the extent to which conserved aromatic residues at −7 of KASH domains (Figure 1B) were required in the context of a longer KASH domain predicted to form disulfide bonds with SUN partners. Mutation of the phenylalanine at −7 in the ANC-1

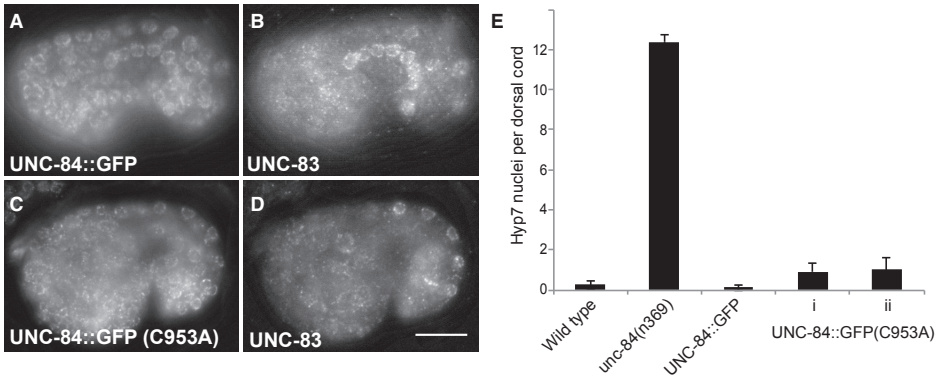

Figure 5. The Conserved Cysteine in UNC-84 Is Not Required for Nuclear Migration
(A–D) Anti-GFP (A and C) and anti-UNC-83 (B and D) immunolocalization in comma-stage embryos. Anterior is left; dorsal is up. Scale bar, 10 μm.
(E) Quantification of nuclear migration defects as in Figure 2. Error bars are 95% CI.

KASH domain did not cause a nuclear anchorage defect in adult *C. elegans* hypodermal cells; an average of 4.3% ± 1.2% (mean ± 95% CI) of hypodermal nuclei per lateral side of an animal were clustered (Figures 4G and 4H), which is not significantly different from the wild-type number of 2.4% ± 1.3% ($p = 0.058$ in a t test compared to wild-type). Thus, the presence of an intermolecular disulfide bond could at least partially compensate for a mutation in the KASH −7 aromatic residue in the UNC-84-ANC-1 interaction. In contrast, expression of an EGFP-mini-nesprin-2G construct harboring a mutation of the tyrosine at −7 in the KASH domain failed to rescue rearward nuclear positioning in nesprin-2-depleted NIH 3T3 fibroblasts during centrosome orientation (Figure 6). These results suggest that the conserved aromatic residues at the −7 position of KASH domains may be necessary for the transmission of forces generated by the actin cytoskeleton to move nuclei, whereas they are dispensable for resisting the forces experienced by nuclei anchored to the actin cytoskeleton in moving *C. elegans* animals. In agreement with this, our molecular dynamics results showed that despite the detachment of residues 0 to −17 in the KASH(Y-7A) mutation, the remaining residues (−18 to −23) remained intact due to the presence of the intermolecular disulfide bond (Figure 3).

Modeling Force Transfer across LINC Complexes by Molecular Dynamics

Our working model predicts that mechanical forces generated in the cytoskeleton are transferred across the nuclear envelope through LINC complexes and that disulfide bonds between SUN and KASH domains are important for the transfer of forces. We therefore modeled how SUN-KASH interactions would be affected with and without the disulfide bond. We used molecular dynamics to simulate constant-velocity pulling on the amino-terminal residue of the KASH peptide of human Nesprin-2 attached to SUN2 at a constant velocity of 0.05 m/s in wild-type (Figure 7A) and the SUN2 (C563A) mutation (Figure 7B). Each simulation was run three times. In a previous study, we applied tension on KASH domains by exerting a constant force on each KASH peptide [35]. As opposed to constant-force simulations, in this study, constant-velocity pulling was used and the changes in the magnitude of forces that the complex was able to withstand were extracted. In the SUN2 (C563A) mutation model, the KASH peptide begins to detach from the SUN protomer under virtually zero forces and both KASH peptides and the KASH lids of SUN domains are stretched to accommodate the pulling (Figures 7B and 7C). In contrast, the wild-type KASH peptide remains closely associated with the SUN trimer throughout the simulation, withstanding significantly higher forces, up to 250 pN ($N = 29{,}700$; $p < 0.0001$, obtained from a two-sample Kolmogorov-Smirnov test) (Figure 7C). Instead, the pulling forces are transferred past the SUN-KASH interaction and SUN domain and are relieved by stretching the coiled-coil domains (formed by α3) of SUN2 (Figures 7A, 7C, and 7D).

DISCUSSION

Interactions between conserved SUN and KASH domains form the core of the nuclear envelope-spanning LINC complex [3–5, 15, 41]. Here, we performed structural/functional analyses of the three interaction interfaces between SUN and KASH proteins. The C-terminal 4 residues of KASH proteins (0 to −3) interact with a binding pocket in SUN protomer P1, residues −4 to −14 interact with a cleft that is formed between the "KASH lid" of P1 and the core of the adjacent P2 protomer, and residues −15 to −23 interact with the surface of P2 [6]. We found that mutating any of the three interfaces disrupted the formation of LINC complexes and/or reduced the transfer of forces generated in the cytoplasm to the nucleoskeleton. Our results uncovered potential regulatory mechanisms for the formation and function of LINC complexes.

Mutational analysis of the two interfaces at the C terminus of KASH domains (consisting of KASH residues 0 to −14) showed they were necessary *in vivo* to move *C. elegans* hypodermal nuclei. These results are supported by the previous findings that the C-terminal 18 residues of the Nesprin-2 KASH domain are sufficient for binding SUN2 *in vitro* [6] and that the extension

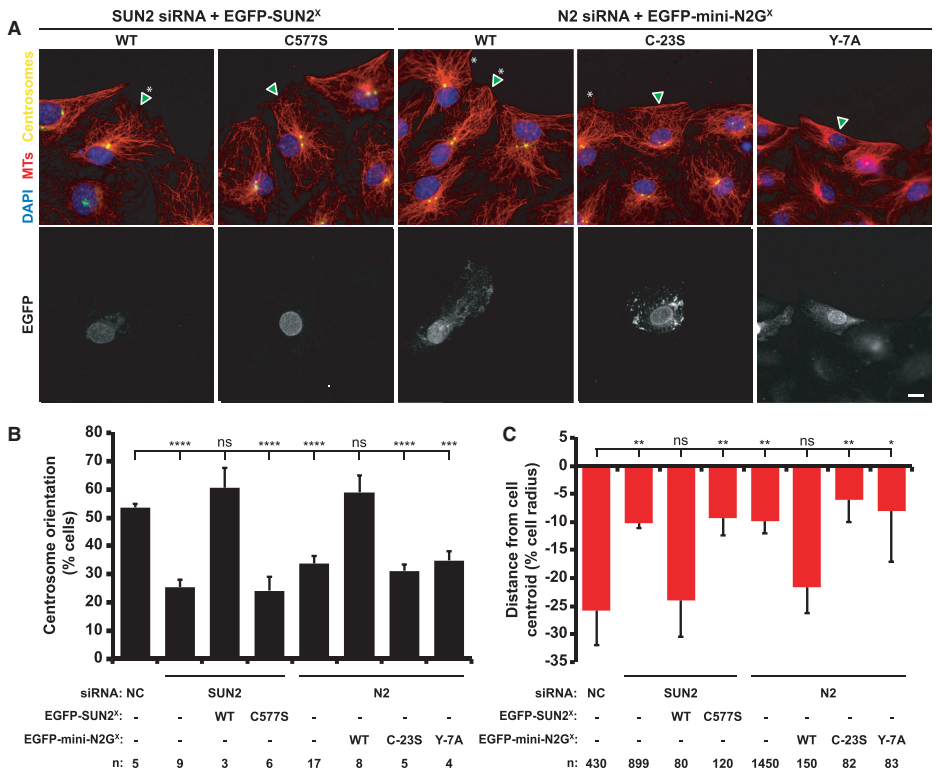

Figure 6. SUN2 C577 and Nesprin-2G C-23 Are Required for Rearward Nuclear Positioning during Centrosome Orientation

(A) Representative epifluorescence images of centrosome orientation in NIH 3T3 fibroblasts treated with siRNA and expressing the indicated cDNA constructs (arrowheads and bottom row of images). Asterisks, oriented centrosomes. Scale bar, 10 μm. MTs, microtubules.

(B) Centrosome orientation in the cells described in (A).

(C) Average nuclear positions from the cells described in (B). The cell center is defined as "0." Positive values are toward the leading edge, and negative values are away.

Two-tailed t tests were used to calculate p values (*p < 0.05, **p < 0.01, ***p < 0.001, ****p < 0.0001; ns, not significant). Error bars are 95% CI.

of the C terminus of KASH prevents its ability to interact with SUN2 *in vitro* [6, 33].

We also tested the extent to which the conserved aromatic residue at position −7 of KASH proteins functions in LINC assembly in our various experimental models and found significant differences. In *C. elegans* hyp7 precursors, UNC-83(Y-7A) expressed at endogenous levels localized to the nuclear envelope, but nuclear migration failed (Figures 3A–3E). These results suggest UNC-83(Y-7A) can weakly interact with UNC-84 at a level sufficient for localization to the nuclear envelope, but the interaction is unable to sustain the forces transferred across the LINC complex during nuclear migration. Our molecular dynamics simulations support this model. Without the tyrosine at position −7, KASH was unable to reach into the cleft between the two SUN protomers, resulting in the loss of several important interactions between the KASH tyrosine and a conserved motif on SUN (E552–S557 of SUN2; Figure 3). Likewise, the −7 tyrosine in the mouse nesprin-2G KASH domain was required for rearward nuclear migration and centrosome orientation in NIH 3T3 cells (Figure 6). In contrast, hypodermal syncytial nuclei were anchored normally in *anc-1(F-7A)* mutant animals. Perhaps the cysteine at −23 of KASH is sufficient to overcome the ANC-1(F-7A) mutation for nuclear anchorage, but both the −23 cysteine and the −7 tyrosine are required in NIH 3T3 cell rearward nuclear movements. Together, these findings suggest that the forces transmitted by LINC complexes required to move nuclei in polarizing fibroblasts may be greater than those required to anchor *C. elegans* hypodermal nuclei.

The third KASH-SUN interaction interface (−15 to −23) may solidify KASH-SUN complexes by forming an intermolecular disulfide bond between highly conserved cysteine residues in certain SUN and KASH pairs. Such a disulfide bond was observed between transiently expressed SUN and KASH proteins in HeLa cells [6]. We propose a model where the regulation of this third interface might enable a SUN protein homo-trimer to switch between different KASH proteins. In *C. elegans*, the SUN

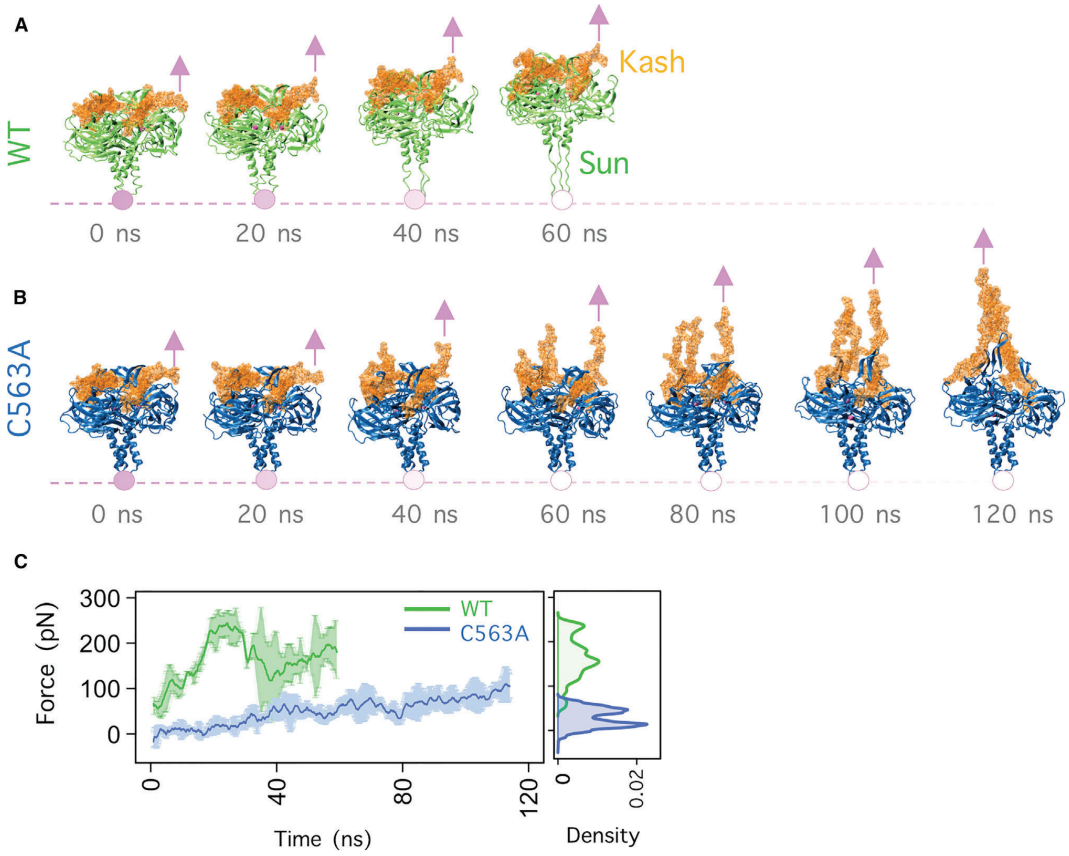

Figure 7. Modeling Force Transfer across LINC Complexes

(A and B) Snapshots of the trajectory of wild-type (A) and C563A (B) SUN2-KASH2 complexes under constant-velocity pulling. Pink arrows represent the location and direction of the applied constant velocity. Pink circles represent the fixed atoms.

(C) Forces on each KASH peptide required to displace the SUN-KASH complex at a constant velocity for wild-type (green) and C563A (blue) averaged over three molecular dynamics simulation runs. Error bars are the range. Right: a density plot shows the forces on each KASH peptide at each time point throughout the three simulations.

protein UNC-84 would first interact with the KASH protein UNC-83, which lacks the conserved cysteine, to move hypodermal nuclei. Then, UNC-84 would primarily interact with ANC-1 to anchor hypodermal nuclei. Because nuclear anchorage occurs over longer timescales, it might be advantageous to stabilize the UNC-84-ANC-1 interaction with a disulfide bond. The conserved cysteines in SUN2 and nesprin-2 were also necessary for actin-dependent rearward nuclear positioning during centrosome orientation in NIH 3T3 fibroblasts. In this manner, the rearward nuclear positioning in fibroblasts may be analogous to nuclear anchorage in the *C. elegans* hypodermis, as both processes use giant KASH proteins to tether nuclei to actin networks.

In further support of our proposed model for the role of an intermolecular disulfide bond in LINC complex function, molecular dynamics simulations suggested that the disulfide bond allows for maximal force transduction across the nuclear envelope. In the absence of a disulfide bond, constant pulling rapidly stretched KASH domains and the KASH lid of SUN domains. Only ~50 pN of force was transferred across the interface without the disulfide bond. In contrast, the presence of SUN-KASH intermolecular disulfide bonds transferred the forces on the KASH peptides directly to the coiled-coil trimerization domain in the luminal parts of SUN proteins while maintaining the stability of the SUN-KASH interface in our simulations. In this case, forces could be transferred across the LINC complex and ultimately to the nucleoskeleton and/or chromatin. These findings suggest that higher forces and/or a more stable interaction may be required to anchor nuclei to actin networks more permanently, versus the interactions to microtubules during *C. elegans* nuclear migration that are only required for brief

times. It is likely that other nuclear movements or other roles of LINC complexes in human development and disease will have a similar mode of regulation.

If the cell regulates the formation and reduction of the predicted SUN-KASH intermolecular disulfide bond, an interesting question is how it might do so. There are three protein disulfide isomerases in *C. elegans*. However, these three genes are understudied and their expression patterns could be developmentally regulated. A second possibility is that pulling across a disulfide bond could expose it to reduction [42]. Third, it has been proposed that the AAA+ ATPase Torsin could regulate the formation of LINC complexes [38, 43–45]. Future experiments could distinguish between these and other possible regulatory mechanisms.

The KASH domains in *C. elegans* UNC-83 and mammalian KASH5 are well conserved but significantly shorter than those in other KASH proteins. Nevertheless, both bind canonical SUN proteins UNC-84 in *C. elegans*, or SUN1 and SUN2 in mammals [7, 8, 15, 28]. UNC-83 and KASH5 are transiently required during development, whereas ANC-1 and the other Nesprins tend to play longer-term roles. For example, UNC-83 is required for a few specific nuclear migration events that take ~10–30 min during *C. elegans* development [26, 27]. After migration, nuclei remain anchored in place for days by way of the interaction of ANC-1 with the actin cytoskeleton [14]. Similarly, KASH5 only functions a short time during meiotic prophase I [28], whereas other Nesprins function just before and after this narrow window [4]. These findings suggest that evolution has maintained the disulfide bond in *C. elegans* and mammalian LINC complexes that function long term and/or require maximal force transduction but selected against the disulfide bond in LINC complexes that function transiently. The disulfide bond and third interaction domain may have been lost in KASH5 and UNC-83 after the divergence of nematodes, insects, and vertebrates, as both canonical KASH proteins in *Drosophila*, Klarsicht and MSP-300, have the conserved cysteine [5].

In summary, we have demonstrated here that all three interaction interfaces between conserved SUN and KASH proteins contribute to LINC complex function in nuclear positioning. Our findings from *C. elegans* development, mammalian cultured fibroblasts, and molecular dynamics simulations have led to a more complete mechanistic understanding of SUN-KASH interactions, which form the core of LINC complexes. Because LINC complexes are central to a multitude of cell and developmental functions and have been implicated in multiple pathologies [4, 5, 15, 46, 47], our mechanistic findings are likely to be important for understanding a variety of cell and developmental processes.

STAR★METHODS

Detailed methods are provided in the online version of this paper and include the following:

- KEY RESOURCES TABLE
- CONTACT FOR REAGENT AND RESOURCE SHARING
- EXPERIMENTAL MODEL AND SUBJECT DETAILS
- METHOD DETAILS
  - *C. elegans* CRISPR/Cas9 editing
  - Nuclear migration and anchorage assays in *C. elegans*
  - NIH 3T3 fibroblast manipulations
  - Immunofluorescence
  - Molecular Dynamics
- QUANTIFICATION AND STATISTICAL ANALYSIS

SUPPLEMENTAL INFORMATION

Supplemental Information includes one table and can be found with this article online at https://doi.org/10.1016/j.cub.2018.08.001.

ACKNOWLEDGMENTS

We thank Thomas Schwartz, Ulrike Kutay, and members of the Starr, Mofrad, and Luxton laboratories for helpful discussions. This work was supported by the NIH (R01GM073874 to D.A.S.; R21NS095109 to G.W.G.L.; and AR007612 to N.J.H.), National Science Foundation (CAREER award CBET-0955291 to M.R.K.M.), Natural Sciences and Engineering Research Council of Canada (to Z.J.), Dystonia Medical Research Foundation (to G.W.G.L.), and American Cancer Society Illinois Division (PF-13-094-01-CGC to N.E.C.).

AUTHOR CONTRIBUTIONS

Conceptualization, N.E.C., Z.J., M.R.K.M., G.W.G.L., and D.A.S.; Investigation, N.E.C., Z.J., A.S., V.A.V., B.E., H.H., N.J.H., L.A.H., and B.M.W.; Formal Analysis, all authors; Writing – Original Draft, N.E.C., Z.J., M.R.K.M., G.W.G.L., and D.A.S.; Writing – Review & Editing, all authors.

DECLARATION OF INTERESTS

N.E.C. is currently employed as a scientific editor at *Cell Reports*, which is a part of Cell Press.

Received: December 27, 2017
Revised: June 18, 2018
Accepted: August 1, 2018
Published: September 20, 2018

REFERENCES

1. Bone, C.R., and Starr, D.A. (2016). Nuclear migration events throughout development. J. Cell Sci. *129*, 1951–1961.
2. Gundersen, G.G., and Worman, H.J. (2013). Nuclear positioning. Cell *152*, 1376–1389.
3. Burke, B., and Roux, K.J. (2009). Nuclei take a position: managing nuclear location. Dev. Cell *17*, 587–597.
4. Ungricht, R., and Kutay, U. (2017). Mechanisms and functions of nuclear envelope remodelling. Nat. Rev. Mol. Cell Biol. *18*, 229–245.
5. Starr, D.A., and Fridolfsson, H.N. (2010). Interactions between nuclei and the cytoskeleton are mediated by SUN-KASH nuclear-envelope bridges. Annu. Rev. Cell Dev. Biol. *26*, 421–444.
6. Sosa, B.A., Rothballer, A., Kutay, U., and Schwartz, T.U. (2012). LINC complexes form by binding of three KASH peptides to domain interfaces of trimeric SUN proteins. Cell *149*, 1035–1047.
7. McGee, M.D., Rillo, R., Anderson, A.S., and Starr, D.A. (2006). UNC-83 is a KASH protein required for nuclear migration and is recruited to the outer nuclear membrane by a physical interaction with the SUN protein UNC-84. Mol. Biol. Cell *17*, 1790–1801.
8. Crisp, M., Liu, Q., Roux, K., Rattner, J.B., Shanahan, C., Burke, B., Stahl, P.D., and Hodzic, D. (2006). Coupling of the nucleus and cytoplasm: role of the LINC complex. J. Cell Biol. *172*, 41–53.
9. Haque, F., Lloyd, D.J., Smallwood, D.T., Dent, C.L., Shanahan, C.M., Fry, A.M., Trembath, R.C., and Shackleton, S. (2006). SUN1 interacts with nuclear lamin A and cytoplasmic nesprins to provide a physical connection between the nuclear lamina and the cytoskeleton. Mol. Cell. Biol. *26*, 3738–3751.

10. Padmakumar, V.C., Libotte, T., Lu, W., Zaim, H., Abraham, S., Noegel, A.A., Gotzmann, J., Foisner, R., and Karakesisoglou, I. (2005). The inner nuclear membrane protein Sun1 mediates the anchorage of Nesprin-2 to the nuclear envelope. J. Cell Sci. *118*, 3419–3430.
11. Malone, C.J., Fixsen, W.D., Horvitz, H.R., and Han, M. (1999). UNC-84 localizes to the nuclear envelope and is required for nuclear migration and anchoring during *C. elegans* development. Development *126*, 3171–3181.
12. Bone, C.R., Tapley, E.C., Gorjánácz, M., and Starr, D.A. (2014). The *Caenorhabditis elegans* SUN protein UNC-84 interacts with lamin to transfer forces from the cytoplasm to the nucleoskeleton during nuclear migration. Mol. Biol. Cell *25*, 2853–2865.
13. Rothballer, A., and Kutay, U. (2013). The diverse functional LINCs of the nuclear envelope to the cytoskeleton and chromatin. Chromosoma *122*, 415–429.
14. Starr, D.A., and Han, M. (2002). Role of ANC-1 in tethering nuclei to the actin cytoskeleton. Science *298*, 406–409.
15. Luxton, G.W.G., and Starr, D.A. (2014). KASHing up with the nucleus: novel functional roles of KASH proteins at the cytoplasmic surface of the nucleus. Curr. Opin. Cell Biol. *28*, 69–75.
16. Janota, C.S., Calero-Cuenca, F.J., Costa, J., and Gomes, E.R. (2017). SnapShot: nucleo-cytoskeletal interactions. Cell *169*, 970–970.e1.
17. Wang, W., Shi, Z., Jiao, S., Chen, C., Wang, H., Liu, G., Wang, Q., Zhao, Y., Greene, M.I., and Zhou, Z. (2012). Structural insights into SUN-KASH complexes across the nuclear envelope. Cell Res. *22*, 1440–1452.
18. Hennen, J., Hur, K.-H., Saunders, C.A., Luxton, G.W.G., and Mueller, J.D. (2017). Quantitative brightness analysis of protein oligomerization in the nuclear envelope. Biophys. J. *113*, 138–147.
19. Hennen, J., Saunders, C.A., Mueller, J.D., and Luxton, G.W.G. (2018). Fluorescence fluctuation spectroscopy reveals differential SUN protein oligomerization in living cells. Mol. Biol. Cell *29*, 1003–1011.
20. Sosa, B.A., Kutay, U., and Schwartz, T.U. (2013). Structural insights into LINC complexes. Curr. Opin. Struct. Biol. *23*, 285–291.
21. Zhou, K., and Hanna-Rose, W. (2010). Movers and shakers or anchored: *Caenorhabditis elegans* nuclei achieve it with KASH/SUN. Dev. Dyn. *239*, 1352–1364.
22. Starr, D.A., and Han, M. (2005). A genetic approach to study the role of nuclear envelope components in nuclear positioning. Novartis Found. Symp. *264*, 208–219, discussion 219–230.
23. Luxton, G.W.G., Gomes, E.R., Folker, E.S., Vintinner, E., and Gundersen, G.G. (2010). Linear arrays of nuclear envelope proteins harness retrograde actin flow for nuclear movement. Science *329*, 956–959.
24. Gomes, E.R., Jani, S., and Gundersen, G.G. (2005). Nuclear movement regulated by Cdc42, MRCK, myosin, and actin flow establishes MTOC polarization in migrating cells. Cell *121*, 451–463.
25. Chang, W., Antoku, S., and Gundersen, G.G. (2016). Wound-healing assays to study mechanisms of nuclear movement in fibroblasts and myoblasts. In Electron Microscopy Methods in Molecular Biology, S. Shackleton, P. Collsa, and E.C. Shirmer, eds. (Springer), pp. 255–267.
26. Fridolfsson, H.N., and Starr, D.A. (2010). Kinesin-1 and dynein at the nuclear envelope mediate the bidirectional migrations of nuclei. J. Cell Biol. *191*, 115–128.
27. Starr, D.A., Hermann, G.J., Malone, C.J., Fixsen, W., Priess, J.R., Horvitz, H.R., and Han, M. (2001). unc-83 encodes a novel component of the nuclear envelope and is essential for proper nuclear migration. Development *128*, 5039–5050.
28. Horn, H.F., Kim, D.I., Wright, G.D., Wong, E.S.M., Stewart, C.L., Burke, B., and Roux, K.J. (2013). A mammalian KASH domain protein coupling meiotic chromosomes to the cytoskeleton. J. Cell Biol. *202*, 1023–1039.
29. Roux, K.J., Crisp, M.L., Liu, Q., Kim, D., Kozlov, S., Stewart, C.L., and Burke, B. (2009). Nesprin 4 is an outer nuclear membrane protein that can induce kinesin-mediated cell polarization. Proc. Natl. Acad. Sci. USA *106*, 2194–2199.
30. Zhen, Y.-Y., Libotte, T., Munck, M., Noegel, A.A., and Korenbaum, E. (2002). NUANCE, a giant protein connecting the nucleus and actin cytoskeleton. J. Cell Sci. *115*, 3207–3222.
31. Zhang, Q., Skepper, J.N., Yang, F., Davies, J.D., Hegyi, L., Roberts, R.G., Weissberg, P.L., Ellis, J.A., and Shanahan, C.M. (2001). Nesprins: a novel family of spectrin-repeat-containing proteins that localize to the nuclear membrane in multiple tissues. J. Cell Sci. *114*, 4485–4498.
32. Zhang, X., Xu, R., Zhu, B., Yang, X., Ding, X., Duan, S., Xu, T., Zhuang, Y., and Han, M. (2007). Syne-1 and Syne-2 play crucial roles in myonuclear anchorage and motor neuron innervation. Development *134*, 901–908.
33. Stewart-Hutchinson, P.J., Hale, C.M., Wirtz, D., and Hodzic, D. (2008). Structural requirements for the assembly of LINC complexes and their function in cellular mechanical stiffness. Exp. Cell Res. *314*, 1892–1905.
34. Bone, C.R., Chang, Y.-T., Cain, N.E., Murphy, S.P., and Starr, D.A. (2016). Nuclei migrate through constricted spaces using microtubule motors and actin networks in *C. elegans* hypodermal cells. Development *143*, 4193–4202.
35. Jahed, Z., Shams, H., and Mofrad, M.R.K. (2015). A disulfide bond is required for the transmission of forces through SUN-KASH complexes. Biophys. J. *109*, 501–509.
36. D'Alessandro, M., Hnia, K., Gache, V., Koch, C., Gavriilidis, C., Rodriguez, D., Nicot, A.-S., Romero, N.B., Schwab, Y., Gomes, E., et al. (2015). Amphiphysin 2 orchestrates nucleus positioning and shape by linking the nuclear envelope to the actin and microtubule cytoskeleton. Dev. Cell *35*, 186–198.
37. Lawrence, K.S., Tapley, E.C., Cruz, V.E., Li, Q., Aung, K., Hart, K.C., Schwartz, T.U., Starr, D.A., and Engebrecht, J. (2016). LINC complexes promote homologous recombination in part through inhibition of nonhomologous end joining. J. Cell Biol. *215*, 801–821.
38. Saunders, C.A., Harris, N.J., Willey, P.T., Woolums, B.M., Wang, Y., McQuown, A.J., Schoenhofen, A., Worman, H.J., Dauer, W.T., Gundersen, G.G., and Luxton, G.W. (2017). TorsinA controls TAN line assembly and the retrograde flow of dorsal perinuclear actin cables during rearward nuclear movement. J. Cell Biol. *216*, 657–674.
39. Folker, E.S., Östlund, C., Luxton, G.W.G., Worman, H.J., and Gundersen, G.G. (2011). Lamin A variants that cause striated muscle disease are defective in anchoring transmembrane actin-associated nuclear lines for nuclear movement. Proc. Natl. Acad. Sci. USA *108*, 131–136.
40. Luxton, G.W.G., Gomes, E.R., Folker, E.S., Worman, H.J., and Gundersen, G.G. (2011). TAN lines: a novel nuclear envelope structure involved in nuclear positioning. Nucleus *2*, 173–181.
41. Razafsky, D., and Hodzic, D. (2009). Bringing KASH under the SUN: the many faces of nucleo-cytoskeletal connections. J. Cell Biol. *186*, 461–472.
42. Wiita, A.P., Ainavarapu, S.R.K., Huang, H.H., and Fernandez, J.M. (2006). Force-dependent chemical kinetics of disulfide bond reduction observed with single-molecule techniques. Proc. Natl. Acad. Sci. USA *103*, 7222–7227.
43. Starr, D.A., and Rose, L.S. (2017). TorsinA regulates the LINC to moving nuclei. J. Cell Biol. *216*, 543–545.
44. Gerace, L. (2004). TorsinA and torsion dystonia: unraveling the architecture of the nuclear envelope. Proc. Natl. Acad. Sci. USA *101*, 8839–8840.
45. Sosa, B.A., Demircioglu, F.E., Chen, J.Z., Ingram, J., Ploegh, H.L., and Schwartz, T.U. (2014). How lamina-associated polypeptide 1 (LAP1) activates Torsin. eLife *3*, e03239.
46. Calvi, A., and Burke, B. (2015). LINC Complexes and Their Role in Human Disease (John Wiley & Sons).
47. Cartwright, S., and Karakesisoglou, I. (2014). Nesprins in health and disease. Semin. Cell Dev. Biol. *29*, 169–179.
48. Cain, N.E., Tapley, E.C., McDonald, K.L., Cain, B.M., and Starr, D.A. (2014). The SUN protein UNC-84 is required only in force-bearing cells to maintain nuclear envelope architecture. J. Cell Biol. *206*, 163–172.
49. Brenner, S. (1974). The genetics of *Caenorhabditis elegans*. Genetics *77*, 71–94.

50. Dickinson, D.J., Ward, J.D., Reiner, D.J., and Goldstein, B. (2013). Engineering the *Caenorhabditis elegans* genome using Cas9-triggered homologous recombination. Nat. Methods *10*, 1028–1034.

51. Paix, A., Folkmann, A., Rasoloson, D., and Seydoux, G. (2015). High efficiency, homology-directed genome editing in *Caenorhabditis elegans* using CRISPR-Cas9 ribonucleoprotein complexes. Genetics *201*, 47–54.

52. Phillips, J.C., Braun, R., Wang, W., Gumbart, J., Tajkhorshid, E., Villa, E., Chipot, C., Skeel, R.D., Kalé, L., and Schulten, K. (2005). Scalable molecular dynamics with NAMD. J. Comput. Chem. *26*, 1781–1802.

53. Humphrey, W., Dalke, A., and Schulten, K. (1996). VMD: visual molecular dynamics. J. Mol. Graph. *14*, 33–38, 27–28.

54. Palazzo, A.F., Joseph, H.L., Chen, Y.J., Dujardin, D.L., Alberts, A.S., Pfister, K.K., Vallee, R.B., and Gundersen, G.G. (2001). Cdc42, dynein, and dynactin regulate MTOC reorientation independent of Rho-regulated microtubule stabilization. Curr. Biol. *11*, 1536–1541.

55. Dickinson, D.J., Pani, A.M., Heppert, J.K., Higgins, C.D., and Goldstein, B. (2015). Streamlined genome engineering with a self-excising drug selection cassette. Genetics *200*, 1035–1049.

56. Arribere, J.A., Bell, R.T., Fu, B.X.H., Artiles, K.L., Hartman, P.S., and Fire, A.Z. (2014). Efficient marker-free recovery of custom genetic modifications with CRISPR/Cas9 in *Caenorhabditis elegans*. Genetics *198*, 837–846.

57. Paix, A., Schmidt, H., and Seydoux, G. (2016). Cas9-assisted recombineering in *C. elegans*: genome editing using in vivo assembly of linear DNAs. Nucleic Acids Res. *44*, e128.

58. Richardson, C.D., Ray, G.J., DeWitt, M.A., Curie, G.L., and Corn, J.E. (2016). Enhancing homology-directed genome editing by catalytically active and inactive CRISPR-Cas9 using asymmetric donor DNA. Nat. Biotechnol. *34*, 339–344.

59. Liu, Z., Kirch, S., and Ambros, V. (1995). The *Caenorhabditis elegans* heterochronic gene pathway controls stage-specific transcription of collagen genes. Development *121*, 2471–2478.

STAR★METHODS

KEY RESOURCES TABLE

REAGENT or RESOURCE	SOURCE	IDENTIFIER
Antibodies		
mouse monoclonal anti-UNC-84	[48]	L72/6
mouse monoclonal anti-UNC-83	[27]	1209D7
rabbit polyclonal anti-GFP	Novus Biologicals	RRID:AB_10003058; NB600-308
mouse monoclonal anti-GFP	Clontech	RRID:AB_10013427; JL-8
rabbit polyclonal anti-pericentrin	Covance	RRID:AB_291635; PRB-432C
rat monoclonal anti-tyrosinated α-tubulin	European Collection of Animal Cultures	YL1/2
AlexaFluor secondary antibody 488 donkey anti-rabbit	Thermo Fisher	Cat#A-21206
AlexaFluor secondary antibody 555 goat anti-mouse	Thermo Fisher	Cat#A-21422
AlexaFluor secondary antibody 594 donkey anti-mouse	Thermo Fisher	Cat#R37115
Lipofectamine RNAiMAX	Thermo Fisher	Cat#13778075
Fluoromount-G	Thermo Fisher	Cat#00-4958-02
Bacterial and Virus Strains		
E. coli OP50	*Caenorhabditis* Genetics Center	N/A
Chemicals, Peptides, and Recombinant Proteins		
LPA	Avanti Polar Lipids	Cat#857130P
tetramisole	Sigma-Aldrich	Cat#L9756
Cas9 protein	QB3 UC Berkeley	N/A
Critical Commercial Assays		
Lipofectamine RNAiMAX	Thermo Fisher	Cat#13778150
Q5 Site-directed mutagenesis kit	New England Biolabs	Cat#E0554
Experimental Models: Cell Lines		
NIH 3T3 fibroblasts	ATCC	ATCC CRL-1658
Experimental Models: Organisms/Strains		
C. elegans strain: *wild type*	[49]	N2
C. elegans strain: *unc-84(n369)*	[11]	MT369
C. elegans strain: *unc-83(e1408)*	[27]	CB1408
C. elegans strain: *anc-1(e1873)*	[14]	CB3440
C. elegans strain: *unc-83(yc26[unc-83::gfp::kash + LoxP])V*	[34]	UD473
C. elegans strain: *unc-84(yc24[unc-84::gfp+LoxP])X*	[37]	UD476
C. elegans strain: *unc-19(ed3)I, yc28[unc-83::gfp::kash+A, LoxP::unc-19(+)::LoxP]V.*	this paper	UD478
C. elegans strain: *unc-84(yc35[unc-84(C953A)::gfp + LoxP])X*	this paper	UD497 & UD498
C. elegans strain: *anc-1(*yc48*[kash(CC,-24,-23,AA)]);dpy-10*	this paper	UD558
C. elegans strain: *unc-83(yc50[unc-83::gfp::kash(Y-7A) +LoxP])V*	this paper	UD568
C. elegans strain: *ycEx249[p_{col-19}::gfp::lacZ, p_{myo-2}::mCherry]*	this paper	UD522
C. elegans strain: *anc-1(yc56[F-7A]) I; ycEx249[p_{col-19}::gfp::lacZ, p_{myo-2}::mCherry]*	this paper	UD584
Oligonucleotides		
See Table S1	N/A	N/A
Recombinant DNA		
p_{eft-3}::*Cas9* + Empty sgRNA	gift from Bob Goldstein [50]	pDD162; Addgene plasmid # 47549
unc-83::gfp::kash homologous repair template	[34]	pSL718
unc-83::gfp::kash+A homologous repair template	this paper	pSL724

(*Continued on next page*)

Continued

REAGENT or RESOURCE	SOURCE	IDENTIFIER
Cas9 sgRNA construct for *unc-83* ctatgataattgtgtccac	[34]	pSL715
Cas9 sgRNA construct for *unc-84* gttgtgtcaacaagatgct	this study	pSL771
Cas9-sgRNA vector	gift from Geraldine Seydoux [51]	AP568-2; Addgene plasmid # 70047
promoterless *gfp::lacZ::nls* expression construct	gift from Andrew Fire	pPD96.04; Addgene plasmid #1502
$p_{col\text{-}19}$*::gfp::lacZ::nls* expression construct	this paper	pSL779
SUN2 siRNA rescuing construct	[23]	EGFP-SUN2^{WT}
SUN2 siRNA rescuing construct with C577S	this paper	EGFP-SUN2^{C577S}
Nesprin-2G siRNA rescuing construct	[23]	EGFP-mini-Nesprin-2^{WT}
Nesprin-2G siRNA rescuing construct with C-23S	this paper	EGFP-mini-Nesprin-2G$^{C\text{-}23S}$
$p_{myo\text{-}2}$*::mCherry*	gift from Erik Jorgensen	pCFJ90; Addgene plasmid # 19327
Software and Algorithms		
NAMD with CHARMM27 Molecular dynamics	[52]	http://www.ks.uiuc.edu/Development/Download/download.cgi?PackageName=NAMD
Langevin's piston and Hoover's method	[52]	N/A
VMD	[53]	http://www.ks.uiuc.edu/Development/Download/download.cgi?PackageName=VMD
LAS X Life Science	Leica	https://www.leica-microsystems.com/products/microscope-software/details/product/leica-las-x-ls/
NIS-Elements software	Nikon	https://www.nikoninstruments.com/Products/Software/NIS-Elements-Confocal/NIS-Elements-Viewer
ImageJ	NIH	https://imagej.nih.gov/ij/
R	The R Foundation	https://www.r-project.org/
Excel	Microsoft	https://products.office.com/en-US/excel

CONTACT FOR REAGENT AND RESOURCE SHARING

Further information and requests for resources and reagents should be directed to and will be fulfilled by the Lead Contact, Daniel A. Starr (dastarr@ucdavis.edu).

EXPERIMENTAL MODEL AND SUBJECT DETAILS

Caenorhabditis elegans were cultured on nematode growth medium plates spotted with OP50 bacteria and maintained at 15°C or room temperature (approximately 22°C). N2 was used as the wild-type control strain [49]. Some strains were provided by the *Caenorhabditis* Genetics Center, funded by the National Institutes of Health Office of Research Infrastructure Programs (P40 OD010440). Only healthy animals that were not used in previous procedures and were naive to testing were used. See the Key Resources Table for strain list.

Low-passage NIH 3T3 fibroblasts (authenticated by ATCC and of unknown sex) were cultured in DMEM with 10% bovine calf serum (Thermo Fischer). For polarization assays, cells were serum starved for 2 days, wounded and stimulated with 10 μM LPA (Avanti Polar Lipids) [24, 54]. Cells were grown at 37°C in 5% CO_2.

METHOD DETAILS

C. elegans CRISPR/Cas9 editing

Knock-in strains were constructed using CRISPR/Cas9-mediated genome editing [50, 55–57]. Some Cas9 targeting sequences were cloned into pDD162 ($p_{eft\text{-}3}$*::Cas9* + Empty sgRNA, a gift from Bob Goldstein, Addgene plasmid # 47549) [50], using Q5 site-directed mutagenesis (New England Biolabs). For others, guideRNAs were synthesized and pre-complexed with purified Cas9 protein. Targeting sequences for each strain are listed in Table S1.

unc-83::gfp::kash(+A) was generated using *unc-19(ed3)* rescue [34, 50]. An alanine codon was inserted before the stop into pSL718 [34] using Q5 site-directed mutagenesis to create the homologous repair template pSL724, which was used with

Cas9-sgRNA construct pSL715 and injection markers as reported [50] to make UD478: *unc-19(ed3)I, yc28[unc-83::gfp::kash+A, LoxP::unc-19(+)::LoxP]V*.

The *unc-84::gfp(C953A)* mutation was introduced into *unc-84::gfp* (UD476) by CRISPR co-conversion with single stranded oligodeoxyribonucleotide repair templates containing *unc-84(C953A)* and *dpy-10(cn64)* [51, 56], using Cas9-sgRNA constructs pSL771 and AP568-2 (gift from Geraldine Seydoux, Addgene plasmid #70047) [51]. Two independent integrated lines were isolated and analyzed UD497 and UC498: *yc35[unc-84(C953A)::gfp + LoxP]X*.

The *anc-1(yc48)*, *anc-1(yc56)*, and *unc-83(yc50)* mutations were made by directly injecting RNA/Cas9 complexes into *C. elegans* gonads [56–58]. To make *anc-1(yc48)*, 17.5 μM of pre-complexed Alt-R CRISPR *anc-1* crRNA #1 (synthesized by Integrated DNA technologies, see Table S1), tracrRNA (Integrated DNA Technologies), and Cas9 purified protein (QB3 Berkeley) were injected with 6 μM ssDNA repair templates (Integrated DNA Technologies, see Table S1). *anc-1(yc48)* mutates cysteine residues at −23 and −24 of the KASH domain to alanines to make ANC-1(CC-23-24AA) in strain UD558. To make *unc-83(yc50)* and *anc-1(yc56)*, 4 μg crRNA against *unc-83* or crRNA #2 against *anc-1*, 1.25 μg crRNA against *dpy-10*, 10 μg tracrRNA (Dharmacon), 25 μg of Cas9 protein, 1.1 μg ssDNA repair template (See Table S1), and 0.15 μg ssDNA repair for *dpy-10* in a total of 10 μL was injected into young adult gonads [57]. *unc-83(yc50)* mutates the conserved tyrosine at residue 967 of UNC-83 to make UNC-83(Y-7A) in strain UD568. *anc-1(yc56)* mutates the conserved phenylalanine at position −7 from the C terminus of ANC-1 to make ANC-1(F-7A).

A fluorescent marker to identify hypodermal nuclei in the adult animal was constructed by insertion of a 1 kb fragment upstream of the *col-19* gene [59] into pPD96.04 (gift from Andrew Fire, Addgene plasmid #1502) to create $p_{col\text{-}19}$*::gfp::lacZ* (pSL779). N2 animals were injected with pSL779 at 40 ng/μl, pBluescript SK+ at 50ng/μl, and pCFJ90 at 2 ng/μl to make strain UD522: *ycEx249[*$p_{col\text{-}19}$*::gfp::lacZ,* $p_{myo\text{-}2}$*::mCherry]*. Transgenic animals were identified by red fluorescent pharynx in larval stages. Green hypodermal nuclei were observed in transgenic animals beginning at the L4 molt. The marker was introduced into other strains by crossing to UD522 transgenic males.

Nuclear migration and anchorage assays in *C. elegans*

Defects in hyp7 nuclear migration were quantified by counting the number of hyp7 nuclei found abnormally, using Nomarski optics, in the dorsal cords of L1 or L2 hermaphrodites. We scored all the hyp7 nuclei abnormally in the dorsal cord between the second bulb of the pharynx and the anus [12, 27]. Hyp7 nuclear clustering was assayed in adult animals expressing $p_{col\text{-}19}$*::gfp::lacZ*. Young adult hermaphrodites were mounted on 2% agarose pads with 10 mM tetramisole in M9 buffer. Nuclei were counted as clustered if within 10% nuclear diameter proximity to another nucleus in the same focal plane along the longitudinal axis of the worm, as determined by DIC microscopy. Contacts between nuclei on the perpendicular axis were not counted, as the marker could not distinguish seam cell nuclei in proximity to hyp7 nuclei from clusters of hyp7 nuclei. Only nuclei situated between the pharynx and the anus were counted, as nuclei near the mouth and at the very end of the tail were observed to cluster in wild-type animals. Only one lateral side of each animal was scored.

For both the nuclear migration and anchorage assays, *C. elegans* animals of the appropriate age were randomly selected at the dissecting microscope for scoring using the compound microscope and all scorable animals on the slide were counted. Animals were only scored if the entire animal was easily viewable. Although the genotypes were not blinded, animals from multiple plates were included in the datasets. In one case, the *unc-84::gfp(C953A)* mutant, two independently generated lines were assayed.

NIH 3T3 fibroblast manipulations

siRNA experiments were performed using 50nM siRNA duplexes (Shanghai GenePharma), which were transfected using Lipofectamine RNAiMAX (Thermo Fisher). The noncoding, Nesprin-2G, and SUN2 siRNA sequences were previously validated and listed in Table S1 [23]. EGFP-SUN2^{C577S} was made by *in vitro* mutagenesis of EGFP-SUN2^{WT} [23]. EGFP-mini-Nesprin-2G$^{C\text{-}23S}$ was similarly generated from EGFP-mini-Nesprin-2^{WT} [23]. The primers used to generate these constructs are in Table S1. Purified plasmid DNA was microinjected into NIH 3T3 cell nuclei at concentrations between 5 and 30 μg/mL [38]. Injections were performed on a TS100 microscope (Nikon) equipped with a chrome-free infinity Apochromat long working distance apodized dark low 20Å~/NA 0.4 objective (3-mm working distance) and a Narishige NT-88 β [27, 48].

Immunofluorescence

For *C. elegans* experiments: Anti-UNC-84 mouse monoclonal antibody L72/6 [48] was used at 1:100 dilution. Mouse monoclonal anti-UNC-83 antibody 1209D7 [27] was used undiluted. Rabbit polyclonal anti-GFP antibody NB600-308 (Novus Biologicals) was used at 1:500 dilution. AlexaFluor secondary antibodies 488 donkey anti-rabbit, 555 goat anti-mouse, and 594 donkey anti-mouse (Thermo Fisher) were used at 1:500 dilution. Images were captured with a HCX Plan Apochromat 63, 1.40 NA objective on a compound microscope (DM6000) with LAS X software. Images were uniformly enhanced using the background subtraction and brightness/contrast commands in ImageJ.

For experiments with NIH 3T3 cells: NIH 3T3 fibroblasts were cultured in DMEM with 10% bovine calf serum (Thermo Fischer Scientific) on number 1.5 coverslips. Fibroblasts were serum starved for 2 d, wounded, and stimulated with 10 μM LPA for 2 hr before being fixed in in −20° methanol for 10 min. The fixed cells were then stained as follows. Anti-EGFP mouse monoclonal antibody JL-8 (Clontech) was used at a 1:200 dilution, anti-percentrin rabbit polyclonal antibody PRB-432C (Covance) was used at 1:200 dilution. Anti-tyrosinated α-tubulin rat monoclonal antibody YL1/2 (supernatant collected from hybridomas purchased from the European Collection of Animal Cell Cultures, Salisbury, UK) was used at 1:50 dilution. Goat anti-mouse, -rabbit, and -rat secondary antibodies

conjugated to AlexaFluor488, AlexaFluor555, AlexaFluor594, AlexaFluor650 (Thermo Fisher) were used at 1:200 dilution. Stained cells were mounted on slides using Fluoromount (Thermo Fisher).

Images were obtained with a Nikon Eclipse Ni-E microscope driven by NIS-Elements software using a Nikon oil immersion 40Å~/1.30 NA Plan Fluor Eco-Glass oil immersion objective lens (0.20-mm working distance), a Lumencor SOLA solid state white-light excitation subsystem, and a Photometrics CoolSNAP ES2 12-bit 20-MHz digital monochrome charge-coupled device camera. A custom DAPI filter for the SOLA light source was used, which consisted of an ET 395/25Å~excitation filter and an ET 460/50-m emission filter purchased from Chroma Technology Corp (Bellows Falls, VT). EGFP (C-FL EGFP hard coat high signal to noise Zero Shift; Nikon), Texas Red (C-FL Texas Red hard coat high signal to noise Zero Shift; Nikon), and Cy5 (C-FL CY5 hard coat high signal to noise Zero Shift; Nikon) filter sets were also used.

To quantify centrosome orientation, a fibroblast is divided by drawing a ''v'' that begins and ends at the left- and rightmost wound-edge, respectively. The middle of the ''v'' is defined by the center of the nucleus. The cell is scored as having an oriented centrosome if the centrosome resides within the ''v'' between the nucleus and the wound-edge. Since the ''v'' occupies ~1/3 of the cell, ~33% of wound-edge cells will have an oriented centrosome. Experiments were repeated at least 3 times.

To quantify nuclear positioning, fluorescence images of the stained cells described above were pseudocolored, combined and aligned such that the wound-edge was parallel to the x axis using ImageJ. Custom-made MATLAB software (MathWorks, Natick, MA) was then used to calculate the cell centroid and equivalent radius of the wound-edge cells, which were outlined by hand. Segmentation was used to identify the centroid of the nucleus and therefore the position of the organelle. A vector representing the distance from the nuclear centroid to the cell centroid was drawn and resolved into x and y coordinates (parallel and perpendicular to the leading edge, respectively). Measurements were normalized to cell size to allow for comparison between cells. Only the y-coordinate was used in plots as the x-coordinate (position of the nuclear centroid or centrosome along the x axis) did not change significantly. The difference between the cell centroid and the nucleus centroid or centrosome was then divided by the radius to determine the percentage of the cell radius the nucleus traveled.

Regarding the wounded fibroblast monolayer assay for rearward nuclear positioning during centrosome orientation, at least three independent biological replicates were performed and analyzed for each experiment. To compensate for the lack of blinding, five images of at least eighty cells were collected from three different wounds and all of the scorable wound edge cells were analyzed for the non-injected control experiments. For the injected experiments, all of the scorable EGFP-positive wound edge cells were analyzed. Cells were deemed unscorable if they were not entirely visualized within the field of view of an image.

Molecular Dynamics

All molecular dynamics simulations were performed with NAMD using the CHARMM27 force field [52] and visualized using VMD software [53]. The crystal structure used in these simulations was obtained from the protein data bank (PDB ID: 4DXS). Mutations were introduced using the VMD mutator plugin. All modeled structures were then solvated in water and an ion concentration of 150 mM of KCl and 50 μM of $CaCl_2$ was added to each system. Next, periodic boundary conditions were applied in all three directions and the systems were minimized for 5000 steps and equilibrated for ~3ns at 1 atm and 310 K using Langevin's piston and Hoover's method [52], For constant velocity pulling experiments, we attached a dummy atom to the position of the center of mass of the amino-terminal residue of the KASH peptide (C-23) via a virtual spring and fixed the C-terminal residue of SUN2. We then measured the forces between the dummy atom and C-23 using NAMD [52] as the dummy atom was moved at a constant velocity of 0.05 m/s.

QUANTIFICATION AND STATISTICAL ANALYSIS

The *C. elegans* nuclear migration and anchorage data in Figures 2, 3, 4, 5, and 6 are displayed as means with 95% CI as error bars; t tests were performed on indicated comparisons and the sample sizes were at least 20. For Figure 6 pertaining to the NIH 3T3 cells, sample sizes are indicated within the figure. Molecular dynamic simulations were performed in triplicate, plots were prepared using R software. The mean and range of data are shown in Figure 7C. A two-sample Kolmogorov-Smirnov test was performed to determine whether the observed difference in average forces obtained from molecular dynamics simulations is significantly lower in C563A versus wild-type. This test was conducted using the ks.test function in R *stats* package.

Current Biology, Volume *28*

Supplemental Information

Conserved SUN-KASH Interfaces Mediate LINC Complex-Dependent Nuclear Movement and Positioning

Natalie E. Cain, Zeinab Jahed, Amy Schoenhofen, Venecia A. Valdez, Baila Elkin, Hongyan Hao, Nathan J. Harris, Leslie A. Herrera, Brian M. Woolums, Mohammad R.K. Mofrad, G.W. Gant Luxton, and Daniel A. Starr

Table S1. Oligonucleotides used in this study. Related to STAR Methods.

oligonucleotides used for targeting Cas9 in *C. elegans*				
Plasmid or RNA	Target	DNA or RNA target	Strain	Reference
pSL715	*unc-83* 5' of TM domain	ctatgataattgtgtccac	UD478 UNC-83+A	[34]
pSL771	*unc-84* SUN domain	gttgtgtcaacaagatgct	UD497, 498 UNC-84(C953A)	This study
crRNA	*unc-83* KASH domain	ccgcauguaaccuaugugaa	UD568 UNC-83(Y-7A)	This study
crRNA	*anc-1* #1 KASH domain	cauugcgacgacgaguacug	UD558 ANC-1(CC-AA)	This study
crRNA	*anc-1* #2 KASH domain	caguacucgucgucgcaaug	UD584 ANC-1(F-7A)	This study
AP568-2 or crRNA	*dpy-10*	gcuaccauaggcaccacgag	co-CRISPR	[54]

oligonucleotides used CRISPR/CAS9 repair templates			
Repair target	ssODN Sequence	Strain	Reference
unc-84(yc35) UNC-84(C953A)	gttgactatgccctggagagctcaggtggagctgttgtgtcgac aagagcctcagagacgtacaaaagctacacaaggctggaa	UD497, 498	This study
unc-83(yc50) UNC-83(Y-7A)	ctattatcacgtgttcggaaaaccatttggcccgcatgtcaccgc tgtcaatggaccaccaccggtttaactgaatcatcagtattctga ttgaaatccc	UD568	This study
anc-1(yc48) ANC-1(CC-23-24AA)	gcactgcttgttctacttatgggagccgcttgtttggttccacactg tgatgatgaatatgctgctcaacttctcaataatttcgctaaaagtt ttgacccttcgctagaattc	UD558	This study
anc-1(yc56) ANC-1(F-7A)	gacgacaaagatcccgttggagacgggtactcagaactgcttt gccacttcaggtttgtttatatttttaatattaataactaatgtctctc attttcaggcactgcttgttctacttatgggagccgcttgtttggttc cacattgtgatgatgaatactgttgccaacttctcaataatttcgct aaaagttttgacccttcgctagaagccgtaaacggcccgccac cattttaatctttaatttttatttttcattactattcactattgtttcattc	UD584	This study
dpy-10(cn64)	cacttgaacttcaatacggcaagatgagaatgactggaaacc gtaccgcatgcggtgcctatggtagcggagcttcacatggcttc agaccaacagcctat	co-CRISPR	[52]

siRNA sequences for tissue culture		
siRNA target	siRNA Sequence	Reference
noncoding	uucuccgaacgugucacgutt	[23]
Nesprin-2G	ccaucauccugcacuuucatt	[23]
SUN2	gggucauucugcagccagatt	[23]
primers for making mutations in siRNA rescue constructs		
Rescue construct	Sequence	Reference
EGFP-SUN2^{C577S}	gaggagccagtgttatcagcacccgctcctctgagacttatg-agaccaagacggcac	This study
EGFP-SUN2^{C577S}	gtgccgtcttggtctcataagtctcagaggagc-gggtgctgataacactggctcctc	This study
EGFP-mini-Nesprin-2G^{C-23S}	gactacagcagcacccaggc	This study
EGFP-mini-Nesprin-2G^{C-23S}	gcctgggtgctgctgtagtc	This study
EGFP-mini-Nesprin-2G^{Y-7A}	ccaccaacgggccacct	This study
EGFP-mini-Nesprin-2G^{Y-7A}	cccgcagcatggggtaga	This study

Chapter III

Role of KASH domain lengths in the regulation of LINC complexes

Zeinab Jahed, **Hongyan Hao**, Vyom Thakkar, Uyen T. Vu, Venecia A. Valdez, Akshay Rathish, Chris Tolentino, Samuel C. J. Kim, Darya Fadavi, Daniel A. Starr, and Mohammad R. K. Mofrad

MBoC July 2019

Zeinab Jahed and Mohammad R. K. Mofrad designed the *in silco* experiments and wrote the manuscript. Hongyan Hao and Daniel A. Starr designed the *in vivo* experiments and wrote the manuscript related to Figure 5 and Figure 6 together. Venecia A. Valdez generated the *unc-83::anc-1KASH* worm strain. Hongyan Hao conducted the rest of the in vivo experiments and created figures related to Figure 5 and Figure 6.

MBoC | ARTICLE

Role of KASH domain lengths in the regulation of LINC complexes

Zeinab Jahed[a], Hongyan Hao[b], Vyom Thakkar[a], Uyen T. Vu[a], Venecia A. Valdez[b], Akshay Rathish[a], Chris Tolentino[a], Samuel C. J. Kim[a], Darya Fadavi[a], Daniel A. Starr[b], and Mohammad R. K. Mofrad[a,c,*]

[a]Molecular Cell Biomechanics Laboratory, Departments of Bioengineering and Mechanical Engineering, University of California, Berkeley, Berkeley, CA 94720; [b]Department of Molecular and Cellular Biology, University of California, Davis, Davis, CA 95616; [c]Molecular Biophysics and Integrative Bioimaging Division, Lawrence Berkeley National Laboratory, Berkeley, CA 94720

ABSTRACT **The linker of the nucleoskeleton and cytoskeleton (LINC) complex is formed by the conserved interactions between Sad-1 and UNC-84 (SUN) and Klarsicht, ANC-1, SYNE homology (KASH) domain proteins, providing a physical coupling between the nucleoskeleton and cytoskeleton that mediates the transfer of physical forces across the nuclear envelope. The LINC complex can perform distinct cellular functions by pairing various KASH domain proteins with the same SUN domain protein. For example, in *Caenorhabditis elegans*, SUN protein UNC-84 binds to two KASH proteins UNC-83 and ANC-1 to mediate nuclear migration and anchorage, respectively. In addition to distinct cytoplasmic domains, the luminal KASH domain also varies among KASH domain proteins of distinct functions. In this study, we combined in vivo *C. elegans* genetics and in silico molecular dynamics simulations to understand the relation between the length and amino acid composition of the luminal KASH domain, and the function of the SUN–KASH complex. We show that longer KASH domains can withstand and transfer higher forces and interact with the membrane through a conserved membrane proximal EEDY domain that is unique to longer KASH domains. In agreement with our models, our in vivo results show that swapping the KASH domains of ANC-1 and UNC-83, or shortening the KASH domain of ANC-1, both result in a nuclear anchorage defect in *C. elegans*.**

Monitoring Editor
Dennis Discher
University of Pennsylvania

Received: Feb 4, 2019
Revised: Apr 10, 2019
Accepted: Apr 11, 2019

INTRODUCTION

The double-layered nuclear envelope acts as a physical barrier between the constituents of the nucleus and the cytoplasm. The linker of the nucleoskeleton and cytoskeleton (LINC) complexes span this physical barrier and regulate the physical connection between the interior of the nucleus and the cytoplasm during various cellular functions. Through this physical connection, the LINC complex withstands and transfers mechanical forces across the nuclear envelope (Lombardi *et al.*, 2011; Cain *et al.*, 2014; Arsenovic and Conway, 2018; Jahed and Mofrad, 2018, 2019). LINC complexes are composed of Sad1/UNC-84 (SUN) proteins that are anchored to the inner nuclear membrane (INM), and Klarsicht/ANC-1/SYNE homology (KASH) proteins that are anchored to the outer nuclear membrane (ONM). The large cytoplasmic domains of KASH proteins bind to various elements of the cytoskeleton, whereas their 10–30 amino acid KASH domains reside in the perinuclear space (PNS) where they bind to SUN proteins (Figure 1). Several SUN–KASH pairs have been identified to date and each performs distinct functions within the cell (Padmakumar *et al.*, 2005; Crisp *et al.*, 2006; McGee *et al.*, 2006; Kim *et al.*, 2015; Jahed *et al.*, 2016).

Interestingly, different KASH domain proteins can independently bind to the same SUN protein to mediate distinct cellular functions.

This article was published online ahead of print in MBoC in Press (http://www.molbiolcell.org/cgi/doi/10.1091/mbc.E19-02-0079) on April 17, 2019.

*Address correspondence to: Mohammad Mofrad (mofrad@berkeley.edu).

Abbreviations used: CC, coiled-coil; ELEC, electrostatic; INM, inner nuclear membrane; KASH, *Klarsicht*, *ANC-1*, *SYNE* homology; LINC, linker of the nucleoskeleton and cytoskeleton; MD, molecular dynamics; NE, nuclear envelope; ONM, outer nuclear membrane; RMSF, root-mean-square fluctuations; SUN, *Sad-1* and UNC-84.

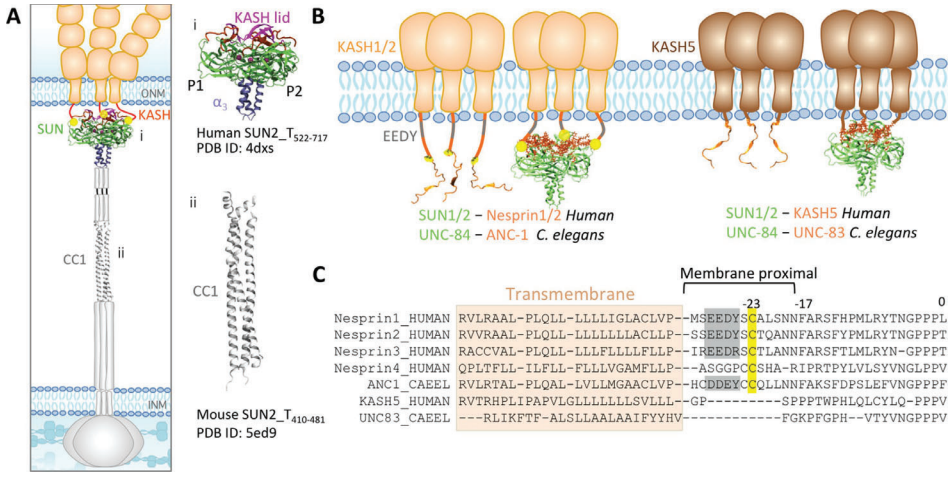

FIGURE 1: Structure of LINC complexes at the nuclear envelope. (A) Schematic representation of LINC complex: inner nuclear membrane (INM) protein SUN, and outer nuclear membrane (ONM) protein KASH. (i) Structure of the human SUN2–KASH2 hexamer and (ii) structure of the coiled-coil (CC1) region of mouse SUN2. (B) Model of SUN–KASH interactions at the ONM. SUN1 or SUN2 in humans binds to Nesprin1, Nesprin2. In *C. elegans*, ANC-1 binds to UNC-84. KASH5 (human), and UNC-83 (*C. elegans*) are shorter in the length of their KASH domains and also bind to SUN1/2 and UUNC-84, respectively. (C) Sequences of transmembrane and KASH domains of longer KASH domains (Nesrpin1–4 in humans and ANC-1 in *C. elegans*), as well as shorter KASH domains (KASH5 in humans and UNC-83, KDP-1, and ZYG-12 in *C. elegans*). The transmembrane domains are highlighted; a conserved C-23 and EEDY motif are highlighted on the sequences of KASH domains of longer lengths, namely, Nesprin1–3 and ANC-1.

For example, in mammals the SUN protein SUN1 can transiently associate with KASH protein KASH5 in the PNS, and with telomeres in the nucleus to mediate microtubule-dependent meiotic chromosome movement (Horn *et al.*, 2013b). On the other hand, SUN1 can bind to Nesprin1 and Nesprin2 to mediate actin-dependent nuclear movement (Padmakumar *et al.*, 2005; Haque *et al.*, 2006; Yu *et al.*, 2011; Nishioka *et al.*, 2016). Similarly, in *Caenorhabditis elegans* SUN protein UNC-84 transiently binds to KASH protein UNC-83 in embryonic hypodermal cells to mediate microtubule-dependent nuclear migration during development (Starr *et al.*, 2001; McGee *et al.*, 2006; Fridolfsson *et al.*, 2010; Bone *et al.*, 2014). Later, the same SUN protein UNC-84 independently binds to a different KASH protein, ANC-1, to anchor nuclei in place for several days (Starr and Han, 2002; Cain *et al.*, 2018).

Crystal structure of the SUN–KASH complex

The crystal structure of the conserved regions of SUN2 in complex with the KASH domain of Nesprin1/2 revealed a trimeric SUN domain that binds to three KASH peptides simultaneously (Figure 1; PDB ID: 4DXS; Sosa *et al.*, 2012, 2013). In this structure, residues 0 to –17 of each KASH peptide of Nesprin2 bind in a groove formed by two neighboring promoters of the SUN trimer. This groove is formed by an ~20 residue β-hairpin extending from the SUN domain of protomer 1, known as the "KASH-lid," and the β-sandwich core of SUN protomer 2 (Figure 1; Sosa *et al.*, 2012). After interactions with this groove, membrane proximal regions consisting of residues –18 to –23 interact exclusively with protomer 2. The SUN–KASH interaction is further enhanced by a disulfide bond formed between cysteine –23 on KASH and conserved cysteine 563 on protomer 2 of SUN2. The remaining membrane proximal residues of KASH between –23 and the transmembrane domain (residues –24 to –30), including a conserved EEDY motif are thought to not interact with SUN.

Despite being well conserved, the luminal domains of KASH5 and UNC-83 are much shorter than the luminal domains of mammalian Nesprins 1–4, *C. elegans* ANC-1 (Figure 1). Both UNC-83 and KASH5 lack the membrane proximal interaction domain, including the conserved cysteine at –23 (Figure 1), which is suggested to form a disulfide bond with the SUN domain (Sosa *et al.*, 2012; Jahed *et al.*, 2015; Cain *et al.*, 2018). Interestingly, UNC-83 and KASH5 have relatively short-term roles in nuclear migration and meiotic chromosome movements, respectively. Herein, we combined in silico molecular dynamics (MD) simulations with in vivo *C. elegans* genetics to explore the role of the KASH domain length in the dynamics and function of LINC complexes. Specifically, we asked: how does the SUN–KASH complex with a shorter KASH domain withstand and transmit tensile forces compared with longer KASH domains? Does swapping long and short KASH domains between ANC-1 and UNC-83 disrupt nuclear positioning? What is the role of the membrane proximal residues in the dynamics of the LINC complex at the membrane? Our results show that the specific length of the KASH domain is important for force transmission and LINC function in vivo and in simulations. Our results also suggest that the membrane proximal EEDY motifs of longer KASH domains may play a role in anchoring the SUN–KASH complex to the ONM.

RESULTS

Longer KASH domains transfer higher forces

We previously developed a molecular model of the LINC complex under tensile forces and showed that the presence of a conserved cysteine residue at position –23 plays an important role in nuclear positioning, and the transmission of maximal forces across the complex (Jahed *et al.*, 2015; Cain *et al.*, 2018; Jahed and Mofrad, 2018). In this work, we set out to determine whether the length of the KASH domain bound to SUN also affects nuclear positioning and force transmission across LINC. To this end, we deleted

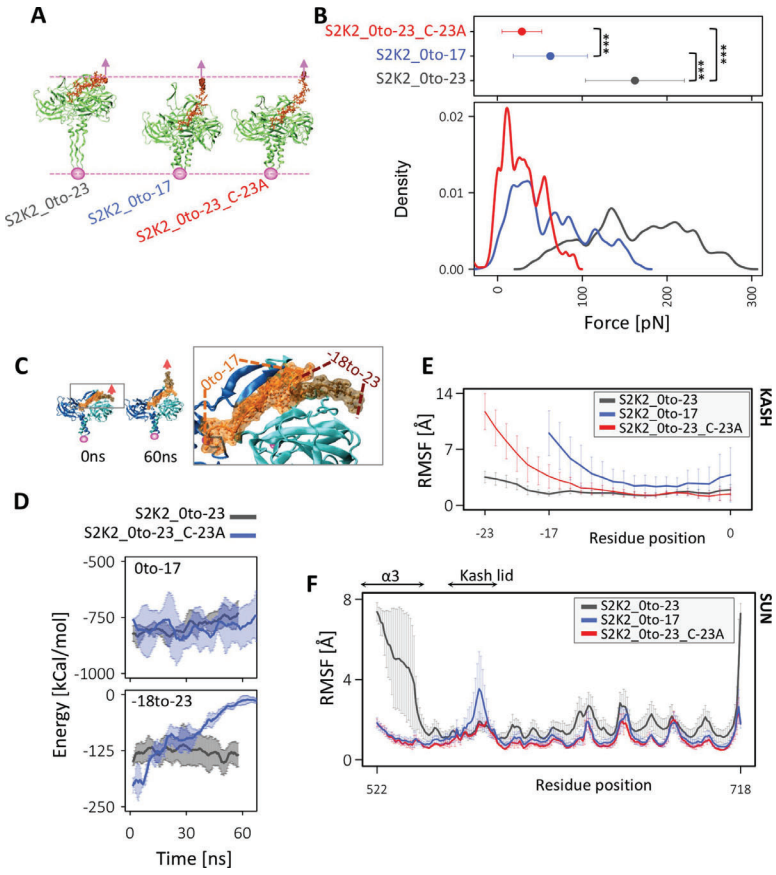

FIGURE 2: Force transmission from KASH to SUN. (A) Representative images of the final simulation frames of each SUN–KASH model after 60 ns of pulling. (B) Magnitude of forces required to pull on KASH for 60 ns at 0.5 Å/ns (i.e., total displacement of 30 Å), average values of force for three independent 60-ns simulation runs are shown at the top (averaged over time and simulation run; error bars correspond to 1 SD), density plots are shown at the bottom; ***, *P* value < 2.2e-16). (C) Conformation of S2K2_0to-23_C-23A model before and after force application showing the detachment of residues –18 to –23 and zoomed view of SUN2–KASH2 interaction showing residues 0 to –17 and residues –18 to –23. (D) Nonbonded interaction energies between residues 0 and –17 and SUN trimer (top) or residues –18 to –23 (bottom) in S2K2_0to-23_C-23A indicating the dispensability of residues –18 to –23 in the absence of C-23. (E) Average RMSF of KASH peptides under force, where average RMSF values of each KASH residue are also averaged over three independent simulation runs, and three KASH peptides of the SUN2–KASH hexamer in each run. Error bars show the range of data over three runs and three KASH peptides in each run. (F) Average RMSF of SUN under force where average RMSF values of each SUN2 residue are also averaged over three independent simulation runs, and three SUN2 protomers of the SUN2–KASH2 hexamer in each run. Error bars show the range of data over three runs and three SUN2 protomers in each run.

residues in the membrane proximal part of KASH domains (–18 to –23) and obtained a model of SUN2 in complex with a shorter length KASH2 peptide (S2K2_0to-17). We then compared the molecular mechanisms of force transmission across this model with the previously developed models of SUN2-KASH2, namely, S2K2_0to-23 and S2K2_0to-23_C-23A by applying forces at a constant velocity of 0.5 Å/ns to the membrane proximal end residue of the KASH peptide in each model (Figure 2A). The forces required to displace the KASH peptide by 30 Å (equivalent to pulling for 60 ns at 0.5 Å/ns) were compared among the three models (Figure 2A). Note that the reported forces were averaged over the 60 ns simulation times as well as over three independent runs for each model where forces were sampled at 2000 fs (Figure 2B). These results suggest that the model with the longest KASH domain, which contains C-23, can withstand average forces that are on average 97 pN higher than S2K2_0to-17 and 131 pN higher than S2K2_0to-23_C-23A (*p* value < 2.2e-16; Figure 2B). Interestingly, a short KASH domain, S2K2_0to-17, endured significantly higher forces than the longer KASH with a cysteine mutation, S2K2_0to-23_C-23A (*p* value < 2.2e-16) suggesting that in the absence of C-23, a longer KASH domain would transmit forces less efficiently than a 17-residue-long KASH domain (Figure 2B). We therefore hypothesized that in the absence of C-23, residues –18 to –23 interfere with the stability of the SUN–KASH complex under tensile forces. This could be a reason why these residues were rapidly lost in KASH peptides that lack C-23 (i.e., mammalian KASH5 and *C. elegans* UNC-83; see Figure 1C). To test this, we calculated the nonbonded interaction energies between two regions of the KASH peptide (region1: residues 0 to –17, or region2: residues –18 to –23; Figure 2C), and the SUN2 trimer in the S2K2_0to-23 and S2K2_0to-23_C-23A models. Our results show that the energies of both regions are highly stable under force in the S2K2_0to-23 model (Figure 2D). Additionally, the energy between region1 and the SUN2 trimer is highly stable under force in the S2K2_0to-23_C-23A model (Figure 2D). However, once C-23 is mutated, region2 consisting of residues –18 to –23 dissociates with the SUN2 trimer under force, and the energies between this region and the SUN2 trimer abruptly reduces to zero (Figure 2, C and D). These results suggest that KASH domains that lack the cysteine residues at position –23, can transmit higher forces if residues between positions –18 and –23 are also absent.

In our previous models of SUN2–KASH2 under tension, we had also shown that forces applied on KASH are directly transmitted to the coiled-coil regions of SUN2 formed by α3, in the S2K2_0to-23 model, but not in the S2K2_0to-23_C-23A. This was evident from the average root-mean-square fluctuations (RMSF) of KASH (Figure 2E) and SUN2 (Figure 2, E and F) in each model under tension. We computed and compared the RMSF of SUN2 and KASH in the S2K2_0to-17 model with the previous models all pulled for 60 ns (30 Å displacement; Figure 2, E and F). As shown in Figure 2E, in the S2K2_0to-23_C-23A model, the highest RMSF values are observed in residues –23 to –17, indicating that forces on residue –23 result in

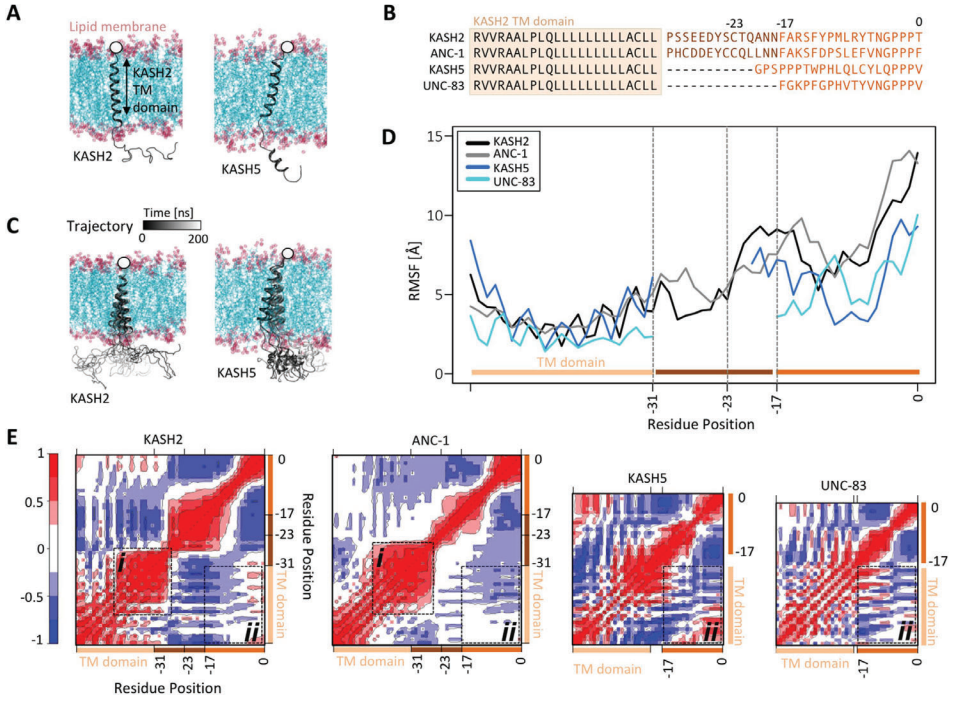

FIGURE 3: Dynamics of KASH peptides at the outer nuclear membrane. (A) Molecular dynamics (MD) model of KASH domain proteins anchored to the outer nuclear membrane (KASH2 and KASH5 are shown on the left and right, respectively). Each structural model consists of the transmembrane domain of KASH2 embedded in the membrane, and the luminal domain of the corresponding KASH domain protein (i.e., KASH2, ANC-1, KASH5, or UNC-83). The position of the Cα atoms of the terminal residue on the cytoplasmic side is fixed (shown with a white circle). (B) Sequences used for modeling the KASH domain proteins KASH2, ANC-1, KASH5, and UNC-83. All models consist of the same transmembrane domain. (C) The trajectories of KASH2 (left) and KASH5 (right) over 200 ns MD simulation time. (D) Average RMSF of KASH2, ANC-1, KASH5, and UNC-83 (a gap is shown between residue –17 or –20 and the TM domain for KASH5 and UNC-83 to better compare the fluctuations of KASH domains). (E) Dynamic cross-correlation heatmap between various regions of each model averaged over MD simulation time. Positive cross-correlations represent fluctuations/displacements in the same direction, whereas negative cross-correlation values represent fluctuations/displacements in the opposite direction. (i) Dynamical cross-correlation between the TM domains and luminal domain residues immediately after the TM domain in KASH2 and ANC-1. (ii) Dynamical cross-correlation between the TM domains and residues 0 to –17 in KASH2, ANC-1, KASH5, and UNC-83.

fluctuations in residues –23 to –17 of the KASH peptide in this model. Similarly, the average RMSF values of residues of the KASH peptide in the S2K2_0to-17 model indicate that forces on the end residue of this KASH peptide (residue –17) result in fluctuations in all residues of the KASH peptide. On the other hand, in the S2K2_0to-23 model, the RMSF values of all KASH residues are very small compared with the other two models indicating that forces on the end residue of KASH do not result in fluctuations of the KASH peptide in this model. Instead, in the S2K2_0to-23 model, forces on KASH result in fluctuations in SUN, and most prominently in the α3 regions as shown in Figure 2F. In the S2K2_0to-17, some forces are transferred to the KASH-lids of SUN, resulting in higher RMSF values for these regions. These results suggest that forces are most efficiently transmitted to the CC regions of SUN in longer KASH peptides.

Conserved EEDY motif links SUN–KASH to the membrane

The results from our model of SUN2–KASH2 under force provided insights into the mechanism of force transfer along the LINC complex for various lengths of KASH peptides. In the next step, we asked whether the length of the KASH peptide would alter the dynamics of KASH at the membrane. To answer this question, we developed a model of luminal KASH domains of KASH2, ANC1, KASH5, and UNC-83 using homology modeling. To model the anchorage of KASH domains to the outer nuclear membrane, we also included a transmembrane (TM) domain in each model (Figure 3, A and B). For all four KASH peptides, the TM domain was modeled using the sequence of the TM domain of KASH2 (Figure 3B). All TM domains were inserted into a lipid bilayer as shown in Figure 3A. After relaxation and equilibration of the model (see *Materials and Methods* for more details), the position of the Cα atoms of the terminal residue on the cytoplasmic side of the TM domains of all four models were fixed in position (Figure 3A). Finally, the dynamics of the four models embedded in the membrane were monitored over 180 ns MD simulation times. Representative trajectories of the positions of KASH2 and KASH5 at the membrane are shown over the 180 ns simulation time in Figure 3C. To compare the dynamics of all four models, we computed the average RMSF of all residues in each KASH peptide (Figure 3D), as well as the average dynamical

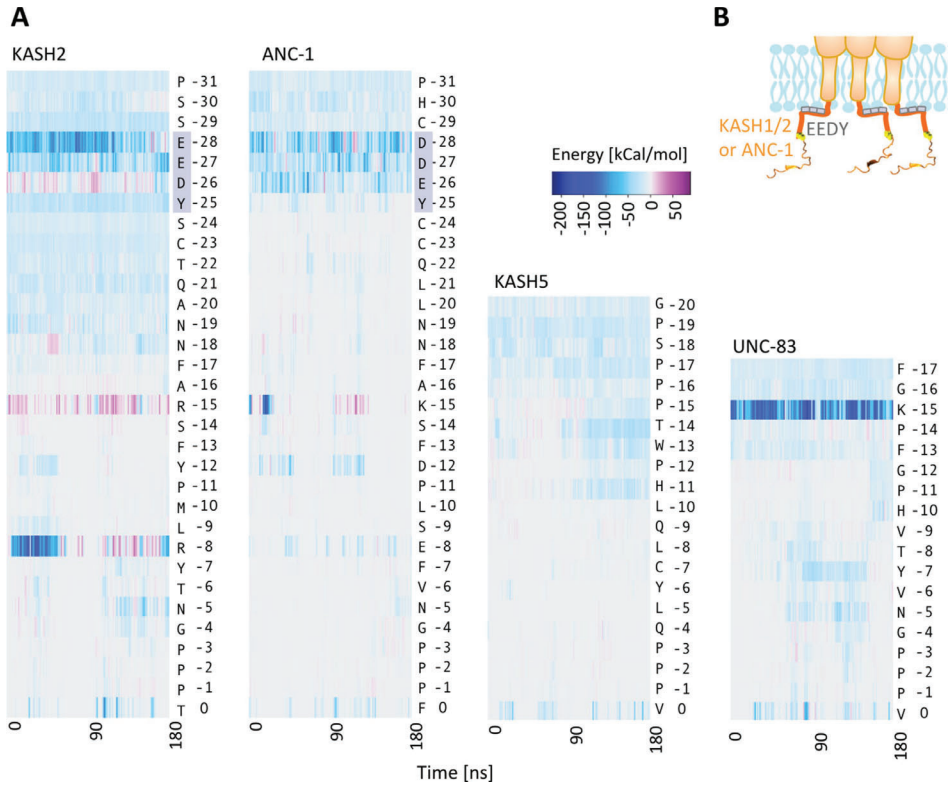

FIGURE 4: Interactions of KASH domains with the outer nuclear membrane. (A) Total nonbonded interaction energies between all residues of the luminal KASH domains of KASH2, ANC-1, KASH5, and UNC-83, and the lipid membrane over simulation time. The conserved EEDY motif in KASH2 and ANC-1 interacts with the membrane. (B) Schematic representation of EEDY motif interacting with the outer nuclear membrane.

cross-correlation of residues over the simulation time (Figure 3E). To better compare the fluctuations of similar residue positions in KASH peptides of various lengths, the RMSF values shown in Figure 3D were aligned based on sequence alignment of the residues as shown in Figure 3B (hence the gap between positions –31 and –20 in KASH5, and –31 and –17 in UNC-83). For KASH2 and ANC-1, the residues immediately after the TM domain (–31 to –23) exhibited lower fluctuations compared with residues –23–0 and the RMSF increased after residue –23 in these two models. The dynamical cross-correlation analysis also revealed a strong positive correlation between the fluctuations of end residues of the TM domain, and the luminal residues immediately after the TM domain in KASH2 and ANC-1 (Figure 3Ei). On the other hand, the TM domain did not show significant correlations with residues 0 to –17 in KASH2 or ANC-1, but showed strong negative correlations between the same regions in KASH5 and UNC-83 (Figure 3Eii). These results suggest that the movement of the KASH peptide is correlated with the TM domain distinctly in the four different KASH peptides. In ANC-1 and KASH2, the residues immediately after the TM domain move in the same direction as the TM domain, in other words their movements are coupled with the movement of their TM domains, and the remaining luminal residues either move in the opposite direction (residues –27 to –14 in KASH2) or show no significant correlation with the TM domain (residues –14–0 in KASH2 and –23–0 in ANC-1). In KASH5 and UNC-83, the KASH domain residues 0 to –17 move in the opposite direction as the TM domain. This is also evident from the trajectory of KASH5 shown in Figure 3C where the luminal domain moved farther to the right as the TM domain moves to the left over the simulation time.

We predicted that interactions with the lipid membrane may be responsible for the reduced fluctuations in residues –31 to –23 in KASH2 and ANC-1, so we calculated the nonbonded interaction energies between each KASH peptide and the lipid membrane. The total pairwise nonbonded interaction energies were calculated between each residue in the four KASH peptides and the lipid membrane over simulation time as shown in Figure 4A. These results show that in KASH2, an EEDY motif forms long-term nonbonded interactions with the lipid membrane over the time of our simulations. ANC-1 also has a similar DDEY motif at the same position, which also interacts with the membrane (Figure 4, A and B). No such domains are present in the KASH domains of KASH5 or UNC-83; however, a lysine residue at position –15 (K-15) in UNC-83 also formed strong nonbonded interactions with the lipid membrane. The results obtained from our MD simulations suggest that the conserved EEDY in longer KASH domains may alter the dynamics of the KASH domain by binding to the lipid membrane.

Swapping KASH domains disrupts LINC function in vivo

Our simulations (Figure 2, A and B) predict that shorter KASH proteins can transmit more forces across LINC complexes than longer

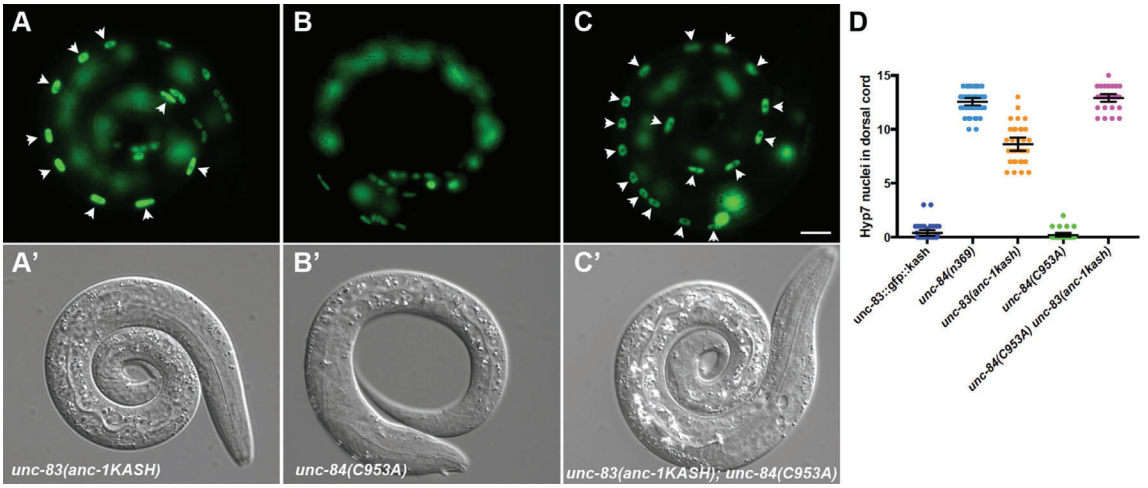

FIGURE 5: Nuclear migration defects in KASH-swap alleles in *C. elegans*. (A–C) Lateral view of L1 animals in a background expressing hypodermal nuclear GFP. (A'–C') Corresponding DIC images of the same animals. (A) *unc-83(yc55[anc-1kash])*; strain UD597. (B) *unc-84(yc35[C953A])*; strain UD605. (C) *unc-83(yc55[anc-1kash]) unc-84(yc35[C953A])*; strain UD604. Arrowheads mark nuclei that are abnormally in the dorsal cord, representing failed migrations. Scale bar, 10 µm. (D) Quantification of nuclear migration defects. Each point represents the number of nuclei in the dorsal cord of a single animal. Means with 95% CI error bars are shown.

KASH domains with mutant cysteines at –23. We set out to test this prediction in the context of a live, developing organism where nuclear positioning is easily followed—the hypodermis of *C. elegans* (Starr and Han, 2002; Fridolfsson *et al.*, 2010). We investigated how changing the lengths of the UNC-83 or ANC-1 KASH domains affected their in vivo function in *C. elegans* developing hypodermal cells using our established nuclear migration and nuclear anchorage assays (Bone *et al.*, 2014; Cain *et al.*, 2018; Fridolfsson *et al.*, 2018). We first used our nuclear migration assay to test the ability of different KASH peptides to mediate nuclear movements in embryonic hyp7 precursors. We hypothesized that longer KASH domains with a cysteine at –23 would form a stable interaction with SUN proteins and mediate nuclear migration normally. Unexpectedly, replacing the shorter KASH domain in *unc-83* with the longer KASH from *anc-1* to make *unc-83 (anc-1KASH)*, caused a significant nuclear migration defect with 8.4 ± 0.9 (mean ± 95% CI) nuclei in the dorsal cord (Figure 5, A and D). This *unc-83(anc-1KASH)* nuclear migration defect was intermediate, significantly less severe than *unc-84* or *unc-83* null animals (Starr *et al.*, 2001; Bone *et al.*, 2014) but significantly more defective than wild type (Figure 5D; $P < 0.0001$). Our simulations indicated that LINC complexes with longer KASH domains including a cysteine at –23 are able to transmit more force than shorter KASH domains, but our in vivo experiments showed that the longer KASH domain with a –23 cysteine somehow interferes with nuclear migration in embryonic hyp7 precursors. Thus, the longer ANC-1 KASH domain might inhibit the migratory function of UNC-83(ANC-1 KASH) by forming overly stabilized SUN–KASH interactions containing a disulfide bond between UNC-83(ANC-1KASH) and UNC-84.

We then tested the extent to which removing the possibility of a disulfide bond between UNC-83 and UNC-84 might affect nuclear migration. We previously showed that mutating of the conserved cysteine in the SUN domain of UNC-84 in *unc-84(C953A)* mutants had no effect on nuclear migration in the presence of the shorter, wild-type KASH domain of UNC-83 (Cain *et al.*, 2018). We engineered a LINC complex with a long KASH domain but a mutation in the cysteine in the SUN domain so that no disulfide bond could form. *unc-84(C963A); unc-83(anc-1KASH)* double mutants had a completely penetrant nuclear migration defect (Figure 5, C and D). Thus, consistent with our simulations (Figure 2), in the absence of a disulfide bond between SUN and KASH in vivo, a short KASH domain appears more functional than a long one.

After nuclei move using the KASH protein UNC-83, they anchor in place using the giant KASH protein ANC-1 (Starr and Han, 2002). We tested the hypothesis that the longer KASH domain of ANC-1 is required for efficient nuclear anchorage. We replaced the long KASH domain of endogenous ANC-1 with the shorter UNC-83 KASH domain to make *anc-1(unc-83KASH)* mutant animals. We observed a significant nuclear anchorage defect with 11.5 ± 2.0 (mean ± 95% CI) percent of nuclei clustered in *anc-1(unc-83KASH)* animals compared with 2.4 ± 1.3 percent of nuclei clustered in wild type ($P = 0.0005$ in a one-way analysis of variance with multiple comparisons; Figure 6, A, C, and E). However, the *anc-1(unc-83KASH)* nuclear anchorage defect was not as severe as the *unc-84(null)* with 26.4 ± 5.3 percent clustered nuclei ($P < 0.0001$; Figure 6, B, C, and E), supporting our simulations that a short KASH is at least partially functional. Alternatively, we deleted 11 residues from –28 to –18 of the endogenous ANC-1 KASH domain to make *anc-1(ΔD-N)* mutant animals, which had 15.0 ± 2.2 percent nuclei clustered (Figure 6, D and E). Thus, both *anc-1(ΔD-N)* and *anc-1(unc-83KASH)* had similar defects ($P = 0.40$), suggesting that either short KASH domain is partially functional to anchor nuclei.

In conclusion, our in vivo data are consistent with a model that a short KASH domain can transmit forces more efficiently than a long KASH without a disulfide bond. However, it is important to note that comparing the function of short KASH domains to long KASH

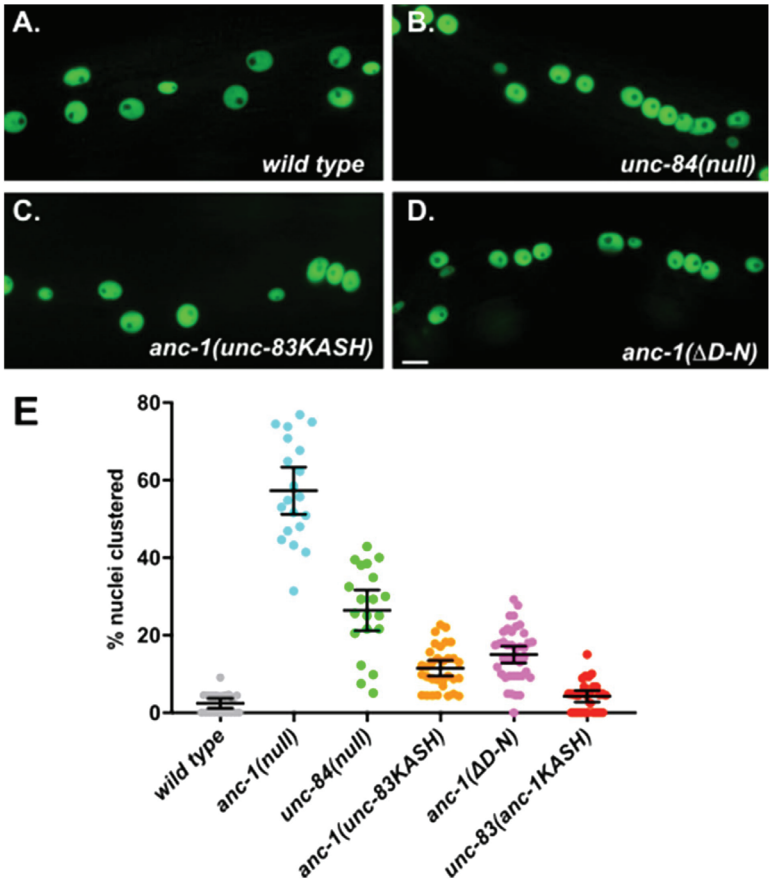

FIGURE 6: Nuclear anchorage defects in KASH-swap alleles in *C. elegans*. (A–D) Lateral views of young adult *C. elegans* are shown. Hypodermal nuclei are marked with nuclear GFP from *ycEx249* in the following genetic backgrounds: (A) wild type; strain UD522. (B) *unc-84(n369)*; strain UD532. (C) *unc-83(yc55[anc-1kash])*; strain UD582. (D) *anc-1(yc60[ΔD-N])*; strain UD589. Scale bar, 10 μm. (E) Quantification of nuclear anchorage defects. Each point represents the percentage of clustered nuclei in one side of a single animal. Means with 95% CI error bars are shown.

domains stabilized by disulfide bonds to SUN proteins is more difficult to interpret, because other factors may be involved in vivo that are missing in our simulations.

Transfer of forces beyond the SUN domain

We showed that for long KASH peptides, forces on the terminal residue of the KASH domain were transferred to the trimeric CC domains of SUN (Figure 2). We next asked how tensile forces are further transmitted across the trimeric CC domains of SUN. Using the solved crystal structure of CC1 of SUN2, we applied tensile forces on the C-terminal residue of each of its three protomers, namely, P1, P2 and P3, while fixing their N-terminal residues (Figure 7A). To determine the dynamics of CC1 under force, we compared the per-residue RMSF values of P1, P2, and P3 in force and no force conditions (Figure 7B). We expected the forces applied at the C-terminus to be further transferred to the N-terminus of CC1. Indeed, the highest fluctuations were observed at the two terminal residues of each protomer when forces were applied, indicating that some of the forces at the C-terminus are directly transferred to the N-terminus. Surprisingly, the RMSF values of residues at the central core of each protomer of CC1 were significantly lower under force as compared with a no force condition (Figure 7B), indicating that the fluctuations in these regions are reduced when CC1 is under tensile forces (Figure 7B). Next, to obtain further insights into the dynamics of CC1 under force and to determine how the fluctuations of various residues across protomers are coupled, we also calculated the dynamical cross-correlations between residues on P1, P2, and P3 in our simulations (Figure 7, C and D). Our results show that the residues at the central core of CC1 exhibit strong positive correlations (i.e., move together in the same direction). On the other hand, the C-terminal residues on which forces are applied show strong negative correlations with the residues at the central core of CC1 (Figure 7, C and D). Specifically, the C-terminal residue of each protomer correlates negatively with the central residues of itself, as well the other two protomers (P2 and P3; Figure 7D), indicating that these regions move in opposite directions during our simulations. These results suggest that cytoskeletal forces may be translated to the residues at the central core of CC1, resulting in some conformational changes in these regions.

DISCUSSION

There is direct evidence that the LINC complex is subject to tension at the nuclear envelope, and that the transmission of forces across the LINC complex is essential for several cellular functions (Grady *et al.*, 2005; Bone *et al.*, 2014; Arsenovic *et al.*, 2016; Arsenovic and Conway, 2018). Various KASH proteins pair with SUN proteins to mediate distinct functions of the cell (Jahed *et al.*, 2016, 2018). In addition to their distinct cytoplasmic domains, the transluminal domains of KASH proteins which bind to SUN proteins are also different in length. Specifically, shorter KASH proteins lack a conserved membrane proximal domain that is responsible for additional interactions with SUN proteins (Figure 1). Our results suggest that the lack of this membrane proximal domain reduces the amount of force that the SUN–KASH complex can withstand. Furthermore, our MD simulations show that an EEDY motif, conserved in the membrane proximal domain of long KASH domains including Nesprin1–3 and ANC1, can interact with the lipid membrane (Figures 1 and 4). The interaction of KASH with the lipid membrane could provide additional anchorage points, which would potentially provide even higher LINC stability under force. In agreement with these findings, we found that the membrane proximal domain of ANC-1 is required for nuclear anchorage in *C. elegans* and a shorter KASH domain is only partially functional

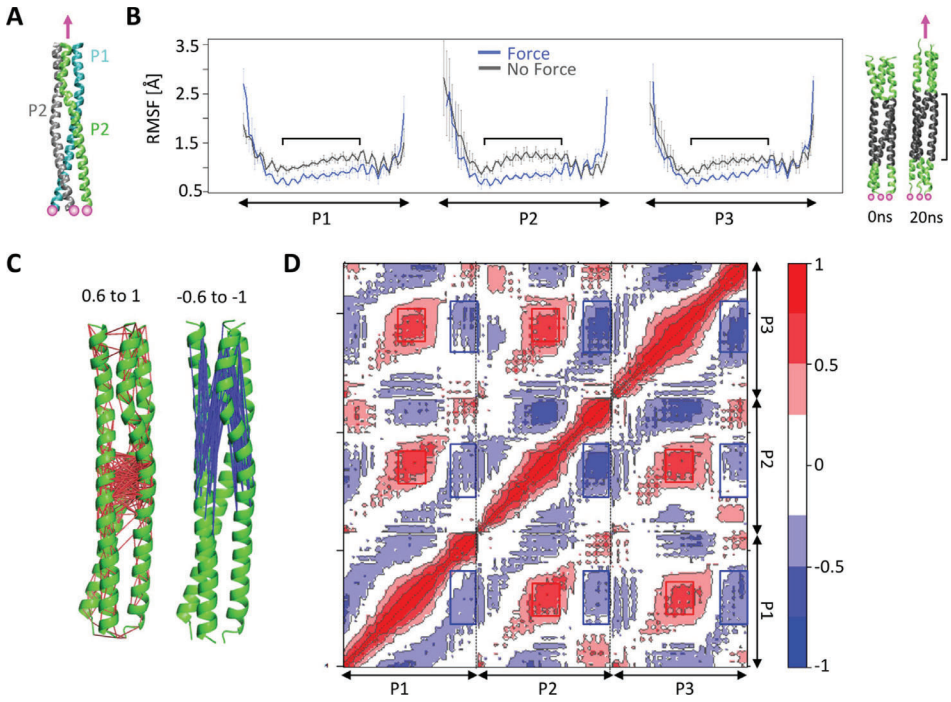

FIGURE 7: Force transmission across the CC domain of SUN2. (A) Model of CC1 of SUN2 under force. Three protomers in the SUN2 CC1 trimer (P1, P2, and P3) were pulled at a constant velocity in the direction shown with a pink arrow. Forces were applied to the C-terminal residue of each protomer while the Cα residues of the N-terminal residues were fixed (shown with pink circles). (B) RMSF of CC1 protomers (P1, P2, and P3) under force, compared with a no force control. Average values are shown for three independent simulation runs, and error bars show data spread. Regions where the RMSF is different between the two conditions are indicated on the plot and mapped onto the structure on the left. (C, D) Dynamic cross-correlation between various regions of each model under force, averaged over MD simulation time. Positive cross-correlations (red) represent fluctuations/displacements in the same direction, whereas negative cross-correlation values (blue) represent fluctuations/displacements in the opposite direction. The residues that are positively correlated with a correlation value between 0.6 and 1 are connected with red lines and residues that are negatively cross-correlated with a correlation value between –0.6 and –1 are connected with blue lines in C, while corresponding residues are represented with red and blue boxes in D.

to anchor nuclei. Although our results suggest that this membrane proximal EEDY domain is important for the function of longer KASH proteins, it is important to note that in mammals, Nesprin4 lacks this membrane proximal EEDY motif (Figure 1). Nesprin4 is known to be important for microtubule-dependent nuclear positioning (Roux *et al.*, 2009; Horn *et al.*, 2013a). However, compared with Nesprin1 and Nesprin2, the dynamics of Nesprin4 are poorly understood and the implications of missing the EEDY motif between the cysteine and the transmembrane helix are unclear and require further investigations.

Why would different LINC-dependent processes require KASH domains of various lengths? There are several differences between the various processes mediated by different SUN–KASH pairs. One major difference is the time scale of the SUN–KASH interaction, which is only a few minutes for KASH5 during meiosis prophase I, and UNC-83 during nuclear migration in development. On the other hand, Nesprin2 and ANC-1 are required for their respective functions for up to several days. Therefore, one explanation is that the additional interactions between the membrane proximal domains of longer KASH domains, with SUN or the lipid membrane, facilitates the more long-term functions of the LINC complexes that employ KASH proteins with longer KASH domains. Unexpectedly, we also found that the longer KASH domain of ANC-1 can significantly inhibit the migratory function of UNC-83 (Figure 5, A and D), which suggests that the addition of a membrane proximal domain to short KASH proteins can also inhibit their function. These results further confirm that the specific length of the KASH domain is important for specific LINC complex functions. An undesirable formation of disulfide bonds between SUN and the membrane proximal domain of longer KASH, or potential interactions of the EEDY motif of the membrane proximal domain of KASH with the membrane may be the mechanism by which longer KASH domains inhibit functions that require shorter KASH domains, but this would require further testing. In this work, we discuss the differences in the luminal KASH domains in the regulation of LINC complexes. However, the differences between SUN proteins are also important to note. Although the KASH binding sites of SUN1 and SUN2 are highly conserved (Lei *et al.*, 2009; Hennen *et al.*, 2017, 2018; Jahed *et al.*, 2018), there are several structural differences in these proteins that could lead to distinct functions of SUN1 and SUN2

(Jahed *et al.*, 2018; Xu *et al.*, 2018). The pairing of KASH domains with distinct SUN domains could further diversify the functions and regulations of LINC complexes and would be intriguing to investigate further.

It is important to note that there are also several other important differences between the functions of ANC-1 and UNC-83 in nuclear anchorage and migration. For example, ANC-1 anchors the LINC complex to the actin cytoskeleton during nuclear anchorage, whereas UNC-83 is linked to microtubules through motor proteins. Therefore, the magnitude and direction of forces generated during these two distinct processes may also vary and may explain the higher force tolerance of longer KASH proteins for their respective functions.

Finally, our MD results imply that forces are more efficiently transmitted from KASH to the CC regions of SUN in longer KASH domains (Figure 2). Our simulations show that forces on the CC region of SUN can induce conformational changes in the CC domains (Figure 7). Interestingly, studies have shown that the CC domain of SUN2 is not a stable trimeric coiled coil in solution, due to structural defects such as hydrophilic residues in its interhelical packing core (Nie *et al.*, 2016). Our simulations suggest that tensile forces on the LINC complex may induce conformational changes in the interhelical packing core of the CC domains, and hence, the conformation of these regions is likely different under force than that observed in solution.

In summary, we show that the presence or absence of a membrane proximal domain in KASH proteins plays an important role in the specific functions of LINC under force.

MATERIALS AND METHODS

Model of SUN2-KASH2 complex

We downloaded the solved structure of the human SUN2 trimer in complex with three KASH peptides of human Nesprin2 from the Protein Data Bank (PDB ID: 4DXS; Sosa *et al.*, 2012) and visualized using visual molecular dynamics (VMD) software (Humphrey *et al.*, 1996). The KASH peptides in this solved structure were 23 residues long and this modeled structure was accordingly labeled as S2K2_0to-23 in the text. A structural model for a shorter KASH (S2K2_0to-17) in complex with SUN2 was developed by residue deletion in VMD software (Humphrey *et al.*, 1996). The model for KASH in complex with cysteine mutant SUN2 (S2K2_0to-23_C-23A) was also developed as before using the mutator tool in VMD (Jahed *et al.*, 2015; Cain *et al.*, 2018). To apply tensile forces on the SUN–KASH complex we attached a dummy atom to the position of the center of mass of the N-terminal residue of the respective KASH peptide at position –23 for S2K2_0to-23 and S2K2_0to-23_C-23A, or position –17 for S2K2_0to-17, via a virtual spring. The position of the C-terminal residue of SUN2 was also fixed in all models. We then measured the forces between the dummy atom and C-23 using NAno-scale Molecular Dynamics (NAMD; Phillips *et al.*, 2005) as the dummy atom was moved at a constant velocity of 0.05 m/s. A moving window average was applied to the force data using the filter function in R with convolution. All plots were prepared using R software.

Model of KASH in the membrane

Peptides of various lengths were modeled using the Phyre2 Protein Fold Recognition Server in Intensive mode (Kelley *et al.*, 2015). The sequence of the transmembrane domain of Nesprin2 was used for all models, which preceded the KASH domains of KASH2, ANC-1, KASH5, and UNC-83 (sequences are shown in Figure 3B). The transmembrane domain was predicted as an alpha helix for all models and all KASH domains were predicted to be disordered as expected. The modeled KASH peptides were anchored to a diacylglycerol and phospholipid membrane (POPC), which was modeled using the VMD membrane plug-in. To remove any overlap between the modeled disordered KASH domains and the lipids, we first fixed all residues of the alpha helical transmembrane domains of all models and applied a constant velocity to the end residue of each KASH peptide at a constant velocity of 0.05 m/s. The alpha helical transmembrane domains of all four KASH peptides were then inserted perpendicular to the lipid membrane and overlapping lipids were removed. The system was then solvated and ionized and all waters in the membrane region were deleted. Because we assembled the system manually, several minimization and equilibration steps were taken before the final simulations presented in the *Results* section. First, we performed a simulation in which we fixed all atoms in the system except lipid tails to obtain a fluid-like lipid bilayer (Humphrey *et al.*, 1996; Phillips *et al.*, 2005). Second, we performed a minimization and equilibration step in which harmonics constraints were applied to the four KASH proteins permitting lipids, water, and ions to adapt to the shape of the proteins. Third, the constraints on the proteins were removed and the full system was equilibrated for 60 ns. The average RMSD values of each KASH protein were monitored during equilibration and plateaued in the 60-ns simulation times. In the final simulations, the end residues of the transmembrane domains were fixed in place to resemble the immobile large cytoplasmic domains of KASH proteins, and simulations were conducted for 180 ns.

MD simulations

MD simulations were performed using NAMD scalable MD with the CHARMM force field (Phillips *et al.*, 2005). Periodic boundary conditions were applied in all three directions. To calculate long-range electrostatic interactions during MD simulations with periodic boundary conditions, particle mesh Ewald (PME) was used with a 1-Å maximum space between grid points. Simulations were performed at a constant temperature of 310 K and a constant pressure of 1 atm using the Langevin piston method and Hoover's method during minimization and equilibration.

Trajectory analyses

Dynamical residue cross-correlation heatmaps and atomic RMSF over MD trajectories were evaluated using the rmsf() function in the R Bio3D package (Grant *et al.*, 2006). Total nonbonded interaction energies (electrostatic and van der Waals) were calculated using VMD and NAMD energy with the cutoff for nonbonded interactions set to 12 Å, and using a switching function with a switching distance of 10 Å (Phillips *et al.*, 2005). All plots were generated using the plot() or heatmap.2() functions of the R gplot package.

C. *elegans* strains and CRISPR/Cas9 editing

C. elegans were cultured on nematode growth medium plates spotted with OP50 bacteria (Stiernagle, 2006). Strains used are listed in Table 1. Some strains were provided by the *Caenorhabditis* Genetics Center, funded by the National Institutes of Health Office of Research Infrastructure Programs (P40 OD010440). Knock-in strains were constructed by CRISPR/Cas9 genome editing using the *dpy-10* co-CRSPR technique (Arribere *et al.*, 2014; Paix *et al.*, 2016). The *anc-1(yc54[unc-83kash])*, *unc-83(yc55[unc-83::gfp::anc-1kash])*, and *anc-1(yc60[ΔD-N])* alleles were generated by injecting CRISPR guide RNAs (crRNAs; Table 2; synthesized by IDT or Dharmacon) precomplexed with purified Cas9 protein (UC Berkeley QB3) and universal tracrRNA (IDT or Dharmacon) along with repair

Strain	Genotype	Reference
N2	Wild type	Brenner, 1974
UD399	*unc-84(n369) X; ycIs10[$p_{col\text{-}10}$nls::gfp::lacZ]*	Bone *et al.*, 2014
UD473	*unc-83(yc26[unc-83::gfp::kash+LoxP])V*	Bone *et al.*, 2016
UD522	*ycEx249[$p_{col\text{-}19}$nls::gfp::lacZ, $p_{myo\text{-}2}$mCherry]*	Cain *et al.*, 2018
UD532	*unc-84(n369) X; ycEx249[$p_{col\text{-}19}$nls::gfp::lacZ, $p_{myo\text{-}2}$mCherry]*	Cain *et al.*, 2018
UD538	*anc-1(e1873) I; ycEx249[$p_{col\text{-}19}$nls::gfp::lacZ, $p_{myo\text{-}2}$mCherry]*	Cain *et al.*, 2018
UD582	*unc-83(yc55[unc-83::gfp::anc-1kash+LoxP])V; ycEx249[$p_{col\text{-}19}$nls::gfp::lacZ, $p_{myo\text{-}2}$mCherry]*	This study
UD588	*anc-1(yc54[unc-83kash])I; ycEx249[$p_{col\text{-}19}$nls::gfp::lacZ, $p_{myo\text{-}2}$mCherry]*	This study
UD589	*anc-1(yc60[ΔD-N])I; ycEx249[$p_{col\text{-}19}$nls::gfp::lacZ, $p_{myo\text{-}2}$mCherry]*	This study
UD594	*anc-1(yc54[unc-83kash])I; unc-83(yc55[unc-83::gfp::anc-1kash+LoxP])V; ycEx249[$p_{col\text{-}19}$nls::gfp::lacZ, $p_{myo\text{-}2}$mCherry]*	This study
UD597	*unc-83(yc55[unc-83::gfp::anc-1kash+LoxP])V; ycIs10[$p_{col\text{-}10}$nls::gfp::lacZ]*	This study
UD605	*unc-84(yc35[unc-84::(C953A)::gfp])X; ycIs10[$p_{col\text{-}10}$nls::gfp::lacZ]*	This study
UD604	*unc-83(yc55[unc-83::gfp::anc-1kash+LoxP])V unc-84(yc35[unc-84::(C953A)::gfp])X; ycIs10[$p_{col\text{-}10}$nls::gfp::lacZ]*	This study
UD603	*unc-83(yc26[unc-83::gfp::kash];ycI9[$P_{col\text{-}10}$nls::gfp::lacZ]*	This study

TABLE 1: *C. elegans* strains in this study.

Gene target	crRNA sequence	DNA repair template sequence	Starting strain	New strain	Reference
anc-1	acuuaugggagcc-gcuuguu	caggtttgtttatatttttttaatattaataactaatgtctctcattttcaggcactgctt-gttctcctcatgggagctgcctgccttgttttcggaaaaccatttggtccgcatgta-acctatgtgaatggaccaccaccggtttaatctttaatttttttattttcattactattcac-tattgtttcattcatcatgaacctgcccccatacatcccagttg	N2	UD580	This study
unc-83	ccgcauguaaccuau-gugaa	ctggcagcgctcgcagcgattttctattatcacgtgccacattgcgacgacgag-tactgttgccaacttctcaataatttcgctaaaagttttgacccttcgctagaattcgta-aacgggccaccaccattttaactgaatcatcagtattctgattgaaatccc	UD473	UD581	This study
anc-1	caguacucgucgucg-caaug	caggcactgcttgttctacttatgggagccgcttgtttggttccacactgttttgc-taagagttttgacccttcgctagaattcgtaaacgggccaccaccatttttaatc	N2	UD592	This study
dpy-10	gcuaccauaggcac-cacgag	cacttgaacttcaatacggcaagatgagaatgactggaaaccgtaccgcatgcggt-gcctatggtagcggagcttcacatggcttcagaccaacagcctat	Co-CRISPR		Arribere *et al.*, 2014

TABLE 2: crRNA and repair templates used in this study.

templates as single-strand DNA oligonucleotide (ssODN) or double-strand DNA (dsDNA; Table 2; IDT or Dharmacon) into *C. elegans* gonads (Paix *et al.*, 2015, 2016). crRNA and repair templates against *dpy-10* were coinjected to identify animals where the Cas9 was active (Arribere *et al.*, 2014; Paix *et al.*, 2016). Edited animals were identified by PCR and restriction digests. The edited strains were backcrossed to UD522 (Cain *et al.*, 2018) to lose *dpy-10* mutations and introduce *ycEx249[$p_{col\text{-}19}$nls::gfp::lacZ, $p_{myo\text{-}2}$mCherry]* to mark hypodermal nuclei with GFP.

Nuclear migration and anchorage assays in *C. elegans*

Nuclear migration in embryonic hyp7 precursors was quantified by counting nuclei abnormally localized in the dorsal cord of L1 larvae as previously described (Starr *et al.*, 2001; Bone *et al.*, 2014). Hyp7 nuclear anchorage was assayed in adult animals expressing nuclear GFP from *ycEx249[$p_{col\text{-}19}$nls::gfp::lacZ, $p_{myo\text{-}2}$mCherry]*; nuclei were scored as clustered if one nucleus contacted another along the longitudinal axis of the worm (Cain *et al.* 2018). Contacts between nuclei on the perpendicular axis were not counted, as the marker could not distinguish seam cell nuclei in proximity to hyp7 nuclei from clusters of hyp7 nuclei. Only nuclei situated between the pharynx and the anus were counted. Only one lateral side of each animal was scored.

ACKNOWLEDGMENTS

This work was supported by the National Science Foundation through grant CMMI-1538707 and the National Institutes of Health through grant R01 GM073874. In addition, this research used resources of the National Energy Research Scientific Computing Center (NERSC), a Department of Energy Office of Science user facility supported by the Office of Science of the United States Department of Energy under contract no. DE-AC02-05CH11231.

REFERENCES

Arribere JA, Bell RT, Fu BXH, Artiles KL, Hartman PS, Fire AZ (2014). Efficient marker-free recovery of custom genetic modifications with CRISPR/Cas9 in *Caenorhabditis elegans*. Genetics 198, 837–846.

Arsenovic PT, Conway DE (2018). The LINC complex. Methods Mol Biol 1840, 59–71.

Arsenovic PT, Ramachandran I, Bathula K, Zhu R, Narang JD, Noll NA, Lemmon CA, Gundersen GG, Conway DE (2016). Nesprin-2G, a component of the nuclear LINC complex, is subject to myosin-dependent tension. Biophys J 110, 34–43.

Bone CR, Chang Y-T, Cain NE, Murphy SP, Starr DA (2016). Nuclei migrate through constricted spaces using microtubule motors and actin networks in *C. elegans* hypodermal cells. Development 143, 4193–4202.

Bone CR, Tapley EC, Gorjanacz M, Starr DA (2014). The *Caenorhabditis elegans* SUN protein UNC-84 interacts with lamin to transfer forces from the cytoplasm to the nucleoskeleton during nuclear migration. Mol Biol Cell 25, 2853–2865.

Brenner S (1974). *Caenorhabditis elegans*. Methods 77, 71–94.

Cain NE, Jahed Z, Schoenhofen A, Valdez VA, Elkin B, Hao H, Harris NJ, Herrera LA, Woolums BM, Mofrad MRK, *et al.* (2018). Conserved SUN-KASH interfaces mediate LINC complex-dependent nuclear movement and positioning. Curr Biol 28, 3086–3097.e4.

Cain NE, Tapley EC, McDonald KL, Cain BM, Starr DA (2014). The SUN protein UNC-84 is required only in force-bearing cells to maintain nuclear envelope architecture. J Cell Biol 206, 163–172.

Crisp M, Liu Q, Roux K, Rattner JB, Shanahan C, Burke B, Stahl PD, Hodzic D (2006). Coupling of the nucleus and cytoplasm: role of the LINC complex. J Cell Biol 172, 41–53.

Fridolfsson HN, Herrera LA, Brandt JN, Cain NE, Hermann GJ, Starr DA (2018). The LINC complex. Methods Mol Biol 1840, 163–180.

Fridolfsson HN, Ly N, Meyerzon M, Starr DA (2010). UNC-83 coordinates kinesin-1 and dynein activities at the nuclear envelope during nuclear migration. Dev Biol 338, 237–250.

Grady RM, Starr DA, Ackerman GL, Sanes JR, Han M (2005). Syne proteins anchor muscle nuclei at the neuromuscular junction. Proc Natl Acad Sci USA 102, 4359–4364.

Grant BJ, Rodrigues APC, ElSawy KM, McCammon JA, Caves LSD (2006). Bio3d: an R package for the comparative analysis of protein structures. Bioinformatics 22, 2695–2696.

Haque F, Lloyd DJ, Smallwood DT, Dent CL, Shanahan CM, Fry AM, Trembath RC, Shackleton S (2006). SUN1 interacts with nuclear lamin A and cytoplasmic nesprins to provide a physical connection between the nuclear lamina and the cytoskeleton. Mol Cell Biol 26, 3738–3751.

Hennen J, Hur KH, Saunders CA, Luxton GWG, Mueller JD (2017). Quantitative brightness analysis of protein oligomerization in the nuclear envelope. Biophys J 113, 138–147.

Hennen J, Saunders CA, Mueller JD, Luxton GWG (2018). Fluorescence fluctuation spectroscopy reveals differential SUN protein oligomerization in living cells. Mol Biol Cell 29, 1003–1011.

Horn HF, Brownstein Z, Lenz DR, Shivatzki S, Dror AA, Dagan-Rosenfeld O, Friedman LM, Roux KJ, Kozlov S, Jeang KT, *et al.* (2013a). The LINC complex is essential for hearing. J Clin Invest 123, 740–750.

Horn HF, Kim DI, Wright GD, Wong ESM, Stewart CL, Burke B, Roux KJ (2013b). A mammalian KASH domain protein coupling meiotic chromosomes to the cytoskeleton. J Cell Biol 202, 1023–1039.

Humphrey W, Dalke A, Schulten K (1996). VMD—visual molecular dynamics. J Mol Graph 14, 33–38.

Jahed Z, Fadavi D, Vu UT, Asgari E, Luxton GWG, Mofrad MRK (2018). Molecular insights into the mechanisms of SUN1 oligomerization in the nuclear envelope. Biophys J 114, 1190–1203.

Jahed Z, Mofrad MR (2019). The nucleus feels the force, LINCed in or not! Curr Opin Cell Biol 58, 114–119.

Jahed Z, Mofrad MRK (2018). Mechanical LINCs of the nuclear envelope: where SUN meets KASH. Extrem Mech Lett 20, 99–103.

Jahed Z, Shams H, Mofrad MRK (2015). A disulfide bond is required for the transmission of forces through SUN-KASH complexes. Biophys J 109, 501–509.

Jahed Z, Soheilypour M, Peyro M, Mofrad MRK (2016). The LINC and NPC relationship—it's complicated! J Cell Sci 129, 3219–3229.

Kelley LA, Mezulis S, Yates CM, Wass MN, Sternberg MJE (2015). The Phyre2 web portal for protein modelling, prediction and analysis. Nat Protoc 10, 845–858.

Kim DI, Birendra K, Roux KJ (2015). Making the LINC: SUN and KASH protein interactions. Biol Chem 396, 295–310.

Lei K, Zhang X, Ding X, Guo X, Chen M, Zhu B, Xu T, Zhuang Y, Xu R, Han M (2009). SUN1 and SUN2 play critical but partially redundant roles in anchoring nuclei in skeletal muscle cells in mice. Proc Natl Acad Sci USA 106, 10207–10212.

Lombardi ML, Jaalouk DE, Shanahan CM, Burke B, Roux KJ, Lammerding J (2011). The interaction between nesprins and sun proteins at the nuclear envelope is critical for force transmission between the nucleus and cytoskeleton. J Biol Chem 286, 26743–26753.

McGee MD, Rillo RS, Anderson A, Starr DA (2006). UNC-83 is a KASH protein required for nuclear migration and is recruited to the outer nuclear membrane by a physical interaction with the SUN protein UNC-84. Mol Biol Cell 17, 1790–1801.

Nie S, Ke H, Gao F, Ren J, Wang M, Huo L, Gong W, Feng W (2016). Coiled-coil domains of SUN proteins as intrinsic dynamic regulators. Structure 24, 80–91.

Nishioka Y, Imaizumi H, Imada J, Katahira J, Matsuura N, Hieda M (2016). SUN1 splice variants, SUN1_888, SUN1_785, and predominant SUN1_916, variably function in directional cell migration. Nucleus 7, 572–584.

Padmakumar VC, Libotte T, Lu W, Zaim H, Abraham S, Noegel AA, Gotzmann J, Foisner R, Karakesisoglou I (2005). The inner nuclear membrane protein Sun1 mediates the anchorage of Nesprin-2 to the nuclear envelope. J Cell Sci 118, 3419–3430.

Paix A, Folkmann A, Rasoloson D, Seydoux G (2015). High efficiency, homology-directed genome editing in *Caenorhabditis elegans* using CRISPR-Cas9 ribonucleoprotein complexes. Genetics 201, 47–54.

Paix A, Schmidt H, Seydoux G (2016). Cas9-assisted recombineering in *C. elegans*: genome editing using in vivo assembly of linear DNAs. Nucleic Acids Res 44, e128.

Phillips JC, Braun R, Wang W, Gumbart J, Tajkhorshid E, Villa E, Chipot C, Skeel RD, Kalé L, Schulten K (2005). Scalable molecular dynamics with NAMD. J Comput Chem 26, 1781–1802.

Roux KJ, Crisp ML, Liu Q, Kim D, Kozlov S, Stewart CL, Burke B (2009). Nesprin 4 is an outer nuclear membrane protein that can induce kinesin-mediated cell polarization. Proc Natl Acad Sci USA 106, 2194–2199.

Sosa BA, Kutay U, Schwartz TU (2013). Structural insights into LINC complexes. Curr Opin Struct Biol 23, 285–291.

Sosa BA, Rothballer A, Kutay U, Schwartz TU (2012). LINC complexes form by binding of three KASH peptides to domain interfaces of trimeric SUN proteins. Cell 149, 1035–1047.

Starr DA, Han M (2002). Role of ANC-1 in tethering nuclei to the actin cytoskeleton. Science 298, 406–409.

Starr DA, Hermann GJ, Malone CJ, Fixsen W, Priess JR, Horvitz HR, Han M (2001). Unc-83 encodes a novel component of the nuclear envelope and is essential for proper nuclear migration. Development 128, 5039–5050.

Stiernagle T (2006). Maintenance of *C. elegans*. WormBook, 1–11.

Xu Y, Li W, Ke H, Feng W (2018). Structural conservation of the autoinhibitory domain in SUN proteins. Biochem Biophys Res Commun 496, 1337–1343.

Yu J, Lei K, Zhou M, Craft CM, Xu G, Xu T, Zhuang Y, Xu R, Han M (2011). KASH protein Syne-2/Nesprin-2 and SUN proteins SUN1/2 mediate nuclear migration during mammalian retinal development. Hum Mol Genet 20, 1061–1073.

Chapter IV

The Nesprin-1/-2 ortholog ANC-1 regulates organelle positioning in C. elegans independently from its KASH or actin-binding domains

Hongyan Hao, Shilpi Kalra, Laura E. Jameson, Leslie A. Guerrero, Natalie E. Cain, Jessica Bolivar, Daniel A. Starr

eLife April 2021

Hongyan Hao and Daniel A. Starr designed the experiments, wrote and edited the manuscript together. Shilpi Kalra generated the CRISPR strain *UD728*, and generated some strains for Figure 4 and Figure 9 under Hongyan Hao's guidance. Shilpi Kalra performed the analysis for Figure 4E, 4F, 11C-F. Laura E. Jameson generated the CRISPR strain UD578 and UD615 under Leslie A. Guerrero's guidance. Laura E. Jameson performed the image analysis in Figure 11A and B. Natalie generated the *UD535* strain and performed the experiment in Figure 1 supplement. Jessica Bolivar participated in generating the strain UD668 and UD669 under Hongyan Hao's guidance. All the rest of the experiments and figures are performed by Hongyan Hao.

RESEARCH ARTICLE

The Nesprin-1/-2 ortholog ANC-1 regulates organelle positioning in *C. elegans* independently from its KASH or actin-binding domains

Hongyan Hao, Shilpi Kalra, Laura E Jameson, Leslie A Guerrero, Natalie E Cain, Jessica Bolivar, Daniel A Starr*

Department of Molecular and Cellular Biology, University of California, Davis, Davis, United States

Abstract KASH proteins in the outer nuclear membrane comprise the cytoplasmic half of linker of nucleoskeleton and cytoskeleton (LINC) complexes that connect nuclei to the cytoskeleton. *Caenorhabditis elegans* ANC-1, an ortholog of Nesprin-1/2, contains actin-binding and KASH domains at opposite ends of a long spectrin-like region. Deletion of either the KASH or calponin homology (CH) domains does not completely disrupt nuclear positioning, suggesting neither KASH nor CH domains are essential. Deletions in the spectrin-like region of ANC-1 led to significant defects, but only recapitulated the null phenotype in combination with mutations in the transmembrane (TM) span. In *anc-1* mutants, the endoplasmic reticulum ER, mitochondria, and lipid droplets were unanchored, moving throughout the cytoplasm. The data presented here support a cytoplasmic integrity model where ANC-1 localizes to the ER membrane and extends into the cytoplasm to position nuclei, ER, mitochondria, and other organelles in place.

***For correspondence:** dastarr@ucdavis.edu

Competing interests: The authors declare that no competing interests exist.

Funding: See page 26

Received: 14 July 2020
Accepted: 11 April 2021
Published: 16 April 2021

Reviewing editor: Maddy Parsons, King's College London, United Kingdom

Introduction

Cellular organization is an essential process. Organelles are interconnected and mostly constrained to specific subcellular locations when they are not actively transported longer distances by cytoskeletal motor proteins (***van Bergeijk et al., 2016***). For example, nuclear positioning is essential for a wide variety of cellular and developmental processes, including fertilization, cell division, cell polarization, gametogenesis, central-nervous system development, and skeletal muscle function (***Bone and Starr, 2016***; ***Gundersen and Worman, 2013***). Defects in nuclear positioning are associated with multiple neuromuscular diseases (***Calvi and Burke, 2015***; ***Folker and Baylies, 2013***; ***Gundersen and Worman, 2013***). Furthermore, the Golgi apparatus and centrosomes are often found next to the nucleus, while the ER and mitochondria are usually spread throughout the cell (***van Bergeijk et al., 2016***). The cellular tensegrity model posits that organelles are physically coupled to the cytoskeleton, plasma membrane, and extracellular matrix so that the cell acts as a single mechanical unit (***Jaalouk and Lammerding, 2009***; ***Wang et al., 2009***). The mechanisms that maintain cellular tensegrity and how it relates to organelle positioning are poorly understood, especially in vivo.

Nuclei are connected to the rest of the cell by LINC (linker of nucleoskeleton and cytoskeleton) complexes. SUN (Sad-1/UNC-84) proteins integral to the inner nuclear membrane and KASH (Klarsicht, ANC-1, and SYNE homology) proteins that span the outer nuclear membrane interact with each other in the perinuclear space to form LINC complexes. The cytoplasmic domains of KASH proteins interact with various components of the cytoskeleton (***Luxton and Starr, 2014***), while the nucleoplasmic domains of SUN proteins interact with lamins. Thus, LINC complexes bridge the

nuclear envelope and mechanically couple the nucleoskeleton to the cytoskeleton (**Chang et al., 2015**; **Lee and Burke, 2018**; **Starr and Fridolfsson, 2010**). LINC complex inhibition reduces the stiffness and increases the deformability of the entire cytoplasm in mammalian tissue culture cells, even far from the nuclear envelope and beyond the predicted reach of LINC complexes (**Gill et al., 2019**; **Stewart-Hutchinson et al., 2008**). Whether LINC complexes maintain the mechanical properties of the cytoplasm in vivo is relatively unexplored.

Here, we investigate the role of LINC complexes with giant KASH proteins in organelle positioning in *Caenorhabditis elegans*. Most of the hypodermis of an adult *C. elegans* consists of a giant syncytium, the hyp7, containing 139 evenly-spaced nuclei that are anchored in place (**Altun and Hall, 2009**). Furthermore, *C. elegans* have invariant developmental lineages, are optically clear, and are easily genetically manipulated, making the hyp7 an ideal in vivo model to study organelle positioning. A LINC complex made of the KASH protein ANC-1 and the SUN protein UNC-84 is responsible for nuclear anchorage in *C. elegans* (**Starr, 2019**). UNC-84 is a canonical SUN protein that is orthologous to mammalian SUN1 and SUN2 and is the only known SUN protein in postembryonic somatic tissues in *C. elegans* with a nucleoplasmic domain that interacts directly with the lamin protein LMN-1 (**Bone et al., 2014**). ANC-1 is an exceptionally large protein of up to 8545 residues with two tandem calponin homology (CH) domains at its N terminus and a KASH domain at its C terminus (**Starr and Han, 2002**). ANC-1 orthologs *Drosophila* MSP-300 and mammalian Nesprin-1 Giant (G) and -2G have similar domain arrangements (**Starr and Fridolfsson, 2010**). Unlike MSP-300, Nesprin-1G, and -2G, which each contains greater than 50 spectrin-like repeats, ANC-1 consists of six tandem repeats (RPs) of 903 residues that are almost 100% conserved with each other at the nucleotide level (**Liem, 2016**; **Rajgor and Shanahan, 2013**; **Starr and Han, 2002**; **Zhang et al., 2001**). While spectrin-like repeats have not been identified in the ANC-1 RPs, most of ANC-1 is predicted to be highly helical, like spectrin (**Starr and Han, 2002**). The CH domains of ANC-1 interact with actin filaments in vitro and co-localize with actin structures in vivo, while the KASH domain of ANC-1 requires UNC-84 for its localization to the outer nuclear membrane (**Starr and Han, 2002**). UNC-84 is thought to interact with lamins to connect LINC to the nucleoskeleton while ANC-1 extends away from the outer nuclear membrane into the cytoplasm to tether nuclei to actin filaments (**Starr and Han, 2002**).

Evidence from multiple systems suggests that giant KASH orthologs might not solely function as nuclear tethers. We have observed that hyp7 syncytia in *anc-1* null animals display a stronger nuclear positioning defect than *unc-84* null animals (**Cain et al., 2018**; **Jahed et al., 2019**) and mitochondria are unanchored in *anc-1*, but not in *unc-84* mutants (**Starr and Han, 2002**). These results suggest that ANC-1 has LINC complex-independent roles for anchoring nuclei and mitochondria. Likewise, mitochondria and the ER are mispositioned in *Drosophila msp-300* mutant muscles (**Elhanany-Tamir et al., 2012**). Finally, it remains to be determined if the CH domains of ANC-1 are necessary for nuclear anchorage. Mouse Nesprin-1 and -2 have isoforms lacking CH domains (**Duong et al., 2014**; **Holt et al., 2016**) and Nesprin-1 CH domains are dispensable for nuclear positioning during mouse skeletal muscle development (**Stroud et al., 2017**).

To address these ambiguities, we use ANC-1 to examine how giant KASH proteins position nuclei and other organelles. We find that for nuclear anchorage, the ANC-1 KASH domain plays a relatively minor role, and the CH domains are dispensable. Rather, multiple large cytoplasmic domains and the C-terminal transmembrane (TM) span of ANC-1 are required for nuclear anchorage. Moreover, in *anc-1* null mutants, the entire cytoplasm is disorganized, and the ER is unanchored and moves freely throughout the cytoplasm. Together, our results support a model in which ANC-1 associates with ER membranes to regulate the mechanical properties of the cytoplasm, thereby anchoring nuclei, mitochondria, ER, and other organelles.

Results

ANC-1 promotes proper nuclear anchorage through a LINC complex-independent mechanism

Loss-of-function mutations in *anc-1* disrupt the even spacing of hyp7 syncytial nuclei (**Cain et al., 2018**; **Starr and Han, 2002**). We use the number of nuclei in contact with each other as a metric for hyp7 nuclear anchorage defects (**Cain et al., 2018**; **Fridolfsson et al., 2018**). In wild type

(WT) animals, very few hyp7 nuclei were touching. In contrast, over 50% of hyp7 nuclei were clustered with at least one other nucleus in *anc-1(e1873)* null mutants. Significantly fewer hyp7 nuclei were unanchored in *unc-84(n369)* null mutants (***Figure 1C***). This trend was also observed in adult syncytial seam cells (***Figure 1—figure supplement 1***). Throughout this manuscript, we call nuclear anchorage defects that are statistically similar to *anc-1* null mutants as severe, defects statistically similar to *unc-84* null mutants but still significantly worse than wild type as mild, and defects statistically between *anc-1* and *unc-84* null mutants as intermediate.

The greater severity of the nuclear anchorage defect in *anc-1* null mutants compared to *unc-84* suggests that ANC-1 plays additional roles in nuclear positioning independently of its SUN partner UNC-84. We used CRISPR/Cas9 gene editing to delete the luminal peptides of the ANC-1 KASH domain (***Figure 1D***). We predicted the *anc-1*(ΔKASH) mutants would abrogate the interaction between ANC-1 and UNC-84 and phenocopy *unc-84*(*null*) animals. Two independent *anc-1*(ΔKASH) mutants exhibited mild nuclear anchorage defects similar to those observed in *unc-84(null)* mutants (***Figure 1B–C***). Together, these results suggest that the SUN/KASH interaction only partially contributes to nuclear anchorage, implicating the large cytoplasmic domain of ANC-1 as the major player in nuclear positioning.

The ANC-1 N-terminal CH domains are not required for hyp7 nuclear positioning

We next deleted the CH domains at the N terminus of the largest isoforms of ANC-1, which are predicted to interact with actin, and replaced them with GFP using CRISPR/Cas9 gene editing. Hyp7 nuclei did not cluster in *anc-1*(ΔCH) mutants (***Figure 2B***). Thus, the CH domains of ANC-1 are not required for hyp7 nuclear anchorage.

Nesprin-1 and -2 have multiple splice isoforms, many of which are missing the CH domains (***Rajgor et al., 2012***; ***Stroud et al., 2017***). We hypothesized a shorter *anc-1* isoform lacking the CH domains would be sufficient for nuclear anchorage. RNAseq and expressed sequence tag data published on WormBase (***Harris et al., 2020***) suggest that *anc-1* has at least three isoforms (***Figure 2A***). We tested whether a shorter isoform lacking CH domains, *anc-1b*, is sufficient for hyp7 nuclear anchorage. RNAi constructs targeting the 5′ exons specific to the *anc-1a/c* long isoforms did not cause nuclear anchorage defects (***Figure 2A–B***). However, RNAi targeting a repetitive region in all three predicted isoforms caused severe nuclear anchorage defects (***Figure 2A–B***). We also analyzed four nonsense mutations. Alleles that are predicted to disrupt the longer *anc-1a/c* isoforms but not the shorter *anc-1b* isoform, *anc-1*(W427*), and *anc-1*(W621*) were normal for nuclear anchorage. In contrast, both *anc-1*(Q1603*) and *anc-1*(Q2878*) alleles, which are predicted to add premature stop codons to all three predicted isoforms, led to severe nuclear anchorage defects (***Figure 2A–B***). These results suggest that the shorter *anc-1b* isoform lacking the CH domains is sufficient for nuclear anchorage.

We next tested whether *anc-1b* is expressed in hyp7. First, 5′ RACE (Rapid amplification of cDNA ends) was used to identify the start of the *anc-1b* predicted transcript (***Figure 2C***). The RACE product contained an SL1 sequence at its 5′ end, suggesting this represents the end of a bona fide transcript (***Figure 2D***). To test if the *anc-1b* isoform is expressed in hyp7, we fused the *anc-1b* promoter and ATG to an *nls::gfp::lacZ* reporter and expressed it in transgenic animals. The *anc-1b* promoter drove GFP expression in hyp7 (***Figure 2E***, yellow arrows). Taken together, these results suggest the conserved CH domains are not necessary for hyp7 nuclear anchorage and the *anc-1b* isoform expressed in the hypodermis plays a major role in hyp7 nuclear anchorage.

Spectrin-like domains of ANC-1b are required for nuclear anchorage

We predicted that the six tandem repeats (RPs) of ANC-1 function analogously to the spectrin-like domains of Nesprin-1 and -2. We modeled the structure of pieces of the ANC-1 RPs using the protein-folding prediction software QUARK (***Xu and Zhang, 2012***; ***Xu and Zhang, 2013***) and found that they are predicted to form helical bundles remarkably similar to the structure of spectrin (***Figure 3A,D***; ***Grum et al., 1999***), suggesting the tandem repeats are analogous to spectrin-like domains.

We next tested the necessity of the ANC-1 spectrin-like repeats and the neighboring cytoplasmic domains for nuclear anchorage by making in-frame deletions of portions of *anc-1* using CRISPR/

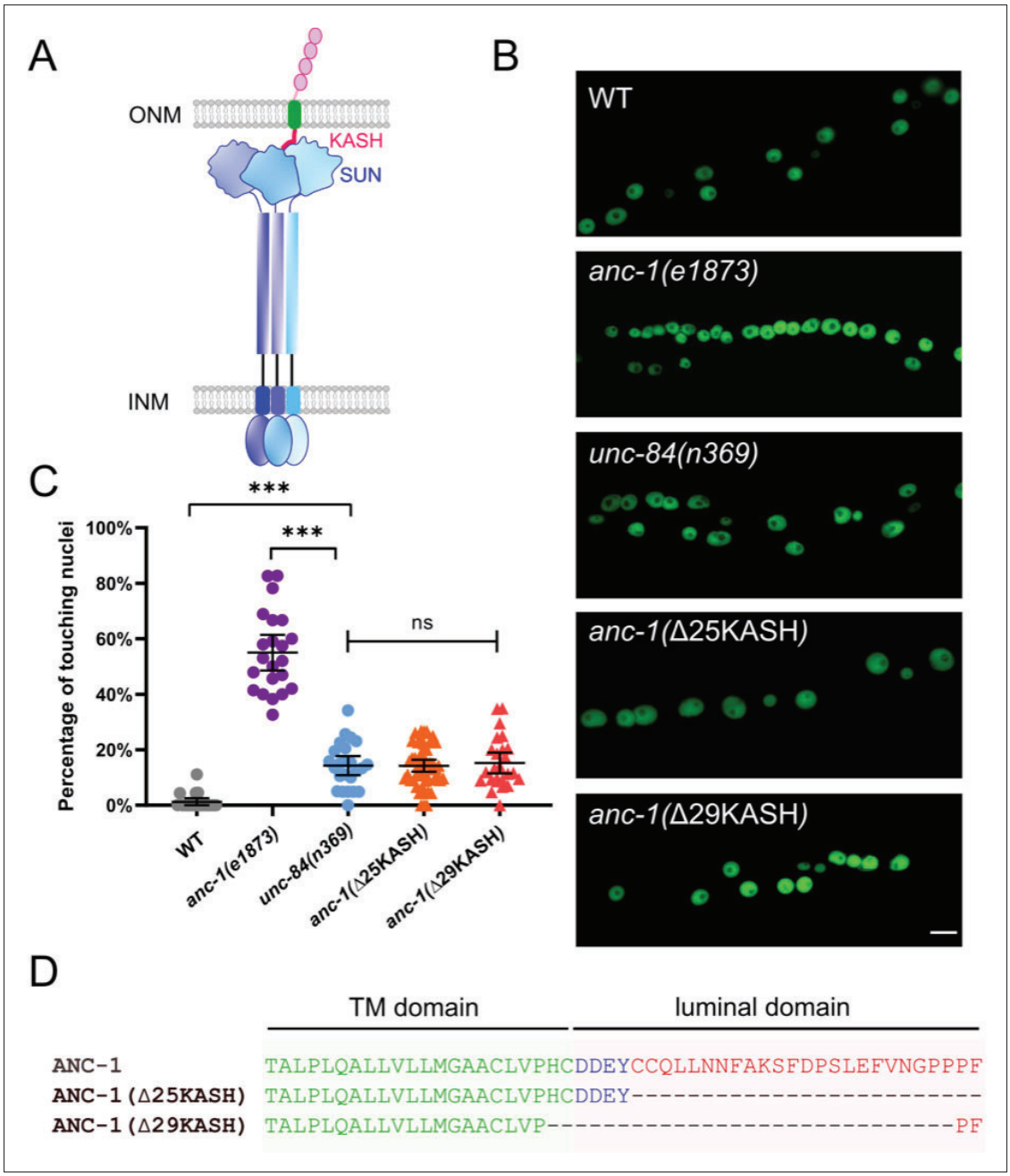

Figure 1. ANC-1 has a linker of nucleoskeleton and cytoskeleton (LINC) complex-independent role in anchoring nuclei. (**A**) Model of the LINC complex. Trimers of the SUN protein UNC-84 (purple and blue) and the KASH protein ANC-1 (red, green, and pink, only one of the trimers is shown) form the LINC complex, which spans the outer nuclear membrane (ONM) and inner nuclear membrane (INM). (**B**) Lateral views of adult *C. elegans* expressing hypodermal nuclear GFP in wild type (WT) or indicated mutants. Scale bar, 10 μm. (**C**) Quantification of nuclear anchorage defects. Each point

Figure 1 continued on next page

Figure 1 continued

represents the percentage of touching nuclei on one side of a young adult animal. Means with 95% CI error bars are shown. ANOVA and Tukey's multiple comparisons tests were used for statistical analysis; ns means not significant, $p>0.05$; ***$p\leq0.001$. $n \geq 20$ for each strain. (**D**) Sequences of the transmembrane (TM) domain and the luminal domain of ANC-1 showing the deletions analyzed.
The online version of this article includes the following figure supplement(s) for figure 1:

Figure supplement 1. Nuclear anchorage defects in seam cell syncytia.

Cas9-mediated gene editing. The N-terminal fragment 1 (F1) contains 1969 residues of ANC-1b from the start codon to the start of the RPs and fragment 2 (F2) contains the 277 residues between the RPs and the C-terminal transmembrane span (***Figure 3A***). The deletion of the F1 domain or all six RPs caused intermediate nuclear anchorage defects (***Figure 3B–C***). ANC-1b with only one of the normal six repeats had an intermediate nuclear anchorage defect that was significantly greater than in wild type but not as severe as the *anc-1*(Δ6RPS) mutant (***Figure 3C***). In contrast, the *anc-1*(ΔF2) mutant had no nuclear anchorage defect (***Figure 3C***). Since the *anc-1*(Δ6RPS) and *anc-1*(ΔF1) defects were less severe than *anc-1* null alleles, we made double mutants with *unc-84*(*n369*) to see if mutations in the cytoplasmic portions of ANC-1 were synergistic with mutations in the KASH domain. Both *anc-1*(ΔF1); *unc-84*(*n369*) and *anc-1*(Δ6RPS); *unc-84*(*n369*) double mutants significantly enhanced the nuclear anchorage defects of the single mutations (***Figure 3C***). However, the hyp7 nuclear anchorage defects in *anc-1*(ΔF1); *unc-84*(*n369*) and *anc-1*(Δ6RPS); *unc-84*(*n369*) double mutants were still less severe than *anc-1*(*e1873*) null mutants, suggesting that multiple parts of ANC-1b mediate proper hyp7 nuclear positioning (***Figure 3C***). Together, these results indicate that (1) F1 and the RPs play roles in nuclear anchorage, (2) multiple repeats are necessary for normal function, and (3) the F2 region is dispensable for hyp7 nuclear positioning.

The ER is unanchored in *anc-1* mutants

In addition to nuclear positioning, ANC-1 functions in mitochondria distribution and morphology in the hypodermis and muscle cells (***Hedgecock and Thomson, 1982***; ***Starr and Han, 2002***). We therefore asked if ANC-1 also anchors other organelles. We characterized the ER in live hyp7 syncytia of *anc-1* and *unc-84* mutants using a single-copy GFP::KDEL marker (*pwSi83*; gift of Barth Grant). In wild type, the ER formed a network evenly distributed throughout hyp7 (***Figure 4A***). We used blind scoring to classify single images of each animal's ER as normal (evenly distributed in what appeared to be sheets), mild defects (lots of sheet-like structures, but occasionally not uniformly spread throughout the syncytium), strong defects (considerable mispositioning and clustering of ER, but still in large units), or severe defects (complete mispositioning and extensive fragmenting of the ER) (***Figure 4*** and ***Figure 4—figure supplement 1***). About a third of wild type adults had normally distributed ER, while the rest had mild ER positioning defects, perhaps due to the pressure on the worm from the coverslip (***Figure 4A–B***). However, ER networks in *anc-1* null mutants were severely disrupted and often fragmented (***Figure 4A–B***). We also observed the dynamics of the ER in live animals. In wild type animals, the hypodermal ER was anchored as an interconnected network and exhibited limited motion while the animal crawled (***Figure 4C,E–F***, ***Video 1***). However, in *anc-1* null mutants, ER fragments drifted apart and often formed large aggregates, suggesting that the anchorage of the ER network was disrupted (***Figure 4D–F***, ***Video 2***). To quantify this phenotype, we measured the change in distance between distinct points over time. In wild type, the average distance change between parts of the ER was less than 1 μm per second, whereas in *anc-1* mutants, the average change in distance more than doubled (***Figure 4E***), suggesting that the ER had lost its overall interconnectivity and that fragments were unanchored from the rest of the ER.

We next examined whether UNC-84 is required for ER positioning. Still images of *unc-84(n369)* null mutants scored blindly were similar to wild type ER (***Figure 4A–B***). However, in some videos of *unc-84(n369)* mutants, there were slight changes in the organization of the ER over time (***Video 3***), suggesting that *unc-84* null mutants had a minor ER positioning defect. Most *anc-1*(Δ29KASH) mutants had mild defects in ER positioning, and only about a quarter had more severe defects, significantly less than *anc-1(e1873)* null mutants. In contrast, more than 80% of *anc-1*(Δ6RPS) animals had strong or severe ER positioning defects, similar to *anc-1* null mutants (***Figure 4A–B***). These

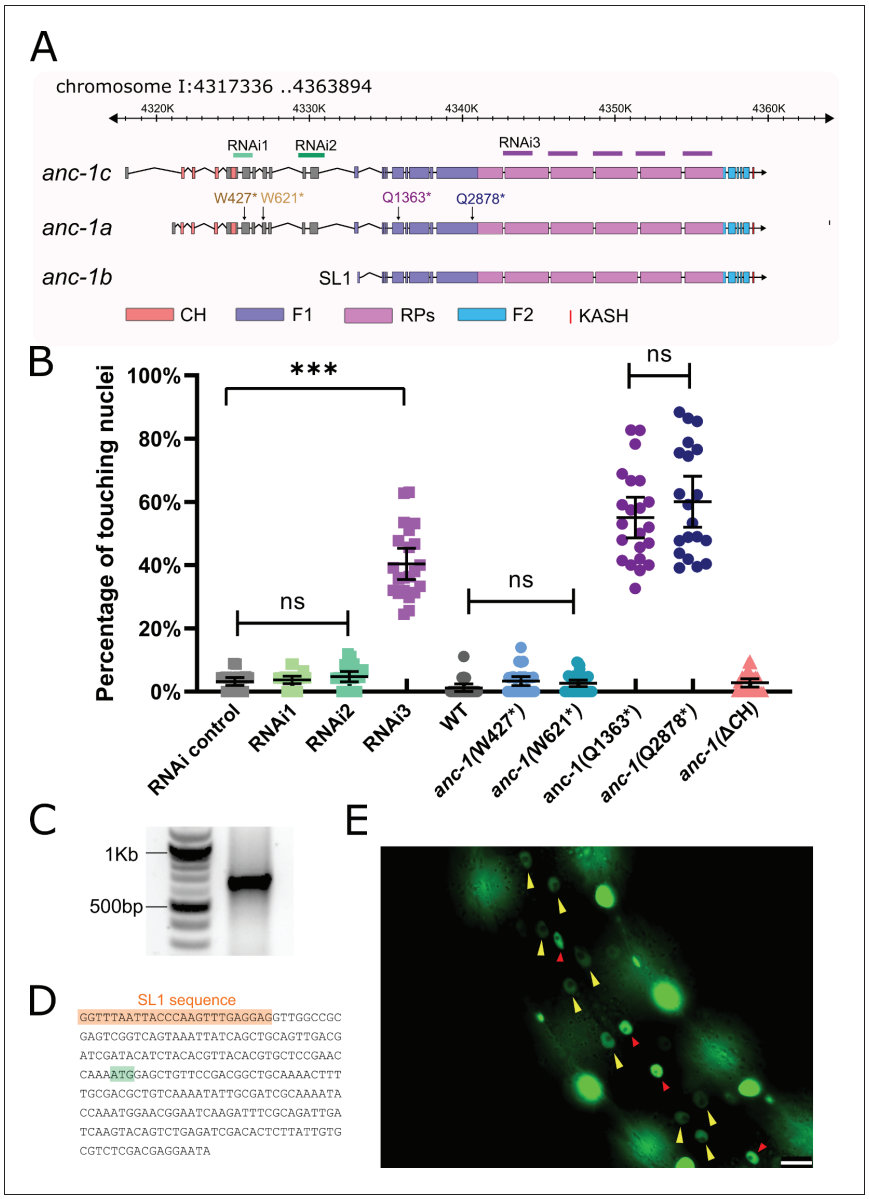

Figure 2. *anc-1b* is the major isoform in hyp7 nuclear anchorage. (**A**) Schematic gene structure of *anc-1a*, *b*, and *c* isoforms (modified from the J-Brower in Wormbase). Domains are color-coded. CH = calponin homology; F1 = fragment one from the ATG of ANC-1b to the beginning of the repeats; RPs = the six exact repeats of about 900 residues each; F2 = fragment two from the end of the repeats to the transmembrane (TM) span; WT = wild type; and KASH = Klarsicht, ANC-1, Syne homology, in this case referring to the residues in the lumen of the nuclear envelope. The target regions of RNAi constructs are labeled. Premature stop mutations are indicated using the numbering the *anc-1a* isoform. (**B**) Quantification of nuclear anchorage defects in *anc-1* mutant and RNAi animals. Means with 95% CI are shown in the graph. ANOVA and Tukey's multiple comparisons tests were used for statistical analysis. ns, not significant, $p>0.05$; ***$p\leq0.001$. $n \geq 20$ for each strain. (**C**) An agarose gel showing

Figure 2 continued on next page

Figure 2 continued

the 5'-RACE products on the right lane. (**D**) Partial sequence of the 5'-RACE product. An SL1 sequence (orange) adjacent to the 5' end of the *anc-1b* transcript was identified. The predicted start codon is in light green. (**E**) Lateral view of a worm showing the expression of nls::GFP driven by *anc-1b* promoter. Yellow arrows mark hyp7 nuclei; the red arrows mark seam cell nuclei; and the bright, unmarked nuclei are in muscle cells. Scale bar, 10 µm.

results indicated that ANC-1 is essential for ER positioning through mostly LINC complex-independent mechanisms.

ANC-1 localizes to ER membranes

Since ANC-1 functions, in part, independently of LINC complexes at the nuclear envelope and because ANC-1 regulates ER positioning, we hypothesized that ANC-1 localizes to multiple membranes, including those away from the nuclear envelope. To study the localization of ANC-1, we tagged endogenous ANC-1 with GFP using CRISPR/Cas9 gene editing. The tag was placed either at the N-terminus of ANC-1b, or between the six tandem RPs and the F2 region to see if the opposite ends of ANC-1 localize to different structures (***Figure 5A***). Both strains were nearly wild type for hyp7 nuclear positioning (***Figure 5B***). Both GFP::ANC-1b and ANC-1::GFP::F2 localized in similar

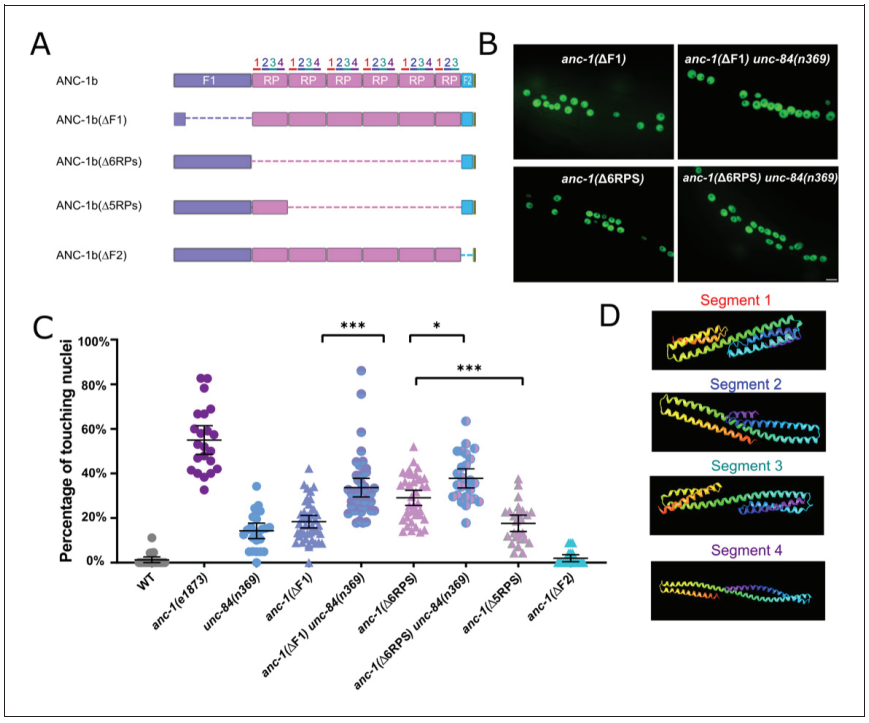

Figure 3. Cytoplasmic domain deletion analysis of ANC-1b. (**A**) Schematics of the ANC-1b cytoplasmic domain deletions. (**B**) Lateral views are shown of young adult *C. elegans* expressing hypodermal nuclear GFP in the indicated genotypes. Scale bar, 10 µm. (**C**) Quantification of nuclear anchorage in the wild type (WT) as well as *anc-1b* domain deletion mutants. Each point represents the percentage of touching nuclei on one side of a young adult animal. Means with 95% CI error bars are shown. ANOVA and Tukey's multiple comparisons tests were used for statistical analysis. *p≤0.05; **p≤0.01; ***p≤0.001. n ≥ 20 for each strain. The data in the first three columns, WT, *anc-1(e1873)*, and *unc-84(n369)* are duplicated from ***Figure 1C*** and copied here for easy reference. (**D**) QUARK result for three fragments in the tandem repeats (RPs). The positions of the fragments are indicated in 3A.

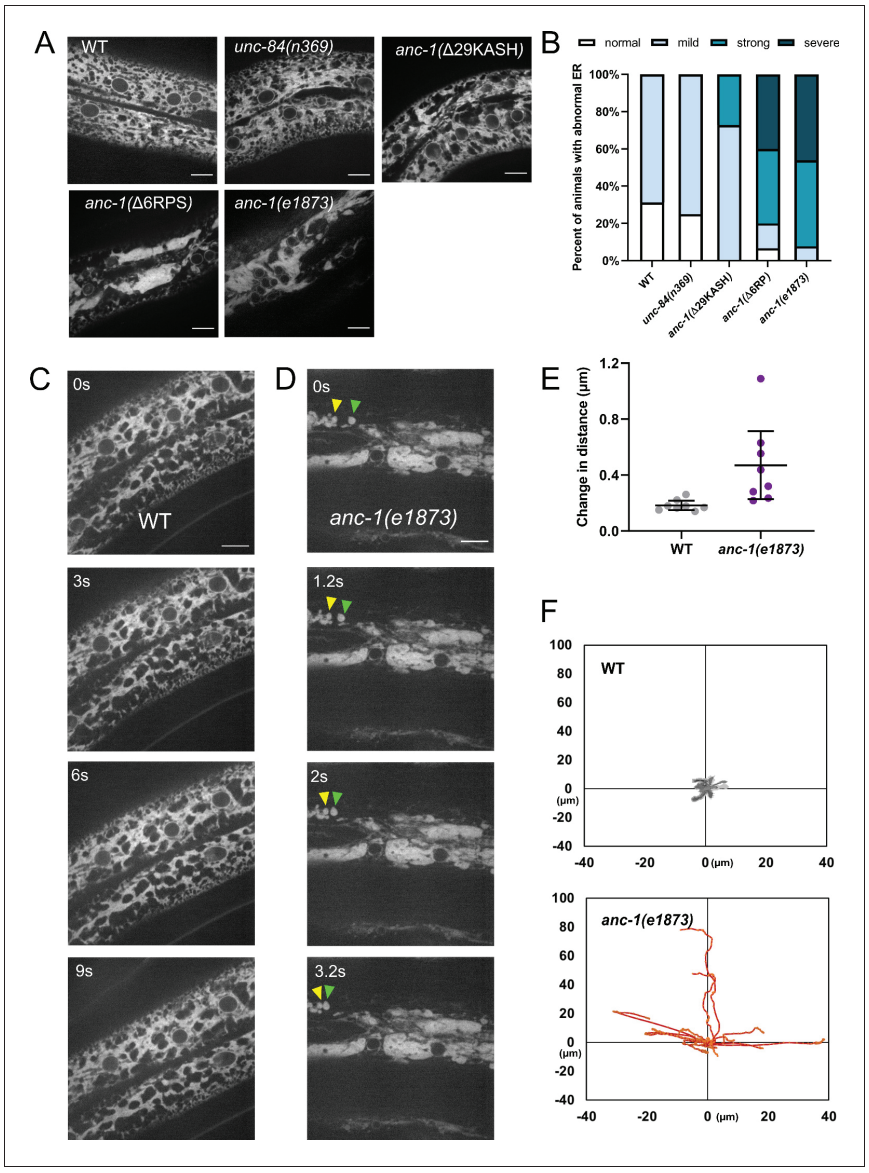

Figure 4. The ER is mispositioned in *anc-1* mutants. (**A**) Representative images of the hyp7 ER labeled with the GFP::KDEL marker in the young adult animals. (**B**) Scoring of the ER positioning defects. ER images of the listed strains were mixed and randomized for blind analysis by multiple researchers. n ≥ 11 for each strain. (**C–D**) Time-lapse images of hyp7 GFP::KDEL marker (**C**) over 9 s in wild type (WT) or (**D**) over 3.2 s in *anc-1* null. Arrowheads show two fragments of ER that changed their relative distance from one another over a short period of time. (**E–F**) To quantify ER displacement, three spots on each WT and *anc-1(e1873)* movie were tracked. The average change in distance between two points in 200 ms intervals is plotted in (**E**). The trajectories of the relative movements of each spot apart from the others are shown in (**F**). Eight movies of each strain were analyzed. Scale bar, 10 μm for all the images.

The online version of this article includes the following figure supplement(s) for figure 4:

Figure 4 continued on next page

Figure 4 continued

Figure supplement 1. Raw data for ER morphology assays.

patterns throughout the cytoplasm of adult hyp7 syncytia (***Figure 5C–D***). To examine the localization of the ANC-1b isoform alone, we introduced a premature stop codon mutation to disrupt the longer *anc-1a* and *c* isoforms in the GFP::ANC-1b strain, which did not significantly change GFP::ANC-1b localization (***Figure 5E***). These data are consistent with our model that *anc-1b* plays the major role in hyp7 nuclear positioning.

We next examined whether the cytoplasmic domains of ANC-1b are required for localization. Deletion of the F1 domain did not dramatically change localization of GFP::ANC-1b (***Figure 5F***). However, deletion of the six tandem repeats enriched GFP::ANC-1b around the nuclear envelope (***Figure 5G***), as did the deletion of five of the six repeats (***Figure 5H***). However, the intensity of the six repeat deletion mutant is significantly less than wild type GFP::ANC-1b (***Figure 5—figure supplement 1***), making it possible that the phenotype is due to less ANC-1 being present. Yet, the deletion mutant is significantly enriched at the nuclear envelope (***Figure 5—figure supplement 1B–C***), supporting the hypothesis that the defect is due to a loss of ANC-1 repeats at the general ER. The nuclear envelope enrichment of GFP::ANC-1b(Δ5RPs) was not observed when *unc-84* was mutated (***Figure 5I***), suggesting the nuclear envelope enrichment of GFP::ANC-1b is UNC-84-dependent.

The ANC-1 localization pattern in ***Figure 6*** is consistent with a model where ANC-1 localizes to ER membranes. In this model, a construct containing the transmembrane span near the C-terminus of ANC-1 but lacking the C-terminal, luminal part of the KASH domain would be sufficient for ER localization. Deletion of both the transmembrane span and the luminal parts of KASH with CRISPR/Cas9 resulted in a significantly worse nuclear anchorage defect than deleting only the luminal KASH domain (***Figure 6B***). Similarly, ER positioning defects were worse in *anc-1*(ΔTK) than in *anc-1* (Δ25KASH) animals (***Figure 6C***). We next examined the role of the neck region, which is located immediately adjacent to the cytoplasmic side of the transmembrane span. When GFP was knocked-in between the neck region and the transmembrane span to make *anc-1(yc36[anc-1::gfp3Xflag::kash])*, it caused a significant nuclear anchorage defect (***Figure 6A–B***). Moreover, extending the deletion in *anc-1*(ΔF2), which had no hyp7 nuclear anchorage defect (***Figure 3C***), an additional nine residues to remove the neck, caused a significant nuclear anchorage defect (***Figure 6A–B***). This suggests that the neck region next to the transmembrane span of ANC-1 plays a role in nuclear positioning, perhaps by targeting the C-terminus of ANC-1 to a membrane.

As shown above, a double mutant that lacks both the ANC-1 repeat region and LINC complex function in the form of an *unc-84(null)* had an intermediate defect (***Figure 3B***). This suggests that a third domain of ANC-1, in addition to the luminal portions of KASH and the RPs, is involved in positioning nuclei. To test this hypothesis, we made an *anc-1(gfp::anc-1b::Δ6rps::Δtk)* mutant line and found that it had a severe nuclear anchorage defect that was not significantly different from the *anc-1(e1873)* null mutant (***Figure 6B***). Together, these data support a model in which the transmembrane span is important for targeting ANC-1 to the ER/nuclear envelope membrane where ANC-1 then positions the ER and nuclei via LINC complex-independent mechanisms.

To further examine the role of the transmembrane span in ER and nuclear positioning, we

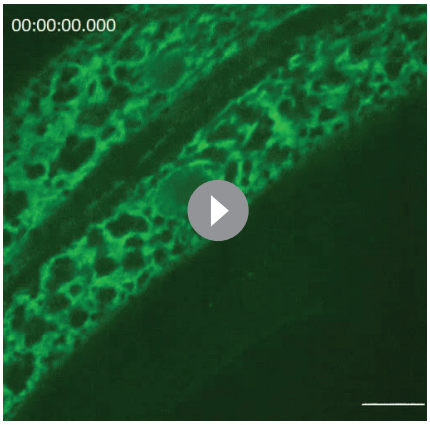

Video 1. The ER is anchored in wild type (WT) hyp7. An example video of the hyp7 ER in young adult wild type *C. elegans* expressing *pwSi83[p_{hyp7}gfp::kdel]*. Images were captured at the interval of 0.2 s for 10 s. Scale bar, 10 μm.
https://elifesciences.org/articles/61069#video1

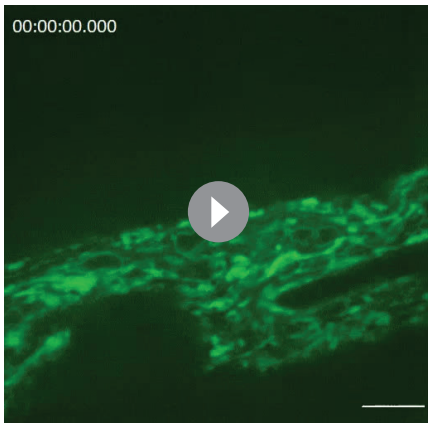

Video 2. The ER is unanchored in *anc-1(e1873)* mutant hyp7. An example video of the hyp7 ER in the young adult *anc-1(e1873)* mutant *C. elegans* expressing *pwSi83[p_{hyp7}gfp::kdel]*. Images were captured at the interval of 0.2 s for 10 s. Scale bar, 10 µm.
https://elifesciences.org/articles/61069#video2

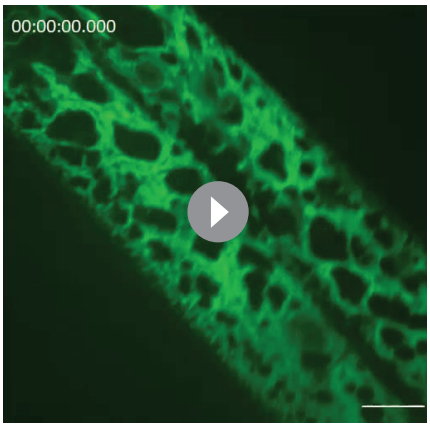

Video 3. ER positioning in *unc-84(null)* mutant hyp7. An example of one of the most severe ER positioning defects observed is shown in a video of the hyp7 ER in the young adult *unc-84(n369)* mutant *C. elegans* expressing *pwSi83[p_{hyp7}gfp::kdel]*. Images were captured at the interval of 0.25 s for 4 s. Scale bar, 10 µm.
https://elifesciences.org/articles/61069#video3

observed the co-localization of ANC-1 with an ER membrane marker (***Figure 7***). A single-copy hypodermal-specific mKate2::TRAM-1 ER marker strain (***Rolls et al., 2002***) was generated and crossed with GFP::ANC-1b. The wild type GFP::ANC-1b fusion protein localized similarly to the ER marked by mKate2::TRAM-1 (***Figure 7A***). We used the ImageJ plug-in ScatterJ to quantify the co-localization and the Pearson's correlation coefficient averaged from 17 images (***Figure 7G***). Our second GFP construct, ANC-1::GFP::F2, also co-localized with the ER (***Figure 7B,G***). Similar results were obtained when co-localizing mKate2::ANC-1b and GFP::KDEL, but since the GFP::KDEL was overexpressed and significantly brighter than the mKate2::ANC-1b, we only present the analyses with GFP ANC-1 fusion proteins co-localizing with mKate2::TRAM-1, which is expressed at lower levels from a single-copy transgene. In contrast, GFP::ANC-1b did not co-localize with lipid droplets or mitochondria (***Figure 7—figure supplement 1***).

Deleting the luminal portion of the KASH domain from GFP::ANC-1b (GFP::ANC-1b::ΔKASH) did not significantly change its localization pattern relative to the wild type construct (***Figure 7C,G***). In contrast, deletion of both the luminal KASH peptide and the transmembrane span (GFP::ANC-1b::ΔTK) resulted in many cases where GFP::ANC-1b::ΔTK almost normally localized to the ER (***Figure 7D,G***) while in other animals it localized in parts of the cytoplasm that lacked ER (***Figure 7E, G***). Deletion of the repeat regions in GFP::ANC-1b::Δ6RPS led to a re-localization away from the general ER (***Figure 7F–G***). Together, these results suggest that (1) ANC-1b has a similar distribution pattern as the ER and (2) that the transmembrane span and repeat regions, but not the luminal KASH domain, plays roles ANC-1 ER localization. The ANC-1 localization pattern is consistent with the above findings that *anc-1*(Δ6RPS) *anc-1*(ΔTK) mutants had intermediate nuclear and ER positioning defects, worse than *anc-1*(Δ25KASH) mutants.

Other organelles are mis-localized in *anc-1* mutants

Our imaging showed that both nuclei and the ER are both unanchored and move freely throughout the cytoplasm. Furthermore, our deletion analyses cast significant doubt on the old tethering model. In our new model, without ANC-1, the entire cytoplasm is disconnected and multiple organelles are likely flowing freely throughout the cytoplasm. We therefore used the MDT-28::mCherry (***Na et al., 2015***) marker to follow lipid droplets (***Figure 8***, ***Videos 4–5***) and the mitoLS::GFP marker to follow mitochondria (***Figure 9***, ***Videos 6–7***). In *anc-1* null mutant animals, both lipid droplets and

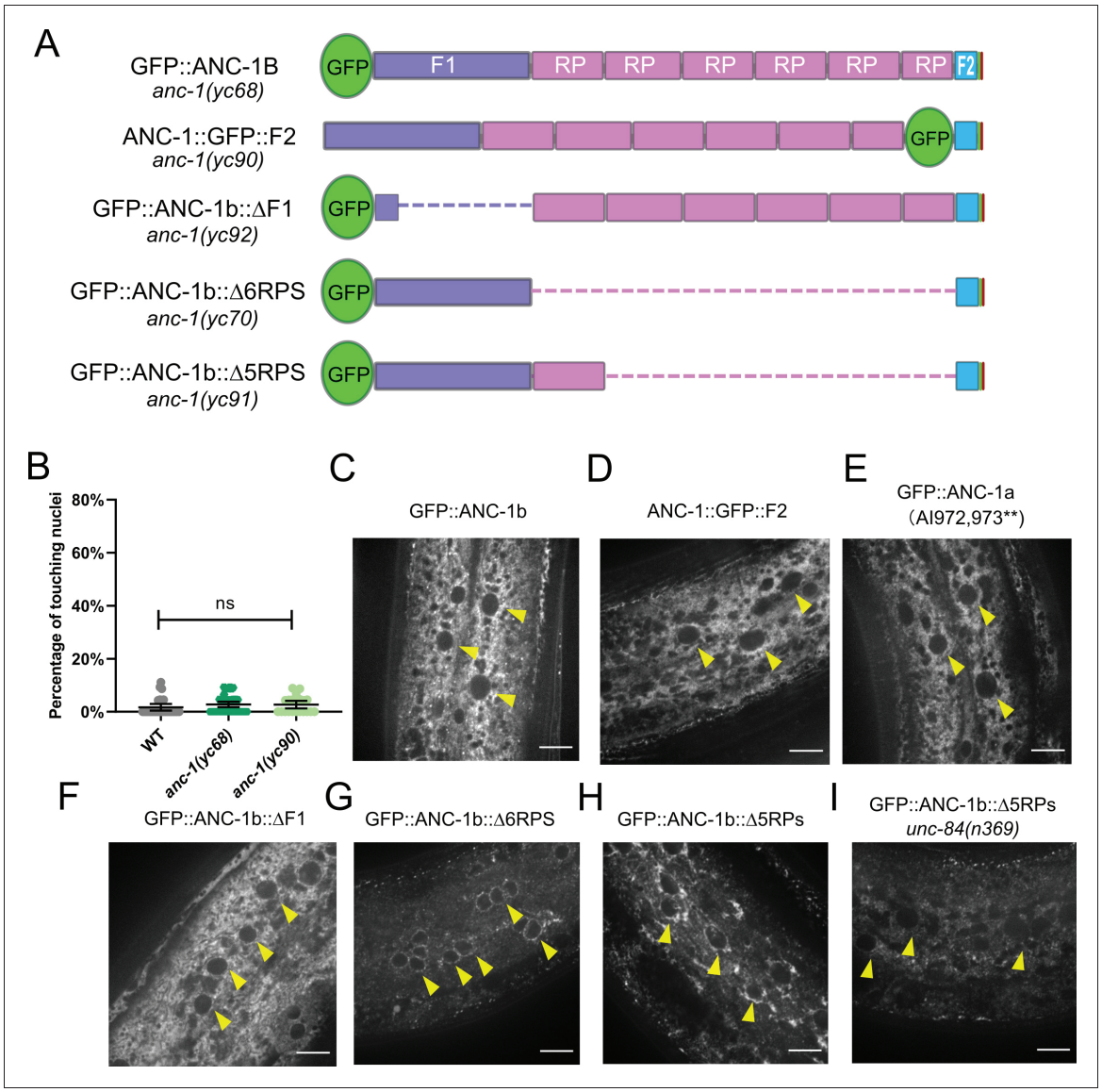

Figure 5. The subcellular localization of ANC-1. (**A**) Schematic depicting the ANC-1 GFP knock-in constructs with or without deletion of ANC-1 cytoplasmic domains. (**B**) Nuclear positioning in GFP::ANC-1b is wild type (WT). Each point represents the percentage of touching nuclei on one side of a young adult animal. Means with 95% CI error bars are shown. ns, not significant ($p>0.05$). $n \geq 20$. (**C–I**) Confocal images of hyp7 subcellular localization in the indicated strains. Yellow arrowheads point to nuclei. Scale bar, 10 μm.

The online version of this article includes the following figure supplement(s) for figure 5:

Figure supplement 1. GFP::ANC-1(Δ6RPS) is expressed at a lower level and is enriched at the nuclear envelope.

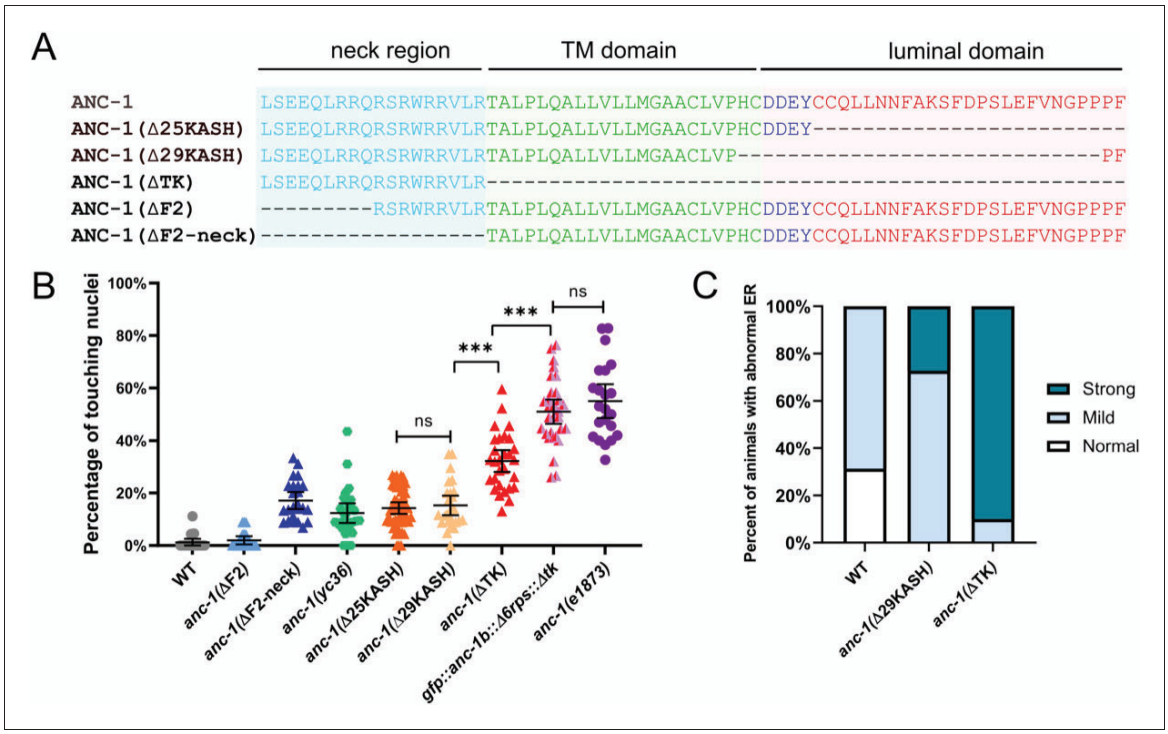

Figure 6. The transmembrane domain of ANC-1 is necessary for nuclear and ER positioning. (**A**) Sequence of deletion in the neck region (blue), transmembrane (TM) span (green), or the luminal domain (red). (**B**) Quantification of nuclear anchorage defects in *anc-1* mutants. Each point represents the percentage of touching nuclei on one side of a young adult animal. Means with 95% CI error bars are shown. n ≥ 20. ANOVA and Tukey's multiple comparisons tests were used in comparisons. ***p≤0.001; ns means p>0.05. The data of wild type (WT), *anc-1*(Δ*F2*), *anc-1*(Δ25KASH), *anc-1*(Δ29KASH), and *anc-1*(*e1873*) are duplicated from ***Figures 1C*** and ***3C*** and copied here for easy reference. (**C**) Qualitative analysis of the ER anchorage defects as in ***Figure 4***. Significantly more *anc-1*(ΔTK) animals show strong ER anchorage defects than *anc*-1(Δ29KASH) mutants (p≤0.01 by Fisher's exact test). Sample sizes were all ≥10.

mitochondria moved in a manner suggesting they were not connected to a network. Furthermore, lipid droplets were often seen in large clusters and mitochondria appeared slightly fragmented. We therefore conclude that ANC-1 is required to interconnect the entire cytoplasm to anchor nuclei, ER, lipid droplets, mitochondria, and likely other organelles to a single network that regulates the integrity of the cytoplasm.

Microtubule networks appear normal in *anc-1* mutants

One hypothesis for ANC-1 function is that it regulates cytoskeletal networks. In this model, mutations in *anc-1* would disrupt the cytoskeleton, causing organelles to lose their attachment to the cytoskeleton and move around freely as shown in ***Figures 4***, ***8*** and ***9***. We therefore examined microtubule organization in the hyp7 syncytia of wild type and *anc-1* null mutant animals. We followed microtubules in live animals with an endogenously expressed microtubule binding protein, GFP::MAPH-1.1 (***Castiglioni et al., 2020***; ***Waaijers et al., 2016***). The density and relative disorganization of the microtubule network in wild type made it difficult to quantify any growth, length, or number parameters of microtubules. Nonetheless, qualitatively, in comparison with the wild type (***Video 8***), microtubules were mostly normal in in *anc-1* null mutant animals (***Figure 10*** and ***Videos 9–10***). The exception was where nuclei had moved back and forth along an anterior-posterior axis, they appear to have cleared a microtubule free channel. These results are more in line with a model where in the

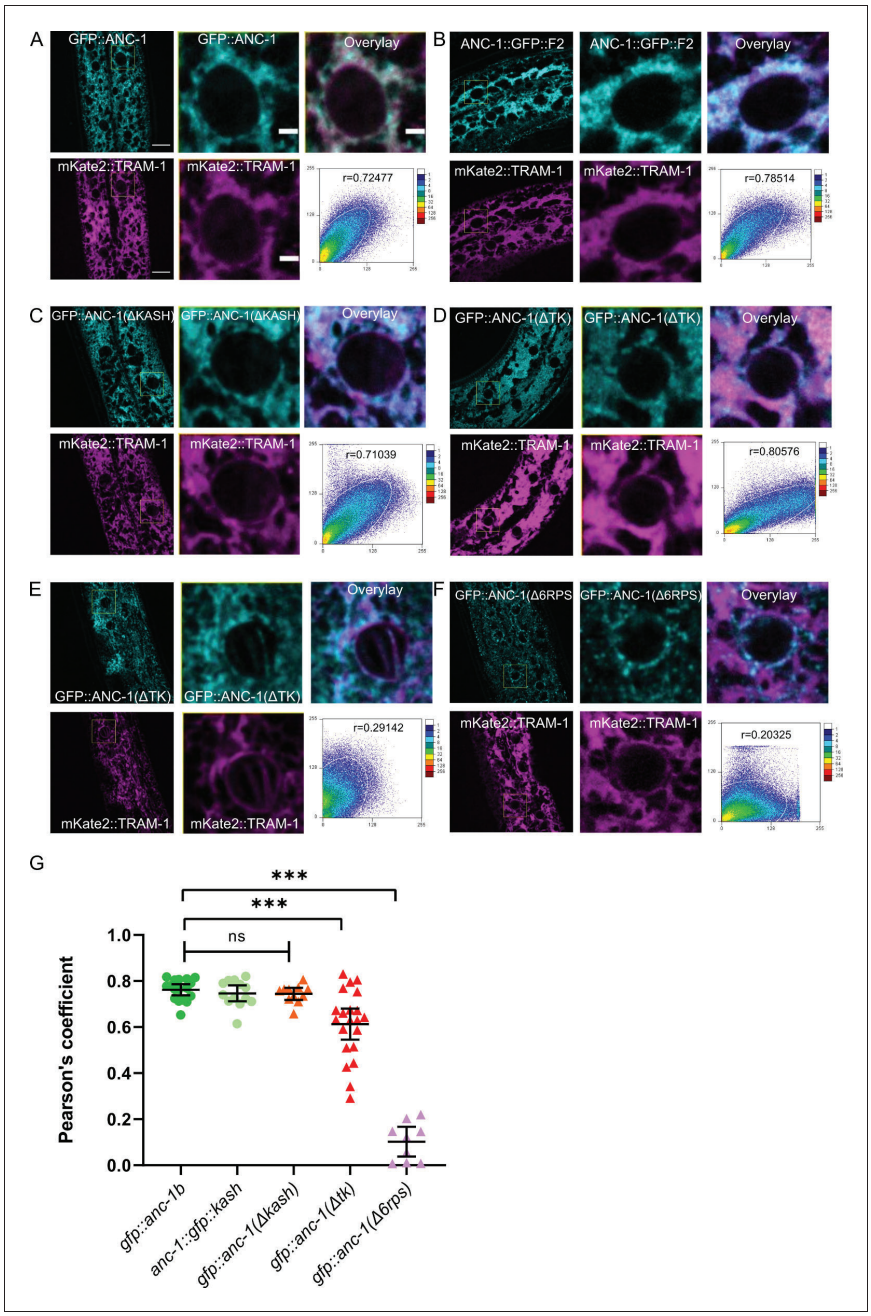

Figure 7. ANC-1 localizes to the ER. ANC-1-GFP fusion protein (cyan) localization with respect to the ER membrane as marked by a mKate::TRAM-1 (magenta) is shown. (**A**) Wild type (WT) GFP::ANC-1b. (**B**) Wild type ANC-1::GFP::F2. (**C**) GFP::ANC-1b::ΔKASH. (**D**) An example of GFP::ANC-1b::ΔTK with good overlap with the ER and (**E**) a GFP::ANC-1b::ΔTK with poor overlap. (**F**) GFP::ANC-1b::Δ6RPS. (**A–F**) For each section, the left two

Figure 7 continued on next page

Figure 7 continued

panels are low magnification of the young adult hypodermis (scale bar, 10 µm) and the middle two panels are a zoom in of the boxed part of the left panels (scale bar, 2 µm). The top right shows the merge of the two channels. The bottom right uses the used ImageJ plug-in ScatterJ to quantify the co-localization and the Pearson's correlation coefficient for overlap is shown as an r value. (**G**) A scatter plot of Pearson's coefficients showing overlap between the indicated GFP and the mKate::TRAM-1 ER membrane marker. Mean ±95% CI are shown. ANOVA and Tukey's multiple comparisons tests were used in comparisons. ***p≤0.001; ns means not significant. The online version of this article includes the following figure supplement(s) for figure 7:

Figure supplement 1. GFP::ANC-1b does not co-localize with lipid droplets or mitochondria.

absence of ANC-1, nuclei move around and disrupt or move microtubules in their way rather than a model where a lack of ANC-1 leads to massive microtubule disruption that then frees nuclei and other organelles to move throughout the syncytia.

Depletion of ANC-1 disrupts nuclear morphology and causes developmental defects

Nuclear shape changes were observed during live imaging in *anc-1* mutants consistent with a model where *anc-1* mutant nuclei are susceptible to pressures from the cytoplasm, perhaps crashing into other organelles that corresponded with dents in nuclei. We therefore quantified nuclear size and

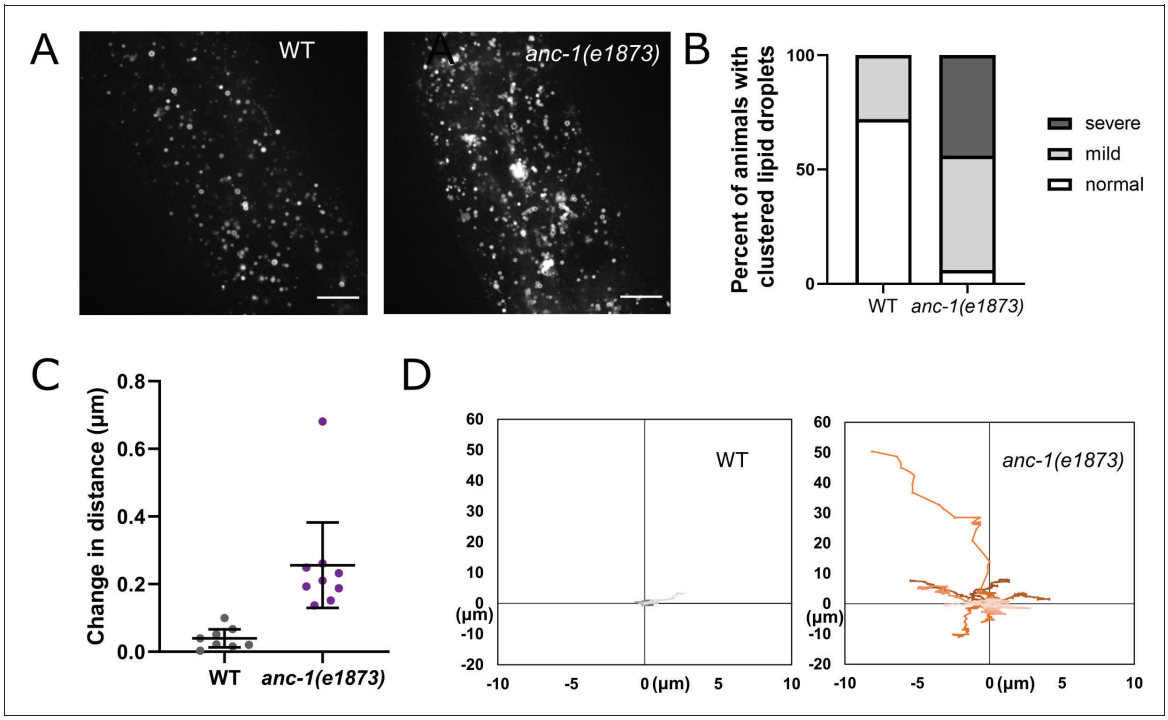

Figure 8. Lipid droplets are mispositioned in *anc-1* mutants. (**A**) Representative images of hyp7 lipid droplets labeled with the $P_{mdt\text{-}28}$*::mdt-28::mCherry* marker in the young adult animals. (**B**) Scoring of the lipid droplet positioning defects. Images were randomized for blind analysis by multiple researchers. n ≥ 11. (**C–D**) Time-lapse images of hyp7 lipid droplets. (**C–D**) The lipid droplet displacement phenotype was quantified as described in ***Figure 4E–F***. The average change in distance between two points in 242 ms intervals is plotted in (**C**). The trajectories of the relative movements of each spot apart from the others are shown in (**D**). Eight movies of each strain were analyzed. Scale bar, 10 µm for all the images. Also see ***Videos 4–5***. WT = wild type.

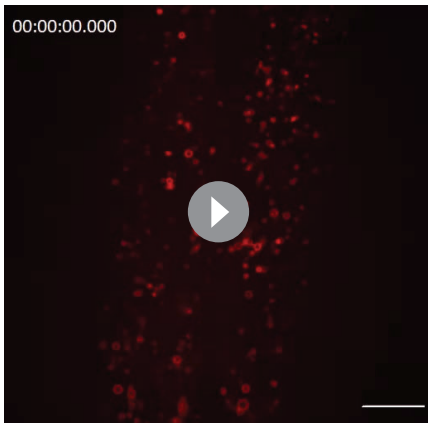

Video 4. Lipid droplets are anchored in wild type (WT) hyp7. An example video of the hyp7 lipid droplets in young adult wild type *C. elegans* expressing *ldrls2 [mdt-28p::mdt-28::mCherry +unc-76(+)]*. Images were captured at the interval of 0.2 s for 10 s. Scale bar, 10 µm.
https://elifesciences.org/articles/61069#video4

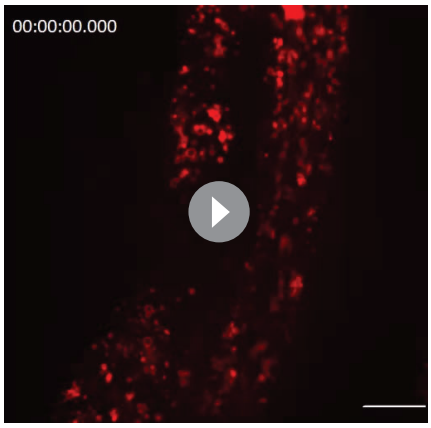

Video 5. Lipid droplets are unanchored in *anc-1(e1873)* mutant hyp7. An example video of the hyp7 lipid droplets in the young adult *anc-1(e1873)* mutant *C. elegans* expressing *ldrls2 [mdt-28p::mdt-28::mCherry +unc-76(+)]*. Images were captured at the interval of 0.24 s for 10 s. Scale bar, 10 µm.
https://elifesciences.org/articles/61069#video5

shape in *anc-1* mutants to better characterize how nuclear and/or ER movements affect the nuclear structure. Adult syncytial hyp7 nuclei were significantly smaller in *anc-1(*Δ6RPS) and *anc-1(e1873)* mutants compared to wild type (***Figure 11A***). Furthermore, the shape of *anc-1(e1873)* hyp7 nuclei, as measured by circularity and solidity, was significantly less round than wild type (***Figure 11B***).

Given the nuclear anchorage, ER positioning, and nuclear shape defects observed in *anc-1* mutants, we examined whether these animals might have other developmental or growth defects. Despite producing fertile adults, *anc-1* null animals had severe developmental defects. The brood size of *anc-1(e1873)* mutants was less than 25% of wild type (***Figure 11C***) and *anc-1(e1873)* mutants had significantly smaller body sizes throughout larval and adult stages (***Figure 11D–F***). Together these results suggest that there are developmental consequences associated with organelle positioning defects in *anc-1* mutants.

Discussion

LINC complexes consisting of giant KASH proteins (*C. elegans* ANC-1, *Drosophila* MSP300, and mammalian Nesprin-1 and -2) and canonical SUN proteins (*C. elegans* UNC-84, *Drosophila* Koi, and mammalian Sun1 and Sun2) are thought to anchor nuclei by tethering them to the cytoskeleton (***Starr and Fridolfsson, 2010***). ANC-1 was thought to connect actin filaments to the nuclear envelope using conserved CH and KASH domains at its N- and C-termini, respectively (***Starr and Han, 2002***). However, results discussed below indicate that this model is not sufficient to explain the role of KASH proteins in the cell. We propose a cytoplasmic integrity model, where giant KASH proteins function, largely independently of LINC complexes at the nuclear envelope and through mechanisms that do not require their CH domains. We find ANC-1 also localizes close to the ER throughout the cell. The large cytoplasmic domains of ANC-1 are required for positioning nuclei, ER, and likely other organelles. In the absence of ANC-1, the contents of the cytoplasm are disconnected from each other, unanchored in place, and sometimes fragmented. The cytoplasm and organelles freely flow throughout the hypodermal syncytia as worms crawl. It appears that ANC-1 is required to organize the entire cytoplasm.

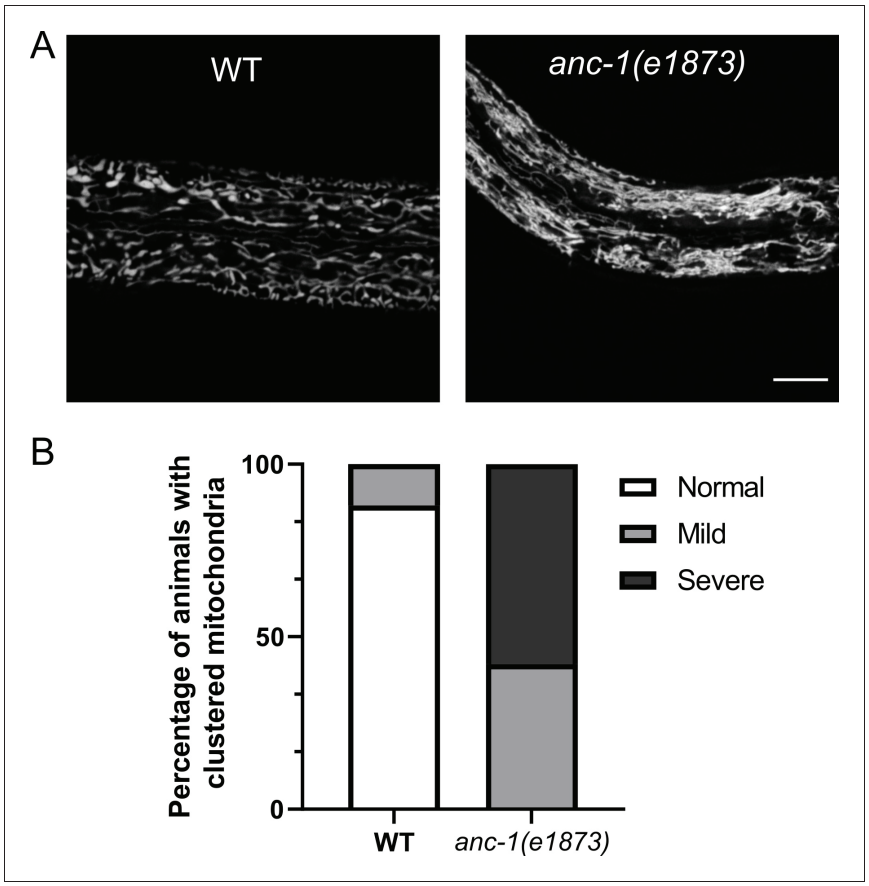

Figure 9. Mitochondria are mispositioned in *anc-1* mutants. (**A**) The hyp7 mitochondria were labeled with the $P_{col\text{-}10}$*::mito::GFP* marker in the L3 animals. (**B**) The mitochondria positioning defect was scored. Images were randomized for blind analysis by multiple researchers. n ≥ 18 for each strain. Scale bar, 10 μm for all the images. Also see ***Videos 6–7***. WT = wild type.

Our finding that ANC-1 works independently of LINC complexes during hyp7 nuclear positioning has significant implications for how the field currently understands the role of LINC complexes in development and disease. A dominant negative approach relies on overexpression of KASH domains to displace endogenous KASH proteins from the nuclear envelope (***Grady et al., 2005***; ***Starr and Han, 2002***; ***Tsujikawa et al., 2007***). Alternatively, a mini-nesprin-2 construct, consisting of the calponin homology and KASH domains with a few spectrin repeats, is commonly used in rescue experiments (***Davidson et al., 2020***; ***Luxton et al., 2010***; ***Ostlund et al., 2009***). If ANC-1 and other giant KASH orthologs have major LINC complex-independent functions, these approaches might have more caveats than previously thought.

We found that the CH domain of ANC-1 is dispensable for ER and nuclear positioning. Similar findings suggest the Nesprin-1 or -2 CH domains are also dispensable for the development of mouse skeletal muscles and the epidermis (***Lüke et al., 2008***; ***Stroud et al., 2017***). Moreover, the CH domains are not required for Nesprin-2 mediated neuronal migration in the developing rat brain (***Gonçalves et al., 2020***). Thus, the significance of the conserved CH domain is not clear. The CH domain of Nesprin-2 is required to form transmembrane actin-associated lines on the nuclear

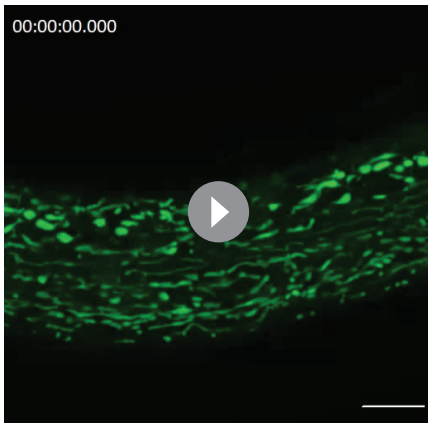

Video 6. Mitochondria are anchored in wild type (WT) hyp7. An example video of hyp7 mitochondria in young adult wild type *C. elegans* as followed by the $P_{col\text{-}10}$*::mitoLS::GFP* marker. Images were captured at the interval of 0.1 s for 10 s. Scale bar, 10 μm.
https://elifesciences.org/articles/61069#video6

envelope during rearward nuclear movement in mouse NIH3T3 fibroblasts polarizing for migration and to accumulate Nesprin-2 at the front of nuclei in cultured mouse embryonic fibroblasts migrating through constrictions (***Davidson et al., 2020***; ***Luxton et al., 2010***).

Most of the other ANC-1 domains, including the C-terminal transmembrane span and the large cytoplasmic repeat regions, are required for nuclear anchorage. Portions of the tandem repeats may be arranged in bundles of three helices, reminiscent of spectrin repeats (***Liem, 2016***). Thus, we hypothesize that ANC-1, like the other giant KASH orthologs MSP300 and Nesprin-1 and -2, consists largely of spectrin repeats with a C-terminal transmembrane domain that attaches ANC-1 to the contiguous ER and outer nuclear membrane.

In general, giant KASH proteins localize strongly to the nuclear envelope in multiple systems (***Starr and Fridolfsson, 2010***). Evidence for giant KASH protein localization to other subcellular locations has been largely ignored or attributed to overexpression artifacts (***Zhang et al., 2001***) or the loss of KASH protein function (***Roux et al., 2009***). Antibodies against ANC-1 mostly localize away from nuclei and are only clearly enriched at the nuclear periphery in the somatic gonad (***Starr and Han, 2002***) and Nesprin-1 localizes to ciliary rootlets (***Potter et al., 2017***). Yet, most models, including the nuclear tethering model, focus primarily on nuclear envelope localization. We found that GFP::ANC-1b was not enriched at the nuclear envelope in most tissues (***Figure 5—***

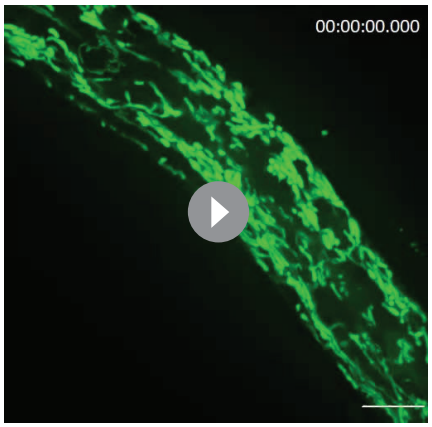

Video 7. Mitochondria are unanchored in *anc-1(e1873)* mutant hyp7. An example video of hyp7 mitochondria in the young adult *anc-1(e1873)* mutant *C. elegans* as followed by the $P_{col\text{-}10}$*::mitoLS::GFP* marker. Images were captured at the interval of 0.1 s for 10 s. Scale bar, 10 μm.
https://elifesciences.org/articles/61069#video7

Video 8. Microtubules in wild type (WT) hypodermal syncytia. A representative clip of the hyp7 in a wild type young adult expressing GFP:: MAPH-1.1 to mark microtubules in cyan and EMR-1::mCherry to mark nuclear envelopes in magenta. Images were at the interval of 1 s for 20 s. Scale bar, 10 μm.
https://elifesciences.org/articles/61069#video8

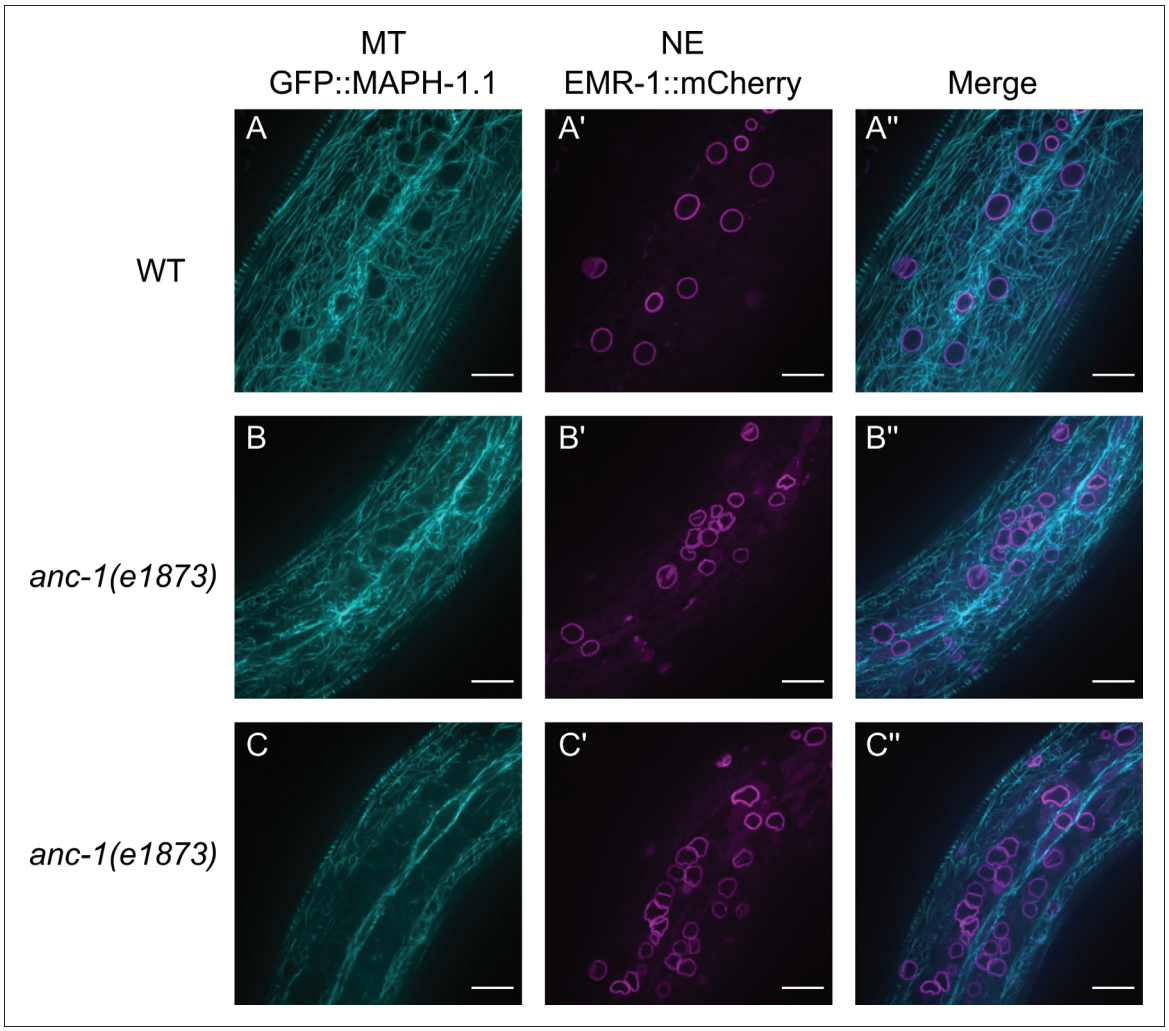

Figure 10. Microtubule organization in *anc-1* mutants. Representative images of microtubules (cyan) and nuclear envelope (NE) (magenta) from the same young adult animals are shown. (**A–A''**) wild type (WT), (**B–B''**) *anc-1(e1873)* mutant animal where the microtubules are mostly normal. (**C–C''**) In other *anc-1(e1873)* animals, microtubule organization is disrupted in the channels where nuclei move. Microtubules are labeled with GFP::MAPH-1.1 and the nuclear envelope is labeled with EMR-1::mCherry. Scale bar, 10 µm. Also see ***Videos 8–10***.

figure supplement 1). Instead, our findings suggest that ANC-1 functions throughout the cytoplasm with its C-terminus in the ER membrane.

We observed that the ER is severely mispositioned in *anc-1* null mutant hypodermal cells. Also, mitochondria are misshaped and mispositioned in the *anc-1* null mutants, but not in *unc-84* nulls (***Hedgecock and Thomson, 1982***; ***Starr and Han, 2002***). Two different mechanisms could explain how nuclei, mitochondria, and the ER are all mispositioned in *anc-1* mutants. First, abnormal organelle clusters could result from a failure in the active positioning process (***Folker and Baylies, 2013***; ***Roman and Gomes, 2018***). Alternatively, organelles could lose physical connections to the rest of the cytoplasm, resulting in organelles being passively pushed around in response to external mechanical forces, such as those generated when the worm crawls. Live imaging favors the second

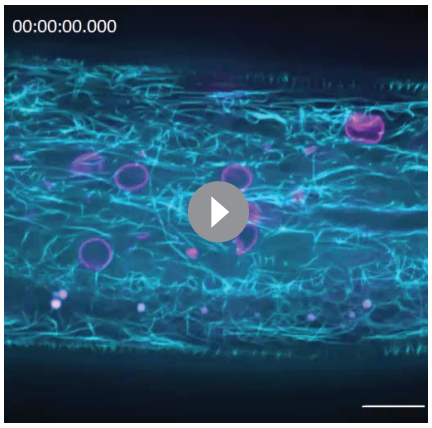

Video 9. Microtubules in *anc-1(null)* hypodermal syncytia. A representative clip of the hyp7 in a *anc-1 (e1783)* mutant young adult expressing GFP:: MAPH-1.1 to mark microtubules in cyan and EMR-1::mCherry to mark nuclear envelopes in magenta. Images were at the interval of 0.845 s for 40 s. Scale bar, 10 μm.
https://elifesciences.org/articles/61069#video9

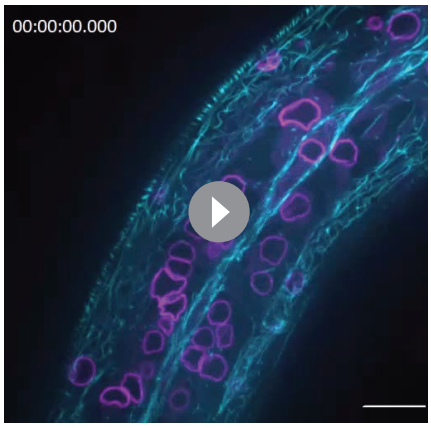

Video 10. Microtubules in *anc-1(null)* hypodermal syncytia. A representative clip of the hyp7 in a *anc-1 (e1783)* mutant young adult expressing GFP::MAPH-1.1 to mark microtubules in cyan and EMR-1::mCherry to mark nuclear envelopes in magenta. Images were at the interval of 0.638 s for 32 s. Scale bar, 10 μm.
https://elifesciences.org/articles/61069#video10

model. As *anc-1* mutant worms bent their bodies, ER fragments rapidly moved in a bulk flow of cytoplasm along with nuclei. The nuclei became misshapen and the ER often fragmented. Nuclei and the ER appeared to be completely detached from any sort of cytoplasmic structural network in *anc-1* mutants. There is precedent that giant KASH proteins could mechanically stabilize the cytoplasm. In cultured mouse NIH3T3 fibroblasts, disrupting KASH proteins leads to the decreased stiffness across the entire cell, as determined by single-particle microrheology experiments (***Stewart-Hutchinson et al., 2008***). Therefore, we propose that ANC-1 and other giant KASH proteins normally function at the ER periphery as important crosslinkers to maintain the mechanical integrity of the cell.

ANC-1 likely maintains the mechanical integrity of the cytoplasm via cytoskeletal networks. Disruption of MSP300 leads to disruption of both actin and microtubule networks in *Drosophila* muscles (***Wang et al., 2015***). Giant KASH proteins can interact with actin independently of their CH domains. ANC-1 binds to AMPH-1/BIN1, which is involved in actin nucleation (***D'Alessandro et al., 2015***), and Nesprin-2 binds to the actin regulators Fascin and FHOD1 (***Jayo et al., 2016***; ***Kutscheidt et al., 2014***). Nesprin-1 interacts with Akap450 to form microtubule organizing centers at the nuclear envelope of mouse muscles (***Elhanany-Tamir et al., 2012***; ***Gimpel et al., 2017***; ***Zheng et al., 2020***). Intermediate filaments and spectraplakins have also been implicated in nuclear positioning (***Ralston et al., 2006***; ***Wang et al., 2015***; ***Zheng et al., 2020***). However, *anc-1* null mutant animals had a reasonably normal microtubule network. Thus, how ANC-1b might directly interact with cytoskeletal components requires further investigations.

In summary, we propose a cytoplasmic integrity model, for how ANC-1 and giant KASH orthologs position nuclei and other organelles. First, ANC-1 is targeted to the ER through its C-terminal transmembrane span. The large cytoplasmic domain of ANC-1 likely consists of divergent spectrin-like repeats that could serve as elastic filaments. ANC-1 filaments could interact with various components of the cytoskeleton, allowing ANC-1 to serve as a cytoskeletal crosslinker to maintain the mechanical integrity of the cytoplasm. However, since at least microtubules are not completely disrupted, ANC-1 likely functions to maintain the mechanical properties of the cytoplasm through other mechanisms. Extracellular mechanical pressure that is generated as the worm bends leads to rapid cytoplasmic fluid flows and positioning defects in nuclei, ER, mitochondria, and likely other

organelles. In this model, ANC-1 maintains cellular connectivity across the cytoplasm by anchoring organelles in place.

Materials and methods

Key resources table

Reagent type (species) or resource	Designation	Source or reference	Identifiers	Additional information
Strain, strain background (*Escherichia. coli*)	OP50	Caenorhabditis Genetics Center (CGC)	OP50	https://cgc.umn.edu/strain/OP50
Strain, strain background (*E. coli*)	DH10B	New England Biolabs (NEB)	C3019H	
Recombinant DNA reagent	pLF3FShC	***Nonet, 2020***	addgene: #153083	https://www.addgene.org/153083/
Recombinant DNA reagent	pSL845	This paper		$P_{y37a1b.5}$*::mKate2::tram-1::tram-1 3'UTR* plasmid to generate the *ycSi2* transgenic *C. elegans strain*
Recombinant DNA reagent	pSL835	This paper		P_{anc-1b}*::nls::gfp::lacZ* Plasmid to generate *ycEx260*
Recombinant DNA reagent	pSL289	This paper		P_{col-10}*::mitoLS::gfp* Plasmid to generate ycEx217

C. elegans genetics

C. elegans strains were maintained on nematode growth medium plates seeded with OP50 *E. coli* at the room temperature (approximately 22˚C) (***Brenner, 1974***). All the strains used in this study are listed in ***Table 1***. Some strains, including N2 (WB Cat# WBStrain00000001, RRID:WB-STRAIN:WBStrain00000001), which was used as wild type, were obtained from the Caenorhabditis Genetics Center, funded by the National Institutes of Health Office of Research Infrastructure Programs (P40 OD010440). Strains VC40007, VC20178, and VC40614 were provided by the *C. elegans* Reverse Genetics Core Facility at the University of British Columbia (***Thompson et al., 2013***). Strain RT3739 (*pwSi83*) was generously provided by Barth Grant (Rutgers University, NJ, USA). UD522 (*ycEx249 [pcol-19::gfp::lacZ, pmyo-2::mCherry]*) was previously described (***Cain et al., 2018***). Male strains of RT3739, UD522, BOX188, LIU2, UD756, UD3, and BN147 were made to cross into *anc-1* or *unc-84* mutants. Alternatively, *pcol-19::gfp::lacZ* was introduced into some mutants by standard germline transformation to make UD736 and UD737 (***Cain et al., 2018***; ***Mello et al., 1991***).

For *anc-1* RNAi feeding experiments, L4 stage animals were transferred onto NGM plates seeded with bacteria expressing dsRNA (***Timmons and Fire, 1998***). The clones from the Ahringer RNAi library (Source Bioscience) (***Kamath and Ahringer, 2003***) were confirmed by Sanger sequencing.

Nuclear anchorage assays were performed as described (***Cain et al., 2018***; ***Fridolfsson et al., 2018***). Briefly, L4 worms with GFP-marked hypodermal nuclei were picked onto fresh plates 20 hr before scoring. Young adults were mounted on 2% agarose pads in ~5 µl of 1 mM tetramisole in M9 buffer (***Fridolfsson et al., 2018***). Syncytial hyp7 nuclei were scored as touching if a nucleus was in contact with one or more neighboring nuclei. Only one lateral side of each animal was scored.

For the brood size assay, starting at the L4 stage, single animals were transferred onto fresh OP50 *E. coli* plates every 24 hr for seven days. The number of embryos laid were counted immediately after the removal of the animal each day.

To measure body size, embryos laid within an hour were collected and cultured for 24 hr and 69 hr to reach the L2 stage and the adult stage, respectively. Animals were mounted on 2% agarose pads in ~5 µl of 1 mM tetramisole in M9 buffer for imaging.

5'-Rapid amplification of cDNA ends (5'-RACE)

Total RNA was extracted from mixed stages of *C. elegans* using the RNeasy kit (QIAGEN). First-strand cDNAs were generated with the ThermoScript RT-PCR system using an *anc-1* antisense

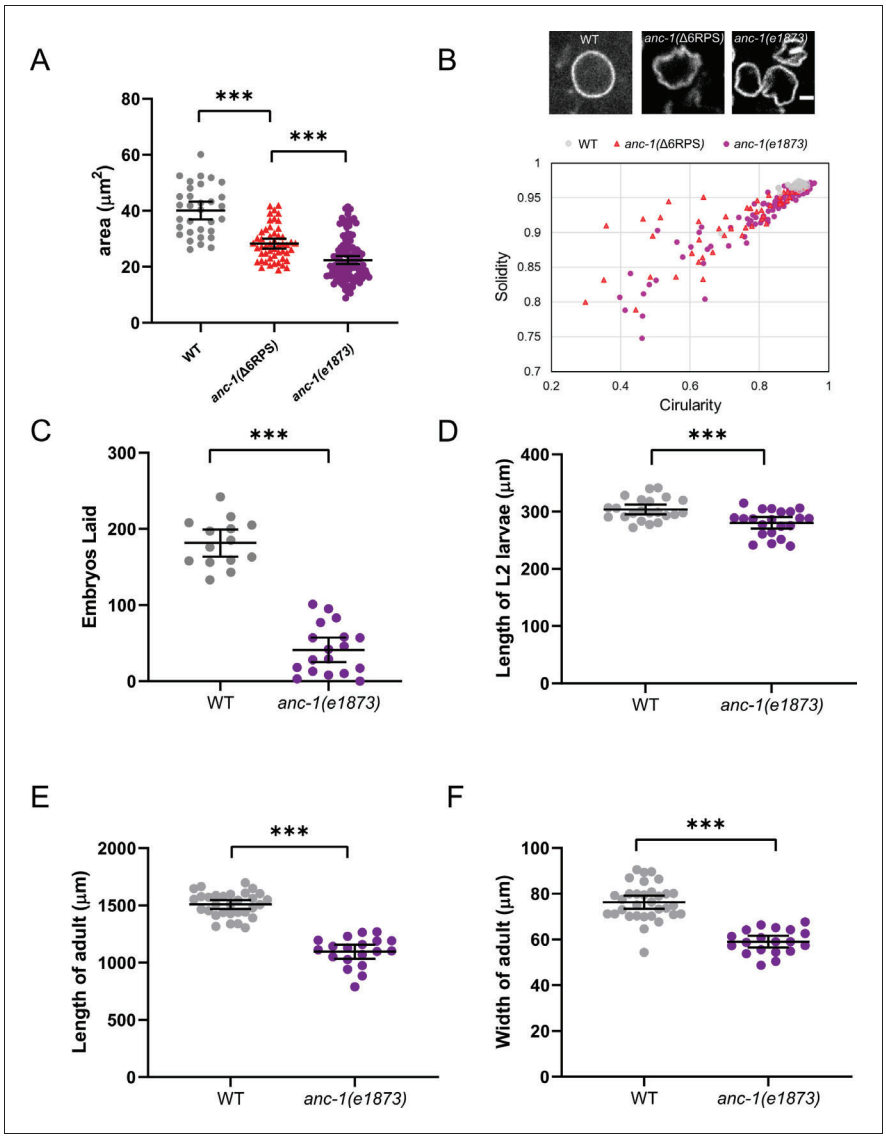

Figure 11. *anc-1* mutants have developmental defects. (**A**) The area of cross-sections of hyp7 nuclei is shown. Each dot represents the area of a single nucleus. n = 32 for wild type (WT), n = 50 for *anc-1*(Δ6RPS), n = 111 for *anc-1(e1873)*. (**B**) Top panel: Representative images of hyp7 nuclei marked by EMR-1::mCherry of WT, *anc-1* (Δ6RPS), and *anc-1(e1873)* mutants. Scale bar, 2 μm. Bottom panel: Plot of the solidity and the circularity. (**C–F**) The brood size (**C**), length of the L2 larvae (**D**), adult length (**E**) and width (**F**) are significantly reduced in *anc-1(e1873)* mutants. Each dot represents a single animal. n ≥ 14 for (**C**) and n ≥ 19 for (**D–F**). Means with 95% CI error bars are shown. Unpaired student two-tail t-test was used for statistical analysis. **p≤0.01; ***p≤0.001.

oligonucleotide (ods2572: 5'-ATAGATCATTACAAGATG-3'). Purification and TdT tailing of the first-strand cDNA were performed by the 5' RACE System for Rapid Amplification of cDNA Ends, version 2.0 (Invitrogen, Cat. No. 18374058). The target cDNA was amplified PCR using the provided 5'

Table 1. *C. elegans* strains in this study.

Strain	Genotype	Reference
N2	Wild type	
UD522	*ycEx249[p_{col-19}::gfp::lacZ, p_{myo-2}::mCherry]*	**Cain et al., 2018**
UD532	*unc-84(n369) X; ycEx249*	**Cain et al., 2018**
UD538	*anc-1(e1873) I; ycEx249*	**Cain et al., 2018**
UD578	*anc-1(yc52[Δ25KASH]) I; ycEx249*	This study
UD615	*anc-1(yc69[Δ29KASH]) I; ycEx249*	This study
JR672	*wIs54[scm::gfp] V*	**Terns et al., 1997**
UD457	*unc-84(n369) X; wIs54 V*	This study
UD451	*anc-1(e1873) I; wIs54 V*	This study
VC20178	*anc-1(gk109010[W427*]) I*	**Thompson et al., 2013**
UD737	*anc-1(gk109010[W427*]) I; ycEx 265[p_{col-19}::gfp::lacZ, p_{myo-2}::mCherry]*	This study
VC40007	*anc-1(gk109018[W621*]) I*	**Thompson et al., 2013**
UD736	*anc-1(gk109018[W621*]) I; yc Ex266[p_{col-19}::gfp::lacZ, p_{myo-2}::mCherry]*	This study
VC40614	*anc-1(gk722608[Q2878*]) I*	**Thompson et al., 2013**
UD565	*anc-1(gk722608[Q2878*]) I; ycEx249*	This study
UD535	*anc-1(yc41[anc-1::gfp3Xflag::kash,Δch]) I; ycEx249*	This study
UD608	*ycEx260[p_{anc-1b}::nls::gfp::lacZ]*	This study
UD599	*anc-1(yc62[ΔF1]) I; ycEx249*	This study
UD591	*anc-1(yc61[Δ6RPS]) I; ycEx249*	This study
UD668	*anc-1(yc80[ΔF2]) I; ycEx249*	This study
UD669	*anc-1(yc81[ΔF2-neck]) I; ycEx249*	This study
UD695	*anc-1(yc61[Δ6RPS]) I; unc-84(n369) X; ycEx249*	This study
UD696	*anc-1(yc62[ΔF1]) I; unc-84(n369) X; ycEx249*	This study
UD612	*anc-1(yc68[gfp::anc-1b]) I*	This study
UD655	*anc-1(yc78[Δ5RPS]) I; ycEx249*	This study
UD619	*anc-1(yc68[gfp::anc-1b]) I; ycEx249*	This study
UD694	*anc-1(yc90[anc-1::gfp::F2]) I*	This study
UD697	*anc-1(yc90[anc-1::gfp::F2]) I; ycEx249*	This study
UD618	*anc-1(yc70[gfp::anc-1b::Δ6rps]) I*	This study
UD698	*anc-1(yc91[gfp::anc-1b::Δ5rps]) I*	This study
UD701	*anc-1(yc92[gfp::anc-1b::Δf1]) I*	This study
UD702	*anc-1(yc93[anc-1AI972,973**::gfp]) I*	This study
UD625	*anc-1(yc71[ΔTK]) I; ycEx249*	This study
UD645	*anc-1(yc73[gfp::anc-1b::Δ6rps::Δtk]) I; ycEx249*	This study
RT3739	*pwSi83[p_{hyp7}gfp::kdel]*	A gift from Barth Grant
UD652	*anc-1(e1873) I; pwSi83*	This study
UD679	*unc-84(n369) X; pwSi83*	This study
UD707	*anc-1(yc71[ΔTK]) I; pwSi83*	This study
UD651	*anc-1(yc61[Δ6RPS]) I; pwSi83*	This study
UD672	*anc-1(yc69[Δ29KASH]) I; pwSi83*	This study
UD520	*anc-1(yc36[anc-1::gfp3Xflag::kash]) I*	This study

Table 1 continued on next page

Table 1 continued

Strain	Genotype	Reference
BN147	*bqSi142 [p_{emr-1}::emr-1::mCherry + unc-119(+)] II*	**Morales-Martínez et al., 2015**
BOX188	*maph-1.1(mib12[gfp::maph-1.1]) I*	**Waaijers et al., 2016**
UD649	*maph-1.1(mib12[gfp::maph-1.1]) I; bqSi142 II*	This study
UD650	*anc-1(e1873) I; maph-1.1(mib12[gfp::maph-1.1]) I; bqSi142 II*	This study
UD677	*anc-1(yc61[Δ6RPS]) I; maph-1.1(mib12[gfp::maph-1.1]) I; bqSi142 II*	This study
UD3	*ycEx217[P_{col-10}::mitoLS::GFP, P_{odr-1}::RFP]*	This study
UD676	*anc-1(e1873) I; [P_{col-10}::mitoLS::GFP, P_{odr-1}::RFP]*	This study
LIU2	*ldrIs2 [mdt-28p::mdt-28::mCherry + unc-76(+)].*	**Na et al., 2015**
UD681	*anc-1(e1873) I; ldrIs2*	This study
UD728	*anc-1(yc94[gfp::anc-1b::Δtk]) I*	This study
UD789	*anc-1(yc106[gfp::anc-1b::Δkash]) I*	This study
UD756	*ycSi2[pSL845 $P_{y37a1b.5}$::mKate2::tram-1::tram-1 3'UTR] IV*	This study
NM5179	*jsTi1493[LoxP::mex-5p::FLP:SL2::m NeonGreen::rpl-28p::FRT::GFP::his-58::FRT3] IV*	**Nonet, 2020**
UD778	*anc-1(yc68[gfp::anc-1b]) I; ycSi2*	This study
UD779	*anc-1(yc90[anc-1::gfp::F2]) I; ycSi2*	This study
UD780	*anc-1(yc70[gfp::anc-1b::Δ6rps]) I; ycSi2*	This study
UD781	*anc-1(yc106[gfp::anc-1b::Δkash]) I; ycSi2*	This study
UD782	*anc-1(yc94[gfp::anc-1b::Δtk]) I; ycSi2*	This study
UD783	*anc-1(yc68[gfp::anc-1b]) I; bqSi142*	This study
UD785	*anc-1(yc70[gfp::anc-1b::Δ6rps]) I; bqSi142*	This study
UD790	*anc-1(yc68[gfp::anc-1b]) I; ldrIs2*	This study

RACE Abridged Anchor Primer and an *anc-1* specific primer: ods2574 (5'-GTCGGCGTCTGAAG-GAAAGA-3'). The PCR product was purified using the QIAquick PCR purification kit (QIAGEN) and Sanger sequencing was performed by Genewiz.

Plasmid construction and transformation

To generate plasmid p_{anc-1b}*::nls::gfp::lacZ* (pSL835), a 2.56 kb fragment of genomic DNA upstream of the start codon of *anc-1b* was amplified with primers ods2491 (5'- TACCGAGCTCAGAAAAAA TGACTGTGAGTATAGTCATTTTCCGCT-3') and ods2492 (5'-GTACCTTACGCTTCTTC TTTGGAGCCATTTTGGTTCGGAGCAC-3') to replace the *col-19* promoter of p_{col-19}*::gfp::lacZ* (pSL779) (**Cain et al., 2018**). N2 animals were injected with 45 ng/µl of pSL835, 50 ng/µl of pBluescript SK, and 2.5 ng/µl of pCFJ90 (p_{myo-2}*::mCherry*) (**Frøkjaer-Jensen et al., 2008**) by standard *C. elegans* germline transformation (**Evans, 2006**) to make strain UD608 (*ycEx260[Panc-1b::nls::gfp::lacZ-2]*). Plasmid P_{col-10}*::mitoLS::gfp* (pSL289) and the odr-1::rfp co-injection marker were injected into N2 young adults to generate UD3 *ycEx217[P_{col-10}::mitoLS::GFP, Podr-1::RFP]* transgenic strain. Flp Recombinase-Mediated Cassette Exchange (RMCE) method was used to generate strain UD756 *ycSi2[pSL845 $P_{y37a1b.5}$::mKate2::tram-1::tram-13'UTR]* (**Nonet, 2020**). pLF3FShC was a gift from Michael Nonet (Addgene plasmid # 153083; http://n2t.net/addgene:153083; RRID:Addgene_153083). To generate plasmid pSL845, the $P_{y37a1b.5}$*::mKate2* fragment amplified from pSL843 (primers: ods2785 and ods2787) and the *tram-1* fragment amplified from the *C. elegans* genomic DNA (primers: ods2788 and ods2789) were inserted into plasmid pLF3FShC through Sap I Golden Gate Assembly (**Nonet, 2020**).

Primers sequences are:

ods2785: 5′-CCGTAAGCTCTTCGTGGGTTGCAGAAAAATATTTCACTGTTTC-3′;
ods2787: 5′-GCAACAGCTCTTCGCTCCGGAACCTCCACGGTGTCCGAGCTTGGA-3′;
ods2788 5′-GCAACAGCTCTTCGGAGGTGGATCTGGAGGTGTTAAGCCGCAAGGAGG-3′;
ods2789: 5′-GCAACAGCTCTTCGTACATGTAATAAAATATAAGAAAACGCTG-3′.

CRISPR/Cas9 mediated gene editing

Knock-in strains were generated using a *dpy-10* Co-CRISPR strategy (**Arribere et al., 2014**; **Paix et al., 2015**; **Paix et al., 2017**). All crRNA and repair template sequences are in **Table 2**. An injection mix containing 0.12 µl *dpy-10* crRNA (0.6 mM) (Horizon Discovery/Dharmacon), 0.3 µl target gene crRNA (0.6 mM) for one locus editing or 0.21 µl of each crRNA (0.6 mM) for multi-loci editing and 1.46 µl (one locus) or 1.88 µl (two loci) universal tracrRNA (0.17 mM) (Horizon Discovery/Dharmacon) precomplexed with purified 7.6 µl of 40 µM Cas9 protein (UC Berkeley QB3) and 0.29 µl of the *dpy-10* single-strand DNA oligonucleotide (ssODN) (500 ng/µl) repair templates and 0.21 µl ssODN repair template (25 µM) for the target gene editing or up to 500 ng double-strand DNA were injected to the germline of the hermaphrodite young adults. For *anc-1(yc52*[Δ25KASH]*) I, anc-1 (yc69*[Δ29KASH]*) I, anc-1(yc62*[ΔF1]*) I, anc-1(yc61*[Δ6RPS]*) I, anc-1(yc80*[ΔF2]*) I, anc-1(yc78*[Δ5RPS]*) I, anc-1(yc91[gfp::anc-1b::Δ5rps]) I, anc-1(yc70[gfp::anc-1b::Δ6rps]) I, anc-1(yc92[gfp::anc-1b::Δf1]) I, anc-1(yc93[anc-1AI972,973**::gfp]) I, anc-1(yc106[gfp::anc-1b::Δkash]) I, anc-1(yc94[gfp::anc-1b::Δ tk]), I* single-strand DNA (SSD) (synthesized by Integrated DNA Technologies, IDT) was used as repair template. For GFP knock-in strains, double-strand DNA repair templates were amplified with PCR from the plasmids pSL779 for *gfp* using Phusion polymerase and the primers listed in **Table 2** (New England Biolabs) (**Bone et al., 2016**; **Cain et al., 2018**).

Strains *anc-1[yc41(anc-1::gfp3Xflg::kash,Δch)]I* and *anc-1[yc36(anc-1::gfp3Xflag::kash)]I* were generated by Dickinson Self-Excising Drug Selection Cassette (SEC) method (**Dickinson et al., 2015**). In *anc-1[yc41(anc-1::gfp3Xflg::kash,Δch)]I*, both CH domains were deleted (starting with 23KAQK26 and ending with 322QFVR325) and replaced with GFP flanked with 9-residue long linkers (GASGASGAS).

Microscopy and imaging analysis

Images of the nuclear anchorage, worm body size measurements and *anc-1b* promoter reporter assays were collected with a wide-field epifluorescent Leica DM6000 microscope with a 63 × Plan Apo 1.40 NA objective, a Leica DC350 FX camera, and Leica LAS AF software. ANC-1 subcellular localization, the ER marker, and nuclear shape images were taken with a spinning disc confocal microscope (Intelligent Imaging Innovations) with a CSU-X1 scan head (Yokogawa), a Cascade QuantEM 512SC camera (Photometrics), a 100 × NA 1.46 objective (Zeiss or Nikon), and SlideBook software (Intelligent Imaging Innovations). The contrast and levels of the images were uniformly adjusted using ImageJ (National Institutes of Health). Live GFP::KDEL images were acquired at 200 ms or 250 ms intervals using the above spinning disc confocal system. To quantify ER, lipid droplet, and mitochondria positioning defects, images from at least 10 young adults of each strain were scored blindly by three people. In addition, the 'Manual Tracking' plug-in for ImageJ (https://imagej.nih.gov/ij/plugins/track/track.html) was used to track the positions of multiple ER fragments and lipid droplets through a time-lapse series. The relative movements between three different spots per animal were measured over time.

To quantify the fluorescent intensity of GFP::ANC-1B and GFP::ANC-1(Δ6RPs), images were taken under the spinning disc confocal system (100X objective) and the RawIntDen of the was hypodermal area measured by ImageJ. The average fluorescent intensity was calculated by dividing the RawIntDen by the area.

For the ER colocalization analysis, z stack images were taken under the spinning disc confocal system (100X objective) and processed by background subtraction with rolling ball radius of 50.0 pixels. A Region of interest (ROI) of 96 × 96 pixels in the non-nuclear region was cropped to use ScatterJ plugin for co-localization analysis (**Zeitvogel et al., 2016**).

For some adult animals, Image J 'Stitching' Plug-in was used to stitch images with overlap (**Preibisch et al., 2009**). The length of L2 larvae, width and length of the adult animals, as well as the circularity and solidity of the nuclei were measured with Image J.

Table 2. crRNA and repair templates used in this study.

New alleles	Strain	crRNA *	DNA repair template * †,§, ‡
anc-1(yc52[Δ25KASH]) I	N2	CAGUACUCGUCG UCGCAAUG	GCACTGCTTGTTCTACTTATGGGAGCCGCTTGTTTGGTTCCACA cTGtGAtGAtGAaTAtTAATCTTTAATTTTTTATTTTCATTACTATT CACTATTGTTTCATTCATCATGAACCTG
anc-1(yc69[Δ29KASH]) I	N2	CAGUACUCGUCG UCGCAAUG	NHEJ ‡
anc-1(yc41[anc-1::gfp3Xflag::kash,Δch]) I	N2	UUUCAUC UUGAAGAGGUUCG	–AAAATCTATTTTGAAAATTTTCAGATGAGGACGAG<EGFP-3xFLAG > AGATCAGGAGCTAGCGGAGCCATGTTCGGAGAAAGATCACCAATG–
anc-1(yc62[ΔF1]) I	N2	ACUUGAUCAAUCUA UAAUAA	GAAACATGAAAGCAAAGTACATTTTTTTAAAAATCGATT ATTTCagATcGAcCAgGTACAGTCTGAGATCGACACTCTTT CAGACTTCGAGGAGATCGAGCGTGAAATAAACGGCTC ACTCGAAGCTTTCGAAGCCGAG
anc-1(yc61[Δ6RPS]) I	N2	GCGUUCAAUUUC UUCAAAAU UGUUAGUA UUGGCGGCGAGU GGAGCGUUUUG UAAAAGCAA	AAGGTACAAAACATTGGAAAAACATCGATTGACGACG TGAATGTATCTGACTTCGAGGAGATCGAGCGTGAGAT CAATGGCTCCCTTGAGGCTTTCTCTATTTGGGAACG CTTCGTCAAGGCTAAAGATGATTTGTACGATTATTTG GAGAAATTAGAGAACAATGTAAGC
anc-1(yc80[ΔF2]) I	N2	GGAGCGUUUUG UAAAAGCAA UCCAACGGGAUC UUUGUCGU	ACTCTTATTCCGGACCTTGAAGAAAGAGCTTCTATTTG GGAGCGTACTGCTTTGCCACTTCAGGTTTGTT TATATTTTTTAATATTAATA
anc-1(yc36[anc-1::gfp3Xflag::kash]) I	N2	GACAAAGATCCCG TTGGAGA	TCCGACGACAgAGATCtCGcTGGcGcCGcGTACTCA GAACTTCAGGAGCTAGCGGAGCC < EGFP-3xFLAG > tcaggagctagcggagccGCTTTGCCACTTCAGgtttgtttatatttttt
anc-1([yc68[gfp::anc-1b]]) I	N2	CCGUCGGAACAGC UCCAUUU	TCTTAACCTTTTGTTCCATTCACTAATTATTTTCAAT TACAGGAGGTTGGCCGCGAGTCGGTCAGTAAATTA TCAGCTGCAGTTGACGATCGATACATCTACACGTT ACACGTGCTCCGAACTAAG < EGFP > GGAGGTTCCG GAGGTGGATCTGGAGGTGAaCTcTTtCGtCGtCTGCAA AACTTTTGCGACGCTGTCAAAATATTGCGATCGCAAAA TACCAAATGGAACGGAATCAAGATTTCGCAGGTTTGT TTCAAAAGCATCACAAATTAGCGG
anc-1(yc78[Δ5RPS]) I	N2	GGAGCGUUUUG UAAAAGCAA UUCCUCUGGCUU-CAACGAGU	GATCAGCTCAAGTCGGACGATTTGAAGACGGCAGAA AAGGAAATCACTAAtagccTcAAaCCcGAaTCTATTTGG GAaaGaTTcGTtAAgGCtAAAGATGATTTGTACGATT ATTTGGAGAAATTAGAGAACAAT
anc-1(yc90[anc-1::gfp::F2]) I	N2	GGAGCGUUUUG UAAAAGCAA	CCGGACCTTGAAGAAAGAGCTTCTATTTGGGAGCG TGGTGGAAGTGGTGGAGGAAGCGGTGGA < EGFP > GCATGGATGAACTATACAAAGGAGGTTCCGGAGGTGG ATCTGGAGGTTTcGTcAAgGCtAAAGATGATTTGTACG ATTATTTGGAGAAATTAGAGAACA
anc-1(yc70[gfp::anc-1b::Δ6rps]) I	UD612	GCGUUCAAUUUC UUCAAAAU UGUUAGUA UUGGCGGCGAGU GGAGCGUUUUG UAAAAGCAA	AAGGTACAAAACATTGGAAAAACATCGATTGACGAC GTGAATGTATCTGACTTCGAGGAGATCGAGCGTGA GATCAATGGCTCCCTTGAGGCTTTCTCTATTTGGGA ACGCTTcGTcAAgGCtAAAGATGATTTGTACGATTAT TTGGAGAAATTAGAGAACAATGTAAGC
anc-1(yc91[gfp::anc-1b::Δ5rps]) I	UD612	GGAGCGUUUUG UAAAAGCAA UUCCUCUGGCUU-CAACGAGU	GATCAGCTCAAGTCGGACGATTTGAAGACGGCAGA AAAGGAAATCACTAAtagccTcAAaCCcGAaTCTATTT GGGAaaGaTTcGTtAAgGCtAAAGATGATTTGTAC GATTATTTGGAGAAATTAGAGAACAAT
anc-1(yc92[gfp::anc-1b::Δf1]) I	UD612	ACUUGAUCAAUCUA UAAUAA	GAAACATGAAAGCAAAGTACATTTTTTTAAAAATCG ATTATTTCagATcGAcCAgGTACAGTCTGAGATCGAC ACTCTTTCAGACTTCGAGGAGATCGAGCGTGAAAT AAACGGCTCACTCGAAGCTTTCGAAGCCGAG
*anc-1(yc93[anc-1AI972,973**::gfp]) I*	UD612	ACUCACCUCUAGAAA UUCGA	CAAAATTTAGAGCTCAGCAATGAGCAGGACTGTCC AGATtaatgaGgtaccCTAGAGGTGAGTATAGTCA TTTTCCGCTCATTACACTCTT
anc-1(yc71[ΔTK]) I	N2	CAGAACUGC UUUGCCACUUC AUUAAAGAUUAAAA UGGUGG	GAACAACTCCGACGACAAAGATCCCGTTGGAGACG GGTACTCAGATAATCTTTAATTTTTTATTTTCATT ACTATTCACTATTGTTTCATTCATC

Table 2 continued on next page

Table 2 continued

New alleles	Strain	crRNA *	DNA repair template * †,§, ‡
anc-1(yc106[gfp::anc-1b::Δ kash]) I	UD612	CAGUACUCGUCG UCGCAAUG	GCACTGCTTGTTCTACTTATGGGAGCCGCTTGTT TGGTTCCACAcTGtGAtGAtGAaTAtTAATCTTTAAT TTTTTATTTTCATTACTATTCACTATTGTTTCATTCATCATGAACCTG
anc-1(yc94[gfp::anc-1b::Δtk])	UD612	CAGAACUGC UUUGCCACUUC AUUAAAGAUUAAAA UGGUGG	GAACAACTCCGACGACAAAGATCCCGTTGGAGAC GGGTACTCAGATAATCTTTAATTTTTTATTTTCA TTACTATTCACTATTGTTTCATTCATC
anc-1(yc73[gfp::anc-1b::Δ6rps::Δtk]) I	UD618	CAGAACUGC UUUGCCACUUC AUUAAAGAUUAAAA UGGUGG	GAACAACTCCGACGACAAAGATCCCGTTGGAGAC GGGTACTCAGATAATCTTTAATTTTTTATTTTCAT TACTATTCACTATTGTTTCATTCATC
dpy-10(cn64)	Co-CRISPR	GCUACCA UAGGCACCACGAG ***Arribere et al., 2014***	CACTTGAACTTCAATACGGCAAGATGAGAATGAC TGGAAACCGTACCGCATGCGGTGCCTATGGTAGC GGAGCTTCACATGGCTTCAGACCAACAGCCTAT (***Arribere et al., 2014***)

*all nucleotide sequences are displayed as single strand in the 5′ to 3′ orientation.

†In many cases a ssDNA oligonucleotide was used. For larger inserts, a PCR product was used.

§An imprecise NHEJ event led to an in-frame deletion without using the repair template.

¶Underlined sequences introduce silent mutations so the repair template is not cut by Cas9.

‡Underline indicates the silent mutation in the repair template.

Statistical evaluation

The nuclear anchorage quantifying data were displayed as scatter plots with means and 95% CI as error bars. Sample sizes are indicated in the figures. The statistical tests are indicated in the figure legends. When there were limited comparisons. unpaired student t-tests were performed on the indicated comparisons for the nuclear anchorage assay, and Fisher's exact test was used. When multiple comparisons were made, ANOVA and Tukey's multiple comparisons tests were used. Prism nine software was used for the statistical analyses.

Acknowledgements

We thank Gant Luxton, Erin Cram, Charlotte Kelley, and members of the Starr lab, for helpful discussions and editing of the paper. We thank Barth Grant for sharing an unpublished strain, Erin Tapley and Yu-Tai Chang for the mitochondrial GFP strain, and Joshua Morgan for suggestions on nuclear shape measurements. We thank Michael Paddy at the MCB Light Microscopy Imaging Facility, which is a UC Davis Campus Core Research Facility, for microscopy assistance. The 3i Marianas spinning disc confocal used in this study was purchased using NIH Shared Instrumentation Grant 1S10RR024543-01. These studies were supported by the National Institutes of Health grants R01GM073874 and R35GM134859 to DAS.

Additional information

Funding

Funder	Grant reference number	Author
National Institutes of Health	R01GM073874	Daniel A Starr
National Institutes of Health	R35GM134859	Daniel A Starr

The funders had no role in study design, data collection and interpretation, or the decision to submit the work for publication.

Author contributions

Hongyan Hao, Conceptualization, Resources, Data curation, Formal analysis, Supervision, Validation, Investigation, Visualization, Methodology, Writing - original draft, Project administration, Writing - review and editing; Shilpi Kalra, Conceptualization, Formal analysis, Validation, Investigation, Methodology, Writing - review and editing; Laura E Jameson, Resources, Data curation, Formal analysis, Investigation, Writing - review and editing; Leslie A Guerrero, Natalie E Cain, Conceptualization, Resources, Formal analysis, Investigation, Methodology, Writing - review and editing; Jessica Bolivar, Conceptualization, Resources, Investigation, Methodology; Daniel A Starr, Conceptualization, Data curation, Formal analysis, Supervision, Funding acquisition, Validation, Visualization, Methodology, Writing - original draft, Project administration, Writing - review and editing

Author ORCIDs

Hongyan Hao https://orcid.org/0000-0003-0860-2615
Natalie E Cain http://orcid.org/0000-0003-1391-404X
Daniel A Starr https://orcid.org/0000-0001-7339-6606

Decision letter and Author response

Decision letter https://doi.org/10.7554/eLife.61069.sa1
Author response https://doi.org/10.7554/eLife.61069.sa2

Additional files

Supplementary files

- Transparent reporting form

Data availability

The list of strains generated is detailed in Table 1. All data points are displayed in the histograms in the figures.

References

Altun Z, Hall D. 2009. *Epithelial System, Hypodermis*. WormAtlas.

Arribere JA, Bell RT, Fu BX, Artiles KL, Hartman PS, Fire AZ. 2014. Efficient marker-free recovery of custom genetic modifications with CRISPR/Cas9 in *Caenorhabditis elegans*. *Genetics* **198**:837–846. DOI: https://doi.org/10.1534/genetics.114.169730, PMID: 25161212

Bone CR, Tapley EC, Gorjánácz M, Starr DA. 2014. The *Caenorhabditis elegans* SUN protein UNC-84 interacts with Lamin to transfer forces from the cytoplasm to the nucleoskeleton during nuclear migration. *Molecular Biology of the Cell* **25**:2853–2865. DOI: https://doi.org/10.1091/mbc.e14-05-0971, PMID: 25057012

Bone CR, Chang YT, Cain NE, Murphy SP, Starr DA. 2016. Nuclei migrate through constricted spaces using microtubule motors and actin networks in *C. elegans* hypodermal cells. *Development* **143**:4193–4202. DOI: https://doi.org/10.1242/dev.141192, PMID: 27697906

Bone CR, Starr DA. 2016. Nuclear migration events throughout development. *Journal of Cell Science* **129**:1951–1961. DOI: https://doi.org/10.1242/jcs.179788, PMID: 27182060

Brenner S. 1974. The genetics of *Caenorhabditis elegans*. *Genetics* **77**:71–94. PMID: 4366476

Cain NE, Jahed Z, Schoenhofen A, Valdez VA, Elkin B, Hao H, Harris NJ, Herrera LA, Woolums BM, Mofrad MRK, Luxton GWG, Starr DA. 2018. Conserved SUN-KASH interfaces mediate LINC Complex-Dependent nuclear movement and positioning. *Current Biology* **28**:3086–3097. DOI: https://doi.org/10.1016/j.cub.2018.08.001, PMID: 30245107

Calvi A, Burke B. 2015. LINC complexes and their role in human disease. *eLS* **39**:1–8. DOI: https://doi.org/10.1042/BST20110658

Castiglioni VG, Pires HR, Rosas Bertolini R, Riga A, Kerver J, Boxem M. 2020. Epidermal PAR-6 and PKC-3 are essential for larval development of *C. elegans* and organize non-centrosomal microtubules. *eLife* **9**:e62967. DOI: https://doi.org/10.7554/eLife.62067

Chang W, Worman HJ, Gundersen GG. 2015. Accessorizing and anchoring the LINC complex for multifunctionality. *Journal of Cell Biology* **208**:11–22. DOI: https://doi.org/10.1083/jcb.201409047, PMID: 25559183

D'Alessandro M, Hnia K, Gache V, Koch C, Gavriilidis C, Rodriguez D, Nicot AS, Romero NB, Schwab Y, Gomes E, Labouesse M, Laporte J. 2015. Amphiphysin 2 orchestrates nucleus positioning and shape by linking the

nuclear envelope to the actin and microtubule cytoskeleton. *Developmental Cell* **35**:186–198. DOI: https://doi.org/10.1016/j.devcel.2015.09.018, PMID: 26506308

Davidson PM, Battistella A, Déjardin T, Betz T, Plastino J, Borghi N, Cadot B, Sykes C. 2020. Nesprin-2 accumulates at the front of the nucleus during confined cell migration. *EMBO Reports* **21**:e49910. DOI: https://doi.org/10.15252/embr.201949910, PMID: 32419336

Dickinson DJ, Pani AM, Heppert JK, Higgins CD, Goldstein B. 2015. Streamlined genome engineering with a Self-Excising drug selection cassette. *Genetics* **200**:1035–1049. DOI: https://doi.org/10.1534/genetics.115.178335, PMID: 26044593

Duong NT, Morris GE, Lam leT, Zhang Q, Sewry CA, Shanahan CM, Holt I. 2014. Nesprins: tissue-specific expression of epsilon and other short isoforms. *PLOS ONE* **9**:e94380. DOI: https://doi.org/10.1371/journal.pone.0094380, PMID: 24718612

Elhanany-Tamir H, Yu YV, Shnayder M, Jain A, Welte M, Volk T. 2012. Organelle positioning in muscles requires cooperation between two KASH proteins and microtubules. *Journal of Cell Biology* **198**:833–846. DOI: https://doi.org/10.1083/jcb.201204102, PMID: 22927463

Evans T. 2006. *The C. Elegans Research Community Transformation and Microinjection*. WormBook. DOI: https://doi.org/10.1895/wormbook.1.108.1

Folker ES, Baylies MK. 2013. Nuclear positioning in muscle development and disease. *Frontiers in Physiology* **4**:363. DOI: https://doi.org/10.3389/fphys.2013.00363, PMID: 24376424

Fridolfsson HN, Herrera LA, Brandt JN, Cain NE, Hermann GJ, Starr DA. 2018. Genetic analysis of nuclear migration and anchorage to study LINC complexes during development of *Caenorhabditis elegans*. *Linc Complex: Methods and Protocols* **1840**:163–180. DOI: https://doi.org/10.1007/978-1-4939-8691-0_13

Frøkjaer-Jensen C, Davis MW, Hopkins CE, Newman BJ, Thummel JM, Olesen SP, Grunnet M, Jorgensen EM. 2008. Single-copy insertion of transgenes in *Caenorhabditis elegans*. *Nature Genetics* **40**:1375–1383. DOI: https://doi.org/10.1038/ng.248, PMID: 18953339

Gill NK, Ly C, Kim PH, Saunders CA, Fong LG, Young SG, Luxton GWG, Rowat AC. 2019. DYT1 dystonia Patient-Derived fibroblasts have increased deformability and susceptibility to damage by mechanical forces. *Frontiers in Cell and Developmental Biology* **7**:103. DOI: https://doi.org/10.3389/fcell.2019.00103, PMID: 31294022

Gimpel P, Lee YL, Sobota RM, Calvi A, Koullourou V, Patel R, Mamchaoui K, Nédélec F, Shackleton S, Schmoranzer J, Burke B, Cadot B, Gomes ER. 2017. Nesprin-1α-Dependent microtubule nucleation from the nuclear envelope via Akap450 is necessary for nuclear positioning in muscle cells. *Current Biology* **27**:2999–3009. DOI: https://doi.org/10.1016/j.cub.2017.08.031

Gonçalves JC, Quintremil S, Yi J, Vallee RB. 2020. Nesprin-2 recruitment of BicD2 to the nuclear envelope controls dynein/Kinesin-Mediated neuronal migration in Vivo. *Current Biology* **30**:3116–3129. DOI: https://doi.org/10.1016/j.cub.2020.05.091, PMID: 32619477

Grady RM, Starr DA, Ackerman GL, Sanes JR, Han M. 2005. Syne proteins anchor muscle nuclei at the neuromuscular junction. *PNAS* **102**:4359–4364. DOI: https://doi.org/10.1073/pnas.0500711102, PMID: 15749817

Grum VL, Li D, MacDonald RI, Mondragón A. 1999. Structures of two repeats of spectrin suggest models of flexibility. *Cell* **98**:523–535. DOI: https://doi.org/10.1016/S0092-8674(00)81980-7, PMID: 10481916

Gundersen GG, Worman HJ. 2013. Nuclear positioning. *Cell* **152**:1376–1389. DOI: https://doi.org/10.1016/j.cell.2013.02.031, PMID: 23498944

Harris TW, Arnaboldi V, Cain S, Chan J, Chen WJ, Cho J, Davis P, Gao S, Grove CA, Kishore R, Lee RYN, Muller HM, Nakamura C, Nuin P, Paulini M, Raciti D, Rodgers FH, Russell M, Schindelman G, Auken KV, et al. 2020. WormBase: a modern model organism information resource. *Nucleic Acids Research* **48**:D762–D767. DOI: https://doi.org/10.1093/nar/gkz920, PMID: 31642470

Hedgecock EM, Thomson JN. 1982. A gene required for nuclear and mitochondrial attachment in the nematode *Caenorhabditis elegans*. *Cell* **30**:321–330. DOI: https://doi.org/10.1016/0092-8674(82)90038-1, PMID: 6889924

Holt I, Duong NT, Zhang Q, Lam leT, Sewry CA, Mamchaoui K, Shanahan CM, Morris GE. 2016. Specific localization of nesprin-1-α2, the short isoform of nesprin-1 with a KASH domain, in developing, fetal and regenerating muscle, using a new monoclonal antibody. *BMC Cell Biology* **17**:26. DOI: https://doi.org/10.1186/s12860-016-0105-9, PMID: 27350129

Jaalouk DE, Lammerding J. 2009. Mechanotransduction gone awry. *Nature Reviews Molecular Cell Biology* **10**:63–73. DOI: https://doi.org/10.1038/nrm2597, PMID: 19197333

Jahed Z, Hao H, Thakkar V, Vu UT, Valdez VA, Rathish A, Tolentino C, Kim SCJ, Fadavi D, Starr DA, Mofrad MRK. 2019. Role of KASH domain lengths in the regulation of LINC complexes. *Molecular Biology of the Cell* **30**:2076–2086. DOI: https://doi.org/10.1091/mbc.E19-02-0079, PMID: 30995155

Jayo A, Malboubi M, Antoku S, Chang W, Ortiz-Zapater E, Groen C, Pfisterer K, Tootle T, Charras G, Gundersen GG, Parsons M. 2016. Fascin regulates nuclear movement and deformation in migrating cells. *Developmental Cell* **38**:371–383. DOI: https://doi.org/10.1016/j.devcel.2016.07.021, PMID: 27554857

Kamath RS, Ahringer J. 2003. Genome-wide RNAi screening in *Caenorhabditis elegans*. *Methods* **30**:313–321. DOI: https://doi.org/10.1016/S1046-2023(03)00050-1, PMID: 12828945

Kutscheidt S, Zhu R, Antoku S, Luxton GW, Stagljar I, Fackler OT, Gundersen GG. 2014. FHOD1 interaction with nesprin-2G mediates TAN line formation and nuclear movement. *Nature Cell Biology* **16**:708–715. DOI: https://doi.org/10.1038/ncb2981, PMID: 24880667

Lee YL, Burke B. 2018. LINC complexes and nuclear positioning. *Seminars in Cell & Developmental Biology* **82**:67–76. DOI: https://doi.org/10.1016/j.semcdb.2017.11.008, PMID: 29191370

Liem RK. 2016. Cytoskeletal integrators: the spectrin superfamily. *Cold Spring Harbor Perspectives in Biology* **8**: a018259. DOI: https://doi.org/10.1101/cshperspect.a018259, PMID: 27698030

Lüke Y, Zaim H, Karakesisoglou I, Jaeger VM, Sellin L, Lu W, Schneider M, Neumann S, Beijer A, Munck M, Padmakumar VC, Gloy J, Walz G, Noegel AA. 2008. Nesprin-2 giant (NUANCE) maintains nuclear envelope architecture and composition in skin. *Journal of Cell Science* **121**:1887–1898. DOI: https://doi.org/10.1242/jcs.019075, PMID: 18477613

Luxton GW, Gomes ER, Folker ES, Vintinner E, Gundersen GG. 2010. Linear arrays of nuclear envelope proteins harness retrograde actin flow for nuclear movement. *Science* **329**:956–959. DOI: https://doi.org/10.1126/science.1189072, PMID: 20724637

Luxton GW, Starr DA. 2014. KASHing up with the nucleus: novel functional roles of KASH proteins at the cytoplasmic surface of the nucleus. *Current Opinion in Cell Biology* **28**:69–75. DOI: https://doi.org/10.1016/j.ceb.2014.03.002, PMID: 24704701

Mello CC, Kramer JM, Stinchcomb D, Ambros V. 1991. Efficient gene transfer in *C. elegans*: extrachromosomal maintenance and integration of transforming sequences. *The EMBO Journal* **10**:3959–3970. DOI: https://doi.org/10.1002/j.1460-2075.1991.tb04966.x, PMID: 1935914

Morales-Martínez A, Dobrzynska A, Askjaer P. 2015. Inner nuclear membrane protein LEM-2 is required for correct nuclear separation and morphology in *C. elegans*. *Journal of Cell Science* **128**:1090–1096. DOI: https://doi.org/10.1242/jcs.164202, PMID: 25653391

Na H, Zhang P, Chen Y, Zhu X, Liu Y, Liu Y, Xie K, Xu N, Yang F, Yu Y, Cichello S, Mak HY, Wang MC, Zhang H, Liu P. 2015. Identification of lipid droplet structure-like/resident proteins in *Caenorhabditis elegans*. *Biochimica Et Biophysica Acta (BBA) - Molecular Cell Research* **1853**:2481–2491. DOI: https://doi.org/10.1016/j.bbamcr.2015.05.020

Nonet ML. 2020. Efficient transgenesis in *Caenorhabditis elegans* Using Flp Recombinase-Mediated Cassette Exchange. *Genetics* **215**:903–921. DOI: https://doi.org/10.1534/genetics.120.303388, PMID: 32513816

Ostlund C, Folker ES, Choi JC, Gomes ER, Gundersen GG, Worman HJ. 2009. Dynamics and molecular interactions of Linker of nucleoskeleton and cytoskeleton (LINC) complex proteins. *Journal of Cell Science* **122**: 4099–4108. DOI: https://doi.org/10.1242/jcs.057075, PMID: 19843581

Paix A, Folkmann A, Rasoloson D, Seydoux G. 2015. High efficiency, Homology-Directed genome editing in *Caenorhabditis elegans* using CRISPR-Cas9 ribonucleoprotein complexes. *Genetics* **201**:47–54. DOI: https://doi.org/10.1534/genetics.115.179382, PMID: 26187122

Paix A, Folkmann A, Seydoux G. 2017. Precision genome editing using CRISPR-Cas9 and linear repair templates in *C. elegans*. *Methods* **121-122**:86–93. DOI: https://doi.org/10.1016/j.ymeth.2017.03.023

Potter C, Zhu W, Razafsky D, Ruzycki P, Kolesnikov AV, Doggett T, Kefalov VJ, Betleja E, Mahjoub MR, Hodzic D. 2017. Multiple isoforms of Nesprin1 are integral components of ciliary rootlets. *Current Biology* **27**:2014–2022. DOI: https://doi.org/10.1016/j.cub.2017.05.066

Preibisch S, Saalfeld S, Tomancak P. 2009. Globally optimal stitching of tiled 3D microscopic image acquisitions. *Bioinformatics* **25**:1463–1465. DOI: https://doi.org/10.1093/bioinformatics/btp184, PMID: 19346324

Rajgor D, Mellad JA, Autore F, Zhang Q, Shanahan CM. 2012. Multiple novel nesprin-1 and nesprin-2 variants act as versatile tissue-specific intracellular scaffolds. *PLOS ONE* **7**:e40098. DOI: https://doi.org/10.1371/journal.pone.0040098, PMID: 22768332

Rajgor D, Shanahan CM. 2013. Nesprins: from the nuclear envelope and beyond. *Expert Reviews in Molecular Medicine* **15**:e5. DOI: https://doi.org/10.1017/erm.2013.6, PMID: 23830188

Ralston E, Lu Z, Biscocho N, Soumaka E, Mavroidis M, Prats C, Lømo T, Capetanaki Y, Ploug T. 2006. Blood vessels and desmin control the positioning of nuclei in skeletal muscle fibers. *Journal of Cellular Physiology* **209**:874–882. DOI: https://doi.org/10.1002/jcp.20780, PMID: 16972267

Rolls MM, Hall DH, Victor M, Stelzer EH, Rapoport TA. 2002. Targeting of rough endoplasmic reticulum membrane proteins and ribosomes in invertebrate neurons. *Molecular Biology of the Cell* **13**:1778–1791. DOI: https://doi.org/10.1091/mbc.01-10-0514, PMID: 12006669

Roman W, Gomes ER. 2018. Nuclear positioning in skeletal muscle. *Seminars in Cell & Developmental Biology* **82**:51–56. DOI: https://doi.org/10.1016/j.semcdb.2017.11.005, PMID: 29241690

Roux KJ, Crisp ML, Liu Q, Kim D, Kozlov S, Stewart CL, Burke B. 2009. Nesprin 4 is an outer nuclear membrane protein that can induce kinesin-mediated cell polarization. *PNAS* **106**:2194–2199. DOI: https://doi.org/10.1073/pnas.0808602106, PMID: 19164528

Starr DA. 2019. A network of nuclear envelope proteins and cytoskeletal force generators mediates movements of and within nuclei throughout *Caenorhabditis elegans* development . *Experimental Biology and Medicine* **244**:1323–1332. DOI: https://doi.org/10.1177/1535370219871965

Starr DA, Fridolfsson HN. 2010. Interactions between nuclei and the cytoskeleton are mediated by SUN-KASH nuclear-envelope bridges. *Annual Review of Cell and Developmental Biology* **26**:421–444. DOI: https://doi.org/10.1146/annurev-cellbio-100109-104037, PMID: 20507227

Starr DA, Han M. 2002. Role of ANC-1 in tethering nuclei to the actin cytoskeleton. *Science* **298**:406–409. DOI: https://doi.org/10.1126/science.1075119, PMID: 12169658

Stewart-Hutchinson PJ, Hale CM, Wirtz D, Hodzic D. 2008. Structural requirements for the assembly of LINC complexes and their function in cellular mechanical stiffness. *Experimental Cell Research* **314**:1892–1905. DOI: https://doi.org/10.1016/j.yexcr.2008.02.022, PMID: 18396275

Stroud MJ, Feng W, Zhang J, Veevers J, Fang X, Gerace L, Chen J. 2017. Nesprin 1α2 is essential for mouse postnatal viability and nuclear positioning in skeletal muscle. *Journal of Cell Biology* **216**:1915–1924. DOI: https://doi.org/10.1083/jcb.201612128, PMID: 28533284

Terns RM, Kroll-Conner P, Zhu J, Chung S, Rothman JH. 1997. A deficiency screen for zygotic loci required for establishment and patterning of the epidermis in *Caenorhabditis elegans*. *Genetics* **146**:185–206. DOI: https://doi.org/10.1093/genetics/146.1.185, PMID: 9136010

Thompson O, Edgley M, Strasbourger P, Flibotte S, Ewing B, Adair R, Au V, Chaudhry I, Fernando L, Hutter H, Kieffer A, Lau J, Lee N, Miller A, Raymant G, Shen B, Shendure J, Taylor J, Turner EH, Hillier LW, et al. 2013. The million mutation project: a new approach to genetics in *Caenorhabditis elegans*. *Genome Research* **23**: 1749–1762. DOI: https://doi.org/10.1101/gr.157651.113, PMID: 23800452

Timmons L, Fire A. 1998. Specific interference by ingested dsRNA. *Nature* **395**:854. DOI: https://doi.org/10.1038/27579, PMID: 9804418

Tsujikawa M, Omori Y, Biyanwila J, Malicki J. 2007. Mechanism of positioning the cell nucleus in vertebrate photoreceptors. *PNAS* **104**:14819–14824. DOI: https://doi.org/10.1073/pnas.0700178104, PMID: 17785424

van Bergeijk P, Hoogenraad CC, Kapitein LC. 2016. Right time, right place: probing the functions of organelle positioning. *Trends in Cell Biology* **26**:121–134. DOI: https://doi.org/10.1016/j.tcb.2015.10.001, PMID: 26541125

Waaijers S, Muñoz J, Berends C, Ramalho JJ, Goerdayal SS, Low TY, Zoumaro-Djayoon AD, Hoffmann M, Koorman T, Tas RP, Harterink M, Seelk S, Kerver J, Hoogenraad CC, Bossinger O, Tursun B, van den Heuvel S, Heck AJ, Boxem M. 2016. A tissue-specific protein purification approach in *Caenorhabditis elegans* identifies novel interaction partners of DLG-1/Discs large. *BMC Biology* **14**:66. DOI: https://doi.org/10.1186/s12915-016-0286-x, PMID: 27506200

Wang N, Tytell JD, Ingber DE. 2009. Mechanotransduction at a distance: mechanically coupling the extracellular matrix with the nucleus. *Nature Reviews Molecular Cell Biology* **10**:75–82. DOI: https://doi.org/10.1038/nrm2594, PMID: 19197334

Wang S, Reuveny A, Volk T. 2015. Nesprin provides elastic properties to muscle nuclei by cooperating with spectraplakin and EB1. *Journal of Cell Biology* **209**:529–538. DOI: https://doi.org/10.1083/jcb.201408098, PMID: 26008743

Xu D, Zhang Y. 2012. Ab initio protein structure assembly using continuous structure fragments and optimized knowledge-based force field. *Proteins: Structure, Function, and Bioinformatics* **80**:1715–1735. DOI: https://doi.org/10.1002/prot.24065, PMID: 22411565

Xu D, Zhang Y. 2013. Toward optimal fragment generations for ab initio protein structure assembly. *Proteins* **81**: 229–239. DOI: https://doi.org/10.1002/prot.24179, PMID: 22972754

Zeitvogel F, Schmid G, Hao L, Ingino P, Obst M. 2016. ScatterJ: an ImageJ plugin for the evaluation of analytical microscopy datasets. *Journal of Microscopy* **261**:148–156. DOI: https://doi.org/10.1111/jmi.12187, PMID: 25515182

Zhang Q, Skepper JN, Yang F, Davies JD, Hegyi L, Roberts RG, Weissberg PL, Ellis JA, Shanahan CM. 2001. Nesprins: a novel family of spectrin-repeat-containing proteins that localize to the nuclear membrane in multiple tissues. *Journal of Cell Science* **114**:4485–4498. PMID: 11792814

Zheng Y, Buchwalter RA, Zheng C, Wight EM, Chen JV, Megraw TL. 2020. A perinuclear microtubule-organizing centre controls nuclear positioning and basement membrane secretion. *Nature Cell Biology* **22**:297–309. DOI: https://doi.org/10.1038/s41556-020-0470-7, PMID: 32066907

Chapter V

Future directions

The TEM sections in Figure V.11 are prepared by Danielle Jorgens and Reena Zalpuri from the electron microscopy lab at UC Berkeley. Shilpi Kalra performed the analysis for Figure V.12E and F using the program developed by Sara Keegan and Liam Holt from the New York University.

V.1 Mechanism and regulation of SUN/KASH interactions *in vivo*

The LINC complexes are conserved across evolution. However, different SUN/KASH pairs facilitate various functions *in vivo*. For example, in *C. elegans*, SUN protein UNC-84 binds to UNC-83, which has a shorter KASH domain and lacks the conserved -23 cysteine, to move nuclei in the embryonic hyp7 precursor cells and the larva P cells (Malone, Fixsen et al. 1999, Bone, Chang et al. 2016, Bone and Starr 2016, Cain, Jahed et al. 2018). However, UNC-84 also interacts with ANC-1, which contain a longer KASH domain, to anchor the nuclei in the hyp7 syncytium and the intestine (Hedgecock and Thomson 1982, Starr and Han 2002). In chapter 2 and chapter 3, we found that the conserved cysteine plays essential roles for the force transmission across the NE. However, swapping the KASH domains of UNC-83 and ANC-1 at least partially disrupted each other's function (Chapter 2). It is still unclear how nuclear migration is affected in the *unc-83(anc-1kash)* embryos. One possibility is that SUN/KASH interaction is regulated differently for long and short KASH domains, leading to a reduced binding affinity to SUN proteins. Interestingly, my very preliminary results indicates that the UNC-83::GFP::ANC-1KASH is still localized on the NE but might be more broadly expressed (Figure V.1). It will be interesting to perform live-imaging to compare the UNC-83::GFP and UNC-83::GFP::ANC-1KASH protein level and subcellular localization during embryonic hyp7 precursor nuclear migration. One challenge is that UNC-83::GFP::KASH signal level is low and the high exposure time is likely to detect dim mitochondria autofluorescence. The future experiments may consider tagging the protein with seven copies of the GFP11 to enhance signal.

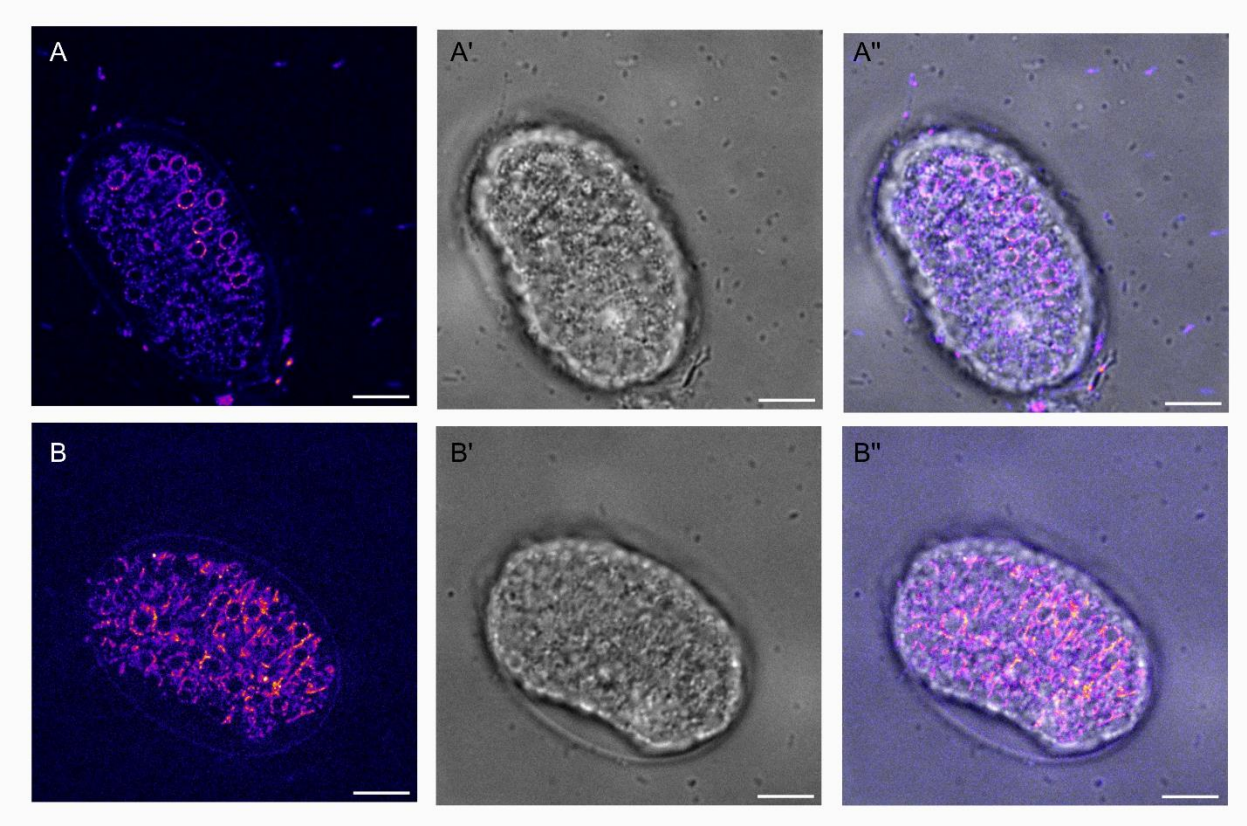

Figure V.1. UNC-83::ANC-1KASH is localized on the NE in the embryonic hyp7 precursors. (A-A') Representative confocal images of endogenous UNC-83::GFP::KASH in pseudo color (LUT fire) (A) and the DIC bright field image (A') are merged on the right (A''). (B-B'') Representative confocal images of endogenous UNC-83::GFP::ANC-1KASH in pseudo color (LUT fire) (B) and the DIC bright field image (B') are merged on the right (B''). Scale bar, 10μm.

In chapter 4, I found that the endogenous GFP-tagged ANC-1 protein is not enriched on the NE in the hyp7 syncytium (Figure II.5). Without the tandem repeats, the protein is enriched on the NE in a UNC-84-dependent manner but there are still cytoplasmic portions. UNC-83 is also expressed and localized on the NE in the adult hypodermis (Figure V.2). It would be interesting to check if UNC-83::GFP::ANC-1KASH is on the NE at the same level as UNC-83::GFP in the adult hyp7 syncytium. UNC-84 and UNC-83 are not uniformly localized on the NE (Figure V.2) (Malone, Fixsen et al. 1999, Starr and Han 2002), indicating they may some high-order oligomerization structures. The adult *C. elegans* hypodermis could potentially be a good in vivo

model to study: 1) What is the oligomerization state of the SUN/KASH proteins? Does SUN protein form LINC complexes with a mixture of two KASH proteins? For example, colocalization analysis of different fluorescent tagged UNC-83 and ANC-1(ΔRPs) would help to address this question; 2) What is the turn-over rate of the LINC complexes? Photoconvertible fluorescent proteins might be used to measure the lifetime of the assembled LINC complexes.

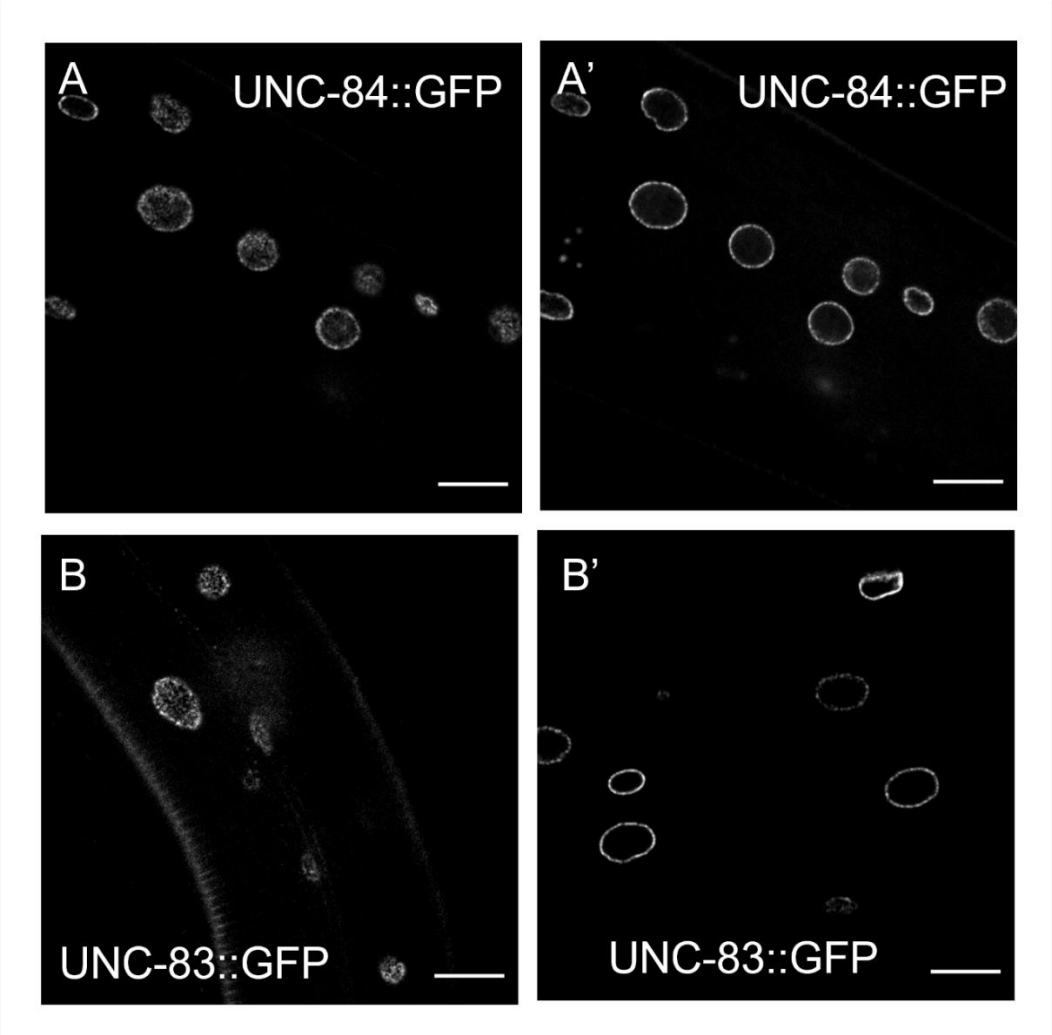

Figure V.2. UNC-84 and UNC-83 are not uniformly localized on the nuclear envelop (NE) in the hypodermis of young adult *C. elegans*. Representative confocal images of endogenous UNC-84::GFP (A, top view and A', cross section) and UNC-83::GFP::KASH (B, top view and B', cross section). Scale bar, 10μm.

In Chapter 4, I charactered a KASH-independent role of ANC-1 on nuclear positioning and organelle anchorage. Interestingly, overexpression the dominant negative KASH (DNKASH) containing the last 349 amino acids of ANC-in the adult hypodermis causes nuclear anchorage defects (Figure V.3 A and D). However, the mcherry::tagged DNKASH protein is not localized on the NE and form puncta or tubule-like structures (Figure V.3 B,C,E). Interestingly, these tubule-like structures are sometimes under motion. Mitochondria colocalization analysis indicates that these puncta are not on the mitochondria (Figure V.4). I have also checked shorter versions (100 residues and 63 residues) of the DNKASH and found similar results. It will be interesting to know if these tubule structures are newly formed ER and if the KASH peptides favors those structures. The promoter I use to overexpress the DNKASH constructs only start to express in late L4s. It is possible that the newly expressed KASH proteins cannot properly localize without extra UNC-84. In the future, a promoter turns on earlier in development could be used to test this hypothesis. In addition, it would be interesting to test if the KASH domain of UNC-83 is localized on the NE in the hypodermis. ANC-1 is enriched on the NE in other tissues like spermatheca, it is not clear if there is any mechanism in these tissues to promote SUN/KASH interaction or the interaction of ANC-1's cytoplasmic domains with other structures are inhibited. It is important as the field moves forward to be aware that the DNKASH approach used by so many is not likely as simple as the literature implies. We do not understand how overexpression of KASH leads to these phenotypes.

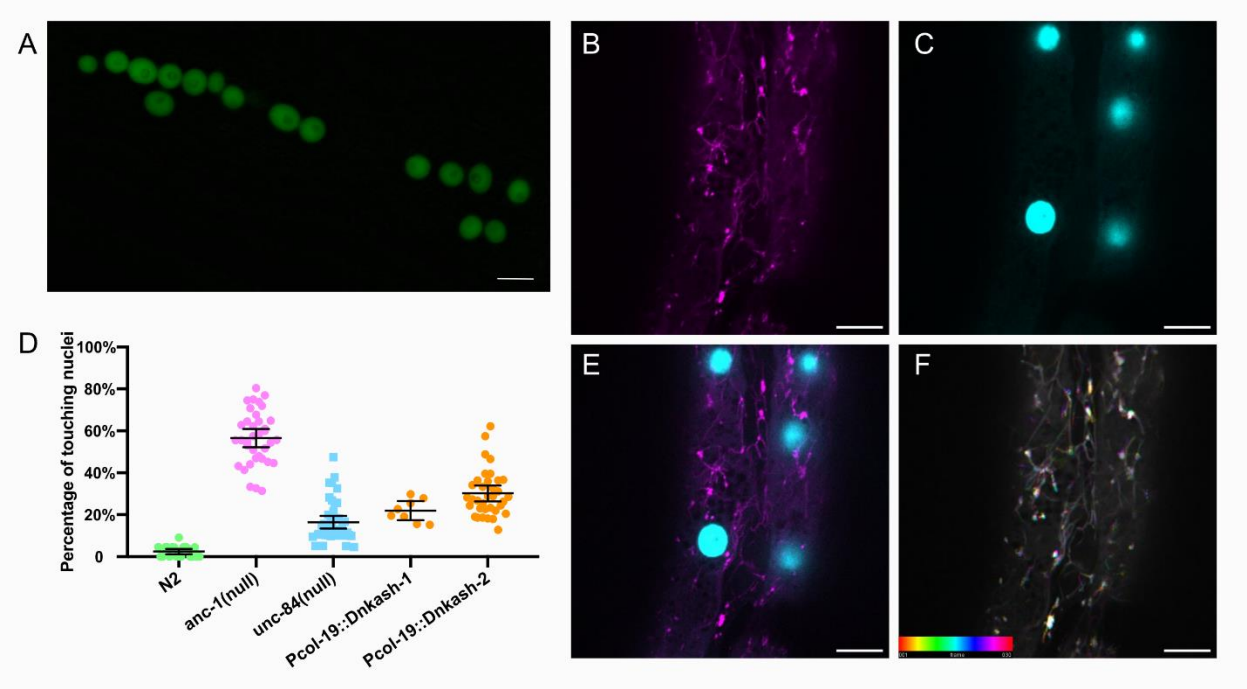

Figure V.3. The dominant negative KASH (DNKASH) is not localized on the NE in the hypodermis of *C. elegans* adults. (A) Lateral view of adult *C. elegans* expressing hypodermal nuclear GFP (green) in the DNKASH overexpression strain. (D) Quantification of nuclear anchorage defects in the DNKASH overexpression strains. Each dot represents the percentage of touching nuclei on one side of a young adult animal. Means with 95% CI error bars are shown. n ≥ 8. (B, C, E and F) Representative confocal images of mCherry::DNKASH (B, magenta), nuclear GFP (C, cyan) and the merge of two channels (E) in the adult hypodermis. (F) Image representing 30 frames of mCherry::DNKASH time-lapse sequences with spectrum color coding. The average time interval is 792.93 ms. Scale Bar, 10µm.

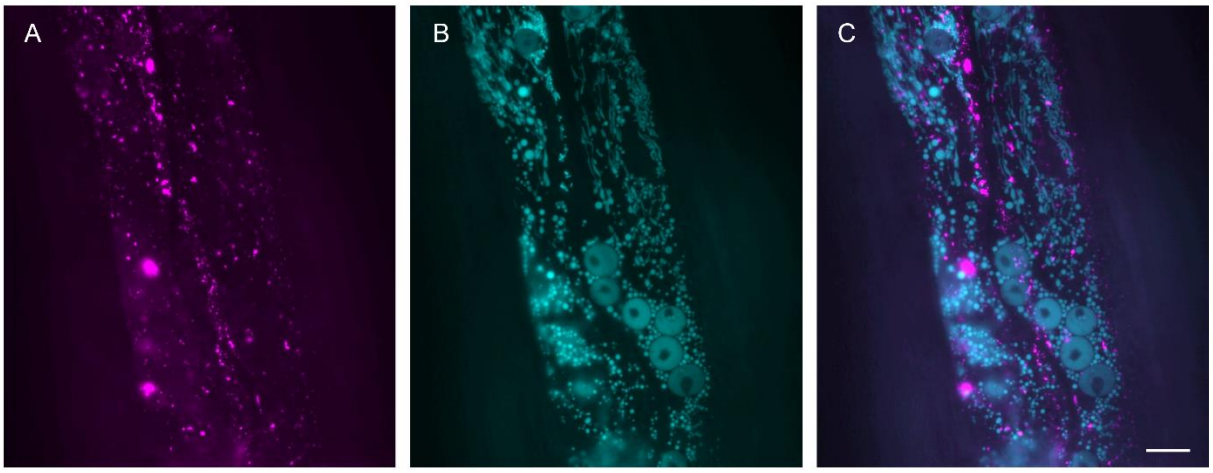

Figure V.4. The mCherry::DNKASH is not colocalized with mitochondria. Confocal images of mCherry::DNKASH in magenta (A), mito::GFP and nuclear GFP in cyan (B) and the merge of two channels (C). Scale Bar, 10µm.

V.2 UNC-83's role in preventing micronuclei in the hypodermis

UNC-83 is the KASH protein interacts with kinesin-1 and dynein to move nuclei in the embryonic hyp7 precursor and larval P cells. Interestingly, even long after the nuclear migration events, UNC-83 is persistently expressed and localized on the nuclear envelop in the *C. elegans* adult hypodermis. It is unclear what is the role of UNC-83 in the adult hypodermis. One hypothesis is that UNC-83 contributes to nuclear anchorage through tethering the syncytial nuclei to the microtubule. However, *unc-83* null mutants do not show nuclear anchorage defects (Figure V.5 C). In the *anc-1* mutants, nuclei group together and form clusters. It is also possible that UNC-83 only plays important roles in nuclear anchorage when *anc-1* is depleted. If this hypothesis is correct, we would expect more severe nuclear anchorage defects in *unc-83* and *anc-1* double mutants. On the other hand, UNC-83 could be the cause of nuclear movement and clustering in the syncytium when ANC-1 mediated nuclear anchorage is depleted. In this case, mutation in *unc-83* would suppress the nuclear cluster phenotype of *anc-1* mutants. Preliminary observation

indicates that double mutant of *unc-83* and *anc-1* still has severe nuclear anchorage defects, it would be interesting to carefully quantify it.

Micronuclei are small nuclear structures separate from the primary nucleus (Fenech, Kirsch-Volders et al. 2011, Krupina, Goginashvili et al. 2021). While characterizing nuclear anchorage defects of *unc-83* mutants, I found an increase of micronuclei in the in the adult seam cell and hyp7 syncytium of *unc-83(e1408)* mutants (Figure V.5 B and D). Interestingly, the SUN protein mutant *unc-84(n369)* null does not cause significant increase of micronuclei. Further experiments are needed to validate the results. If this phenotype is real, it indicates an UNC-84-independent role of UNC-83. It would be interesting to test if deletion of the KASH domain of UNC-83 cause any increase of the rate of micronuclei.

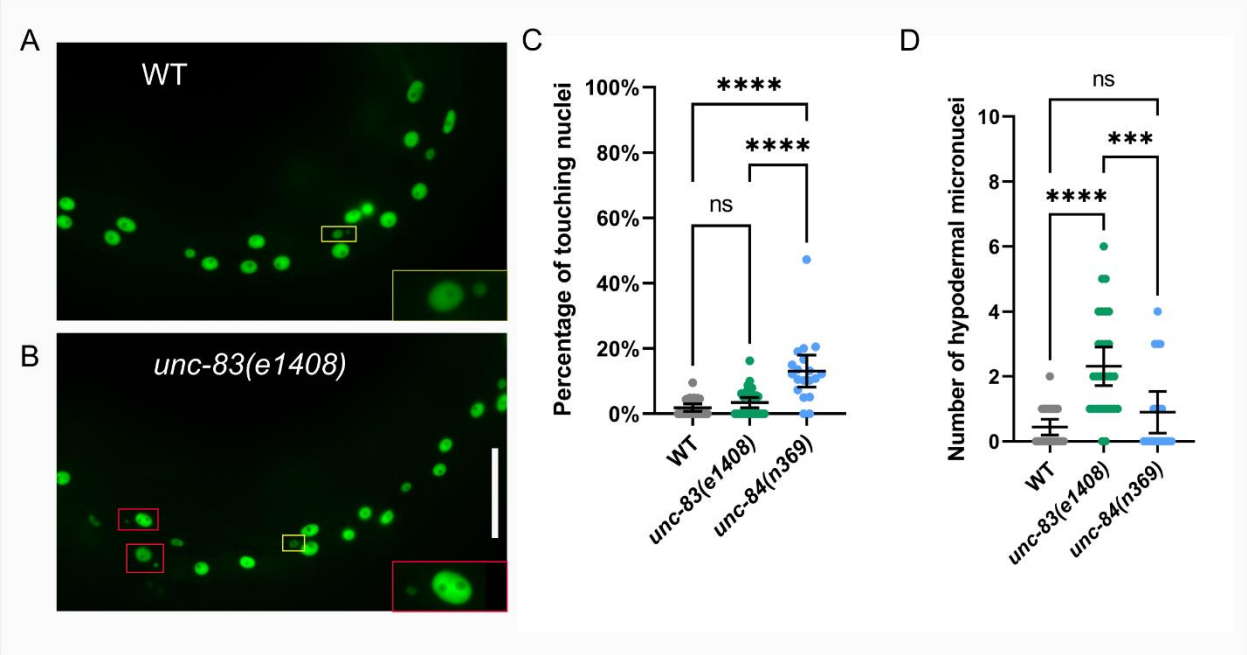

Figure V.5. The number of micronuclei is increased in *unc-83* null mutants. (A-B) Lateral views of young adult C. elegans expressing nuclear GFP marker (green) in the wild-type (WT) (A) and *unc-83(e1408)* (B) animals. The yellow boxes show examples of seam cell micronuclei while the red boxes show examples of hyp7 micronuclei. Scale Bar, 10µm. (C) Quantification of nuclear anchorage defects in the WT, *unc-83(e1408)* and *unc-84(n369)* mutants. Each dot represents the percentage of touching nuclei on one side

of a young adult animal. Means with 95% CI error bars are shown. n ⩾ 20. (D) Quantification of the number of micronuclei in the seam cell and hyp7 syncytium in the WT, *unc-83(e1408)* and *unc-84(n369)* mutants. Each dot represents the number of micronuclei on one side of a young adult animal. Means with 95% CI error bars are shown. n ⩾ 20.

First, micronuclei are DNA containing structures. The current marker we use to quantify micronuclei is NLS-GFP-LacZ. It would be important to use a fluorescent tagged histone marker or Hoescht 33258 staining to test if the micronucleus in the hypodermis contains DNA. It is still possible that the micronuclei we observe in the hypodermis are actually nuclear buds, which is distinguishable from the micronuclei by the thin chromatin bridge connected to the main nucleus (Hatch 2018). Second, micronuclei are mostly caused by defects in chromosome segregation during cell division or nuclear rupture (Krupina, Goginashvili et al. 2021). The adult hermaphrodite hyp7 contains 139 nuclei, 98 of which are derived from seam cell divisions (Altun and Hall 2009). It would be interesting to perform live imaging to test if there are chromosome segregation defects during seam cell division (Altun and Hall 2009). Third, it is possible that UNC-83 helps to maintain the nuclear envelope integrity in the syncytium. Nuclei are connected to the cytoskeleton through the LINC complexes and might be under mechanical stress (Belaadi, Aureille et al. 2016). It is possible UNC-83 associates with the microtubule motors to buffer the force from the cytoplasm on the nuclear envelope. In *anc-1* null mutants where the nuclei are not anchored, I have observed nuclear rotation in the cytoplasm (data not shown). It would be interesting to test if the nuclear rotation in *anc-1* mutants is UNC-83-dependent through live imaging with the strain UD961 (double mutant of *unc-83* and *anc-1* with the *mcherry::emr-1* nuclear envelop marker). Last, the daughters of seam cells become tetraploids once fused to hyp7. However, there are 23 nuclei that are fused to the hyp7 embryonically and remain diploid. Thus, although sharing the same cytoplasm, the nuclei in the syncytium might be

different in age and size. It would be interesting to test if the micronuclei are more likely occur in the seam-derived or the embryonically fused nuclei.

V.3 Function of the cytoplasmic domains of ANC-1

V.3.1 Deletion of fragment1 (F1) causes mild ER anchorage defects

In Chapter 4, I have shown that deletion of the F1 domain causes nuclear anchorage defects. However, it was not clear how F1 deletion affects nuclear positioning or if F1 also functions in ER anchorage. I have crossed the F1 deletion strain to a hyp7 specific GFP::KDEL ER marker and found that the mutant has mild ER defects (Figure V.6 B-B''). In the wild type (Figure V.6 A-A''), there are more ER connect to the nucleus, while in the F1 deletion mutants less ER is surrounding the nucleus. Further analysis on the amount of ER close to the nuclear envelope (within 2μm, for example) may help to characterize the phenotype. Interestingly, preliminary observation indicates that the KASH deletion and TK deletion may also increase the ER free region surrounding the nucleus (data not shown). It might be possible that ANC-1 functions to connect the ER and the nuclear envelop in a LINC-dependent manner. It is still mysterious how the F1 region might also contribute to the ER-nuclear connection.

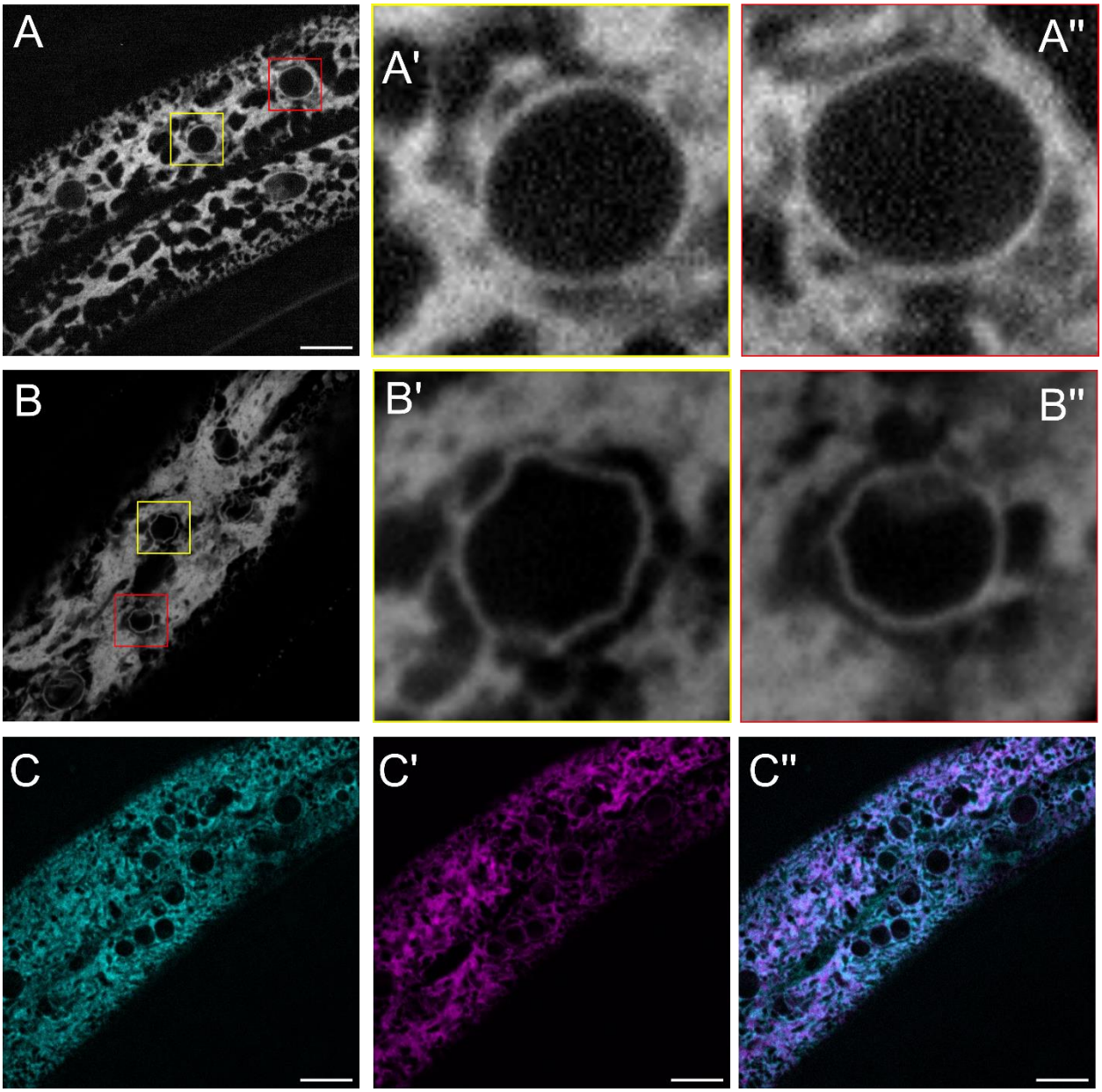

Figure V.6. Deletion of the fragment 1 (F1) of ANC-1 causes mild ER anchorage defects. Representative confocal image of GFP::KDEL labled ER in the hyp7 syncytium of the wild-type (A-A'') and *anc-1*(ΔF1) (B-B'') young adults are shown. A' and A'' are enlared image in the yellow and red boxes from A. B' and B'' are enlared image in the yellow and red boxes from B. (C-C'') Confocal images of GFP::ΔF1 (C, cyan), mKate2::TRAM-1 ER marker (C', magenta) and the merge of two channes (C''). Scale Bar, 10μm.

I have also deleted the F1 region in the GFP::ANC-1B background to test if F1 fragment plays a role in the colocalization of ANC-1 with the ER. As a result, deletion of the F1 region did not exclude the protein from the ER. GFP::ANC-1(ΔF1) is even more broadly expressed in the cytoplasm but is still mostly colocalized with the ER (Figure V.6 C-C''). I have also noticed that sometimes the ER moves slightly in the hyp7 syncytium, which is not as severe as the *anc-1* null. This observation is consistent with the clustering of lipid droplets in the F1 deletion mutants under DIC (Figure V.7 B), which is also not as significant as the *anc-1* null (Figure V.7C).

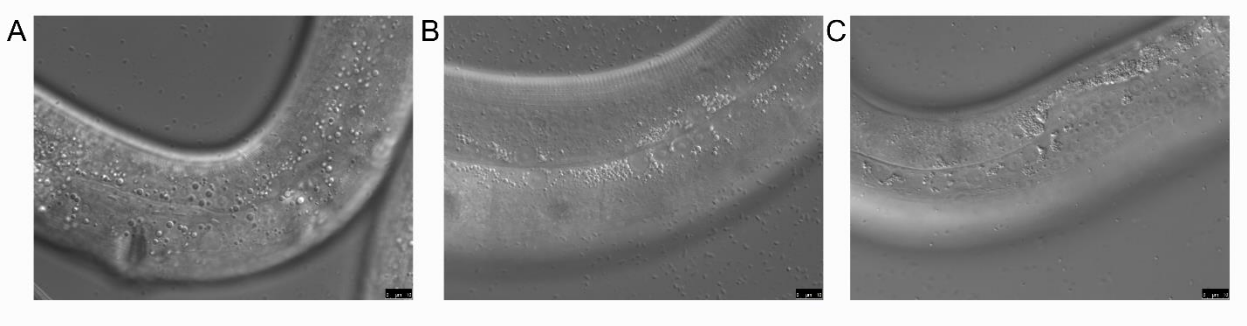

Figure V.7. Lipid droplets form clusters in the *anc-1*(ΔF1) animals. DIC images of the laterview of the hypodermis of young adult wild type (A), *anc-1*(ΔF1) (B) and *anc-1(e1873)* mutants. Scale Bar, 10μm.

V.3.2 Deletion of five of the six RPs causes protein subcellular localization and ER defects

In chapter 4, I have shown that deletion of five of the six tandem repeats has mild nuclear anchorage defects in compare with deletion of all six repeats. Without all the repeats, the ER is strongly misshaped, and the GFP-tagged protein is excluded from the ER. It was unclear if one repeat was sufficient to localize the protein to the ER and maintain its shape. To answer this question, I imaged the GFP::ANC-1(Δ5RPs) with the mKate2::TRAM-1 ER marker, and found that the ER morphology defect is not as severe as the *anc-1*(Δ6RPs) worms. GFP::ANC-1(Δ5RPs) protein sometimes form bright aggregates (Figure V.8 A, B), which might indicates

the self-interaction of ANC-1 proteins. There are still some ER/GFP::ANC-1(Δ5RPs) colocalization, especially at the bright GFP::ANC-1(Δ5RPs) protein aggregation sites. It is possible that the full-length protein is required to form a meshwork in the cytoplasm, which may function as a skeleton for the ER to be anchored.

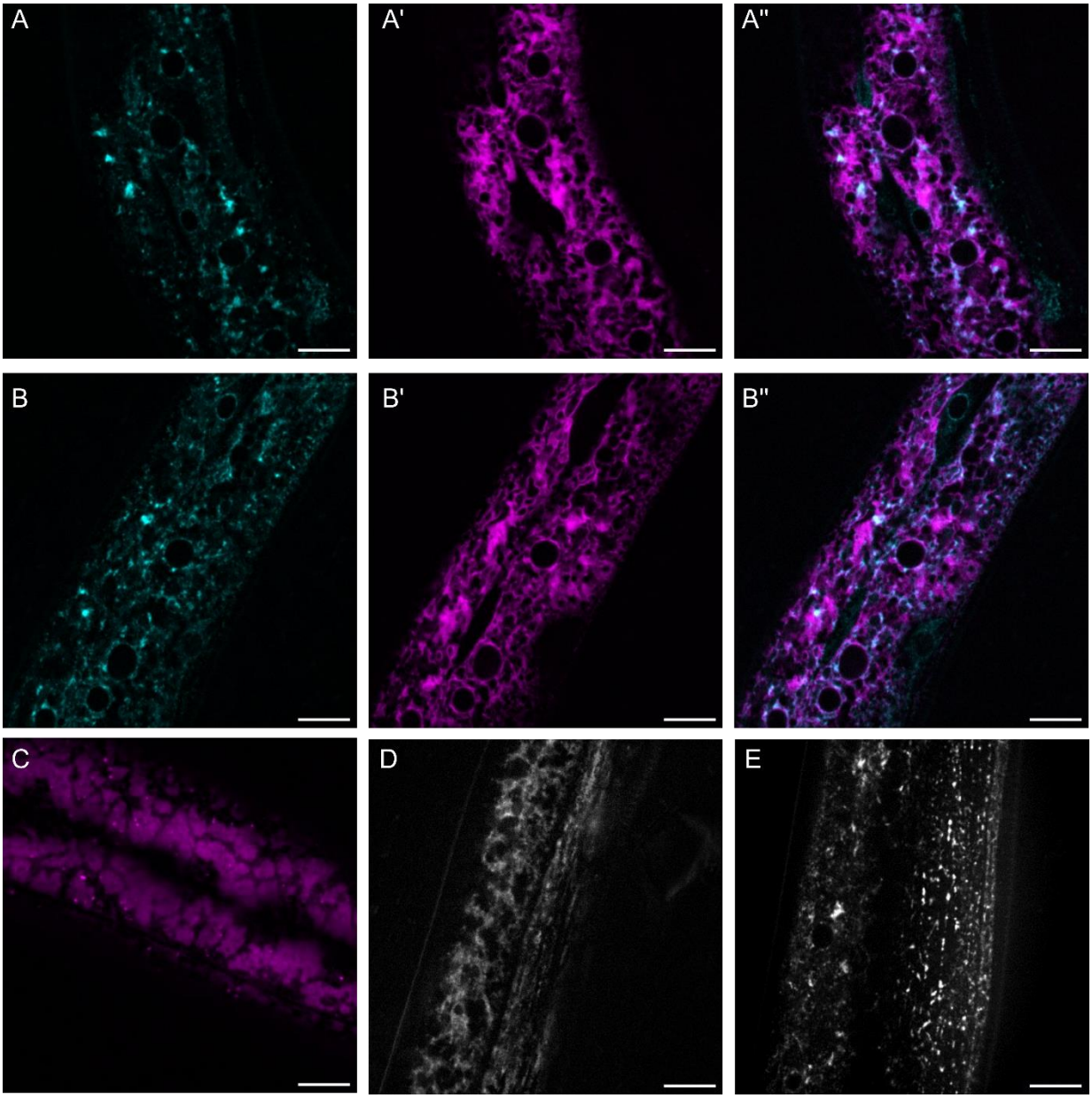

Figure V.8. Subcellular localization of ANC-1(Δ5RPs). (A-A'') and (B-B'') are confocal images of endogenous ANC-1(Δ5RPs) (A and B, cyan), the mKate2::TRAM-1 labeled ER (A' and B', magenta) and

merge of the two channels (A'' and B''). A and B are two different animals. (C) Representive images of the wrmScarlet::1RP (magenta) overexpressed in the hypodermis. (D and E) Confocal images of endogenous GFP::ANC-1 and ANC-1(Δ5RPs) in the adult muscle. Scale Bar, 10μm.

V.3.3 Identify potential binding partners of the F1 and the tandem repeats

F1 and repeat regions play important roles in organelle positioning but the molecular mechanism is poorly understood. It would also be interesting to identify the binding partners of the F1 region. I have created a yeast-2-hybrid bait pSL878 with 582bp (ANC-1B 1552S-2113A) of the F1 region to perform a yeast-two-hybrid screen to identify putative binding partners.

The tandem repeats are predicted to be spectrin-like structures and they are important for ANC-1's association with the ER. However, it is unclear what these repeats bind on the ER. I have cloned a bait plasmid pSL877 with 720bp (ANC-1B 2153L-2872E) of the repeat region for identifying binding partners of this region by yeast-two-hybrid screen.

Another way to identify putative ANC-1 binding partners is through GFP-pull down using the GFP-Trap Magnetic Particles M-270 coupled with mass spectrometry analysis. One drawback of the IP-mass spectrometry experiments is high non-specific background. It might easier to perform the pull-down experiments with both GFP::ANC-1B and GFP::ANC-1(Δ6RPs) strains and analyze the missing protein in the GFP::ANC-1(Δ6RPs) animals. ANC-1 is a very large protein (around 956 KDa) and western-blotting to identify the protein is challenging. I have successfully used the 3-8% NuPAGE Tris-Acetate Gels (ThermoFisher) to identify the repeat deleted proteins (Figure V.9). Future IP-mass spectrometry studies may reveal some putative repeat-binding proteins. It will be exciting to understand what the sceptrin-like repeats interact on the ER.

Moreover, to find putative weak interactors of ANC-1, another approach is to CRISPR tag ANC-1 and ANC-1(Δ6RPs) with BirA* and perform proximity labeling proteomics.

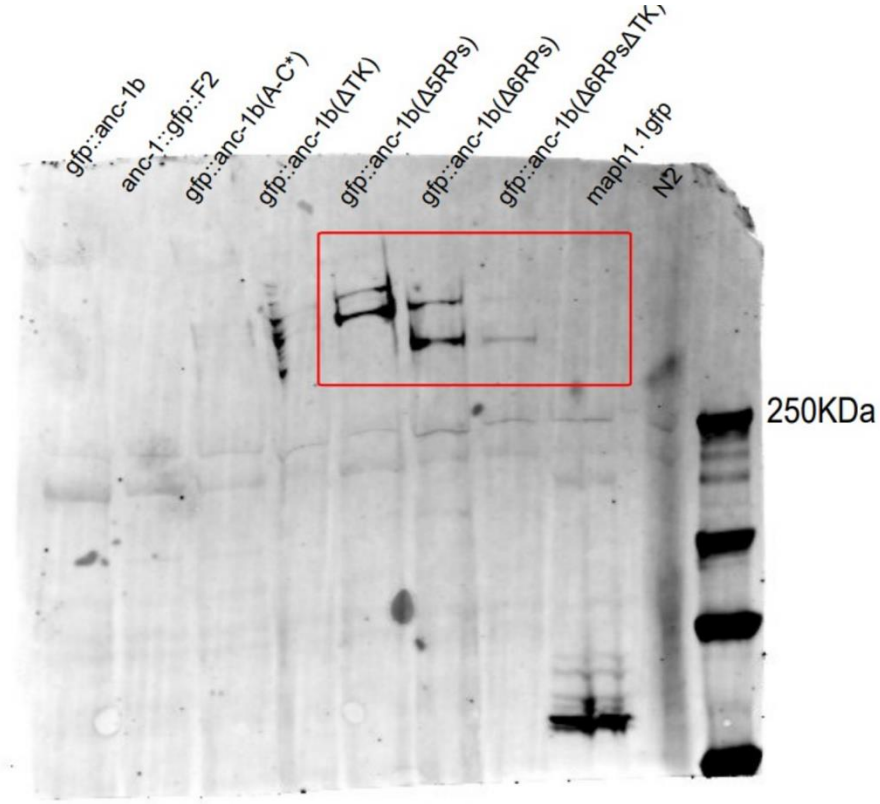

Figure V.9. Western-blot of endogenous GFP::ANC-1 in the whole worm lysates. The red box emphasizes the band of GFP::ANC-1(Δ6RPs) and GFP::ANC-1(Δ5RPs). Top and botom bands might represent the protein of a/c longer isoform and the b shorter isoform, respectively.

V.4 ANC-1's interaction with the ER

V.4.1 Lipin-1 RNAi excludes ANC-1 from the ER

In chapter 4, we characterized the ER morphology defects in *anc-1* mutants and described a strong GFP::ANC-1 correlation with the ER. However, it is not clear if change of the ER morphology will affect ANC-1's function. LIPIN-1 is a phosphatidate phosphatase that converts PA to DAG. RNAi of *lipin-1* changes the morphology of the ER in *C. elegans* early embryos (Golden, Liu et al. 2009). Interestingly, with *lipin-1* RNAi for around 40 hours (Figure V.10 E-H), the ER lost its morphology but GFP::ANC-1 is not colocalized with the misshaped ER. The phenotype is more severe with longer *lipin-1* treatment (Figure V.10 I-L and M-P). It is unclear

how *lipin-1* RNAi affects the ER colocalization of ANC-1. It is possible that some essential binding partners of ANC-1 is affected by *lipin-1* RNAi. The mKate2::TRAM-1 is still localized on the ER. It might be interesting to use proximity labeling proteomics like TurboID to tag TRAM-1 with BirA* and study the missing elements on the ER with *lipin-1* RNAi. It is possible that there are overlapping missing proteins when *lipin-1* is knocked down or the RPs are deleted.

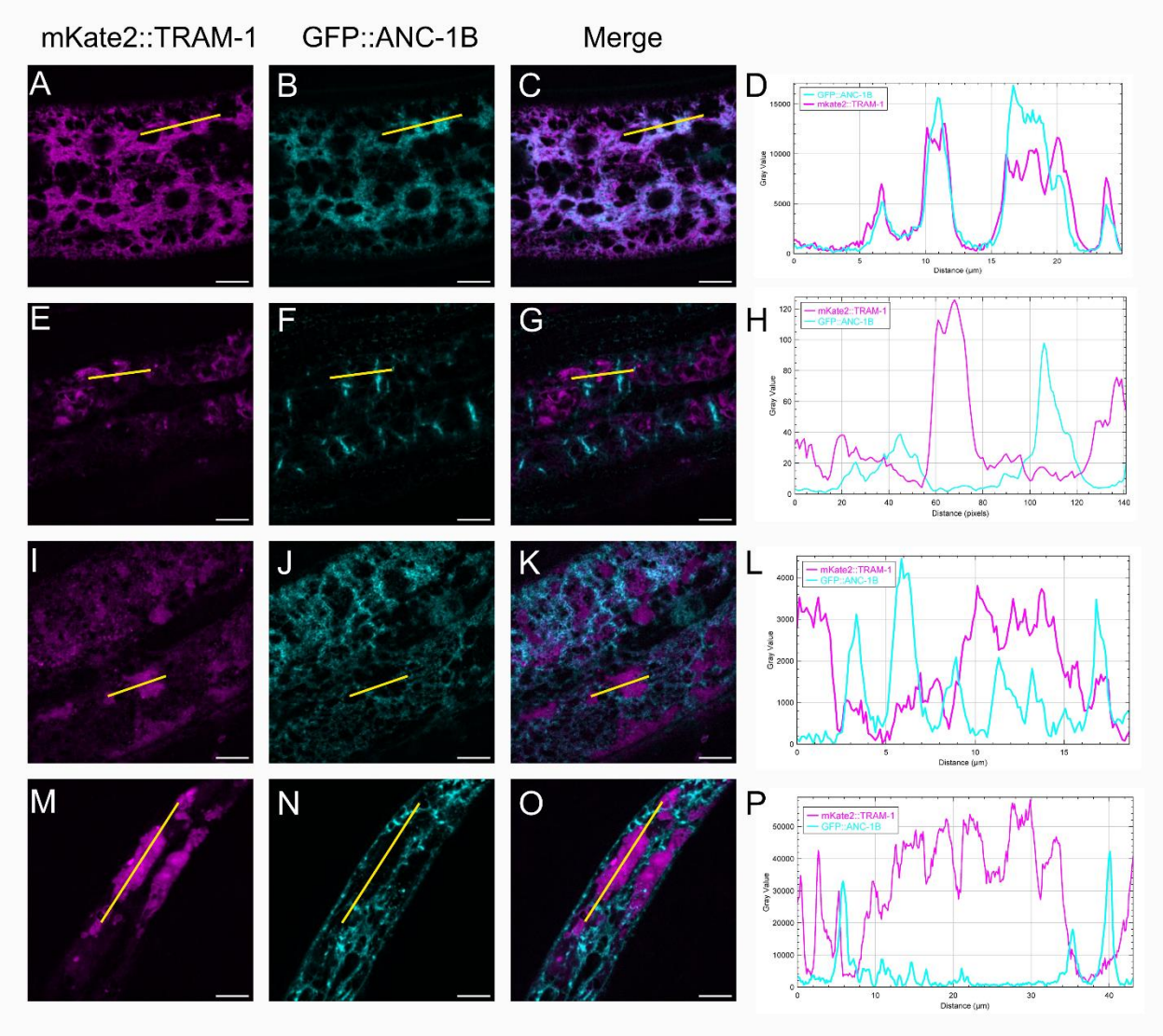

Figure V.10. Lipin-1 RNAi excludes GFP::ANC-1 from the ER. mKate2::TRAM-1 (magenta) and GFP::ANC-1b (cyan) of the control and lipin-1 RNAi treated animals are merged on the right. Line scans are shown on the far right. (A-D) RNAi control animals (E-H) L1 animals on the lipin-1 RNAi plates for

around 40 hours before imaging. (I-L) and (M-P) are two examples of F2 young adult animals on the lipin-1 RNAi plates. Scale Bar, 10μm.

V.4.2 ANC-1 may function as an ER skeleton

The ER is a well-organized structure with tubule-like and sheets-like structures. However, these structures are not well characterized in the *C. elegans* hypodermis. The fluorescent images indicate that the ER might be stacked together in the *anc-1* mutants. It is not clear if the ER changes from tubule-like network to sheets. Although ANC-1's subcellular localization is corelates with the ER, the protein is not uniformly distributed on the ER. There are some areas that ANC-1 is more expressed (Figure V.11 A). It is possible that ANC-1 is forming some sort of meshwork by itself or with other cytoskeleton elements to spread the ER or maintain the structure of the ER. It is not clear if the ER in the regions with higher ANC-1 level is more tubule-like networks than sheets. Preliminary Transmission Electron Microscopy (TEM) images indicates that the ER is organized as branched network in the WT (Figure V.11 A, D and G), while there are more sheets-like structures in the *anc-1(Δ6RPs)* animals (Figure V.11 B, E and H). There is only one worm for each strain, so future studies need to image more samples to characterize how the ER is changed without ANC-1. Two of *anc-1* null mutant worms display a gap between the cuticle and the underneath tissue (Figure V.11 C and F), and the ER is less structured in the mutant. It is not clear if the gap is due to damage in sample processing or is a defect in *anc-1* mutants. It is also not well understood how the ER shape proteins like Alastin-1 or reticulon may function to maintain the shape of ER in the hypodermis or if ANC-1 function with these ER shape proteins to anchor the ER.

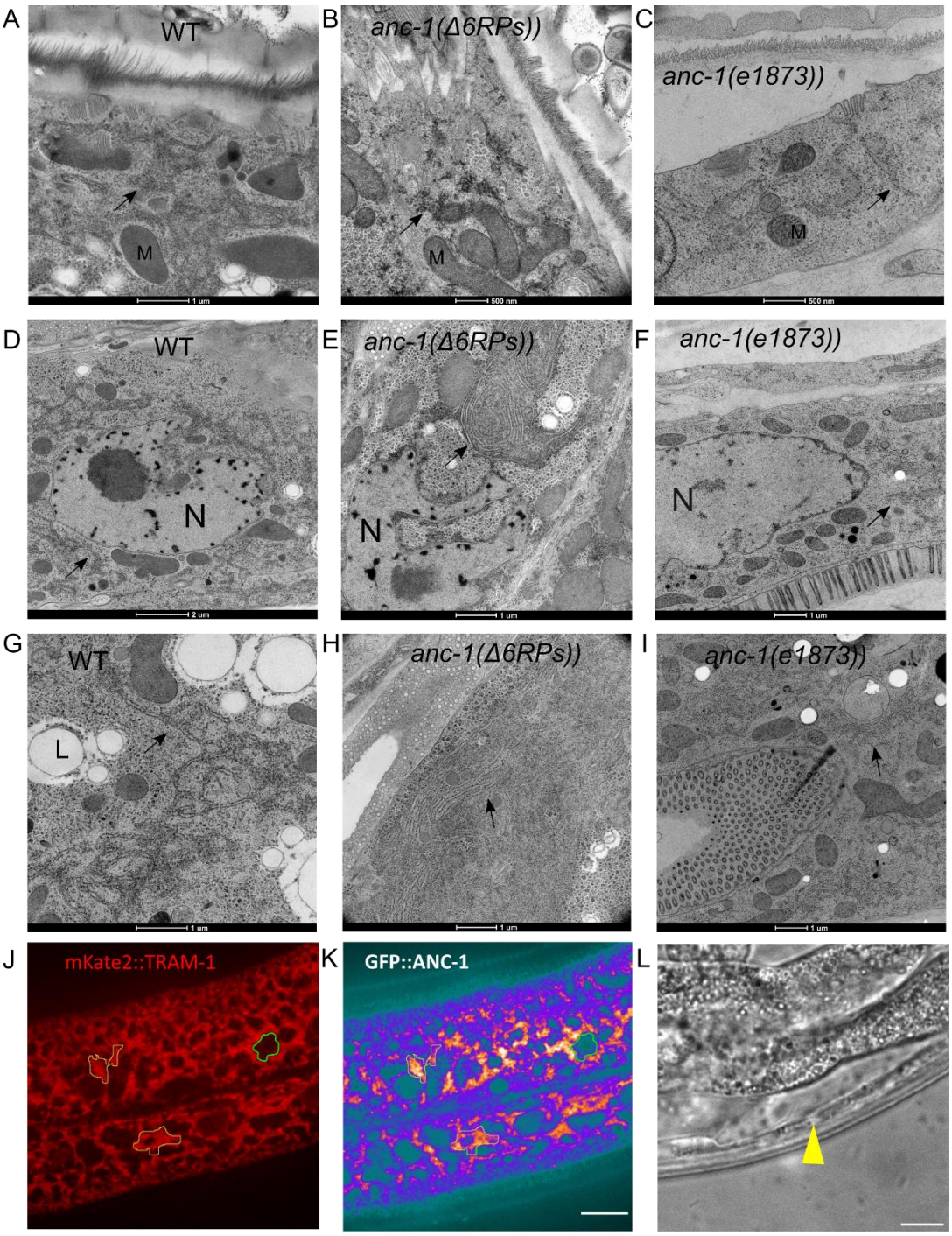

Figure V.11. ER structures in the hypodermal and intestine of wild type and *anc-1* mutants. (A-I) The longitudinal sections of worms examined by transmission electron microscopy (TEM) after High-pressure freezing and freeze substitution (McDonald 2014). (A) WT hypodermis; (B) *anc-1(Δ6RPs)* hypodermis; (C) *anc-1(e1873)* hypodermis; (D and G) WT intestine; (E and H) *anc-1(Δ6RPs)* intestine; (F and I) *anc-*

1(e1873) intestine; Scale bars are shown on the images. N is nucleus; M is mitochondria; L is lipid droplet. (J) mKate2::TRAM-1 marked ER. (K) the endogenous GFP::ANC-1 (Fire LUT). The hand-drew region emphasizes some ER structures with higher GFP::ANC-1 level. Scale Bar, 10μm.

V.5 ANC-1's role in regulating the biophysical properties of the cytoplasm

V.5.1 The mobility of the 40nm genetically encoded multimeric nanoparticles (GEMs) is increased in *anc-1* mutants

In chapter 4, we have observed that the ER, mitochondria, and lipid droplets are not anchored in the *C. elegans* hyp7 syncytium. Interestingly, GFP::ANC-1 is strongly colocalized on the ER but not on lipid droplets or mitochondria. It is unclear how ANC-1 anchors all these organelles. One hypothesis is that ANC-1 regulates the biophysical properties of the cytoplasm, which is required for the anchorage of subcellular organelles. To test this hypothesis, I expressed the recently developed 40nm GEMs (genetically encoded multimeric nanoparticles) (Delarue, Brittingham et al. 2018) in the hyp7 (Figure V.12 A and B), tracked the movement of GEMs (Figure V.12 A' and B'), and compared the effective diffusion coefficient (D_{eff}) (Figure V.12 E) of GEMs in the WT, *anc-1(e1873)* and *unc-84(n369)* mutants (Shilpi Kalra performed the tracking and generated the graph Figure V.12 E and F). Our results indicate that the GEMs move more in the *anc-1* mutant, but not in *unc-84(n369)* relative to the WT. I have also tested the mobility of 40nm GEMs in the intestine and found the similar results (Figure V.12 C-D, C'-D' and F). These results indicate that the cytoplasmic crowding might be altered in the *anc-1* mutants. Notably, there are a large amount of GEM particles trapped and are not moving around in the *C. elegans* tissues. Future analysis should consider filtering those non-mobile particles out.

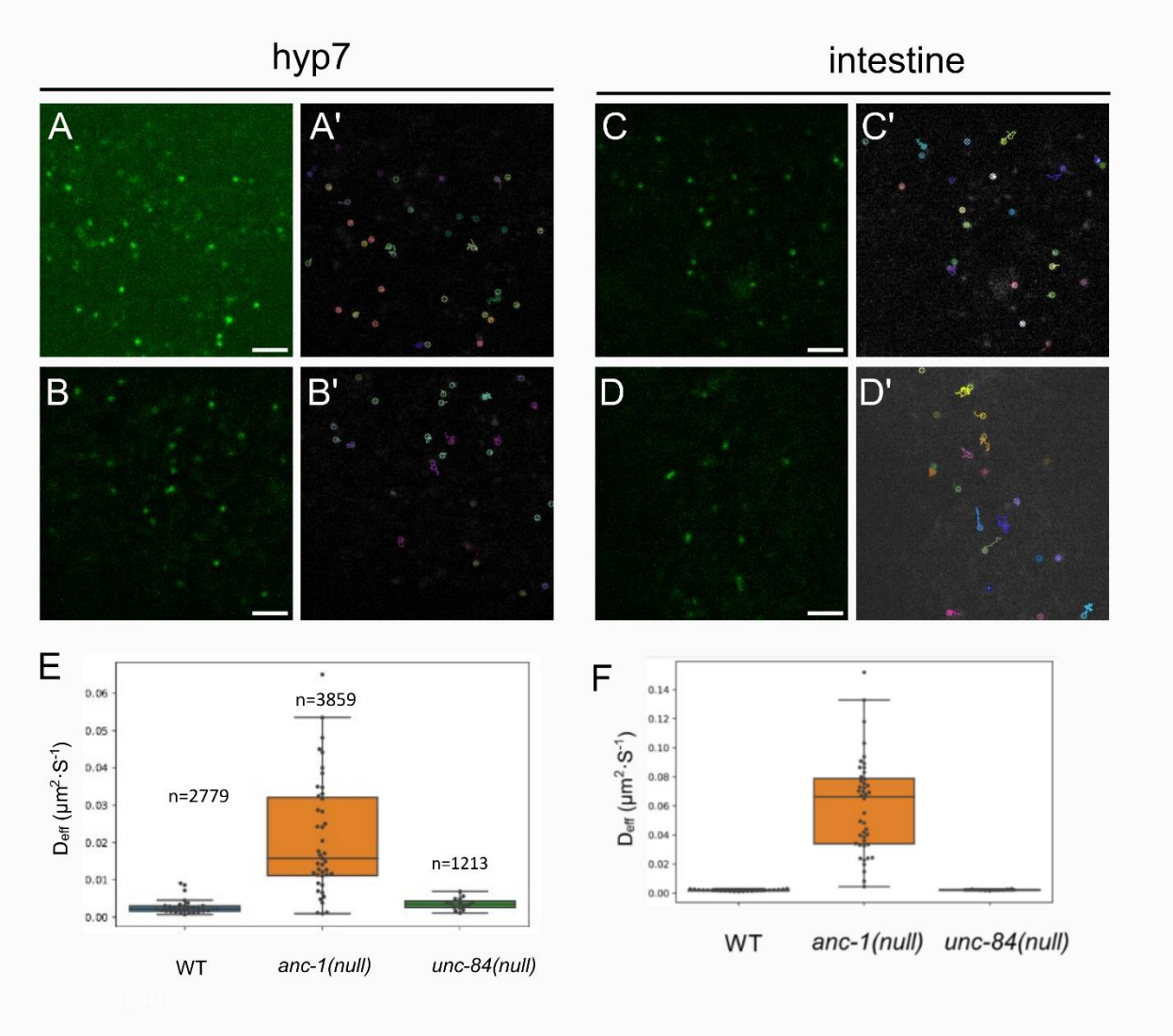

Figure V.12 Nanoparticle's difussion rate is increased in *anc-1* null mutants. (A-B) Representative images of 40nm GEMs in the hyp7 of the wild-type (A) and *anc-1(e1873)* mutant (B). The fluorescent images with single particle trajectories superimposed are shown on the right (A' and B', respectively). (C-D) Representative images of 40nm GEMs in the intestine of the wild-type (C) and *anc-1(e1873)* mutant (D). The fluorescent images with single particle trajectories superimposed are shown on the right (C' and D', respectively). The average time interval is 37ms. Scale bar, 2µm. (F-F) Effective diffusion coefficients (D_{eff}) of 40nm GEMs in the WT (blue), *anc-1(e1873)* (orange), and *unc-84(n369)* (green) in the hyp7 (E) and intestine (F). Each dot represents the medium of Deff for each video. n in figure E represent the number of tracks analyzed.

In addition, I have expressed the 40nm GEMs in the muscle and neurons. GEMs in the muscle are very highly expressed and form aggregates even with GFP RNAi (Figure V.13 A). Further studies may consider using inducible protein expression constructs to control levels of GEMs. One approach I have tried is to use CRISPR/Cas9 gene editing to add the recently established tetracycline-dependent ribozyme switch in the 3' UTR of the hypodermal 40nm GEM strains. Without tetracycline, the ribozyme cleaves the mRNA and no GEM is expressed. In the presentence of tetracycline, the ribozyme is inactivated, and GEMs are expressed (Wurmthaler, Sack et al. 2019). Preliminary results indicate that there is no GEM expression without tetracycline. However, with 1µM tetracycline, there is a robust expression of 40nm GEMs in the adult hyp7. It might be possible to optimize the tetracycline treatment. Otherwise, other approaches should be considered to control the density of the GEMs.

In neurons, the 40nm GEMs driven by the pan-neuronal *rgef-1* promoter are expressed at an appropriate density and are easy to track (Figure V.13 D and E). It might be because that the expression level is enough for GEMs to assembly but not too much to form aggregates. Also, the neurons of *C. elegans* are on the surfaces of the worm, making it easy to image. It would be interesting to know if there is difference in the cellular crowding in the axons and the cell body since ribosome are mainly in the cell body (Rolls, Hall et al. 2002, Noma, Goncharov et al. 2017). ANC-1 is also expressed in neurons (data not shown) and mutations in *anc-1* causes axon guidance defects in the mechanosensory neurons (Tulgren, Turgeon et al. 2014). It would be interesting to test if ANC-1 affects the subcellular crowding in neurons with the neuronal GEM strain. I have crossed a red mechanosensory neuron marker $P_{mec\text{-}7}$*::mRFP (jsIs973 [mec-7p::mRFP + unc-119(+)] III.)* into the $P_{rgef\text{-}1}$*::40nmGEM* strain with or without *anc-1* and *unc-84* null mutations. Preliminary imaging indicates that we can track the GEM mobility in the cell body (Figure V.13 D-D''') or the axon (Figure V.13 E-E'''). Although the 40nm GEMs are not highly expressed in the mechanosensory neurons, it is possible to image more worms to get enough

sample. Future studies could use GEMs to test if ANC-1 plays a role in the cellular crowding in the neurons and if UNC-84 is required in this process.

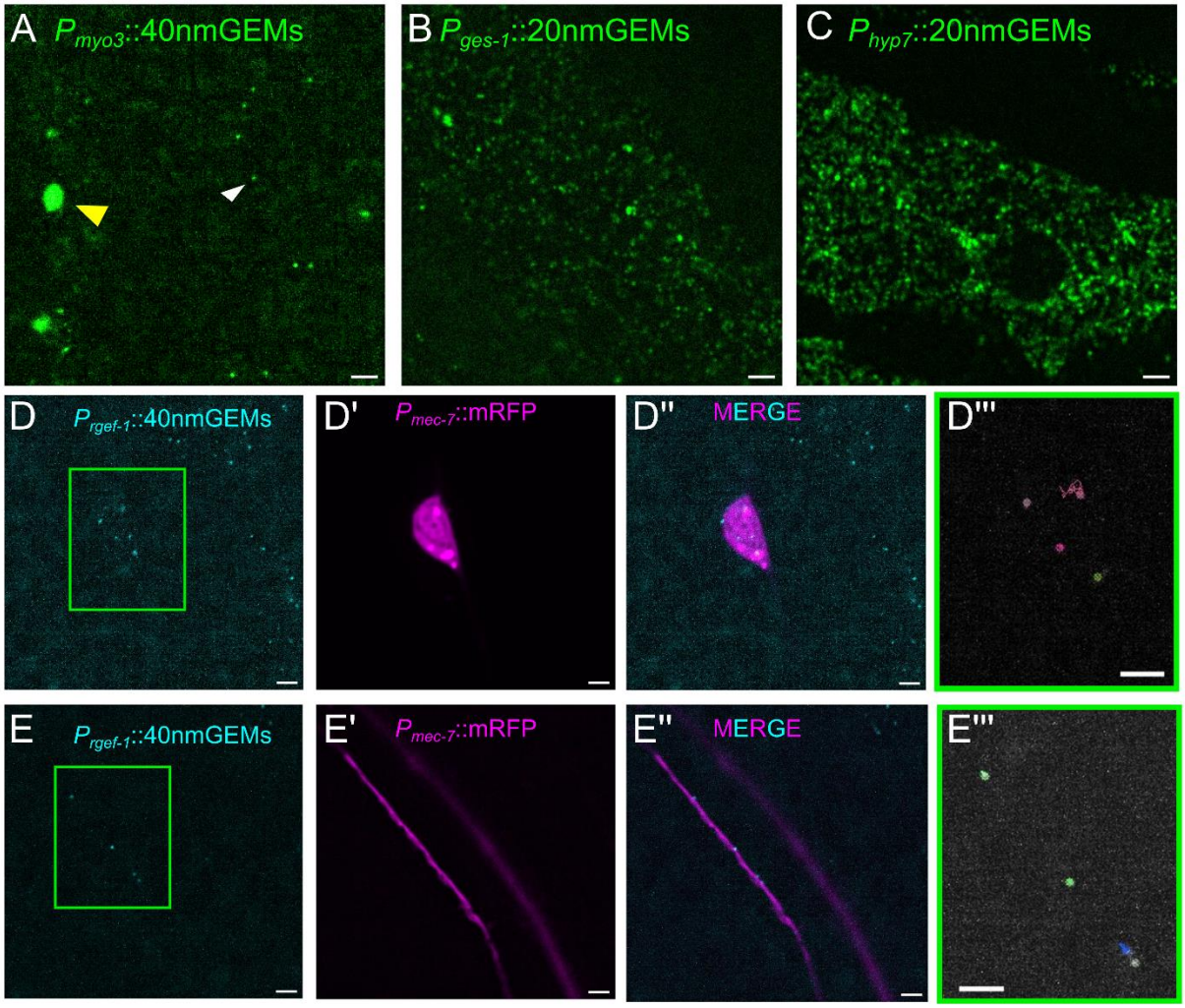

Figure V.13. 40nm GEMs in muscle and neurons and representive images of 20nm GEM strains. (A) 40nm GEMs under the *myo-3* promoter are expressed in single copy in the muscle. Yellow arrow points to the aggregated GEMs; While arrow head points to a GEM particle. (B-C) 40nm GEMs are expressed in single copy under the *ges-1* promoter in the intestine (B) and under the *y37a1b.5* promoter in the hyp7 (C). (D-E''') 40nm GEMs are expressed in single copy under the rgef-1 promoter in neurons (Cyan, D and E) colocalized with the cell body (D-D''') and the axon (E-E''') of P_{mec-7}::mRFP labeled (magenta) mechanosensory neurons. (D''' and E''') Enlarged region in the green boxes of (D) and (E) with tracks

generated by MOSAIC plugin. The Radius is 3, Cutoff is 0, Per/Abs is 0.05 for cell body (D’’’) and 0.02 for axon (E’’’), Linkrage is 2 nd displacement is 10. Scale bar, 2μm.

V.5.2 Knocking-down small ribosome proteins causes nuclear anchorage defects

Recent studies have shown that ribosome concentration plays an important role in the cellular crowding in budding yeast and human tissue culture cells (Delarue, Brittingham et al. 2018). It is not clear if ribosome concentration also affects the cellular crowding in the hyp7 syncytium in *C. elegans*. With the 40nm GEM strain, we can test if the mobility of the GEM particles increases with *rps-15* or *rps-18* RNAi. Rapamycin and mTOR signaling pathway also affect the ribosome concentration (Delarue, Brittingham et al. 2018), we can also test the mobility of GEMs with Rapamycin treatment or *let-363 (mTOC)* RNAi.

Previous preliminary results from an RNAi feeding screen of Chromosome I for nuclear anchorage defects in the lab suggest that RNAi of *rps-15 (ribosomal protein S15)* cause nuclear anchorage defects. The small ribosome protein RPS-15 is involved in nucleolar ribosomal biogenesis and the assembly of RPS-15 into the pre-ribosomes is essential for their nuclear exit (Leger-Silvestre, Milkereit et al. 2004, Rossler, Weigl et al. 2022). Another small ribosome protein RPS-18, which contacts RPS-15 in the small subunit of ribosomes, functions upstream for pre-ribosomes maturation (Leger-Silvestre, Milkereit et al. 2004). Knocking down *rps-15* or *rps-18* causes ribosome biogenesis defects. My nuclear anchorage quantification results showed that *rps-15* and *rps-18* RNAi increased the percentage of touching nuclei in the hyp7 syncytium (Figure V.14 B, C-D), which is even more severe than the *unc-84(null)*. However, the phenotype is not as significant as *anc-1* null mutants. Recently, a large-scale RNAi screen studies identified two different ribosome subunits, *rpl-21* and *rps-22,* that affects ER structure (Maheshwari, Rahman et al. 2021). It would be interesting to test if *rps-15* and *rps-18* RNAi cause ER defects in the hypodermis. It is still not clear if the defects in nuclear positioning and

ER morphology are caused by alteration of cellular crowding or other essential roles of ribosome.

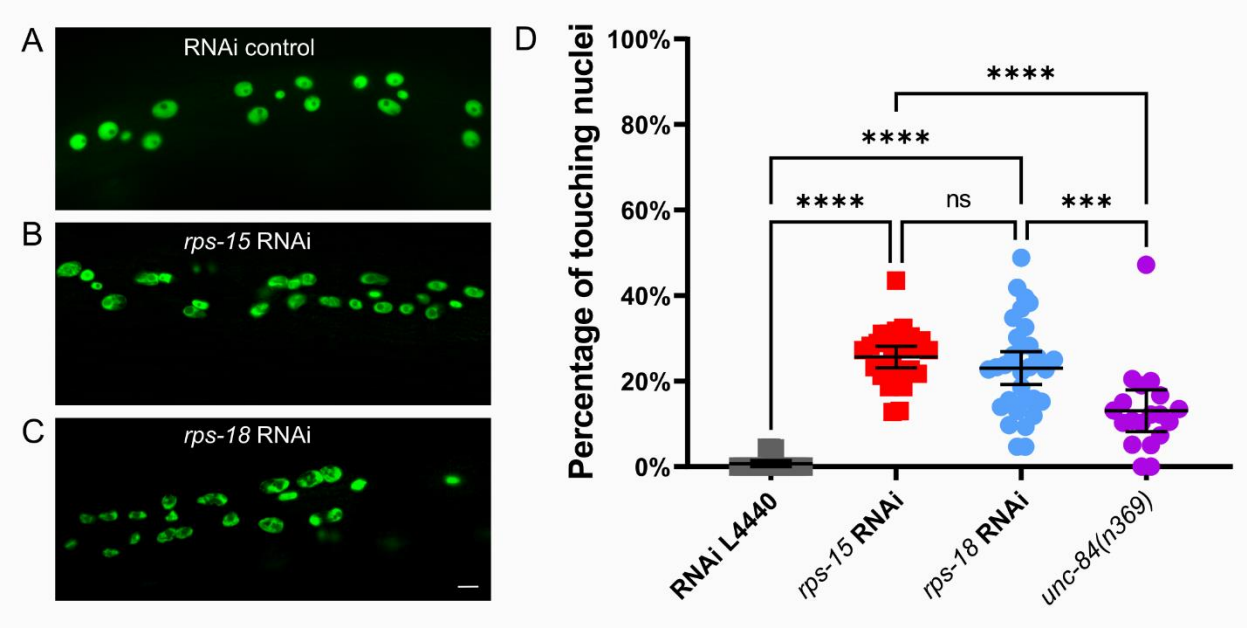

Figure V.14. Knocking down ribosome proteins causes nuclear anchorage defects. (A-C) Lateral view of adult *C. elegans* expressing hypodermal nuclear GFP (green) treated with RNAi control (A), RNAi of *rps-15* (B), and RNAi of *rps-18*. Scale bar, 10μm. (D) Quantification of nuclear anchorage defects in the DNKASH overexpression strains. Each dot represents the percentage of touching nuclei on one side of a young adult animal. Means with 95% CI error bars are shown. n ≥ 20. ns, not significant. P ≤ 0.01 ***, p ≤ 0.01; ****, p ≤ 0.001.

V.5.3 Ribosome distribution maybe altered in *anc-1* mutants

Since ribosomes play a role in cellular crowding, which might affect organelle positioning. I was curious if ribosomes are normal when *anc-1* is knocked down. Most ribosome proteins are essential and tagging GFPs affects their function. The Jin lab has developed split GFP for tissue-specific visualization RPS-18 in *C. elegans* (Noma, Goncharov et al. 2017). The *rps-18* fused to the 11th beta strand of GFP (GFP11) under its own promoter inserted into the genome as a single copy in the *rps-18* null mutant (Noma, Goncharov et al. 2017). The transgene

rescued the null mutant, indicating that GFP_{11}::RPS18 is functional. The larger part of split GFP (GFP1-10) is overexpressed as extrachromosomal arrays under the *col-19* promoter (*juEx5375[Pcol-19-GFP1-10]*). I also used GFP-tagged RPL-29, a component of the ribosome large subunit, to visualize ribosomes (Noma, Goncharov et al. 2017). With RNAi control, the GFP11::RPS-18 and GFP::RPL-29 are ubiquitously expressed in the cytoplasm (Figure V.15 A and D). However, with *anc-1* RNAi, ribosome distribution is disrupted like the ER (Figure V.15 B, E and F; Figure IV.4). I next tested if the regions with brighter GFP::RPS-18 signal are ER-bound ribosomes by CRISPR-tagging RPS-18 with split GFP in the hypodermal mKate2::TRAM-1 ER marker background (both the ER marker and *rps-18* are on chromosome IV, making it challenging to cross the two markers). As a result, the bright ribosome regions are colocalized with the ER (Figure V.15 G-G''' and H-H'''). The GFP or split GFP tagged ribosomes are moving around with the *anc-1* RNAi treatment. It is unclear if the cytoplasmic ribosome concentration is altered, or the distribution of the cytoplasmic ribosomes are altered without ANC-1. Future studies are required to quantify the distribution of ribosomes in the cytoplasm to test if there is a change in the ribosome distribution in *anc-1* mutants. Although challenging, it might be helpful to measure the local ribosome concentration either by analyzing TEM images or fluorescent images in the future (Figure V.11 A-I). It is possible that the ribosome distribution defects cause heterogeneity of cellular crowding in the cytoplasm. It may explain the flow in the cytoplasm in the hyp7 syncytium of *anc-1* mutants. Another possibility is that the change of localization of ribosomes is directly related to the ER anchorage defects in the *anc-1* knock down worms. It is possible that the ER lost anchorage and stack together, creating more room for the ribosomes and decreased ribosome concentrations in the cytoplasm. It would be interesting to measure the ER volume to test if there is more ER-free space in the syncytium.

I have also generated a Split Scarlet-tagged RPS-18 strain (Figure V.15 C), which can be used to image together with GFP-tagged GEMs to test if the local ribosome concentration correlates with GEMs mobility in the wild-type and *anc-1* knockdown worms.

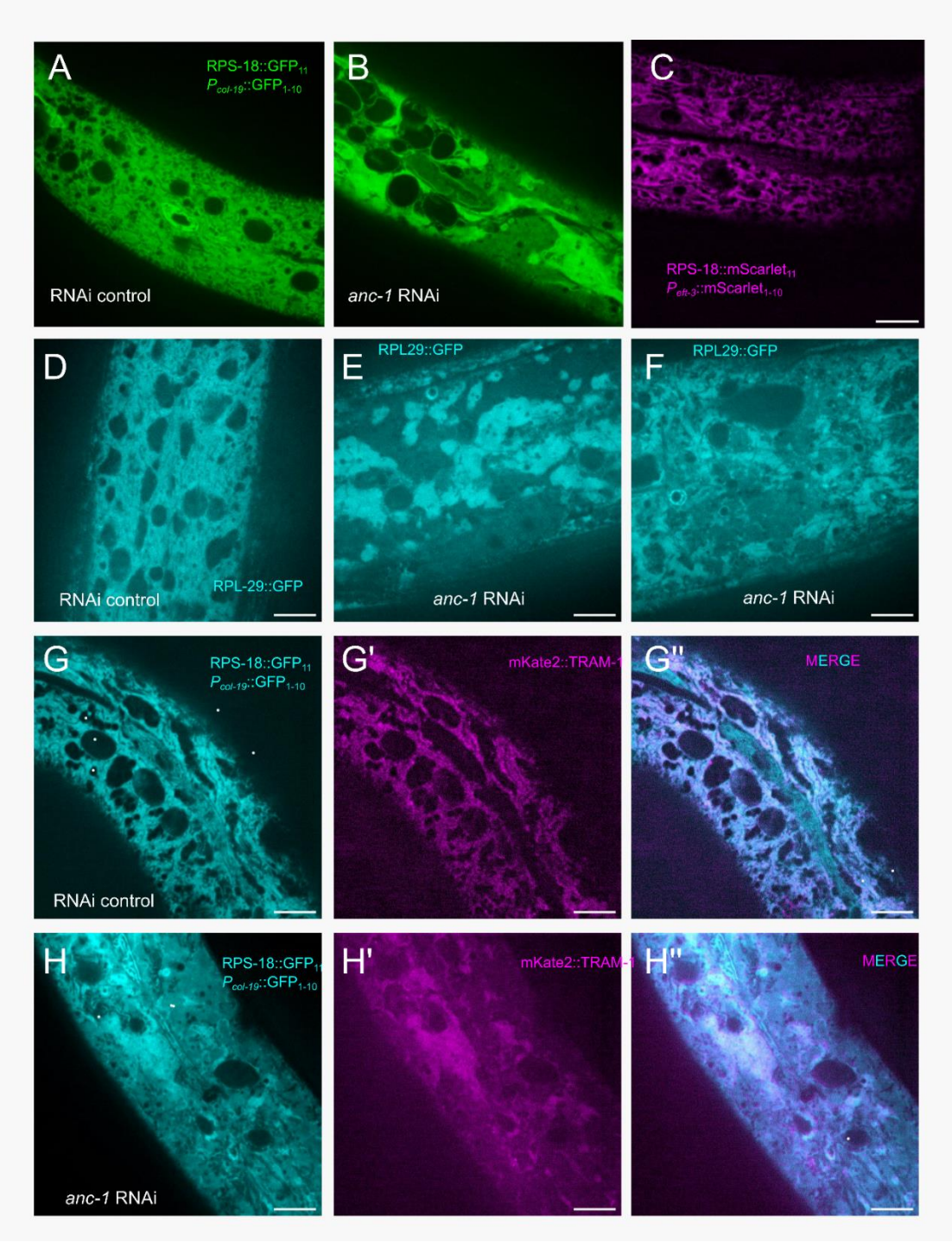

Figure V.15. Ribosome distribution is affected by *anc-1* RNAi. (A-B) Epidermis-specific Split GFP tagged RPS-18 proteins (green) in the young adults with RNAi control treatment (A) and RNAi of *anc-1* (B). (C) Representative confocal image of wrmScarlet11 tagged endogenous RPS-18 in epidermis. (D-F) GFP::RPL29 (cyan) in the young adults with RNAi control treatment (D) and RNAi of *anc-1* (E and F). Split GFP tagged RPS-18 (Cyan, G and H) and mKate2::TRAM-1 labeled ER (magenta G' and H') are merged on the right (G'' and H'') with RNAi control (G-G'') and *anc-1* RNAi (H-H'') treatments. Scale bar, 10μm.

With the present study, I have characterized the KASH-independent function of the giant KASH protein ANC-1 in the anchorage of subcellular organelles in the hyp7 syncytium. The study redirects our attention from nuclear clustering to organelles moving around, which indicates a role of ANC-1 in regulating the organization of the whole cytoplasm. The human ortholog of ANC-1, Nesprin-1 and 2, are involved in many muscular and neurological diseases. It will be interesting to know if the human orthologs also function to organize the cytoplasm, rather than just regulating nuclear positioning. Although the molecular mechanism of how exactly the cytoplasm domains of ANC-1 function is still not clear, further research on identifying ANC-1 binding partners may provide valuable insight into how the cytoplasm is organized. To study the possibility that ANC-1 may regulate the cytoplasmic crowding, I introduced the GEMs to study microrheology in *C. elegans*. Our preliminary results indicate that ANC-1 may regulate the subcellular crowding, but the mechanism is unclear. Although the GEMs are not perfect yet, it could be a great tool to study the biophysical properties of the cytoplasm in various tissues during different developmental processes. Future efforts in optimizing and establishing GEMs as a tool would help to answer many cell biology questions.

References:

Altun, Z. and D. Hall (2009). "Epithelial system, hypodermis." *WormAtlas*. doi:10.3908/wormatlas.1.13 **10**.
Belaadi, N., J. Aureille and C. Guilluy (2016). "Under Pressure: Mechanical Stress Management in the Nucleus." Cells **5**(2).
Bone, C. R., Y. T. Chang, N. E. Cain, S. P. Murphy and D. A. Starr (2016). "Nuclei migrate through constricted spaces using microtubule motors and actin networks in C. elegans hypodermal cells." Development **143**(22): 4193-4202.
Bone, C. R. and D. A. Starr (2016). "Nuclear migration events throughout development." J Cell Sci **129**(10): 1951-1961.
Cain, N. E., Z. Jahed, A. Schoenhofen, V. A. Valdez, B. Elkin, H. Y. Hao, N. J. Harris, L. A. Herrera, B. M. Woolums, M. R. K. Mofrad, G. W. G. Luxton and D. A. Starr (2018). "Conserved SUN-KASH Interfaces Mediate LINC Complex-Dependent Nuclear Movement and Positioning." Current Biology **28**(19): 3086-+.
Delarue, M., G. P. Brittingham, S. Pfeffer, I. V. Surovtsev, S. Pinglay, K. J. Kennedy, M. Schaffer, J. I. Gutierrez, D. Sang, G. Poterewicz, J. K. Chung, J. M. Plitzko, J. T. Groves, C. Jacobs-Wagner, B. D. Engel and L. J. Holt (2018). "mTORC1 Controls Phase Separation and the Biophysical Properties of the Cytoplasm by Tuning Crowding." Cell **174**(2): 338-349 e320.
Fenech, M., M. Kirsch-Volders, A. T. Natarajan, J. Surralles, J. W. Crott, J. Parry, H. Norppa, D. A. Eastmond, J. D. Tucker and P. Thomas (2011). "Molecular mechanisms of micronucleus, nucleoplasmic bridge and nuclear bud formation in mammalian and human cells." Mutagenesis **26**(1): 125-132.
Golden, A., J. Liu and O. Cohen-Fix (2009). "Inactivation of the C. elegans lipin homolog leads to ER disorganization and to defects in the breakdown and reassembly of the nuclear envelope." J Cell Sci **122**(Pt 12): 1970-1978.
Hatch, E. M. (2018). "Nuclear envelope rupture: little holes, big openings." Curr Opin Cell Biol **52**: 66-72.
Hedgecock, E. M. and J. N. Thomson (1982). "A gene required for nuclear and mitochondrial attachment in the nematode Caenorhabditis elegans." Cell **30**(1): 321-330.
Krupina, K., A. Goginashvili and D. W. Cleveland (2021). "Causes and consequences of micronuclei." Curr Opin Cell Biol **70**: 91-99.
Leger-Silvestre, I., P. Milkereit, S. Ferreira-Cerca, C. Saveanu, J. C. Rousselle, V. Choesmel, C. Guinefoleau, N. Gas and P. E. Gleizes (2004). "The ribosomal protein Rps15p is required for nuclear exit of the 40S subunit precursors in yeast." EMBO J **23**(12): 2336-2347.
Maheshwari, R., M. M. Rahman, D. Joseph-Strauss and O. Cohen-Fix (2021). "An RNAi screen for genes that affect nuclear morphology in Caenorhabditis elegans reveals the involvement of unexpected processes." G3 (Bethesda) **11**(11).
Malone, C. J., W. D. Fixsen, H. R. Horvitz and M. Han (1999). "UNC-84 localizes to the nuclear envelope and is required for nuclear migration and anchoring during C-elegans development." Development **126**(14): 3171-3181.
McDonald, K. L. (2014). "Out with the old and in with the new: rapid specimen preparation procedures for electron microscopy of sectioned biological material." Protoplasma **251**(2): 429-448.
Noma, K., A. Goncharov, M. H. Ellisman and Y. Jin (2017). "Microtubule-dependent ribosome localization in C. elegans neurons." Elife **6**.
Rolls, M. M., D. H. Hall, M. Victor, E. H. Stelzer and T. A. Rapoport (2002). "Targeting of rough endoplasmic reticulum membrane proteins and ribosomes in invertebrate neurons." Mol Biol Cell **13**(5): 1778-1791.

Rossler, I., S. Weigl, J. Fernandez-Fernandez, S. Martin-Villanueva, D. Strauss, E. Hurt, J. de la Cruz and B. Pertschy (2022). "The C-terminal tail of ribosomal protein Rps15 is engaged in cytoplasmic pre-40S maturation." RNA Biol **19**(1): 560-574.
Starr, D. A. and M. Han (2002). "Role of ANC-1 in tethering nuclei to the actin cytoskeleton." Science **298**(5592): 406-409.
Tulgren, E. D., S. M. Turgeon, K. J. Opperman and B. Grill (2014). "The Nesprin family member ANC-1 regulates synapse formation and axon termination by functioning in a pathway with RPM-1 and beta-Catenin." PLoS Genet **10**(7): e1004481.
Wurmthaler, L. A., M. Sack, K. Gense, J. S. Hartig and M. Gamerdinger (2019). "A tetracycline-dependent ribozyme switch allows conditional induction of gene expression in Caenorhabditis elegans." Nat Commun **10**(1): 491.